


2009

Characterization of NPRC and its binding partners

Abdel A. Alli

University of South Florida

Follow this and additional works at: <http://scholarcommons.usf.edu/etd>

 Part of the [American Studies Commons](#), and the [Medical Molecular Biology Commons](#)

Scholar Commons Citation

Alli, Abdel A., "Characterization of NPRC and its binding partners" (2009). *Graduate Theses and Dissertations*.
<http://scholarcommons.usf.edu/etd/3672>

This Dissertation is brought to you for free and open access by the Graduate School at Scholar Commons. It has been accepted for inclusion in Graduate Theses and Dissertations by an authorized administrator of Scholar Commons. For more information, please contact scholarcommons@usf.edu.

Characterization of NPRC and Its Binding Partners

by

Abdel A. Alli

A dissertation submitted in partial fulfillment
of the requirements for the degree of
Doctor of Philosophy
Department of Molecular Medicine
College of Medicine
University of South Florida

Major Professor: William R. Gower, Jr., Ph.D.
Denise R. Cooper, Ph.D.
David L. Vesely, MD, Ph.D.
Larry P. Solomonson, Ph.D.

Date of Approval:
November 2, 2009

Keywords: AHNAK1, arrestins, calcium, phospholipase C, phosphorylation

© Copyright 2009, Abdel A. Alli

Table of Contents

List of Tables	v
List of Figures	vi
List of Abbreviations	xii
Abstract	xvii
Introduction	1
Natriuretic Peptides	1
Natriuretic Peptide Receptors	5
β -arrestins	11
G proteins	14
Adenylyl Cyclase	15
AHNAK1/Desmoyokin	17
Arachidonic Acid	20
Phospholipase C	23
Calcium Signaling	24
Adipogenesis	25
Protein Kinases and Phosphatases	28
Cell-cell Junctions	30
RGM1	34
3T3-L1	34
AoSMCs	35
Recombinant Proteins	35

Central Hypothesis and Specific Aims	40
Specific Aim 1	40
Specific Aim 2	40
Specific Aim 3	40
Specific Aim 4	40
Specific Aim 5	40
Chapter 1: Development of a Polyclonal Antibody (JAH84) For Investigations of NPRC	48
Background	49
Materials and Methods	50
Results	56
Discussion	58
Chapter 2: Protein Binding Partners of NPRC	67
Background	68
Materials and Methods	69
Results	74
Discussion	80
Chapter 3: Role of NPRC in Signal Transduction	111
Background	112
Materials and Methods	113
Results	118
Discussion	125
Chapter 4: Post-Translational Modifications of NPRC	161
Background	162
Materials and Methods	163

Results	169
Discussion	175
Chapter 5: Potential Functions of AHNAK1	193
Background	194
Materials and Methods	195
Results	197
Discussion	199
References	211
Appendices	235
Appendix A: EMBOSS alignment needle program results of AHANK1 and AHNAK2	236
Appendix B: Reverse and forward sequence for pACT-NPRC and pBIND-NPRC	239
Appendix C: Sequence for pACT- β -arrestin and pBIND- β -arrestin	240
Appendix D: Reverse and forward sequence for pBIND-AHNAK1	240
Appendix E: Reverse and forward sequence for AHNAK1 construct 2	241
Appendix F: Construction of pACT and pBIND AHNAK1 fusion proteins	242
Appendix G: Construction of pGEX4T3NPRC	243
Appendix H: Sequence for rat GST-NPRC	243
Appendix I: Primers used with the QuikChange site-directed mutagenesis kit	244
Appendix J: Site-directed mutagenesis reaction	244
Appendix K: Cycling parameters for site-directed mutagenesis	

reaction	245
Appendix L: Ligation reaction for construction of pACT and pBIND AHNAK1	245
Appendix M: Restriction digest reaction for verification of pACT and pBIND AHNAK1	245
Appendix N: Reactions and parameters for the subcloning of rat NPRC into pGEX4T3	246
Appendix O: Transfection reagents used for delivery of plasmid DNA or siRNA	247
Appendix P: Relevant publications	248
About the Author	End Page

List of Tables

Table 1	Natriuretic Peptides and their receptors in disease	39
Table 2	Protein expression of natriuretic peptide receptors in various cell lines	39
Table 3	Location of the gene coding for the NPRs	40
Table 4	Sequences for siRNAs used in various experiments	135
Table 5	Solubilization and purification scheme for GST-NPRC	182
Table 6	Various antibodies used to characterize the phosphorylation state of NPRC	182
Table 7	Prediction of NPRC phosphorylation by PKA using the pkaPS algorithm	182

List of Figures

Figure 1	Amino acid structure of the natriuretic peptides.	41
Figure 2	Paradigm of natriuretic peptide synthesis and release.	42
Figure 3	Topology of the natriuretic peptide receptors (NPRs).	43
Figure 4	Diagram showing the role of G proteins in signal transduction.	44
Figure 5	Reactions catalyzed by various enzymes.	45
Figure 6	Role of the second messengers IP ₃ , DAG, and Ca ²⁺ in the phosphatidylinositol system.	46
Figure 7	Phase-contrast microscopy of the cell lines used in the various studies of NPRC.	47
Figure 8	Sequence alignment of the intracellular domain of NPRC from various species.	61
Figure 9	Western blot analysis showing cross-reactivity of various polyclonal antibodies against NPRC.	62
Figure 10	Western blot and densitometric analyses of flag-NPRC using JAH84 antibody.	63
Figure 11	Coomassie blue stained gel (grayscale) after immunoprecipitation of NPRC with JAH84.	64
Figure 12	Western blot analysis of endogenous NPRC protein expression using JAH84 antibody.	65
Figure 13	Immunofluorescence of RGM1 cells using JAH84.	66
Figure 14	Schematic of the far Western (protein overlay assay) technique.	87

Figure 15	Representation of constructs used in the mammalian two-hybrid dual luciferase assay.	88
Figure 16	Sequence alignment of the 37 amino acid cytoplasmic domain of human and rat NPRC.	89
Figure 17	In vitro IP-Western demonstrating the association between NPRC and β -arrestins.	90
Figure 18	Effect of NPRC occupancy on its association with β -arrestins.	91
Figure 19	In vitro GST pulldown assay showing specificity of β -arrestin isoforms for NPRC.	92
Figure 20	Model illustrating the hypothesized role of β -arrestin 1/2 in mediating NPRC signaling.	93
Figure 21	Molecular association of NPRC and AHNAK1 in AoSMC.	94
Figure 22	Molecular association of NPRC and AHNAK1 in RGM1 cells.	95
Figure 23	Molecular association of NPRC and AHNAK1 in 3T3-L1 cells.	96
Figure 24	Identification of AHNAK1 domains that associate with NPRC in AoSMC cells.	97
Figure 25	Specificity of the association between NPRC and AHNAK1.	98
Figure 26	The role of phosphorylation in the association between NPRC and AHNAK1.	99
Figure 27	Effect of NPRC occupancy on the association between NPRC and AHNAK1.	100
Figure 28	Expression of endogenous AHNAK1 and NPR proteins.	101
Figure 29	Expression of endogenous PLC proteins in various cell lines.	102
Figure 30	Assessment of the differentiation of 3T3-L1 cells.	103
Figure 31	Regulation of AHNAK1 and NPR protein expression from day 0 to 6 of 3T3-L1 cell differentiation.	104

Figure 32	Regulation of AHNAK1 and NPR protein expression from day 8 to 12 of 3T3-L1 cell differentiation.	105
Figure 33	Endogenous expression of AHNAK1 and NPRC proteins in mouse adipose tissues.	106
Figure 34	The effect of AHNAK1 translocation in response to PMA treatment in RGM1 cells.	107
Figure 35	Immunofluorescence showing the effect of increased $[Ca^{2+}]_e$ on AHNAK1 translocation in 3T3-L1 preadipocytes.	108
Figure 36	Knockdown of NPRC protein in 3T3-L1 preadipocytes.	109
Figure 37	Role of NPRC knockdown on AHNAK1 subcellular localization.	110
Figure 38	Response to ET-1 in A-10 VSMCs.	136
Figure 39	Intracellular Ca^{2+} mobilization in quiescent AoSMC in response to 1 μ M AA.	137
Figure 40	Intracellular Ca^{2+} mobilization in quiescent AoSMC in response to 25 μ M AA.	138
Figure 41	Intracellular Ca^{2+} mobilization in quiescent AoSMC in response to 25 μ M AA in calcium free medium.	139
Figure 42	Intracellular Ca^{2+} mobilization in quiescent AoSMC in response to 1 μ M TG.	140
Figure 43	Intracellular Ca^{2+} mobilization in quiescent AoSMC in response to 100 μ M AA.	141
Figure 44	Intracellular Ca^{2+} mobilization in quiescent AoSMC in response to 25 μ M PMA.	142
Figure 45	Intracellular Ca^{2+} mobilization in quiescent AoSMC in response to 1 μ M cANF.	143
Figure 46	Intracellular Ca^{2+} mobilization in quiescent 3T3-L1 preadiocytes in response to 100 μ M AA.	144

Figure 47	Intracellular Ca ²⁺ mobilization in quiescent 3T3-L1 preadipocytes in response to 25 μM AA.	145
Figure 48	Intracellular Ca ²⁺ mobilization in quiescent 3T3-L1 preadipocytes in response to 25 μM AA in the absence of extracellular Ca ²⁺ .	146
Figure 49	Intracellular Ca ²⁺ mobilization in quiescent 3T3-L1 preadipocytes in response to 1 μM TG.	147
Figure 50	Intracellular Ca ²⁺ mobilization in quiescent 3T3-L1 preadipocytes in response to 1 μM PMA.	148
Figure 51	Intracellular Ca ²⁺ mobilization in quiescent 3T3-L1 preadipocytes in response to 25 μM PMA.	149
Figure 52	Effect of NPRC knockdown on intracellular Ca ²⁺ mobilization in quiescent 3T3-L1 preadipocytes in response to 25 μM PMA.	150
Figure 53	Effect of overexpression of an pBINDAHNAK1 construct on intracellular Ca ²⁺ mobilization in quiescent 3T3-L1 preadipocytes in response to 1 μM PMA.	151
Figure 54	Effect of overexpression of an pBINDAHNAK1 construct on intracellular Ca ²⁺ mobilization in quiescent 3T3-L1 preadipocytes in response to 25 μM PMA.	152
Figure 55	Effect of AHNAK1 knockdown on intracellular Ca ²⁺ mobilization in quiescent 3T3-L1 preadipocytes in response to 25 μM PMA.	153
Figure 56	Effect of AHNAK1 knockdown on intracellular Ca ²⁺ mobilization in quiescent day 2 differentiated 3T3-L1 preadipocytes in response to 25 μM PMA.	154
Figure 57	Intracellular Ca ²⁺ mobilization in quiescent 3T3-L1 preadipocytes pretreated with AACOCF3 in response to 25 μM PMA.	155

Figure 58	Intracellular Ca ²⁺ mobilization in quiescent 3T3-L1 preadipocytes in response to 1 μM cANF.	156
Figure 59	Comparisons of various intracellular Ca ²⁺ experiments.	157
Figure 60	Proposed role of NPRC in intracellular Ca ²⁺ mobilization through AHNAK1 and AA.	158
Figure 61	Western blot and densitometric analyses showing the effect of increased [Ca ²⁺] _e on AHNAK1 translocation in 3T3-L1 preadipocytes.	159
Figure 62	Effect of increased [Ca ²⁺] _e on [Ca ²⁺] _i mobilization in 3T3-L1 preadipocytes.	160
Figure 63	Construction of recombinant GST-NPRC.	183
Figure 64	Optimization of expression conditions of GST-NPRC.	184
Figure 65	Coomassie blue stained gel showing the purification of GST-NPRC.	185
Figure 66	Confirmation of the sequence of GST-NPRC.	186
Figure 67	Determination of the molecular weight of GST-NPRC under native PAGE conditions.	187
Figure 68	Spontaneous versus ligand-induced dimerization of GST-NPRC.	188
Figure 69	Predicted secondary structure for GST-NPRC.	189
Figure 70	Phosphorylation consensus sequences within the intracellular domain of rat NPRC.	190
Figure 71	In vitro phosphorylation of GST-NPRC.	191
Figure 72	Identification of putative residues and kinases involved in NPRC phosphorylation.	192
Figure 73	Schematic of the junctional complex of epithelial cells.	202
Figure 74	Colocalization of AHNAK1 and ZO-2 proteins in confluent RGM1 cells.	203
Figure 75	Subcellular localization of AHNAK1 in RGM1 cells.	204
Figure 76	Schematic illustrating the various sections of the stomach.	205

Figure 77	Histochemical analysis of representative tissue sections from healthy human organ stomach donors.	206
Figure 78	Western blot analysis of endogenous AHNAK1, NPRA, and NPRC protein expression in healthy human stomach.	207
Figure 79	Immunohistochemistry analysis of endogenous AHNAK1 in healthy human stomach.	208
Figure 80	Knockdown of AHNAK1 protein in RGM1 cells.	209
Figure 81	In vitro permeability assay demonstrating the role of AHNAK1 in maintaining paracellular cellular permeability and the barrier properties of RGM1 cells.	210

List of Abbreviations

7MSRs	seven membrane spanning receptors
AA	arachidonic acid
AJ	adherens junctions
AngII	angiotensin II
ANP	atrial natriuretic peptide
AoSMC	Aortic Vascular Smooth Muscle Cell
BNP	B-type natriuretic peptide
BCA	bicinchoninic acid
BSA	bovine serum albumin
cPLA ₂	cytosolic Ca ²⁺ dependent phospholipase A ₂
CASM	coronary artery smooth muscle cells
CD	circular dichroism
CNP	C-type natriuretic peptide
cAMP	cyclic adenosine monophosphate
cANF/cANP	ANP analog des-[Glu ¹⁸ Ser ¹⁹ Gly ²⁰ Leu ²¹ Gly ²²]-ANF-(4-23)-NH ₂
CYP	cytochrome P450 monooxygenase
DAG	diacylglycerol
DAPI	4',6-diamidino-2-phenylindole
DDA	dideoxyadenosine
DIC	differential interference contrast
DMEM	Dulbecco's modified Eagle's medium

DMSO	dimethyl sulfoxide
DNP	dendroaspis natriuretic peptide
DTT	dithiothreitol
EC	endothelial cell
ECD	extracellular domain
EDTA	ethylenediaminetetraacetic acid
EET	epoxyeicosatrienoic acids
EGF	epidermal growth factor
ET-1	Endothelin-1
FABP	Fatty acid binding protein
FBS	fetal bovine serum
FSK	forskolin
FITC	fluorescein isothiocyanate
FGF	Fibroblast growth factor
GAPDH	glyceraldehyde-3-phosphate dehydrogenase
GAPs	GTPase activating proteins
GDI	Guanosine nucleotide dissociation inhibitors
GDP	guanosine diphosphate
GEFs	guanine nucleotide exchange factors
Gi	inhibitory guanine nucleotide regulatory protein
GPCR	G protein-coupled receptors
GRKs	G protein-coupled receptor kinases
Gs	stimulatory guanine nucleotide regulatory proteins
GST	Glutathione <i>S</i> -transferase
GTP	guanosine-5'-triphosphate

GUK	guanylate kinase
HBSS	Hanks' balanced salt solution
HRP	horseradish peroxidase
IB	inclusion body
IBMX	3-isobutyl-1-methylxanthine
I _{Ca,L}	L-type Ca ²⁺ current
ICD	intracellular domain
IF	intermediate filament
IGF-1	insulin-like growth factor 1
IHD	ischemic heart disease
IHC	immunohistochemistry
Ig	immunoglobulin
IL-6	interleukin 6
IMAC	immobilized metal affinity chromatography
IP	Immunoprecipitation
IP ₃	inositol (1,4,5)-triphosphate
iPLA ₂	cytosolic Ca ²⁺ independent phospholipase A ₂
IPTG	isopropyl β-D-1-thiogalactopyranoside
JAM	junctional adhesion molecule
kDa	kilodalton
KP	kaliuretic peptide
LANP	long-acting natriuretic peptide
LT	leukotrienes
MBP	maltose binding protein
mAb	monoclonal antibody
MAGUK	membrane associated guanylate kinase

MBP	maltose binding protein
MEF	Mouse embryonic fibroblast
mGluRs	metabotropic glutamate receptors
MS	mass spectrometry
MPER	mammalian protein extraction reagent
MWM	molecular weight marker
NCBI	National Center for Biotechnology Information
NP	natriuretic peptide
NEP	neutral endopeptidase 24.11
NPRA	natriuretic peptide receptor A
NPRB	natriuretic peptide receptor B
NPRC	natriuretic peptide receptor C
NSAID	non-steroidal anti-inflammatory drug
pAb	polyclonal antibody
PEG	polyethylene glycol
PBS	phosphate buffered saline
PDGF	platelet-derived growth factor
PGE2	prostaglandin E2
PI	Phosphatidylinositol
PIP ₂	phosphatidylinositol 4,5-bisphosphate
PKA	cAMP-dependent protein kinase
PKB	protein kinase B
PKC	protein kinase C
PHD	Pleckstrin homology domain
PHLPP	PH domain leucine-rich repeat protein phosphatase

PLC	phospholipase C
PMSF	phenylmethylsulphonyl fluoride
PPAR	peroxisome proliferator-activated receptors
Pref-1	preadipocyte factor-1
PG	prostaglandin
RACKs	receptors for activated C-kinase
RGM1	rat gastric mucosa
SDS-PAGE	sodium dodecyl sulfate polyacrylamide gel electrophoresis
SH3	Src homology 3
siRNA	small interfering RNA
SMC	smooth muscle cell
smMLCK	smooth muscle myosin light chain kinase
SOC	store-operated calcium
sPLA ₂	secretory phospholipase A ₂
TBS	tris-buffered saline
TG	thapsigargin
TJ	tight junction
TGF	transforming growth factor
TMD	transmembrane domain
TNF- α	tumor necrosis factor α
Trx	thioredoxin
VD	vessel dilator
VEGF	vascular endothelial growth factor
WB	western blot
ZO	zonula occludens

Characterization of NPRC and Its Binding Partners

Abdel A. Alli

ABSTRACT

The C type natriuretic peptide receptor (NPRC), also known as NPR3 is a widely expressed single transmembrane-spanning protein. NPRC functions as a homodimer at the cell surface for the metabolic clearance of a broad range of natriuretic peptides from circulation. The intracellular domain of NPRC is coupled to inhibitory G proteins and is involved in mediating signal transduction. In order to further elucidate the role of NPRC in signal transduction, a proteomic approach was taken to identify putative protein binding partners for NPRC in different cell-types. An interrogation of the molecular association between NPRC and its identified protein binding partner(s) was carried out in different cell types to identify the specific interacting domains. The physiological role of the association between NPRC and its protein binding partner(s) were investigated *in situ*. Furthermore, NPRC is subject to post translation modifications, including glycosylation and phosphorylation. Although evidence suggests NPRC is phosphorylated on serine residues, the specific amino acid residues that are phosphorylated and the kinases responsible for their phosphorylation has yet to be determined. A recombinant GST-NPRC fusion protein, polyclonal NPRC antibody, kinase prediction algorithm, and several phosphospecific and substrate motif antibodies were utilized to characterize the phosphorylation state of NPRC *in vitro*.

Introduction

Natriuretic Peptides

Natriuretic peptides (NPs) are a family of hormones, which include atrial natriuretic peptide (ANP), B-type natriuretic peptide (BNP), C-type natriuretic peptide (CNP), dendroaspis natriuretic peptide (DNP), and urodilatin [1, 2]. ANP, BNP, CNP, and DNP each contain a conserved 17-amino acid ring structure (Figure 1). Upon secretion, proANP (amino acids 1-126) is cleaved by the serine protease corin [3] into an N-terminus fragment (amino acids 1-98) and a C-terminus fragment (amino acids 99-126) in equimolar amounts [4]. Long-acting natriuretic peptide (LANP) (amino acids 1-30), vessel dilator (VDL) (amino acids 31–67), and kaliuretic peptide (KP) (amino acids 79–98) originate from the N-terminus, while ANP (amino acids 99–126) originates from the C-terminus of the prohormone [5, 6]. Upon secretion proBNP (amino acids 1-108) is cleaved by furin [7], into an N-terminus fragment (amino acids 1-76) and a C-terminus fragment (amino acids 77-108) [7]. A paradigm for the synthesis and processing of ANP [5] and BNP [8] is shown in Figure 2.

Although they are also produced in other tissues, ANP is primarily secreted by atrial myocytes, while BNP is secreted by both the atria and ventricles of the heart [9, 10]. ANP is released from the secretory granules in response to an increase in wall stretch and/or pressure [11], or in response to various factors including catecholamines, glucocorticoids, angiotensin II, and endothelin [12]. For example, endothelin-1 (ET-1) was shown to induce ANP secretion in ventricular cardiomyocytes through an

intracellular signaling pathway mediated by the ET_A receptor involving the production of cAMP and the activation of an nifedipine-sensitive calcium channel [13]. Rebsamen *et al.* also demonstrated that the mechanism in which ET-1 induced ANP secretion involved calcium influx instead of calcium release from intracellular stores [13].

ANP and BNP play an important physiological role in promoting natriuresis and diuresis, inhibiting renin and aldosterone release, and directly influence blood pressure and body fluid homeostasis [14-16]. NPs have been shown to inhibit adenylyl cyclase and decrease cAMP levels in various tissues [17], suppress vascular smooth muscle cell growth [18], inhibit DNA synthesis in cardiac fibroblasts [19], and inhibit cell proliferation in several different cell types through the generation of cyclic guanosine monophosphate (cGMP) [20-23]. NPs have been shown to induce apoptosis in cardiac myocytes [24] and in endothelial cells (EC) [25]. NPs were shown to affect the electrophysiology of the heart [26, 27] and central nervous system [28, 29], and muscle relaxation in the gastrointestinal system [30, 31].

CNP, which lacks the carboxyl-terminal tail, is not known to be natriuretic, although it does possess vasorelaxant activity [32, 33]. CNP complements the endocrine actions of ANP and BNP to lower blood volume and pressure, and has a paracrine role in the regulation of vascular tone [33]. CNP is abundantly produced in the vascular endothelium, and because it does not circulate in large amounts as does ANP and BNP, it is thought to function locally in an autocrine/paracrine way [33]. CNP induces vasodilatation through activation of the B type natriuretic peptide receptor (NPRB) or the C type natriuretic peptide receptor (NPRC) and hyperpolarization of vascular smooth muscle [34]. Evidence has shown that the responses of CNP mediated through NPRB

result in stimulation of EC, but attenuation of smooth muscle cells [35, 36]. CNP has been shown to be an important regulator of endochondral ossification and a major phenotype of CNP-deficient mice is dwarfism, as demonstrated by shortened long bones [37, 38]. Several groups have demonstrated that CNP stimulates bone growth primarily through increased proliferation, mineralization, and extracellular matrix synthesis [37, 39, 40]. Also, Agoston *et al.* demonstrated the ability of CNP to stimulate endochondral bone growth through expansion of the hypertrophic zone of the growth plate [41]. NPs are efficiently removed from the circulation by binding to natriuretic peptide clearance receptor NPRC [42] or by hydrolysis by the enzyme neprilysin or neutral endopeptidase (NEP) [43].

Several distinct phenotypes have been observed for various NPs or NPRs using mouse models, as indicated in Table 1. The overexpression of ANP [44] or NPRA [45] induces a dose-dependent decrease in arterial blood pressure. The deletion of ANP [46] or NPRA [47, 48] in mice leads to cardiac hypertrophy and sudden death. The deletion of CNP or NPRB in mice leads to severe dwarfism [37], while deletion of NPRC results in skeletal overgrowth [49].

Plasma concentrations of ANP and BNP may be considered useful biomarkers of cardiac function [50, 51], since their concentrations increase in response to volume and pressure overload of the heart [11, 52-56]. Accordingly, ANP and BNP secretion is significantly elevated during cardiac failure and their plasma concentrations are proportional to the severity of the condition [52-56]. Resistance to the natural effects of NPs occurs in cardiac failure, especially in patients with the most advanced disease, but short-term infusions in patients have beneficial effects [57, 58].

NPs are also capable of regulating various digestive functions. Sabbatini *et al.* showed ANP and CNP play a role in stimulating pancreatic fluid and protein secretion in a dose-dependent manner when administered intravenously in rats [59]. The activation of NPRC was shown to mediate specific effects of ANP and CNP in the digestive system. CNP was shown to increase amylase secretion in response to NPRC activation and subsequent stimulation of phospholipase C (PLC) in pancreatic acinar cells [60]. At low doses, ANP was found to stimulate bicarbonate, decrease chloride output, and enhance secretin-induced pancreatic secretion in pancreatic duct cells [61]. At high doses, ANP was found to decrease secretin-induced pancreatic secretion through inhibition of adenylyl cyclase activity [61]. ANP and CNP were shown to inhibit spontaneous and sodium dehydrocholate induced bile secretion upon administration into rats [62]. Moreover, ANP was shown to play a role in the regulation of gastric acid secretion through a vagal pathway and also through a paracrine/autocrine pathway [63]. ANP was found to increase gastric acid secretion in rats through a vagal-dependent mechanism when administered into rat's intracerebroventricularly [64]. However, ANP demonstrated a biphasic effect when administered into rats intravenously, as low doses of ANP enhances vagally stimulated gastric secretion and high doses of ANP decreases vagally stimulated gastric secretion [65]. Also, a feedback mechanism has been suggested between ANP and somatostatin. In rat antrum and fundus, ANP was found to stimulates somatostatin secretion through the activation of NPRA, while somatostatin inhibits ANP secretion [66, 67].

Natriuretic Peptide Receptors

One class of natriuretic peptide receptors (NPRs) constitutes the guanylyl cyclase-coupled receptors NPRA and NPRB [68-75]. NPRA preferentially binds ANP and BNP (ANP>BNP>>CNP), while NPRB is more selective for CNP (CNP>>ANP>BNP) [76-78]. The topology of NPRA and NPRB include a large extracellular domain (ECD), a single transmembrane domain (TMD), and an intracellular domain (ICD) consisting of kinase-homology regulatory domain (KHD), and a guanylyl cyclase domain (GCD) [79] (Figure 3). At the basal state, the KHD interacts with the GCD to suppress its activity and upon ligand binding guanylyl cyclase activity is elevated, resulting in the conversion of guanosine triphosphate (GTP) to cGMP [79]. Various desensitizing agents and conditions have been reported to inhibit the guanylyl cyclase-coupled receptors by decreasing their phosphorylation state [80], as phosphorylation is required for their activation [81].

The other class of NPRs constitutes the non-guanylyl cyclase-coupled receptor NPRC. The topology of NPRC consists of a large ECD of ~440 amino acids, a single TMD, and a short 37 amino acid ICD [82]. NPRC exists as monomers and disulfide-linked homodimers with a relative molecular mass of approximately 66 kDa and 130 kDa, respectively [82]. Structural analysis of NPRC by truncation and site-directed mutagenesis studies, followed by binding assays provided evidence that the monomeric form of NPRC is capable of binding NPs with high affinity [83]. Two isoforms, of 67 and 77 kDa, have been identified and both have been reported to form disulfide-linked homodimers and have high affinities for ANP and the NPRC selective agonist, ANP

analog des-[Glu¹⁸Ser¹⁹Gly²⁰Leu²¹Gly²²]-ANF-(4-23)-NH₂ (cANF) [84]. The location of the genes coding for the NPRs is described in Table 3.

NPRC is the most promiscuous of the NPRs and the stoichiometry of the ligand-receptor complex is 1:2 [85]. NPRC has much broader specificity and also binds small peptide analogs [86]. NPRC is widely expressed in a wide range of cells and tissues and represents the majority of the population of NPRs *in vivo* [82]. NPRC protein expression has been reported in human breast adenocarcinoma cells [87], human pancreatic adenocarcinoma cells [88], human renal carcinoma cells [89], human prostate carcinoma cells [90], human medullary thyroid carcinoma cells [91], human glioblastoma cells [92], human colon adenocarcinoma cells [93], human melanoma cells [94], human ovarian adenocarcinoma (HTB-161) cells, human angiosarcoma cells [95], human small cell lung carcinoma (SHP77) cells [96, 97], rat A-10 VSMCs [98], normal rat gastric mucosa (RGM1) cells [99], rat aortic smooth muscle (RASM) cells [99], pancreatic alpha cells [100], human aortic smooth muscle cells (AoSMCs) [99], mouse 3T3-L1 preadipocytes and adipocytes [99]. A summary of the expression profile for the NPRs in various cell lines is shown in Table 2.

The primary function of NPRC is the metabolic clearance of NPs from circulation [82]. Upon ligand binding, the NPRC-ligand complex undergoes endocytosis via clathrin-coated pits, which is thought to be dependent on the integrity of the cytoplasmic domain of NPRC [101]. The complex then dissociates intracellularly in endosomes, followed by hydrolysis of ligand in lysosomes and rapid recycling of receptor back to the cell surface [102]. NPRC locally modulates the physiological effects of the NP system by regulating the availability of NPs at their target organs [49]. Another mechanism for

the metabolic clearance of NPs from circulation is mediated by NEP. Several groups have investigated effects of simultaneously blocking each or both the NPRC and NEP NP degradative pathways in normal animals. Rademaker *et al.* [103], Chiu *et al.* [104], and Kukkonen *et al.* [105] reported the NPRC and NEP systems have an additive effect for the clearance of NPs from circulation. Charles, C *et al.* [106] and Wegner *et al.* [107] demonstrated the NPRC and NEP systems can work in concert or synergistically to modulate the clearance of NPs from circulation.

The extracellular ligand binding domain of NPRC contains several glycosylation sites [108]. The crystal structures of NPRC bound and unbound to ligand suggest glycosylation plays a role in the structural stabilization of the receptor and an indirect role in binding activity [109].

NPRC expression has been demonstrated to be affected under various conditions and by a variety of factors. Sarzani *et al.* demonstrated fasting inhibits natriuretic peptides clearance receptor expression in rat adipose tissue [110]. Chabrier *et al.* reported a decrease in NPR density in response to angiotensin II (Ang II) in rat vascular smooth muscle cells (VSMCs) [111]. Similarly, Yasimoto *et al.* showed Ang II treatment decreased NPRC mRNA levels in cultured rat aortic smooth muscle cells, while NPRA and NPRB were not affected [112]. Boumati *et al.* showed endothelin (ET-1) treatment attenuated NPRC protein expression in A-10 SMCs [113]. Kishimoto *et al.* demonstrated that norepinephrine or isoproterenol downregulates NPRC density mediated by the activation of the β -adrenergic receptor, as the effect was blocked only by a β -selective adrenergic antagonist and not by α 1 or α 2 or β 1 adrenergic antagonists in rat VSMCs [114]. Agui *et al.* demonstrated the differential regulation of NPR in response to

transforming growth factor- β 1 (TGF- β 1) treatment of murine thymic stromal cells, as NPRC expression was augmented and NPRA and NPRB expression was attenuated [115]. However, Sun *et al.* found that platelet-derived growth factor BB (PDGF-BB) and fibroblast growth factor (FGF-1 and FGF-2) treatments downregulated NPRC mRNA in pulmonary arterial smooth muscle cells [116]. Itoh *et al.* showed dehydration causes decrease in NPRA, NPRB, and NPRC mRNA expression in rat glomeruli, as the effect was proposed to be attributed to a lower circulating levels of ANP [117]. Ardaillou *et al.* demonstrated glucocorticoids upregulate NPRC protein expression in cultured human mesangial cells [118]. Lu *et al.* reported vasonatin peptide can decrease the expression of NPRC in cardiac fibroblasts and myocytes under both air-control and hypoxic condition, and the effect is mediated by an increase in intracellular cGMP [119]. Several groups have demonstrated NPRC expression is regulated by ANP itself. Hirata *et al.* reported downregulation of ANP receptors in VSMCs in response to ANP exposure [120]. Arejian *et al.* showed nitric oxide attenuates the expression of natriuretic peptide receptor C in rat aortic vascular smooth muscle cells [121]. Gower *et al.* showed prostaglandin E(2) (PGE(2)) and transforming growth factor (TGF) can decrease NPRC mRNA and protein expression in RGM1 cells [122]. Multiple groups have shown that acute and chronic hypoxia cause the downregulation of NPRC gene expression and binding in rat lung without affecting other NPRs [123-125]. Sun *et al.* demonstrated that NPRC mRNA expression is downregulated in the lungs of hypoxia-adapted mice [125] and rats [124] in response to increased circulating levels of ANP, while NPRA and NPRB mRNA levels were not affected. This group later demonstrated that dietary salt supplementation is able to downregulate NPRC mRNA levels in the kidneys of wild-type

mice and mice with insertion inactivation of the ANP gene independently of endogenous ANP levels, but had no effect on NPRA or NPRB mRNA levels [126]. These findings were consistent with findings from Nagase *et al.* who demonstrated that NPRC gene expression was selectively attenuated in the kidney by chronic salt loading in Dahl salt-sensitive and salt-resistant rats, whereas expression of NPRA and NPRB expression was not affected [127].

The regulation of NPRC in disease has also been documented. Luk *et al.* showed NPRC is downregulated in chronic renal failure rat glomeruli, and is the result of ANF-stimulated cGMP responses [128]. Yoshimoto *et al.* demonstrated NPRC mRNA expression is downregulated in the aorta from stroke prone spontaneously hypertensive rats, while NPRA mRNA expression was upregulated [112]. Similarly, NPRC mRNA expression was found to be downregulated in the aorta [129], as well as in the lung, renal cortex of DOCA-salt hypertensive rats, while ANP levels were elevated [124].

NPRC is an atypical G protein coupled receptor (GPCR), because it lacks the seven transmembrane spanning domains that is a hallmark of traditional serpentine or heptahelical GPCRs [130]. NPRC is coupled to the inhibitory G protein, G_i [31, 82]. NPRC was shown to be negatively coupled to adenylyl cyclase in cultured atrial and ventricular cardiocytes [131-133]. The cytoplasmic domain of rat NPRC was shown to contain G_i activator sequences that inhibit adenylyl cyclase activity [134, 135]. NPRC is coupled to adenylyl cyclase inhibition via α subunits [134] and PLC- β_3 activation via $\beta\gamma$ subunits of G_{i1} and G_{i2} [31]. The ability of NPRC to inhibit adenylyl cyclase has been suggested to contribute to the attenuation of PGE₂-production of lipopolysaccharide-activated macrophages and reduces COX-2-protein and -mRNA levels [136], astrocyte

proliferation [137], and production and release of endothelin from EC [138]. Johnson *et al.* and Kanwal *et al.* demonstrated NPRC mediates inhibition of adenylyl cyclase and neurotransmission through cANF in nerve growth factor-treated PC12 cells [139, 140].

Mouawad *et al.* has shown a possible cross-talk that may exist between the adenylyl cyclase pathway and the PLC pathway in A-10 VSMCs, as the NPRC induced inhibition of adenylyl cyclase and decreased levels of cAMP contributes to NPRC mediated stimulation of PI turnover [141]. They also showed that the cANF (4-23) induced increase in IP₃ production was further increased by the cAMP inhibitor dideoxyadenosine (DDA) and was inhibited by the cAMP inducing agent forskolin (FSK) [141].

NPRC has also been implicated in the modulation of other signaling pathways. Murthy *et al.* has shown NPRC activation by cANF(4-23) can result in the activation of constitutive nitric oxide synthase (NOS) via G_{ia1} and G_{ia2} in gastrointestinal smooth muscle [30]. Prins *et al.* has demonstrated cANF (4-23) can inhibit platelet-derived growth factor (PDGF) and endothelin-3 stimulated mitogen-activated protein kinase (MAPK) activity in astrocytes [142]. Furthermore, NPRC binding to CNP or cANF has been shown to inhibit L-type Ca²⁺ current (I_{Ca,L}) without modulating other voltage-gated Ca²⁺ currents in mouse atrial, ventricular, and sinoatrial node myocytes [26, 143].

The coupling of NPRC to various signaling pathways has provided a mechanism for additional roles of NPRC. For example, several reports have shown NPRC mediates ANP-inhibition of vascular smooth muscle cell proliferation [144] and endothelial cell proliferation [145]. In another report, NPRC was found to mediate cANF induced antiproliferative effects in multiple different neuroblastoma cell lines [146]. Also, the

cAMP inhibition mediated by NPRC has been shown to modulate endothelial cell permeability in coronary EC [147]. NPRC was suggested to be implicated in vascular remodeling and angiogenesis, as cANF was found to inhibit ET and hypoxia-stimulated vascular endothelial cell growth factor (VEGF) transcription and production in VSMCs [148].

The complete absence of NPRC in mice by homologous recombination results in skeletal abnormalities, characterized by hunched backs, dome-shaped skulls, decreased weight, and elongated femurs, tibiae, metatarsals, digital bones, vertebral bodies, and body length [149]. Jaubert *et al.* reported that three mutations involve the *Npr3* gene encoding for NPRC, as well as an NPRC knockout results in a mouse skeletal-overgrowth phenotype, thus implicating a role for NPs in bone growth [149]. The three mutations reported to be within the extracellular domain of NPRC included an *lgj*^{2J} allele displaying a C to T transition at position 283, resulting in a stop codon; a *stri* allele showing a C to A transversion at position 502, leading to an asparagine to histidine substitution; an *lgj* allele exhibiting an in-frame 36-bp deletion between position 195 and 232, causing a truncated protein by 12 amino acids [149].

β -arrestins

The arrestin family consists of cone arrestin [150], visual arrestin [151], β arrestin 1 [152], and β arrestin 2 [153]. Cone arrestin and visual arrestin are almost exclusively expressed in the retina and regulate photoreceptor function, whereas the β -arrestins are virtually ubiquitously expressed and regulate most GPCRs, or seven membrane spanning

receptors (7MSRs) [154-157]. The β -arrestins bind to agonist-activated cell surface GPCRs phosphorylated by G protein-coupled receptor kinases (GRKs) and mediate their homologous desensitization and internalization [158, 159]. The GRK family consists of seven different genes and the seven GRK members are divided into three subfamilies [160]. The first subfamily of GRKs consist of GRK1 and -7, the second subfamily of GRKs consist of the pleckstrin homology domain-containing GRK2 and -3, and the third subfamily of GRKs consist of constitutively membrane bound GRK4, -5, and -6 [161]. Upon GPCR stimulation and activation by agonist, GRKs phosphorylate GPCRs on serine and threonine residues within the carboxyl-terminal tail and/or the third cytoplasmic loop [130, 162-165]. GPCR phosphorylation by GRKs significantly enhances the affinity of the receptor for arrestins, but it is the binding of the β -arrestins to the GPCR that leads to the actual homologous desensitization [154, 166, 167]. In contrast to homologous desensitization mediated by GRK phosphorylation and β -arrestin binding, heterologous desensitization of GPCRs is not dependent on agonist occupancy and instead is mediated by phosphorylation within the cytoplasmic loops and C-terminal tail domains of GPCRs by second-messenger-dependent protein kinases, including protein kinase A and protein kinase C [168].

In addition to their role in desensitization of GPCRs, β arrestins act as adapter proteins to target GPCRs to clathrin-coated pits for endocytosis [154]. The ability of β -arrestins to function as adapter proteins to target GPCRs to components of the clathrin-dependent endocytic machinery is attributed to two motifs within the β -arrestins. The first motif involves the binding of an LIEF sequence located between residues 374 and 377 of β -arrestin 2 [169], to a region between amino acid residues 89 and 100 of the N

terminal domain of the clathrin heavy chain. The other motif involves the binding of β -arrestins to the β 2 adaptin subunit of the heterotetrameric AP-2 adaptor complex through an RxR sequence located between amino acid residues 394 to 396 of β -arrestin 2 [170]. The endocytic function of β -arrestin 1 and 2 are differentially regulated. The endocytic function of β -arrestin 1 is mediated by ERK1 and ERK2 phosphorylation [171], while the endocytic function of β -arrestin 2 is mediated by ubiquitination catalyzed by the E3 ubiquitin ligase Mdm2 in response to agonist binding of the GPCR [172]. The deubiquitinating enzyme ubiquitin-specific protease 33 (USP33) was found to bind to beta-arrestins, resulting in deubiquitination of beta-arrestins [173]. The USP33 and Mdm2 function reciprocally and allow for beta-arrestin complex stability or lability, respectively [173]. This process of sequestration contributes to the attenuation of GPCR signaling and resensitization and downregulation of the GPCR [154]. Receptor downregulation involves a decrease in the density of cell surface receptors and is a slow process that occurs over a period of hours to days [154, 157]. In contrast, receptor desensitization involves a temporary loss of receptor responsiveness to agonist and is a rapid process that begins within seconds of agonist binding [154, 157]. Receptor resensitization requires dephosphorylation of the receptor and the dissociation of the ligand [154]. Multiple studies support the requirement for receptor internalization for resensitization of many GPCRs [174, 175].

Furthermore, the β -arrestins can confer enzymatic activities upon GPCRs by binding directly to signal transduction associated proteins including Src family kinases and components of the MAP kinase and ERK1/2 signaling cascades [154]. The binding of β -arrestin to Src is mediated by interaction between the proline-rich PXXP motifs of

amino acid residues 88-91 and 121-124 of the N terminal domain of β -arrestin 1 and the Src homology (SH) 3 domain of the kinase [154]. One role of the β -arrestin-Src complex is to modulate GPCR endocytosis. The three major classes of MAP kinases of mammalian cells include the ERKs, which play a role in the control of the G0-G1 cell cycle, and the JNKs and p38/HOG1, which play a role in the regulation of growth arrest and apoptosis [154]. Activated MAP kinases phosphorylate various cytoplasmic, membrane, and nuclear substrates. The ability of β -arrestins to serve as scaffolds for MAP kinases allows for the targeting of MAP kinases to specific subcellular locations, increased signaling efficiency, and the dampening of cross talk between MAP kinase cascades [154]. Accordingly, the β -arrestins have significant implications for cellular processes such as chemotaxis and apoptosis [176].

G proteins

Guanine nucleotide regulatory proteins (G-proteins) are a family of GTP-binding proteins that are involved in second messenger signaling cascades [177]. G proteins may refer to two different families of proteins, the Ras subfamily of small GTPases (small G-proteins) and the heterotrimeric G-proteins (large G-proteins). Small GTPases are homologous to the α subunit of heterotrimeric G-proteins [178]. The G-protein is active when bound to GTP and inactive when bound to GDP. The cognate G-protein is activated upon activation of guanine nucleotide exchange factors (GEFs) [179-183], and inactivated upon activation of GTPase activating proteins (GAPs) [184-188]. Guanosine nucleotide dissociation inhibitors (GDI) [189] keep small GTPases in the inactive state. Heterotrimeric G-proteins consist of α , β , and γ subunits [190-194]. There are three

distinct forms of $G\alpha_i$ from different genes, and four forms of $G\alpha_s$ from splicing of a single gene [194]. In the resting state, $G\alpha$ is bound to GDP and associates with $G\beta\gamma$ [192]. The GDP bound heterotrimer is coupled to surface receptors, which increases the receptors affinity for ligand [192]. Upon ligand binding, the activated receptor acts as a guanine nucleotide exchange factor by activating the heterotrimer and increasing the rate of GDP to GTP exchange on $G\alpha$ [192]. The exchange triggers dissociation of $G\alpha$ from $G\beta\gamma$ and the receptor [192]. $G\alpha$ GTP and $G\beta\gamma$ then activate different signaling pathways and effector proteins including adenylyl cyclase [195-197] and PLC [195, 198-200]. Upon disassociation between ligand and receptor, intrinsic GTPase activity of $G\alpha$ hydrolyzes the GTP to GDP and the inactive GDP bound $G\alpha$ associates with $G\beta\gamma$ to begin a new cycle.

Bacterial toxins are useful tools for identifying and investigating the role of G proteins. Pertussis toxin and cholera toxin are known to covalently modify the α subunits of G proteins by ADP-ribosylating specific amino acid residues [201]. Pertussis toxin attenuates the effect of G_i [202, 203], while cholera toxin irreversibly activates the G_s protein resulting in stimulation of adenylyl cyclase [202, 204]. The role of various G proteins in mediating adenylyl cyclase and phospholipase C signal transduction is shown in Figure 4.

Adenylyl cyclase

There are at least nine isoforms of membrane associated adenylyl cyclase (AC) and one isoform of soluble AC [205] that currently exist, and each is characterized by distinct biochemical properties and tissue distribution. The AC isoforms are subdivided

into five distinct families based on their amino acid sequence similarity and functional characteristics [205-207]. The Ca^{2+} CaM-sensitive forms include AC1, AC3, and AC8 [205-207]. The $\text{G}\beta\gamma$ stimulatory forms include AC2, AC4, and AC7 [205-207]. The Ca^{2+} and $\text{G}\alpha_i$ sensitive isoforms include AC5 and AC6 [205-207]. The most divergent membrane bound AC isoform is AC9 and is highly insensitive to the diterpene forskolin [205-207]. The overall most divergent AC isoform is the soluble AC isoform and it maintains similarities to the cyclases found in cyanobacteria [205]. The ACs hydrolyzes ATP to produce pyrophosphate and the second messenger cyclic AMP (cAMP) [206, 207](Figure 5). Elevated levels of pyrophosphate can force AC into a product-bound conformation and inhibit the activity of AC [206, 207]. AC consists of six transmembrane segments and two catalytic domains that extend into the cytoplasm [206, 207]. With the exception of the soluble AC isoform, all other AC isoforms are inhibited by adenosine analogs, or P-site inhibitors [208]. P-site inhibitors inhibit AC activity without competing with ATP binding [208], but instead by binding to a conformation of the enzyme that closely resembles the product bound state, or posttransition state [209]. While all membrane bound AC isoforms are expressed in excitable tissues, such as neurons and muscle, AC1 and AC3 are expressed exclusively in the brain [210] and the soluble form of AC is ubiquitously expressed with high levels in sperm cells [211]. Each AC isoform is activated by alpha subunits of G proteins and some have been found to be activated by various other molecules including forskolin. Non-physiological concentrations of Ca^{2+} in the mM range inhibit all AC isoforms, but AC5 and AC6 are inhibited by concentrations of Ca^{2+} in the μM range from capacitative entry [212] epinephrine, glucagon, prostaglandin, prostaglandin E2 (PGE2), adenosine are known to

activate AC through membrane-bound receptors. Unlike the membrane bound AC isoforms, the soluble AC isoform is unresponsive to hormones, G proteins, and forskolin and its biochemical activity is dependent on the divalent cation Mn^{2+} [211]. Furthermore, the soluble AC isoform displays approximately a 10-fold lower affinity for substrate [213] than the membrane associated AC isoforms [214]. The intracellular domain of G protein coupled receptors interact with the GDP bound heterotrimeric G proteins, resulting in the displacement of bound GDP by GTP and the dissociation of the GTP bound G α subunit and the G $\beta\gamma$ dimer [206, 207]. The GTP bound $G\alpha_s$ family stimulates AC, while the GTP-bound $G\alpha_i$ family inhibits AC [206, 207].

AHNAK1/Desmoyokin

AHNAK, meaning giant in Hebrew or also referred to as Desmoyokin [215] is a large phosphoprotein of approximately 700 kDa [216]. A second AHNAK1-like protein located on chromosome 14q32, AHNAK2, has been identified [217]. The amino terminal domain of AHNAK2 is predicted to contain a PDZ domain [217]. AHNAK1 is encoded by a single exon located on human chromosome 11q12 [218]. AHNAK1 is composed of three distinct structural domains: a short amino terminus domain of 251 amino acids, a large central domain of 4,392 amino acids characterized by 39 highly conserved repeating units each of 126 amino acids, and a large carboxy terminus domain of 1000 amino acids [216].

AHNAK1 expression increases in the G₀ stage of the cell cycle, as quiescent cells contain higher levels of AHNAK1 protein. Among various human cell lines, Shtivelman *et al.* reported AHNAK1 downregulation in neuroblastoma cells, Burkitt lymphomas, and

small cell lung carcinomas [216]. Gentil *et al.* observed AHNAK1 is widely expressed in smooth muscle cells, skeletal muscle, myoepithelium, and myofibroblasts [219]. However, Gentil *et al.* did not observe significant AHNAK1 staining in cells having secretory functions such as the glandular epithelium of the mammary gland, the salivary gland, the stomach, the prostate, or the exocrine and endocrine pancreas [219]. Kingsley *et al.* reported AHNAK1 expression in extraembryonic tissue, mesenchymal cells of the branchial artery, and nasal epithelia and skin [220]. Salim *et al.* found AHNAK1 expression in developing and adult rat peripheral nervous system [221]. AHNAK1 expression was found in small and medium-sized neurons and satellite cells of dorsal root ganglia and Schwann cells [221]. Matza *et al.* found strong AHNAK1 expression in CD4⁺ T cells and less expression in thymocytes [222].

The carboxy terminal domain of AHNAK1 was found to contain nuclear localization sequences and a nuclear export signal [223]. The subcellular localization of AHNAK1 is cell type dependent, as AHNAK1 has been described to be restricted predominantly to cell nuclei and Golgi apparatuses of nonepithelial cells and cytoplasmic or plasma membrane-associated in epithelial cells [216] or upon PKC activation or increase in extracellular calcium [224]. Sussman *et al.* reported phosphorylation of AHNAK1 by PKB contributes its nuclear exclusion in epithelial cells, and that AHNAK1 translocates from the cytosol to the cytosolic side of the plasma membrane during the formation of cell-cell contact and epithelial polarity development [225]. Benaud *et al.* reported that the translocation is regulated by Ca²⁺ dependent cell-cell adhesion and is a reversible process [226]. Hashimoto *et al.* reported AHNAK1 translocates from the cytosol to the plasma membrane in response to increased extracellular calcium in

keratinocytes [224]. AHNAK1 demonstrated a predominantly nuclear distribution in low calcium medium and both a nuclear and cytoplasmic distribution in normal calcium medium [224].

AHNAK1 has been implicated in several different cell type specific functions including neuroblast differentiation [216], tumorigenesis [227], epidermal cell adhesion [228], Ca^{2+} homeostasis regulation [229], regulated exocytosis [230], skeletal muscle regeneration [231], regulation of cell membrane cytoarchitecture [226], maintaining blood brain barrier properties [232], regulation of L-type calcium channels [233, 234], modulation of DNA ligase IV-mediated double-stranded ligation [235], T cell calcium signaling [222, 236], and activation of phospholipase C γ 1 in the presence of Tau or arachidonic acid (AA) [237-239]. Matza *et al.* proposed AHNAK1 helps regulate membrane localization of L-type calcium channels during T cell activation [236]. Benaud *et al.* showed down-regulation of AHNAK1 affects the cell membrane cytoarchitecture of epithelial cells [226]. In addition, AHNAK1 was found to be widely distributed in EC with blood-brain barrier properties and was found to co-localize to the TG protein ZO-1 [232]. These findings suggest a role for AHNAK1 in the regulation of cell adhesion and permeability. Since paracellular permeability and intramembrane diffusion of various components between the apical and basolateral membranes of epithelial cells is attributed to TJs, the expression and role of AHNAK1 in establishing such junctions have been investigated [219]. AHNAK1 has also been identified as a novel autoantigen in systemic lupus erythematosus [240]. Skoldberg *et al.* has shown AHNAK1 contains distinct cleavage sites for granzyme B and caspase-3 [240]. Since a hallmark of many autoantigens in systemic autoimmune disease is the efficient cleavage

by granzyme B to produce fragments distinct from those produced during other forms of apoptosis, AHNAK1 was suggested to be a target of the immune system in autoimmune disease.

AHNAK1 has been shown to associate with several different proteins including the calcium and zinc-binding protein S100b [229], the regulatory β 2 subunit of L-type calcium channels [233], G-actin [241], PLC [237], and PKC [239]. The carboxyl-terminal domain AHNAK1 has also been found to associate with a type of vesicles called enlargosomes, a new population of calcium regulated vesicles capable of fast exocytosis [230, 231].

Phospho analysis revealed AHNAK1 is phosphorylated on serine and threonine residues, and subsequent studies showed it is a substrate of PKA, PKB, and PKC *in vitro*. AHNAK1 was reported to consist of eight potential *in vitro* phosphorylation sites for PKA [233], six potential *in vitro* phosphorylation sites for PKC [234], and seven potential *in vitro* phosphorylation sites for casein kinase II [234]. Phosphorylation of AHNAK1 is important for its subcellular localization and function. AHNAK1 phosphorylation decreases when cells are made quiescent. Phosphorylation of serine 5535 of AHNAK1 by PKB results in nuclear exclusion in MDCK and HeLa cells [225]. The binding affinity between the C1 domain of AHNAK1 and the β 2 subunit of L-type calcium channels decreases by approximately 50% upon PKA phosphorylation [233].

Arachidonic Acid

Arachidonic acid (AA) is a polyunsaturated fatty acid with four double bonds, in which by itself or its metabolites serves multiple roles in living cells [242]. AA and its

metabolites (e.g. eicosanoids) function as modulators to suppress inflammation [243]. The concentration of AA in resting cell is generally described as being low [244]. AA is amphipathic in nature, as its hydrophobic tail can remain in a lipid bilayer, while its polar carboxyl group can emerge into the extracellular aqueous environment [244]. Additionally, the amphipathic nature of AA allows it to readily bind to proteins such as serum albumin [245]. Fatty acid binding proteins (FABPs) [246] and fatty acid transport proteins (FATPs) [247-251] allow for cellular uptake of AA. Liberated AA is metabolized by the cyclooxygenase (COX), lipoxygenase (LO), and cytochrome P450 monooxygenase (CYP) enzymatic pathways [252, 253]. The COX pathway converts AA into prostaglandins (PGs) and is clinically relevant since it is the main target for non-steroidal anti-inflammatory drugs (NSAIDs) [254]. Three COX isoforms exist [255], where COX-1 is virtually ubiquitously expressed in most tissues and COX-2 is thought to be an inducible isoform upregulated by inflammatory stimuli [254, 256-260]. The LO pathway converts AA into leukotrienes (LT), and the lipoxygenases demonstrate regiospecificity during interaction with substrates [261]. Accordingly, the LOs have been designated as arachidonate 5-, 8-, 12-, 15-lipoxygenase (5-LOX, 8-LOX, 12-LOX, and 15-LOX) [244, 262, 263]. In EC, the CYP pathway metabolizes arachidonic acid to four regioisomeric epoxyeicosatrienoic acids, which are then rapidly hydrolyzed to dihydroxyeicosatrienoic acids [264, 265]. Many of the bioactivities of AA is from its conversion to bioactive products such as prostaglandins by oxygenases [242]. The extracellular release of AA allows for the exchange of AA between cells and certain cell types further release AA in response to exogenous AA. AA is known to regulate transcription factors, including the activation of peroxisome-activated receptors (PPARs)

[242]. The hydrolysis of phospholipids by phospholipase A2 (PLA₂) is the primary pathway leading to AA production [266, 267]. Activation of PLA₂ is tightly regulated at both the transcriptional and posttranslational levels. The secretory (sPLA₂), cytosolic Ca²⁺ dependent (cPLA₂), and cytosolic Ca²⁺ independent (iPLA₂) are three types of PLA₂s [266]. The sPLA₂ enzymes have a molecular mass of between 13-19 kDa and lack specificity for arachidonate containing phospholipids [268]. The sPLA₂ enzymes are stored in the secretory granules and released upon the activation of cells, and can increase the activity of cPLA₂ in cell types including EC. Several EC functions, including migration, proliferation, viability, barrier maintenance, adherence, and generation of bioactive mediators are affected by AA metabolites [243]. The cPLA₂ enzymes have a molecular mass of greater than 60 kDa and preferentially hydrolyze arachidonate containing phospholipids [269]. The cPLA₂ enzymes are constitutively expressed in most cells and tissues. The iPLA₂ enzymes have a molecular mass of approximately 85 kDa and are not selective for arachidonate containing phospholipids [270]. Stimulation of cells with pro-inflammatory cytokines and growth factors results in increased expression of cPLA₂ and sPLA₂ [266]. AACOCF₃, a trifluoromethyl ketone analog of AA, is a potent inhibitor of cPLA₂ [271]. Alternatively, AA can be released from membrane phospholipids from hydrolysis of DAG catalyzed by two DAG-lipase [272].

A few reports have provided evidence for a positive correlation between the amount of AA in adipose tissue and the risk of ischemic heart disease (IHD) [273]. Furthermore, AA concentrations in adipose tissue have been found to be positively correlated with body mass index, which is a risk factor for myocardial infarction [273].

Phospholipase C

PLC β , PLC γ , PLC δ , and PLC ϵ are four main subfamilies of PLC [238]. There are four members of the PLC β subfamily, and each are activated by α or $\beta\gamma$ subunits of the heterotrimeric G-proteins in response to agonist binding [198, 238]. PLC β 1 exist as alternatively spliced variants β 1a and β 1b and each show differential tissue distribution and expression [238]. PLC β 2 is highly expressed in cells of hematopoietic origin and is implicated in leukocyte signaling and host defenses [238]. PLC β 3 is widely expressed with high levels in granule cells and the pituitary gland [238]. PLC β 4 exist as alternatively splice variants with the PLC β 4b variant having a unique 10 residue peptide instead of the 162 amino acid carboxy-terminal [238]. PLC β 3 is the only β isoform that is essential as homologous disruption of the PLC β 3 gene is lethal for mice early in development [238]. However, null mutations of the other β isoforms each result in a phenotype representative of the specialized role of that specific isoform [238]. There are two members of the PLC γ subfamily, and each contains two types of SH domains and is believed to be regulated by tyrosine phosphorylation following binding to either growth factor activated receptor kinases or to cytosolic tyrosine kinases of the src family [238]. Alternatively, lipid-derived second messengers have been shown to activate this isozyme [238]. There are four members of the PLC ϵ subfamily and they are activated by Ras and Rho GTPases and contains both guanine nucleotide exchange factor (GEF) and RA (Ras associating) domains [238]. PLC hydrolyzes phosphatidylinositol 4,5-biphosphate (PIP₂) to generate the water soluble inositol 1,4,5-triphosphate (IP₃), which is released into the cytosol and the hydrophobic DAG, which is released into the membrane [238]. IP₃ triggers calcium release from intracellular calcium stores through binding to IP₃

receptors, while DAG is known to activate PKC [238, 274]. Both IP₃ and DAG are important second messengers in various signaling pathways (Figure 6). Moreover, activation of PLC is a key event in cellular signal transduction involved in cell growth, metabolism, secretion, and proliferation [238]

Calcium Signaling

Calcium is a ubiquitous and universal second messenger that plays an important role in the regulation of a wide range of cellular processes [275]. As a second messenger calcium is known to influence cell growth and proliferation [276-283], differentiation [284-287], survival and death [288-291]. Cells possess the necessary machinery to regulate both [Ca²⁺]_e and [Ca²⁺]_i with accuracy and precision by directional Ca²⁺ transport across the plasma membrane and across membranes of intracellular organelles (e.g. endoplasmic reticulum).

The second messenger function of Ca²⁺ extends beyond inside the cell, as many cells express cell surface sensors for Ca²⁺. The best characterized Ca²⁺ sensor is the extracellular-Ca²⁺ sensing receptor (CaR), a GPCR that is able to respond to divalent and trivalent metal ions including Ca²⁺, Mg²⁺, Zn²⁺ and Gd³⁺, extracellular amino acids, and various polycations [292]. A CaR is abundantly expressed in epithelial cells, glial cells, and central and peripheral neurons [293]. CaR couples to various intracellular signal transduction cascades upon activation by ligand [294-297]. CaR is coupled to G_{α_q}/G_{α₁₁} to stimulate intracellular PLC/IP₃/Ca²⁺ signaling, and through PTX-sensitive G_{α_i} to interrupt cAMP production [292, 298]. CaR is also linked to AA production activation of the MAP kinase pathways [292]. Ca²⁺ may act as paracrine messenger via CaR, since

CaRs of neighboring cells are able to respond to changes in $[Ca^{2+}]_e$ as a consequence of $[Ca^{2+}]_i$ signaling. Moreover, Ca^{2+} may act as an autocrine messenger, as export of Ca^{2+} following intracellular Ca^{2+} spiking upon activation of CaR has been reported. Several other membrane proteins have been reported to respond to $[Ca^{2+}]_e$. The metabotropic glutamate receptors (mGluRs), a G-protein coupled receptor that is sensitive to $[Ca^{2+}]_e$ is expressed predominantly in the central nervous system [299]. Hemichannels of adjacent cells that form gap junctions have been reported to be highly responsive to small decreases in $[Ca^{2+}]_e$ [300]. Ion channels, including the ASIC1a/ASIC1b, proton-gated cation channels are responsive to fluctuations in $[Ca^{2+}]_e$ [301].

An increase in $[Ca^{2+}]_i$ may occur from an influx of extracellular calcium via channels in the plasma membrane or from depletion of intracellular calcium stores. In non-excitable cells, a biphasic increase in $[Ca^{2+}]_i$ may occur from store-operated calcium entry (SOC) (also known as capacitative calcium entry) as calcium store depletion triggers an influx of extracellular calcium [293]. SOC helps to replenish intracellular calcium stores and activate various physiological processes [293].

Adipogenesis

Adipose tissue is a type of specialized connective tissue that is composed of several cell types including fibroblasts, macrophages, EC, and adipocytes [302]. White and brown adipocytes derive from fibroblastic precursor cells and constitute the two forms of adipose tissue found in mammals [303]. Brown adipose tissue, which acquires its color from vascularization and densely packed mitochondria, is believed to function as a defense against cold and protection against obesity, but the physiological significance

of brown adipose tissue has been less characterized than white adipose tissue [302]. Adipose tissue store energy in the form of triglycerides and secretes a variety of hormones termed adipokines [302]. Adipokines such as adiponectin, leptin, interleukin 6 (IL-6), tumor necrosis factor α (TNF- α), adipon, visfatin, and leptin are involved in the regulation of energy metabolism [302]. The dysfunction of adipokine production may contribute to the pathogenesis of diseases associated with energy metabolism including insulin resistance and type 2 diabetes [302].

The function of adipose tissue is disregulated in obesity [304], which has been linked with an increase risk of various diseases including cancer, heart disease, hypertension, stroke, and diabetes [305]. Since obesity is characterized by an excess of adipose tissue, pharmacological approaches to modulate adipogenesis, the development of adipocytes from preadipocytes is an attractive solution to this disorder. However, the medical benefits from the direct reduction of adipogenesis is not yet clearly understood. For example, stimulators of adipogenesis are used clinically to reduce hyperglycemia in patients with type 2 diabetes [302]. Also, it would seem increasing brown fat adipogenesis would be beneficial.

Adipogenesis involves a cascade of events leading to the development of adipocytes from preadipocytes. The core constituents of the initial cascade include the CCAAT/enhancer-binding protein β (C/EBP β) and C/EBP δ transcription factors [306]. The core constituents of the second cascade include the peroxisome proliferator-activator receptor γ (PPAR γ) and C/EBP α transcription factors [306]. The C/EBP family members belong to the basic-leucine zipper class of transcription factors [306]. The PPAR γ is a member of the nuclear receptor family and exist as two protein isoforms from alternative

splicing at the 5' end of the gene [307]. The PPAR γ 2 isoform contains 30 additional amino acids at the amino terminus and is highly specific for fat cells [308]. PPAR γ is activated upon binding of ligands to its carboxy terminal domain ligand binding domain [307]. In a model by Rosen and Spiegelman, C/EBP β and C/EBP δ induces the expression of PPAR γ , which in turn activates C/EBP α [302]. PPAR γ and C/EBP α are believed to act synergistically to activate differentiation gene expression [307, 309]. Furthermore, the ADD1/SREBP1 transcription factor has been linked to the activation of PPAR γ by inducing its expression and promoting the production of endogenous PPAR γ ligand [307].

In comparison with other cell lineages, the differentiation of preadipocytes into mature adipocytes *in vitro* closely mimics and recapitulates many of the key features of adipogenesis *in vivo*. These features include cell growth cessation, morphological changes, lipid accumulation, and sensitivity to various hormones including insulin [302]. Several extracellular and intracellular signals, including various hormones growth factors have been shown to influence preadipocyte determination, preadipocyte growth, and terminal differentiation. Insulin is known to induce differentiation and increase lipid accumulation, although preadipocytes express low, if any levels of insulin receptors [302]. Accordingly, the effect of insulin on differentiation was found to be the result of cross-activation of the insulin-like growth factor 1 (IGF-1) receptor [302]. Activation of preadipocyte IGF-1 receptors by IGF-1 or pharmacological doses of insulin results in the activation of several distinct transduction pathways, including ras and akt, which activate adipogenesis via unknown effectors [302]. Furthermore, glucocorticoids are known to induce adipocyte differentiation [306]. Glucocorticoids can be administered in the form

of dexamethasone and activate the glucocorticoid receptor, which belongs to the same superfamily as PPAR γ [118, 306]. Glucocorticoids have been shown to reduce expression of the negative regulator of adipogenesis, preadipocyte factor-1 (pref-1) [302]. Inhibition of adipogenesis involves the activation of MAPK by various cytokines, including TNF- α and IL-1 and growth factors, including PDGF, FGF, and EGF. MAPK phosphorylates PPAR γ leading to repression of differentiation [302].

Protein Kinases and Phosphatases

Protein phosphorylation plays an important role in many physiological processes and is often dysregulated in various pathological conditions. A protein kinase is responsible for the transfer of terminal phosphate of ATP to a hydroxyl group on a protein, while a protein phosphatase is responsible for removal of the phosphate by hydrolysis. Protein kinases and phosphatases have been implicated in various diseases and are major drug targets [310].

The cAMP-dependent protein kinase, or protein kinase A (PKA) is a serine/threonine kinase that is composed of two catalytic subunits and a regulatory subunit dimer [311]. The kinase is rendered inactive when the two catalytic subunits associate with the regulatory subunit to form a tetrameric complex [311]. The kinase becomes active when the intracellular signaling molecule cAMP binds to the regulatory subunit and facilitates dissociation of the complex [311]. The two forms of the heterotetrameric PKA holoenzyme are the type I (RI α and RI β dimer) and type II (RII α and RII β dimer) PKA holoenzymes [312]. Type I PKA is predominantly cytoplasmic, while type II is known to associate with various cellular structures and organelles [313].

The localization of PKA and other signaling enzymes is dependent on its interaction with A-kinase anchoring proteins (AKAPs) [314]. The AKAPs play an important role in the coordination of signaling complexes by connecting upstream activators with downstream targets [314].

PKB, also known as Akt, is a serine/threonine kinase that is activated in the phosphoinositide-3 kinase (PI3K)-dependent pathway [315]. PKB exist as α , β , γ isoforms, each of which are encoded by separate genes [315]. PKB possesses a Pleckstrin homology domain (PHD), which binds to phosphoinositides with high affinity. PKB has been implicated in cell survival, cell cycle, metabolism, and angiogenesis and tumor development. The PH domain leucine-rich repeat protein phosphatase (PHLPP) is the phosphatase responsible for dephosphorylating the hydrophobic motif of PKB [316]. PKB serves a protective role against apoptosis in response to mitochondrial damage, as its activation has been found to reduce ischemia-reperfusion and hypoxia/reoxygenation-induced apoptosis in neuronal cells and in cardiomyocytes by inhibiting the release of cytochrome *c* the activation of caspase-3 and caspase-9 [317, 318].

The PKC family consists of 10 isozymes that are organized into three subclasses according to their second messenger mode of regulation [319]. The conventional PKC isozymes, α , $\beta 1/\beta 2$, and γ respond to DAG and Ca^{2+} [319]. The novel isozymes, δ , ϵ , η , θ respond only to DAG [319]. The atypical isozymes ι , λ , ξ respond to neither to Ca^{2+} nor DAG [319]. A given PKC isozyme can directly oppose the function of another isozyme. For example, PKC δ is known to be proapoptotic and anti-proliferative, while PKC ϵ is known to be anti-apoptotic and proliferative [319]. All members of the PKC family have a conserved C-terminal kinase core and an N-terminal regulatory moiety [319-321]. The

regulatory moiety is responsible for maintaining the enzyme in an autoinhibited state in the absence of a second messenger, targeting the enzyme to specific cellular sites, and mediating protein-protein interactions [319-321]. PKC translocates from the cytosol to the plasma membrane in response to the generation and subsequent binding of the lipid second messengers, Ca^{2+} and DAG [319-321]. Increases in intracellular concentrations of these second messengers results in activation of PKC, while decreases in these second messengers results in inactivation of PKC [319-321]. The C1, C2 and C-terminal tail of PKC help to mediate protein-protein interactions. PKC can interact with various binding partners to target it to different signaling pathways [319-321]. Receptors for activated C-kinase (RACKs), which serve as adaptors for various proteins are responsible for binding to the C2 domain of activated PKC and regulating its activity [319]. Activated PKC that is in the open conformation is susceptible to phosphatases, proteolysis, and degradation [319]. Dephosphorylation at the activation loop, turn motif, and hydrophobic motif renders PKC inactive [321]. Chronic activation of PKC by treatment with phorbol esters and bryostatins results in the loss in enzymatic activity and down-regulation of the enzyme [321]. Maturation of PKC is dependent on phosphorylation at the activation loop, allows for autophosphorylation at the C-terminus, correctly positions residues required for catalysis, and reveals access to the substrate binding site [321].

Cell-cell junctions

The formation and integrity of cell-cell contacts is important for establishing and maintaining the permeability barrier property of endothelial and epithelial cells [322].

Cell-cell contacts between epithelial cells are attributed to the junctional complex, which contains gap junctions, desmosomes, adherens junctions (AJs), and TJs [322, 323].

Gap junctions metabolically and electrically couple neighboring cells together by allowing the passage of second messengers, ions, and small molecules between cytoplasm of adjacent cells [324]. Gap junctions are formed by two unrelated families of proteins, the connexins and the pannexins [324]. Connexin proteins are similar in structure as they contain four transmembrane domains that are connected by two extracellular loops and form the wall or pore of the channels [324]. The connexin proteins are also composed of cytoplasmic N and C terminal domains and a cytoplasmic loop that links the second and third transmembrane domains [324].

Desmosomes help hold epithelial cells together and provide anchoring sites for intermediate filaments [325]. Desmosomal cell-cell attachment is mediated by the transmembrane glycoproteins of the cadherin superfamily, desmoglein and desmocollin [326, 327], in which three known tissue specific isoforms exist for each protein [328]. The cytoplasmic domains of desmoglein and desmocollin connect to intermediate filaments through desmosomal proteins such as plakoglobin, while the extracellular domains connect with their counterparts in adjacent cells [327, 328]. The cell type specific intermediate filament (IF) proteins are arranged into several different sequence homology classes [329]. Classes I and II represent the acidic and basic cytokeratins, respectively [329]. Class III include vimentin, desmin, glial fibrillary acidic protein, and peripherin [329]. Class IV include α -internexin and neurofilament triplet proteins, and nestin [329]. Class V include the nuclear lamins [329].

AJs play an important role in maintaining endothelial and epithelial paracellular permeability [330]. In addition AJs promote cell-cell communication and transfer signals between cells that regulate cell shape and polarity, mediate contact inhibition of cell growth, and increase resistance to apoptosis [330]. The two major protein complexes that exist at AJs of epithelial cells include the cadherin-catenin complex and the nectin-afadin complex [331, 332]. The cadherin-catenin complex is composed of the Ca^{2+} dependent adhesion E-cadherin molecule and the armadillo repeat domain containing family of proteins, p120^{ctn} and β/γ -catenin [331, 332]. The nectin-afadin complex is composed of the Ca^{2+} independent nectin molecule and the PDZ afadin protein [331, 332]. AJs may signal by binding to growth factor receptors and modulate their downstream pathways and internalization, recruit transcriptional co-factors, and activate signaling mediators [331, 332]. Furthermore, AJs play a vital role during development and appear to be dynamic structures during morphogenesis and in resting cells [331, 332].

TJs functions as a permeability barrier and separates the apical and basolateral membrane domains [333]. The biosynthesis of TGs is affected by various signal transduction pathways. Proteins including G proteins, PLC, calmodulin and second messengers including Ca^{2+} and cAMP are important for the assembly of TJs [323]. Three major classes of integral membrane proteins exist at TJs of epithelial and EC. The first class consist of tricellulin, claudins, and occludin all of which contain cytoplasmic N-terminal and C-terminal domains, two extracellular loops, and four transmembrane domains [323, 333]. Claudins constitute the TJ intercellular strands and mediate calcium independent cell-cell adhesion [323, 333]. Claudins directly interact with peripheral PDZ domain containing zonula occluden (ZO) proteins, including ZO-1, ZO-2, and ZO-3

[323, 333]. The ZOs belong to the membrane associated guanylylkinase (MAGUK) family of proteins, which contain a core structure of at least one PDZ domain, a SH3 domain, and a guanylylkinase (GUK) domain [334]. In addition to being present at the TJs of epithelial and EC, ZOs are also present in nonepithelial cells such as astrocytes, fibroblasts, and Schwann cells [335]. Mammalian ZOPs consist of ZO-1, ZO-2, and ZO-3 proteins. ZO-1, a 220 kDa protein and is highly homologous to ZO-2, a 160-kDa protein, and two proteins were found to co-precipitate in epithelial cells [333, 335, 336]. However, the C-terminus of ZO-1 and ZO-2 diverges at the C-terminus and ZO-2 contains an alternatively spliced region, the β -motif [333, 337]. As previously mentioned, the AHNAK1 protein was shown to co-localize with ZO-1 in EC with blood-brain properties [232]. ZO-3, a 130-kDa protein, which was originally described as p130, shows high homology to ZO-1 and ZO-2 but contains a unique proline-rich region [333, 334]. ZO-3 directly interacts with ZO-1 and the cytoplasmic domain of occludin, but not ZO-2 [333, 334]. Occludin may serve a role in the regulation of various signaling cascades attributed to the formation of TJs. At the TJ occludin directly interacts with the ZO-1, ZO-2, and ZO-3 proteins [333]. Occludin indirectly interacts with the actin cytoskeleton and junctional adhesion molecules (JAMs) by interacting with ZO proteins [333]. JAMs contain a single transmembrane domain, a cytoplasmic tail, and an extracellular domain, which contain two Ig-like motifs [333]. The second class consists of Ig-SF members and include JAM-A, CAR, CLMP, ESAM, and JAM4, all of which contain two Ig-like domains [323, 333]. The third class consists of a homologue of the *Drosophila* Crumbs proteins, Crumbs3 (CRB3), which contains a short extracellular domain and a short cytoplasmic domain [323, 333]. In addition to interacting with

claudins, occludin, and junctional adhesion molecule the ZOPs also associate with various cytoplasmic proteins of less defined function [333, 338-340].

RGM1

The rat gastric mucosal (RGM1) cell line (Figure 7C), established by Dr. H. Matsui at the Institute of Physical and Chemical Science (RIKEN) Cell Bank and Institute of Clinical Medicine, University of Tsukuba, Tsukuba, Japan are nontransformed and immortalized gastric surface epithelial cells [341]. RGM1 cells were found to be an excellent model to investigate gastric epithelial restoration *in vitro* [342].

3T3-L1

The establishment of the 3T3-L1 mouse cell line from a continuous strain of 3T3 cells by Green and colleagues is a commonly used model to study adipocyte physiology [343-345]. Undifferentiated, or 3T3-L1 preadipocytes have a fibroblast-like morphology (Figure 7D), but can be differentiated to have an adipocyte-like phenotype and morphology with the signet ring appearance of adipose cells. 3T3-L1 adipocytes recapitulate many of the endocrine and metabolic functions of mature adipocytes *in vivo* [343-345]. Differentiated 3T3-L1 cells (Figure 7D) are sensitive to lipogenic and lipolytic hormones and drugs, including insulin, epinephrine, and isoproterenol [343]. 3T3-L1 cells can be spontaneously converted into adipocytes when maintained in culture with fetal bovine serum alone [345]. Alternative means of triggering spontaneous differentiation of fibroblasts into adipocytes include the expression of constitutively active Akt kinase [346], bisphenol A treatment. The most effective method to induce

differentiation is to treat confluent cultures of 3T3-L1 cells with a combination of insulin, DEX, and MIX [347].

AoSMC

Vascular smooth muscle cells (VSMCs) are important for providing structural support. VSMCs are characterized by the expression of various smooth muscle isoforms of structural genes involved in contraction, including smooth muscle myosin heavy chains (smMHCs), smooth muscle calponin (smCalponin), smooth muscle α -actin (sm α -actin), smooth muscle myosin light chain kinase (smMLCK), and α -tropomyosin [348, 349]. The proliferation, differentiation or change in regulation of VSMCs may contribute to the pathogenesis of atherosclerosis, restenosis and diabetic angiopathy [350]. Human aortic vascular smooth muscle cells (AoSMCs) are shown in Figure 7E.

Recombinant Proteins

Manufactured proteins are useful for various biomedical applications including small molecule drug discovery and the production of therapeutic proteins and vaccines [351]. A renewable source of protein is also useful for other applications such as antibody generation and purification [352], protein structure determination [353], protein-protein interactions studies [354], and post-translational modifications studies. Recent advancements leading to the better understanding of transcription, translation, and protein folding in *Escherichia coli* (*E. coli*) has made it the system of choice for recombinant protein production.

Production of recombinant proteins involves subcloning the gene of interest into an expression vector that is under the control of an inducible promoter. High-throughput purification of human proteins from bacteria has been accomplished [355]. Advantages of using a bacterial system for protein production include rapid growth, high protein yields, practicality, and lower cost compared to mammalian, insect, or yeast cultures. Shortcomings of using a bacterial system for protein production include the lack of specialized post-translational modifications, the absence of eukaryotic chaperones, the lack of specific co-factors, the inability of the protein to form complexes or associations with other proteins, and the failure of the protein to be targeted to subcellular locations. One or a combination of these limitations may contribute to protein aggregation and/or protein mis-folding. Furthermore, membrane proteins such as receptors often pose difficulties in the expression and purification of bacterial systems because of their hydrophobicity [356, 357]. A number of different approaches to manipulate various expression parameters are commonly used to circumvent these problems. For example, reducing the cultivation temperature, reducing the amount of expression inducer, and the co-expression of various chaperones are common strategies to minimize protein misfolding [358]. A typical approach to enhancing the solubility of the overexpressed protein in the host bacteria is the incorporation of a solubility enhancing tag such as maltose binding protein (MBP), thioredoxin (Trx), and GST [355, 359, 360]. Additional advantages of inclusion of a fusion tag include the larger size fusion protein containing a greater number of potentially immunogenic epitopes for antibody generation [361], a means of purification, and the ability to immobilize the fusion protein in various assays.

The overexpression of foreign proteins in bacteria usually results in the production of insoluble aggregates termed inclusion bodies (IBs). IBs are the result of an unbalanced equilibrium between solubilization and *in vivo* protein aggregation [362]. The formation of inclusion body proteins are often thought to be biologically inactive and therefore discarded. However, multiple reports have suggested that aggregation of bacterial inclusion bodies does not imply biologically inactivation of proteins [363, 364]. In fact, the incorporation of the overexpressed foreign protein into bacterial inclusion bodies has been described to be advantageous for several reasons [360]. The recombinant protein may be protected from proteolysis within the inclusion bodies, enriched in the inclusion bodies, and may not be lethal to the host cell when overexpressed. There have been numerous reports of refolding of various proteins including enzymes and receptors from bacterial inclusion bodies. Kiefer *et al.* reported efficient refolding of GST-GPCR-His fusion proteins from bacterial inclusion bodies [365]. The procedure involved solubilization of the inclusion body fusion protein complex, transfer into a neutral detergent, thombin cleavage of the GST, and purification on a nitrilotriacetic acid column [365]. Frangioni and Neel reported efficient recovery of enzymatically active nontransmembrane tyrosine phosphatase GST fusion proteins from bacterial inclusion bodies [366]. The procedure involved solubilizing the fusion proteins with an empirically determined molar ratio of the ionic detergent N-laurylsarcosine (sarkosyl) and the non-ionic detergent Triton X-100 and purification over glutathione agarose beads. In one report, the complexity of inclusion body aggregates were analyzed and separated into subclasses based on their mass [367]. The aggregates of

lower complexity were found to be more efficiently recovered in the presence of molecular chaperones.

The main disadvantages of using a bacterial system for overexpressing a foreign protein of interest include the loss of posttranslational modifications and protein folding. The distinct differences in protein processing between bacterial and eukaryotic systems contribute to the lack of conservation of posttranslational modifications and protein folding of eukaryotic proteins when overexpressed in a bacterial system. Membrane proteins are overexpressed in the cytoplasmic membrane of bacteria, while they are overexpressed in the endoplasmic reticulum membrane of eukaryotes [368]. Also, the rate of polypeptide elongation and the rate of protein folding are considerably higher in prokaryotes than in eukaryotes, which may contribute to protein misfolding [368]. Differences in lipid composition and lack of chaperone proteins between prokaryotic and eukaryotic systems may also contribute to protein misfolding [368]. Glycosylation is often required for correct folding of eukaryotic membrane proteins, but bacterial cells such as *E. coli* do not have the ability to glycosylate proteins [368]. The lack of chaperone proteins, glycosylation machinery, differences in lipid compositions, and the lack chaperone proteins does not eliminate bacterial cells from being used as a host for the production of functional eukaryotic membrane proteins [368]. If desired, it is possible to utilize active kinases to posttranslational modify the protein *in vitro* after expression and purification from bacterial cells. Similarly, it is possible the target protein may spontaneously adopt its native confirmation after being expressed and purified from the bacterial cells, since its structure is largely determined by its amino acid sequence. In

other cases, artificial membranes may be used to induce folding of certain membrane proteins overexpressed in bacterial cells.

Table 1. Natriuretic Peptides and their receptors in disease

Genotype	Phenotype	Reference
ANP/BNP ++	Arterial hypotension	[44]
ANP -/-	Salt-sensitive hypertension, pulmonary hypertension	[46]
BNP -/-	Cardiac fibrosis	[46]
CNP -/-	Dwarfism	[37]
NPRA ++	Arterial hypotension	[45]
NPRA -/-	Cardiac hypertrophy and fibrosis, salt-resistant hypertension	[47, 48]
NPRB -/-	Seizure attacks, infertility	[37]
NPRC -/-	Hypotension, skeletal deformations	[49]

Phenotypes seen in mouse models. ++ represents overexpression, -/- represents deletion

Table 2. Protein expression of natriuretic peptide receptors in various cell lines

Cell line	Assay	NPRA	NPRB	NPRC
NIH 3T3	WB	+	+	++
3T3-L1	WB/IHC	+	+	++
RGM1	WB/IHC	-	-	+++
A-10	WB	+++	+	+++
AoSMC	WB/IHC	+++	+++	++
HeLa	WB/IHC	++	+++	+++
PANC	WB	++	++	++
HEK 293	WB	+	+	++
α TC1	WB	+	+	++
AR42J	WB	+	+	+
BON	WB	+	+	+
HCT-15	WB	+	+	++
HCC-1428	WB	+	+	+
HPAC	WB	+	+	+
KATO III	WB	+	+	+
Min6	WB	+	+	++
MS1VEGF	WB	+	+	+
NCI-N87	WB	+	+	+
SHP-77	WB	+	+	++

+ represents low, ++ represents moderate, and +++ represents high immunoreactivity using polyclonal anti-NPRA, NPRB, or NPRC antibodies.

Table 3. Location of the gene coding for the NPRs

	Mouse	Rat	Human
NPRA	3 47.6 cM	2q34	1q21-q22
NPRB	4 21.5 cM	5q22	9p21-p12
NPRC	15 6.7 cM	2q16	5p14-p13

Central Hypothesis: NPRC is an atypical G protein coupled receptor that associates with various proteins, and plays an important role in signal transduction.

Specific Aim #1: To identify novel NPRC protein binding partners in various cell lines.

Specific Aim #2: To confirm the molecular association and identify the specific interacting domains between NPRC and arrestins and AHNAK1

Specific Aim #3: To determine the role of NPRC in AHNAK1 mediated calcium signaling

Specific Aim #4: To characterize the phosphorylation state of NPRC

Specific Aim #5: To identify novel or putative roles of AHNAK1

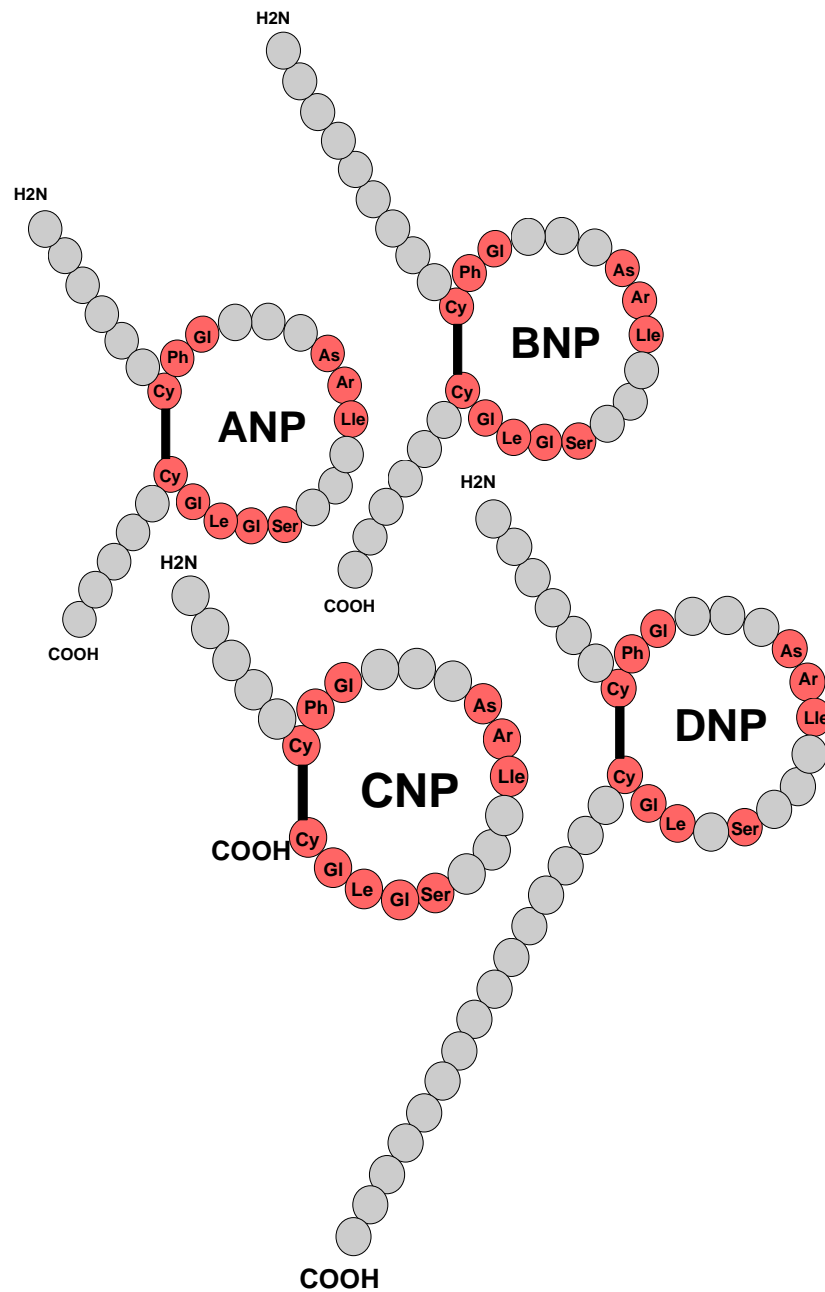


Figure 1. Amino acid structure of the natriuretic peptides. ANP (28 amino acids), BNP (32 amino acids), CNP (22 amino acids), and DNP (38 amino acids) share a similar 17-amino acid disulfide ring structure

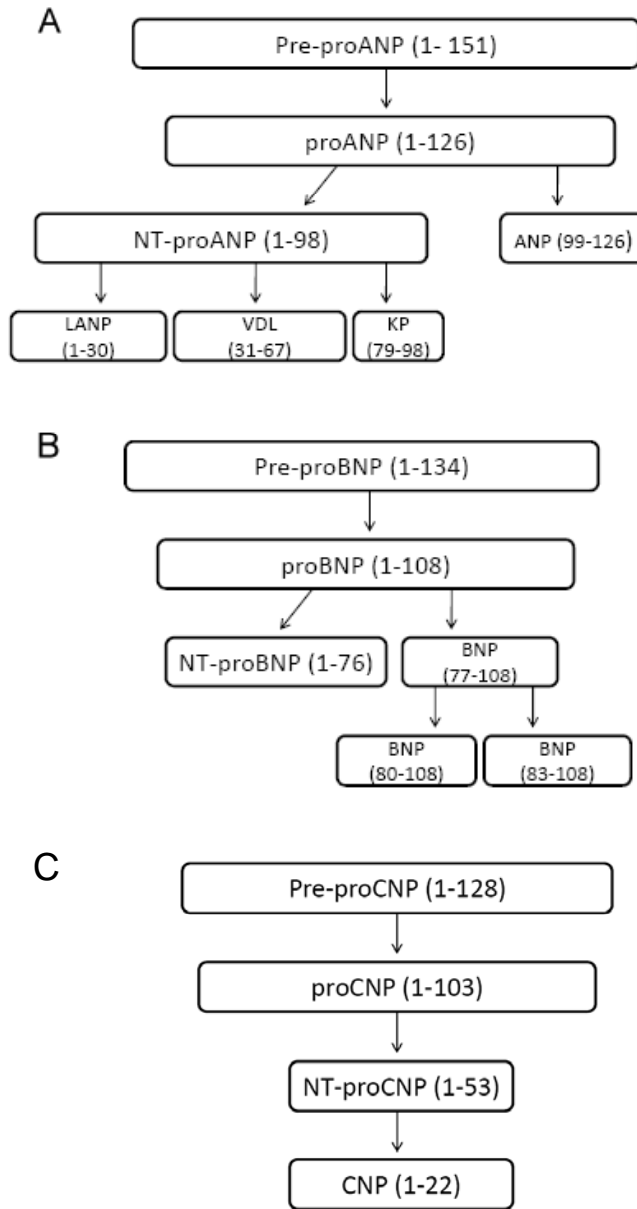


Figure 2. Paradigm of natriuretic peptide synthesis and release
 A: ANP; B: BNP; C: CNP

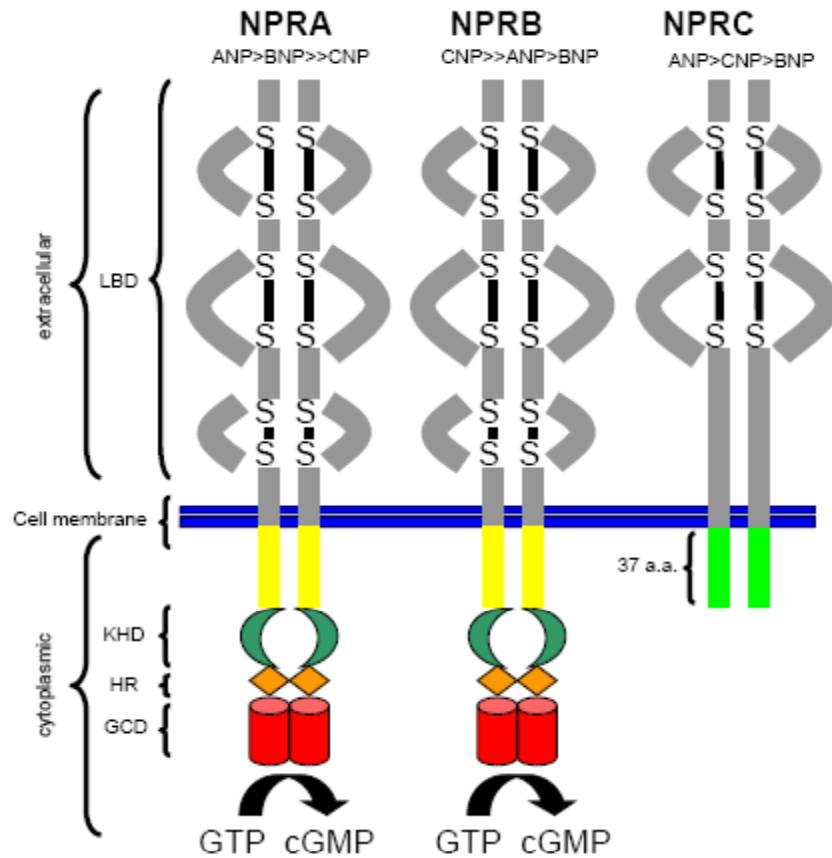


Figure 3. Topology of the natriuretic peptide receptors (NPRs). NPRA, NPRB, and NPRC are single transmembrane spanning receptors and each contains a large extracellular ligand binding domain (LBD). NPRA and -B contain a kinase homology domain (KHD), hinge region (HR), and a guanylyl cyclase domain (GCD). NPRC is devoid of the KHD, HR, and GCD. Instead, NPRC contains a short 37 amino acid (a.a.) intracellular domain.

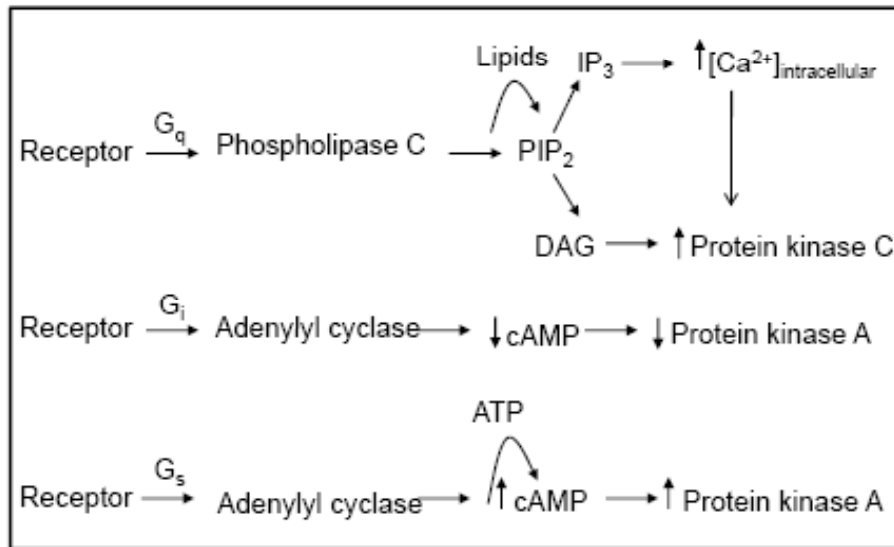


Figure 4. Diagram showing the role of G proteins in signal transduction. Receptors signaling through G_q activate PLC enzymes resulting in the hydrolysis of phosphatidylinositol-4,5-bisphosphate (PIP₂), generating diacylglycerol (DAG) and inositol-1,4,5-triphosphate (IP₃). IP₃ binds to receptors of intracellular stores and Ca²⁺ is released. The second messengers Ca²⁺ and DAG bind to and activate PKC. Receptors signaling through G_i inhibit adenylyl cyclase, resulting in decreased levels of cAMP, and decreased activity of PKA. Receptors signaling through G_s activate adenylyl cyclase, resulting in increased levels of cAMP, and increased activity of PKA.

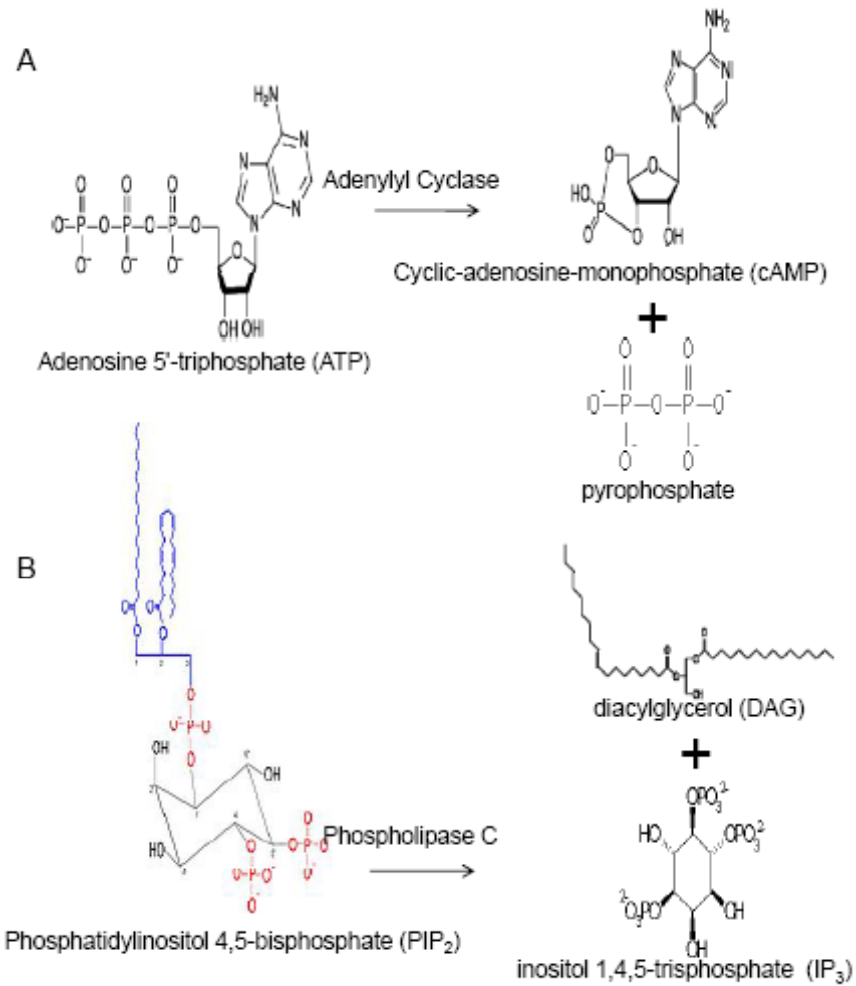


Figure 5. Reactions catalyzed by (A) adenylyl cyclase and (B) phospholipase C

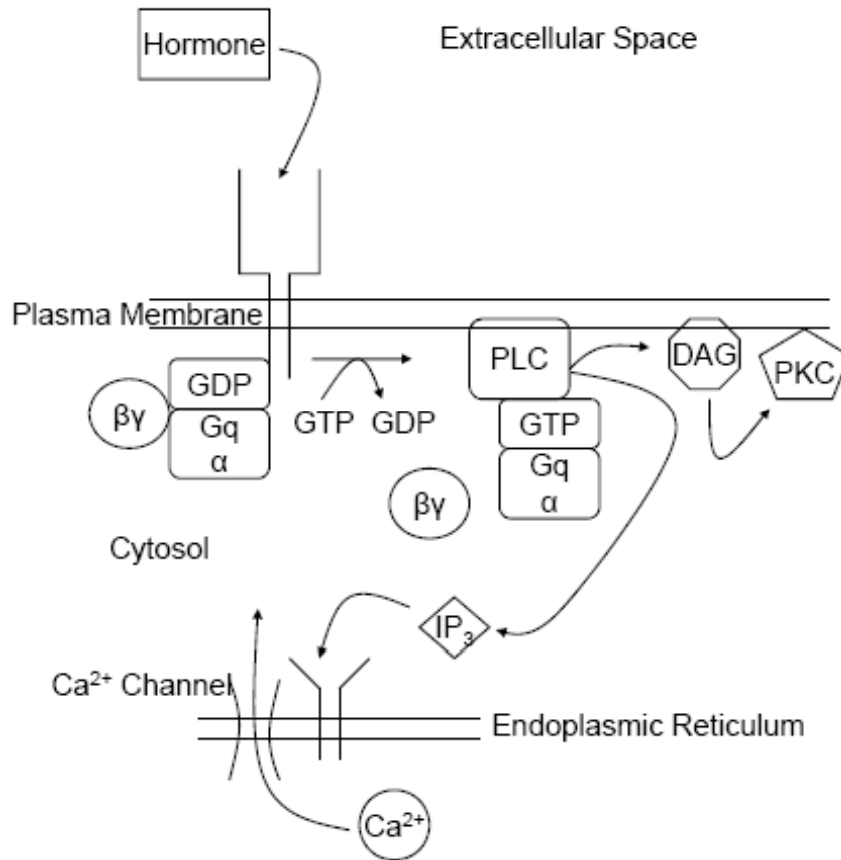


Figure 6. Role of the second messengers IP₃, DAG, and Ca²⁺ in the phosphatidylinositol system. After hormone binds to a specific receptor, the receptor-hormone complex catalyzes GTP-GDP exchange on Gq, and activates it. Active Gq activates PLC, which then cleaves phosphatidyl-inositol 4,5-bisphosphate to IP₃ and DAG. IP₃ binds to specific receptors on the endoplasmic reticulum, releasing sequestered Ca²⁺. DAG and Ca²⁺ activates PKC at the plasma membrane PKC phosphorylates proteins to produce cellular responses to the hormone.

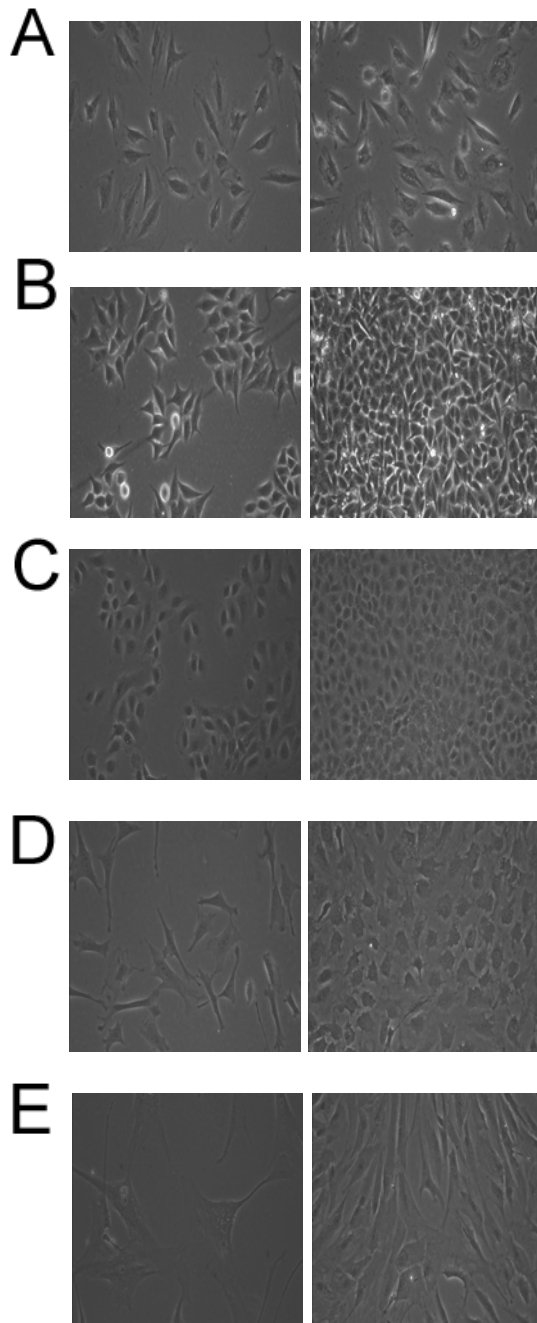


Figure 7. Phase-contrast microscopy of the cell lines used in the various studies of NPRC. (A) A-10 cells were purchased from the ATCC and cultured in DMEM high glucose supplemented with 10 % FBS and maintained at 37 °C, 5% CO₂ in a humidified incubator. (B) HeLa cells were purchased from the ATCC and cultured in DMEM high glucose media supplemented with 10% FBS and maintained at 37 °C, 5% CO₂ in a humidified incubator. (C) RGM1 cells were obtained from Dr. Hirofumi Matsui and cultured in DMEM/Ham's F-12 growth media supplemented with 10% FBS and maintained at 37 °C, 5% CO₂ in a humidified incubator. (D) 3T3-L1 cells were purchased from the ATCC and cultured in DMEM high glucose media supplemented with 10% newborn calf serum and maintained at 37 °C, 10% CO₂ in a humidified incubator. (E) hAoSMC were purchased from Lonza and cultured in smooth muscle growth media supplemented with insulin, hFGF-gentamicin/ amphotericin-B, FBS, hEFG and maintained at 37 °C, 5% CO₂ in a humidified incubator. For panels A-D, subconfluent cells are shown in the left panels and confluent cells are shown in the right panels.

Chapter 1: Development of a Polyclonal Antibody (JAH84) For Investigations of NPRC

Background

Currently, there are very few commercially available antibodies for NPRC. The few commercial antibodies against NPRC that are available demonstrate limited species cross-reactivity, high background, and poor applicability. The only antibody that has been validated for cross-reactivity between multiple species and for use in multiple immunoassays including immunoprecipitation, immunoblotting, and immunohistochemistry is a polyclonal antibody established several years ago by Fujishige *et al.* [369]. Antibodies are useful tools to probe for protein expression, regulation, post-translational modification, interaction, and function. Therefore, there was an urgent need to create an antibody against NPRC that was readily available and would crossreact with different species and could be used to perform different immunoassays in order to allow for various studies of NPRC.

Materials and Methods

Reagents and antibodies

All cell culture plasticware was purchased from Nalge Nunc (Rochester, NY). Precast gels (7.5% resolving with 4% stacking), 10X Tris-buffered saline (TBS), Laemmli sample buffer, Precision plus protein dual color standards, and horseradish peroxidase conjugated goat anti-rabbit secondary antibody were purchased from Bio-Rad (Hercules, CA). Colloidal coomassie blue stain was purchased from Genomic Solutions, Inc. (Ann Arbor, MI). 10X phosphate buffered saline (PBS) was purchased from Fisher Scientific (Fair Lawn, NJ). Protein G agarose was purchased from Upstate Biotechnologies (Lake Placid, NY). Mammalian protein extraction reagent (M-PER), Halt Protease and Phosphatase Inhibitor, Super Signal West Pico Chemiluminescent Substrate, BCA (bicinchoninic acid) protein assays reagents, and Restore Western blot stripping buffer were purchased from Pierce (Rockford, IL). Anti-NPRC antibody directed against the 37 COOH-terminal amino acids of rat NPRC was kindly provided by Dr. K. Omori (Kansai Medical University, Osaka, Japan) [369]. β -actin antibody and anti-mouse secondary antibody were purchased from Sigma (St. Louis, MO). Hybond-C extra nitrocellulose membranes and Hyperfilm ECL were purchased from Amersham Biosciences (Piscataway, NJ). Ponceau Red solution was purchased from Sigma. All other chemicals were purchased from Sigma unless otherwise noted. Texas Red/ FITC-streptavidin, anti-rabbit/anti-mouse biotinylated secondary antibodies, and Vectashield mounting medium with or without 4',6'-diamidino-2-phenylindole hydrochloride (DAPI) were purchased from Vector Laboratories (Burlingame, CA).

Cell Lines and Cell Culture

Human aortic vascular smooth muscle cells (AoSMC) were purchased from Lonza (Walkersville, MD) and were cultured in smooth muscle cell basal medium (SmBM) (Lonza) supplemented with SmGM-2 SingleQuots (Lonza). All other cell lines were purchased from the American type culture collection (ATCC) (Manassas, VA). SHP77 cells were cultured in RPMI 1640. NIH 3T3, HEK293, CCL13, PANC, and HeLa cells were cultured in high glucose Dulbecco's modified Eagle's medium (DMEM) (Gibco Invitrogen; Grand Island, NY). RGM1 cells were cultured in DMEM/F12 Medium (Gibco). With the exception of SmBM, all other media were supplemented with 1X antibiotic/antimycotic (Gibco) and 10% fetal bovine serum (Atlanta Biologicals; Norcross, Atlanta). All cell lines were maintained at 37°C in a 5% CO₂ humidified atmosphere. Only low passaged cells of less than 25 passages were used for experiments.

Polyclonal Antibody Production

A synthetic peptide corresponding to the last 26 amino acids of the cytoplasmic domain of human NPRC was used as the immunogen. The first amino acid of this peptide, a threonine, was replaced with a cysteine and the peptide was conjugated to Keyhole Limpet Hemocyanin (KLH). White New Zealand rabbits were immunized with the conjugated synthetic peptide (BIO-SYNTHESIS, INC.; Lewisville, TX).

SDS-PAGE and Immunoblotting

Proteins were harvested from cells cultured in 100 mm tissue culture dishes by scraping and collecting the lysate in the presence of M-PER. Proteins were harvested

from 50 mg pieces of tissue by moderate homogenization in the presence of tissue protein extraction reagent M-PER. All protein lysates were supplemented with Halt Protease and Phosphatase Inhibitors. Protein was quantified using BCA reagents and 25 µg of protein from cell or tissue lysate prepared in Laemmli sample buffer was loaded onto a 7.5% gradient polyacrylamide precast gel and subjected to SDS-PAGE for 4 hrs. Proteins were electrically transferred onto nitrocellulose membranes at 100 V in Towbin buffer for 75 minutes. In order to confirm the transfer of proteins, membranes were stained with Ponceau red solution. The membranes were destained by washing with 1X TBS and then blocked in 5% (w/v) nonfat milk in 1X TBS at room temperature (RT) for 1 hr. Membranes were washed with 1X TBS and then incubated with anti-NPRC (JAH84; 1:1000 dilution) polyclonal antibody in 5% BSA in TBS at RT for 2 hrs. Membranes were washed and then incubated with horseradish peroxidase conjugated goat anti-rabbit secondary antibody (1:3000 dilution) in blocking solution (5% (w/v) nonfat milk in 1X TBS) at RT for 1 hr. Membranes were washed with 1X TBS and immunoreactive bands were detected by SuperSignal West Pico chemiluminescent substrate and developed using Hyperfilm-ECL. As an internal control membranes were stripped using Restore Western blot stripping buffer and reprobbed with anti-β-actin (1:1000 dilution) and anti-mouse secondary antibody (1:25000 dilution). Precision plus protein dual color standards were used as molecular weight markers.

Immunohistochemistry of Paraffin-embedded Tissue Samples

Paraffin embedded tissues were sectioned and mounted on Superfrost Plus (+) glass slides. The slides were subject to deparaffinization, hydration, and antigen

retrieval. The slides were subject to three exchanges of xylene, two exchanges of 100% ethanol, two exchanges of 95% ethanol, and a single exchange of 80% ethanol, 70% ethanol, 60% ethanol, and reagent grade water for 5 min durations. The slides were then subject to a series of four microwave sessions in 10 mM citrate buffer (pH 6.0) for 5 min durations. The slides were rinsed with reagent grade water for 10 min and then rinsed with 1X PBS for 10 min. The slides were blocked in 8% filtered normal goat serum in 1X PBS at RT for 30 min. The slides were then incubated with anti-NPRC (JAH84; 1:250) polyclonal antibody in blocking solution at RT for 90 min. The slides were washed in 1X PBS and then incubated with anti-rabbit biotinylated secondary antibody (Vector Laboratories; Burlingame, CA) diluted in PBS and filtered normal goat serum at RT for 30 min. The slides were washed in 1X PBS and then incubated with FITC-conjugated streptavidin (Vector Laboratories) (1:50 dilution) in 1X PBS at RT for 30 min. The slides were washed, coverslipped, and mounted with mounting media containing DAPI in Vectashield medium.

Immunofluorescence of Cultured Cells

AoSMC, SHP77, HEK293, CCL13, PANC, and HeLa cells were cultured on type 1 collagen coated chamber slides. At 70% confluency, cells were washed with PBS, and then fixed at -20 °C for 5 minutes in MeOH/Acetone (1:1). Fixed cells were washed with PBS, and then blocked and stained as follows. Slides were incubated at RT for 30 minutes in blocking solution (8% filtered normal goat serum diluted in PBS), and then incubated at RT for 90 minutes with a polyclonal primary antibody (diluted in blocking solution). Slides were washed and incubated at RT for 30 minutes with anti-rabbit

biotinylated secondary antibody. Slides were washed and incubated at RT for 30 minutes in the dark in a solution of Texas Red-conjugated streptavidin (diluted in PBS). Slides were incubated at RT for 30 minutes in a second blocking solution (8% filtered normal horse serum diluted in PBS) and then incubated at RT for 90 minutes with a monoclonal primary antibody (diluted in blocking solution). Slides were washed and incubated at RT for 30 minutes with anti-mouse biotinylated secondary antibody. Slides were washed and incubated at RT for 30 minutes in the dark in a solution of FITC-conjugated streptavidin (diluted in PBS). Finally, slides were washed and coverslips were applied with mounting media containing DAPI in Vectashield medium.

Immunoprecipitation

Proteins were harvested from 100 mm tissue culture dishes as described above. After quantification by the BCA assay, 200 µg of protein was incubated with 4 µl of anti-NPRC (JAH84) polyclonal antibody with end-over-end mixing at 4 °C for 2 hrs. The resulting complexes were incubated with 40 µl of prewashed 50% protein G agarose slurry with end-over-end mixing at 4 °C for 4 hrs. The immunocomplex was washed four times with ice cold PBS and bound proteins were eluted by boiling for 5 minutes in Laemmli sample buffer. Eluted proteins were analyzed by SDS-PAGE and Coomassie blue staining.

MS

Gel bands were excised from Coomassie stained gels. The gel bands were subjected to in-gel tryptic digestion, liquid extraction of the gel fragments, followed by

LC-MS/MS on an LTQ mass spectrometer (Thermo Electron Corporation, Waltham, MA) with an LC packing ultimate dual gradient nano-LC system (Dionex, Sunnyvale, CA) (Proteomics Department at the Moffitt Cancer Center, Tampa FL). The Mascot algorithm (Matrix Science, London UK) was used to search the collected data against the nonredundant rodentia database at the national center for biotechnology information (NCBIInr).

Transient Transfection of FLAG-NPRC

FLAG-NPRC was transfected into COS7 cells using Lipofectamine reagents (Invitrogen; Carlsbad, CA) according to the manufactures instructions. Briefly, cells were seeded in 100 mm dishes and the cells were transfected after reaching 70% confluency. The Lipofectamine diluted in OptiMEM medium was added dropwise to the plasmid DNA (10 μ g/dish) diluted in OptiMEM medium and the complex was briefly incubated at room temperature before adding it dropwise to the cells. Cells were maintained in complete growth medium and cultured for at least 48 hours before harvesting the cells for protein.

Statistics

Results are expressed as the mean \pm SEM. Statistical significance was set at $p < 0.05$. Student's paired t test was used to compare data from two groups.

Results

Polyclonal Antibody Production

Multiple sequence alignments of the intracellular domain of NPRC reveals high homology between various different species (Figure 8). Multiple polyclonal antibodies were created against NPRC (JAH84 and JAH85) (Figure 9), and each appeared to recognize different epitopes of the target antigen and have different crossreactivities among different species (Figure 9). JAH84 and JAH85 each demonstrated a titer of 1:12,800 and the IgG concentration of each was approximately 2.5 mg/mL after purification and after the addition of sodium azide.

Monitoring transient transfection of Flag-NPRC to confirm specificity of JAH84

To demonstrate specificity of JAH84, the transfection efficiency of FLAG-NPRC was determined by immunoblotting with JAH84 and analyzing the immunoreactive bands by densitometry. COS7 cells were transfected with a FLAG-NPRC construct and the transfection efficiency was assessed by immunoblot and densitometric analysis using JAH84 or established anti-NPRC antibody. The presence of an immunoreactive band at 66 kDa corresponding to mock transfection, and at least a three-fold increase in a band at the same molecular weight, but corresponding to FLAG-NPRC was observed after probing with JAH84 (Figure 10). In addition to evaluating the ability of JAH84 to be used in Western blotting, it was evaluated to be used in immunoprecipitation studies (Figure 11). Several putative NPRC binding partners were pulled down with JAH84 (Figure 11). These proteins are identified in the next Chapter.

JAH84 confirms NPRC is the most widely and abundantly expressed NPR subtype

Several normal and abnormal cell lines, corresponding to various tissue origins of mouse, rat, and human species were screened for NPR protein expression by Western blot analysis and/or immunofluorescence. While using rabbit polyclonal antibodies against NPRA, NPRB, or NPRC, NPRC is shown to be the most widely and highly expressed NPR subtype across several different cell lines of various species (Table 2). Western blots, performed using JAH84 show NPRC is expressed in mouse heart, lung, kidney, liver, and pancreas (Figure 12A) and expressed in cell lines corresponding to human aortic vascular muscle derived cells, small cell lung carcinoma cancer-derived cells, embryonic kidney derived cells, hepatocyte-derived liver cells, and pancreatic ductal adenocarcinoma cancer-derived cells (Figure 12B).

JAH84 is applicable for immunohistochemistry analysis

Since antibodies are assay specific in addition to being species specific, the ability of JAH84 to be used in various different immunoassays was investigated. In addition to being able to crossreact with NPRC proteins from various different species by Western blot analysis and pull-down putative NPRC binding partners by immunoprecipitation, JAH84 was able to detect NPRC protein in RGM1 cells by immunofluorescence (Figure 13).

Discussion

Initial attempts to produce a monoclonal antibody to NPRC were unsuccessful. However, multiple polyclonal antibodies to NPRC were produced and assessed for applicability, sensitivity, specificity, and crossreactivity. Of these antibodies, JAH84 detected NPRC protein by multiple immunoassays, was sensitive and specific, and cross-reacted with multiple species.

Polyclonal antibodies generally cost less to produce and have a much faster overall turnaround time for production than monoclonal antibodies. Although polyclonal antibodies may be less specific, and are limited in quantity by the lifespan and size of the host animal, they have a wider range of potential applications than do monoclonal antibodies. One advantage of using a polyclonal antibody instead of a monoclonal antibody in an immunoassay such as immunoprecipitation is a polyclonal antibody is more likely to recognize multiple epitopes of the antigen with varying affinities. It is favorable to have an antibody recognize multiple epitopes while attempting to capture protein binding partners by immunoprecipitation. If the antibody is capable of recognizing multiple epitopes it may be possible to capture a protein-protein interaction if one or more of the antigenic epitopes are masked by the binding sites between the proteins of interest. Another advantage of using a polyclonal antibody in a typical immunoassay such as immunoblotting for screening cell lines or tissues for protein expression is there is a greater likelihood the protein of interest will be detected if it is readily susceptible to proteolysis or is posttranslationally modified. Polyclonal antibodies are generally not homogenous in nature as are monoclonal antibodies, and

because they can recognize different epitopes of the antigen, slight changes of the protein are generally tolerated.

The unique cytoplasmic domain of NPRC as an immunogen was targeted because of the high degree of homology of the extracellular and transmembrane domains between NPRA, NPRB, and NPRC. Since it is possible to predict antigenic determinants of a protein largely from its amino acid sequence, the entire cytoplasmic domain of NPRC was analyzed prior to designing the immunogen. The cytoplasmic domain was found to be antigenic enough to use as an immunogen, based on various immunogenic determinants.

The double bands that are present in immunoblots corresponding to some of the various tissue or cell lysates, indicates the JAH84 antibody detects total NPRC protein, including both unmodified and posttranslationally modified forms. NPRC has been reported to be phosphorylated on serine residues [370], although the specific residues that are phosphorylated and the kinases that are responsible for phosphorylating them have not yet been identified. The double bands at 66 kDa that were observed in some immunoblots and immunoprecipitation experiments may be attributed to NPRC phosphorylation, since only a single band is sometimes observed in the absence of phosphatase inhibitors. Moreover, the multiple bands that were observed in Western blots could also be attributed to other posttranslational modifications such as glycosylation.

The undiluted JAH84 antibody with supplemented with a bacteriostat, 0.05% sodium azide, to preserve its integrity. Several different buffers were tested for dilution of JAH84 for immunoblotting, and determined optimal dilutions for immunoblotting, immunohistochemistry, and immunoprecipitation. A typical attribute of polyclonal

antibodies is high background. Antibodies that produce high background in immunoassays such as immunohistochemistry and immunoblotting after blocking with a common agent may require affinity purification prior to use. JAH84 presented little background in immunostaining of cells and tissues and only a few nonspecific bands in immunoblotting. There was no need to affinity purify our JAH84 antibody prior to its use in various immunoassays.

Antibodies are indispensable tools that are commonly used in several different applications in biological research. As an alternative to detecting NPRC expression by Northern blotting, *in situ* hybridization, and PCR, the antibody presented in this report, JAH84, may be used as a valuable tool to confirm NPRC protein expression by various immunoassays. JAH84 offers several attractive advantages including high sensitivity, high specificity, cross-reactivity between multiple species, low background, minimal optimization, and applicability for discovery or confirmatory purposes.

XP_526959.2 [Pan troglodytes]	RKKYRITTIERRTQQEESNLGKHRELREDSIRSHFSVA
AF231035_1 [Xenopus laevis]	RKKYRITTIERRNQQDDCNLGKHRQLREDSIRSHFSAA
AAH55897.1 [Mus musculus]	RKKYRITTIERRNQQEESNIGKHRELREDSIRSHFSVA
NP_037000.1 [Rattus norvegicus]	RKKYRITTIERRNHQEESNIGKHRELREDSIRSHFSVA
NP_776552.1 [Bos taurus]	RKKYRITTIERRNQQEESNVGKHRELREDSIRSHFSVA
AA88801.1 [Homo sapiens]	RKKYRITTIERRTQQEESNLGKHRELREDSIRSHFSVA

Figure 8. Sequence alignment of the intracellular domain of NPRC from various species. Shaded areas indicate highly conserved amino acid residues. The source of each of the partial sequences shown for NPRC can be traced from the accession numbers given on the left.

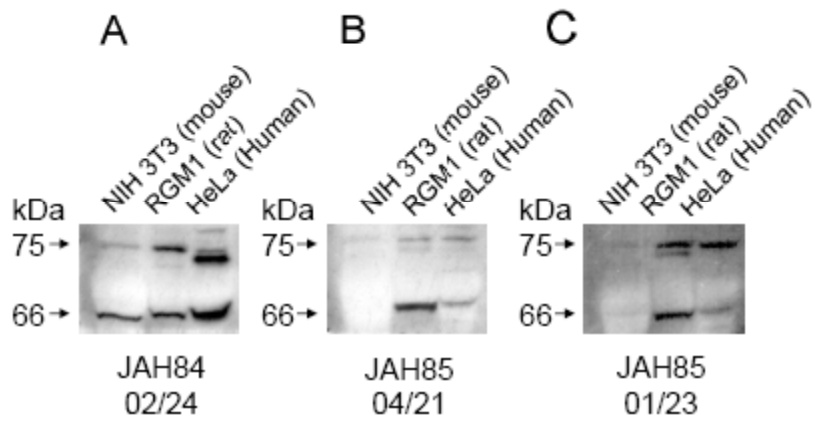


Figure 9. Western blot analysis showing cross-reactivity of various polyclonal antibodies against NPRC. The immunoreactive band at 75 kDa in panel A, was further identified as NPRC, as the band was excised and subject to mass spectrometry analysis for protein identification. The top bands in panes A, B, and C may be nonspecific.

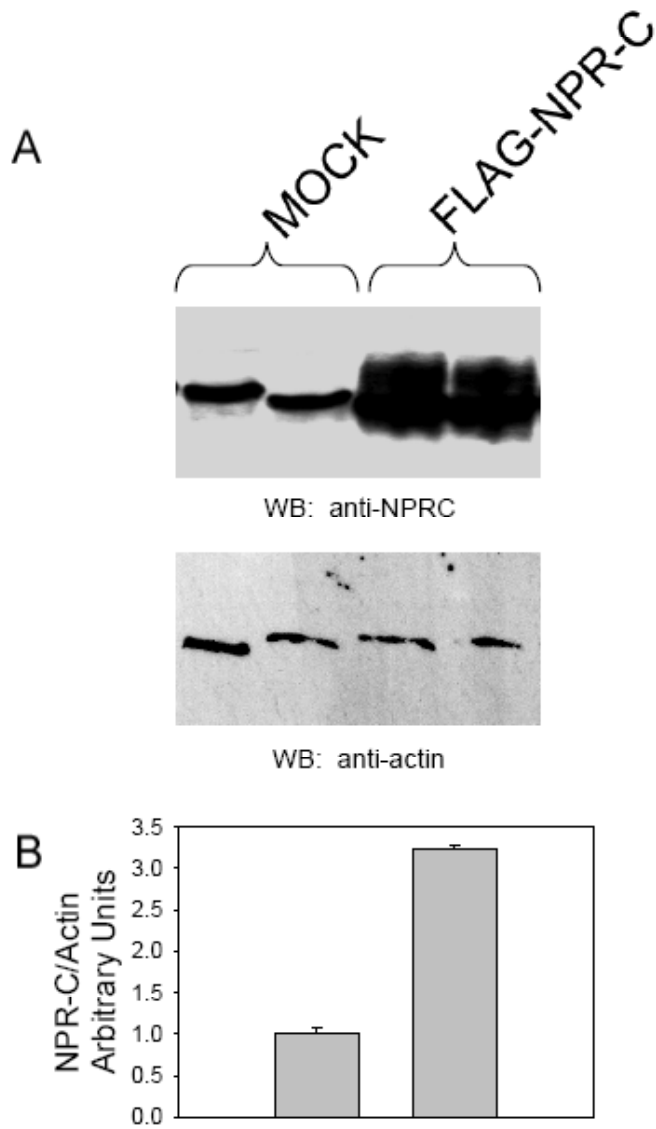


Figure 10. Western blot and densitometric analysis of flag-NPRC using JAH84 antibody. Representative immunoblot (A) and densitometric analysis (B) of FLAG-NPRC 72 hours after transient transfection of COS7 cells. The immunoblot for actin demonstrates equal loading.

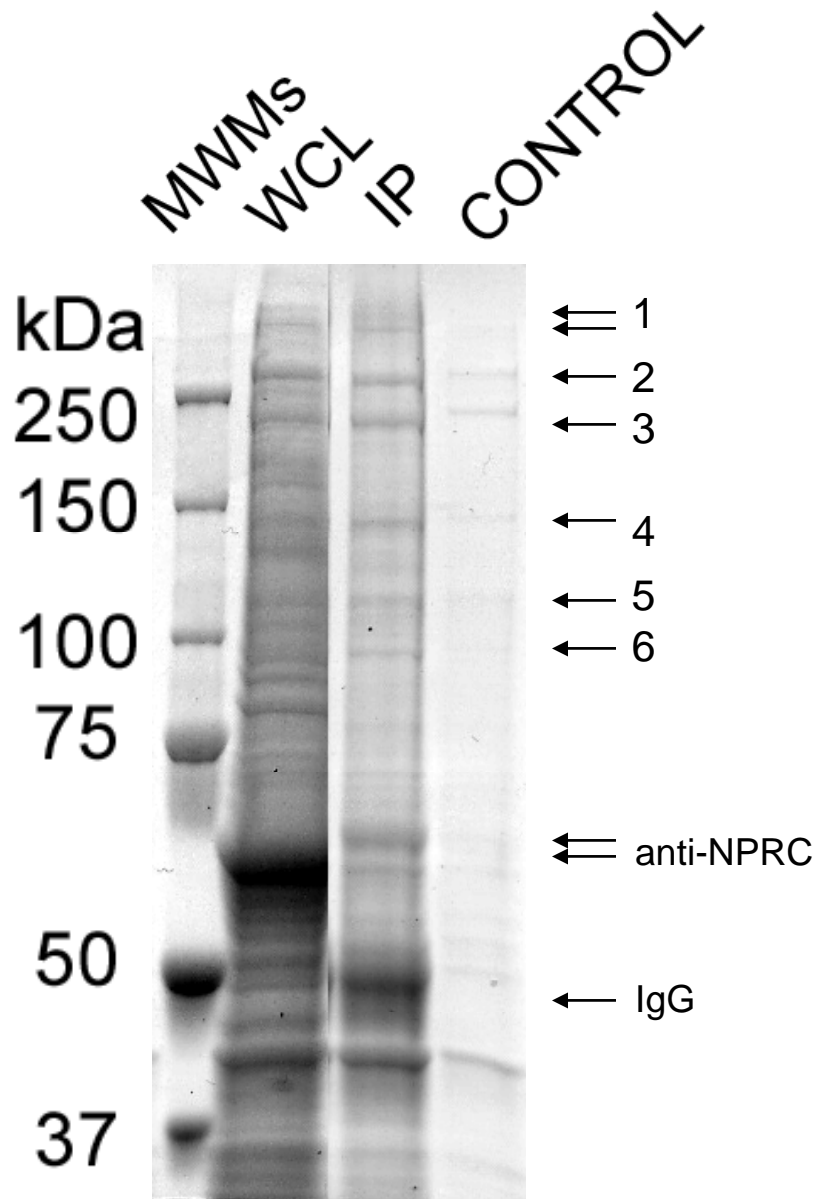


Figure 11. Coomassie blue stained gel (grayscale) after immunoprecipitation of NPRC with JAH84. From left to right (Molecular Weight Markers (MWMs), RGM1 Whole Cell Lysate (WCL), Immunoprecipitation (IP) with JAH84, Control (protein G agarose beads alone). Six putative NPRC binding proteins are indicated by arrows.

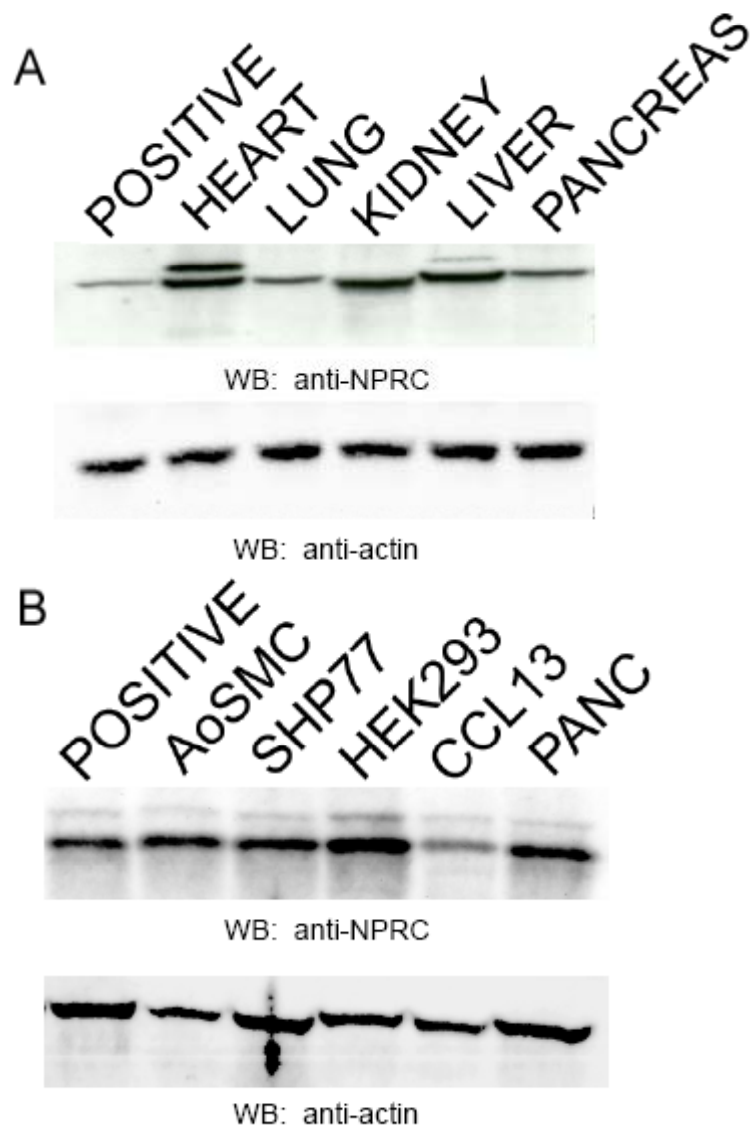


Figure 12. Western blot analysis of endogenous NPRC protein expression using JAH84 antibody. Representative immunoblots showing endogenous NPRC protein expression in various mouse tissues (A) and in various human cell lines (B). Corresponding immunoblots for actin demonstrate equal loading. POSITIVE refers to whole cell lysate positive control.

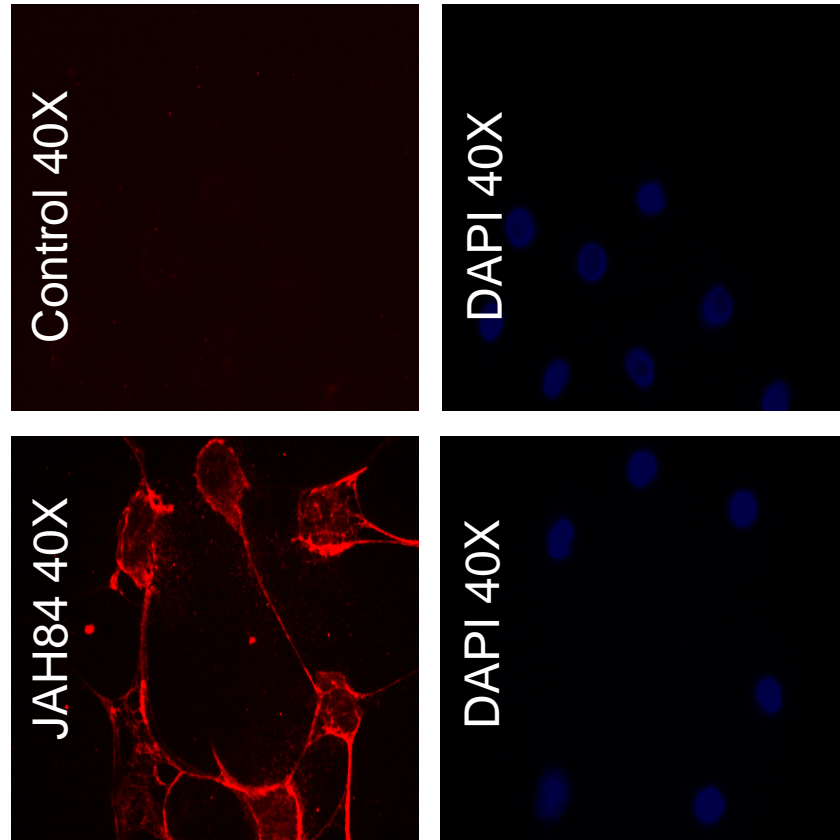


Figure 13. Immunofluorescence of RGM1 cells using JAH84. A: Negative control showing no appreciable positive staining in the absence of specific antibody. B: Nuclear staining of (A) with DAPI C: Strong positive staining is observed when using JAH84 at a dilution of 1:250. D: Nuclear staining of (C) with DAPI.

Chapter 2: Protein Binding Partners of NPRC

Background

NPRC may no longer be considered a biologically silent receptor with the only purpose being the clearance of NPs from circulation. As mentioned earlier, there have been several reports from different groups that have provided evidence of NPRC modulating signaling pathways through G α i. In order to further investigate the role of NPRC in mediating signaling transduction through G α i or independent of G α i, a proteomic approach was taken to identify novel protein binding partners for NPRC in various cell types. The identification of these novel protein-protein associations were confirmed by different methods. The molecular associations were characterized *in vitro* before investigating their functional significance *in situ*, using various cell lines that express endogenous NPRC, as mentioned earlier.

Materials and Methods

Reagents and antibodies

In addition to the reagents and antibodies mentioned in the previous chapter, the following reagents and antibodies were purchased or acquired as described. JAH84 antibody was from our laboratory [371], β -arrestin polyclonal antibody was kindly provided by Dr. R.J. Lefkowitz (Howard Hughes Medical Institute and Duke University Medical Center, Durham, North Carolina), polyclonal AHNAK1 antibody was kindly provided by Dr. Hannelore Haase (Max Delbrück Center, Berlin, Germany), monoclonal AHNAK1 antibody was purchased from Abnova (Taipei City, Taiwan), β -actin antibody was purchased from Sigma (St. Louis, MO). Hybond-C extra nitrocellulose membranes and Hyperfilm ECL were purchased from Amersham Biosciences (Piscataway, NJ). All other chemicals were purchased from Sigma unless otherwise noted. Collagen Type 1 cellware culture slides were purchased from BD Biosciences (Bedford, MA).

Cell Lines and Cell Culture

In addition to various cell lines mentioned in the previous chapter, the rat gastric mucosa cell line (RGM1) was acquired from Dr. Hirofumi Matsui (Riken, Japan) and cultured in a 1:1 mixture of Dulbecco's Modified Eagle's Medium and Ham's Nutrient F-12 (DMEM/F12) supplemented with 10% Fetal Bovine Serum (FBS; Atlanta Biologicals) and 100 U/ml penicillin, 100 μ g/ml streptomycin, and 25 ng/ml fungizone (GIBCO Invitrogen; Grand Island, NY). Cells were grown to confluent monolayers in 100 mm tissue culture dishes or chamber slides at 37°C in a humidified incubator with an atmosphere of 5% CO₂.

Immunoprecipitation

Two hundred µg of total protein cell lysate was incubated with a 1:250 dilution of anti-β-arrestin polyclonal antibody, anti-NPRC polyclonal antibody (OMORI or JAH84 as indicated) or anti-AHNAK1 polyclonal antibody at 4 °C for 2-4 hrs with end-over-end mixing. Complexes were incubated with a 1:10 dilution of prewashed 50% protein G agarose slurry at 4°C for 4-6 hrs with end-over-end mixing. Beads were washed 4X with ice cold M-PER. Immune complexes were eluted in 1X SDS sample buffer and analyzed by SDS-PAGE and Coomassie staining or Western blotting.

SDS-PAGE, Western blotting, and Densitometric analyses

SDS-PAGE and Western blotting was performed as described in the previous Chapter. Densitometry of the immunoreactive bands was performed using the ImageQuant software version 5.2 (Molecular Dynamics, Sunnyvale, CA).

Recombinant fusion protein production

cDNA fragments encoding various AHNAK1 domains were a kind gift from Dr. Takashi Hashimoto (Keio University School of Medicine, Tokyo, Japan). Domains were AHNAK N (residues 2-252), AHNAK M (residues 821-1330), AHNAK C1 (residues 4646-5145), and AHNAK C2 (residues 5146-5643). GST-AHNAK N, GST-AHNAK M, GST-AHNAK C1, and GST-AHNAK C2 were kindly provided by Dr. Silvère M. van der Maarel (Leiden University Medical Center, Leiden, Netherlands) [231]. All constructs were confirmed by DNA sequencing. Plasmids were transformed into competent *E. coli* BL21 (DE3) (Amersham Biosciences) for expression. Positive clones were grown in

2XYT kanamycin medium (16g/L tryptone, 10 g/L yeast extract, 5g/L NaCl, pH 7.0) at 37 °C. Isopropyl-d-thiogalactoside (IPTG) induction was performed at an optical density (OD₆₀₀) of 0.4 by adding IPTG to a final concentration of 0.01 M. GST-AHNAK N was obtained by traditional methods and GST-AHNAK M, C1, C2 were solubilized from inclusion bodies, as described in Chapter 4. Bacterial cells were lysed by sonication, and the fusion protein was batch purified using Glutathione Sepharose 4B. Purity of the fusion protein was analyzed by SDS-PAGE and Coomassie blue staining. Identity of the fusion protein was confirmed by Western blotting and by mass spectrometry (MS) analysis (Proteomics Dept. at the Moffitt Cancer Center, Tampa FL).

GST pull-down assay

Two hundred µg of total protein cell lysate was incubated together with 25 µg of purified GST-β-arrestin 1, GST-β-arrestin 2, GST-AHNAK1 N, GST-AHNAK1 M, GST-AHNAK1 C1, or GST-AHNAK1 C2 (as described above) or 25 µg of purified GST protein at 4 °C for 2 hrs with end-over-end mixing. The resulting complexes were incubated with 40 µl of prewashed 75% glutathione Sepharose slurry at 4 °C for 4 hrs with end-over-end mixing. Beads were washed 4X with 1 mL of ice cold GST lysis buffer (200 mM NaCl, 20 mM Tris-Cl (pH 8.0), 1 mM ethylenediaminetetraacetic acid (EDTA) (pH 8.0), 0.5% Igepal CA-630, 25 µg/mL phenylethylsulfonyl fluoride (PMSF), 2 µg/µl aprotinin, 1 µg/µl leupeptin, 0.7 µg/mL pepstatin). Bound proteins were eluted with 50 µl of 20 mM reduced glutathione in 50 mM Tris-Cl (pH 8.0) and then analyzed by SDS-PAGE and Western blotting.

Overlay binding assay (far-Western)

25 µg of cell lysate was separated by SDS-PAGE and blotted onto nitrocellulose membranes. The blots were blocked in 5% BSA 1X PBS for 1 hr at RT. The membranes were overlaid with purified GST or GST-NPRC (see Chapter 4) in blocking solution for 2 hours at RT, washed with 1X PBS, and probed for GST. A schematic of the overlay binding assay, or far-Western blot is illustrated in Figure 14.

Mammalian two hybrid and dual-luciferase assay

The mammalian two-hybrid and the dual-luciferase reporter assay system (CheckMate; Promega, Madison, Wis) was optimized for investigating the association between NPRC and β -arrestins or NPRC and AHNAK1 *in situ*. A schematic of the mammalian two hybrid assay is illustrated in Figure 15. For the mammalian two-hybrid assay, two positive control vectors that encode and express two proteins known to interact *in vivo*, Id and MyoD, were included in the assay kit for use as pBIND-Id (GAL4-Id) and pACT-MyoD (VP16-MyoD) fusion constructs. In order to confirm the association between NPRC and β -arrestins or AHNAK1 *in situ*, pACT NPRC and pBIND NPRC, pACT β -arrestin1 and pBIND β -arrestin1, pACT AHNAK1 and pBIND AHNAK1 constructs were created as shown in Appendix B-F. Between 48 to 72 hrs after transfection, the cells were lysed with 1X passive lysis buffer (Promega) and the activities of firefly (*Photinus pyralis*) and *Renilla* (*Renilla reniformis*) Luciferases were measured sequentially. The activity of the firefly luciferase reporter was measured first by adding Luciferase assay reagent II (LAR II) to generate a luminescent signal. After quantifying the firefly luminescence, the reaction was quenched, and the *Renilla*

luciferase reaction was initiated simultaneously by adding Stop & Glo[®] reagent to the same sample.

Statistics

Results are expressed as the mean \pm SE of three independent experiments, as indicated. Repeated measures ANOVA was conducted and statistical significance was set at $p < 0.05$. Here, by convention, * $p < 0.05$, ** $p < 0.005$, *** $p < 0.0005$. Student's *t*-test was used to compare two groups and one-way ANOVA was used to compare multiple groups.

Results

The cytoplasmic domain of NPRC contains consensus sequence binding motifs for β -arrestin

The 37 amino acid cytoplasmic domain of both rat and human NPRC contains at least a single consensus sequence binding motif for β -arrestin, as shown in Figure 16. The binding motif consists of a serine or threonine residue followed by any four to five amino acids followed by a serine or threonine residue, (-S/TX4-5S/T) [372]. Although no GRK phosphorylation motifs were identified within the cytoplasmic domain of NPRC, several putative PKA, PKB, and PKC phosphorylation sites were identified using motif scanner (http://scansite.mit.edu/motifscan_seq.phtml) and NetPhos 2.0 (www.cbs.dtu.dk/services/NetPhos) (Figure 16).

NPRC associates with β -arrestin in vitro

Preliminary immunoprecipitation studies were performed using β -arrestin specific antibody to pull-down β -arrestin and its protein bind partners in A-10 VSMCs. Subsequent SDS-PAGE analysis of the elutants from the β -arrestin immunoprecipitation studies, revealed several putative protein binding partners for β -arrestin as indicated by Ponceau staining. Probing the membranes with an antibody against NPRC revealed an immunoreactive band at 66 kDa, corresponding to NPRC (Figure 17A). Similarly, β -arrestins were also shown to associate with NPRC *in vitro* in HeLa cells as indicated by immunoprecipitation studies (Figure 17B). Mouse embryonic fibroblasts (MEF) lacking β -arrestin 1, β -arrestin 2, or both β -arrestin 1 and β -arrestin 2 were evaluated for NPRC expression as they could serve as a nonspecific control while performing

immunoprecipitation studies. Interestingly, Western blot analysis revealed NPRC is expressed in each of the MEF cell lines, with the exception for MEF β -arrestin knockout 1 (Figure 17C).

The in vitro association between NPRC and β -arrestins is dependent on NPRC occupancy

Next, additional immunoprecipitation studies were performed to determine if NPRC associates with β -arrestin in NIH 3T3 cells and if the association was dependent on receptor occupancy. NIH-3T3 cells were treated with 1 μ M cANF for 0, 2, 5, and 20 minutes before harvesting the cells for protein, in the presence of phosphatase inhibitors in order to perform IP-Western blot analysis. The association between NPRC and β -arrestins was significantly augmented with the treatment of cANF over time, as indicated by increasing intensity of the immunoreactive band at 66 kDa corresponding to NPRC shown in Figure 18.

NPRC predominantly associates with β -arrestin 1 in vitro

Afterwards, the ability of NPRC to associate with β -arrestins in RGM1 cells and specificity of the β -arrestin isoform involved in the association was investigated. GST- β -arrestin 1 and 2 were expressed and purified, and then used as bait proteins in GST pull-down assays. GST- β -arrestin 1 was found to be the predominant isoform to be associated with NPRC *in vitro*, although β -arrestin 2 was also able to pull-down NPRC in RGM1 cells, but to a lesser extent (Figure 19).

NPRC associates with AHNAK1 isoform 1

In order to identify other putative NPRC binding partners and to confirm the association between NPRC and β -arrestins, NPRC was immunoprecipitated from AoSMC or RGM1 cell lysates. The elutants were electrically separated by SDS-PAGE, and the resulting bands from Coomassie blue stained gels were excised and subjected to MS analysis for protein identification. While using either AoSMC or RGM1 cell lysates as a source of the prey protein, Coomassie stained gels revealed several bands representing putative NPRC associating proteins, including a high molecular weight double band above 250 kDa. For experiments utilizing AoSMC lysate, Mascot results of the excised double band revealed multiple signature peptides corresponding to human AHNAK1 isoform 1 (Figure 21). Similarly, for experiments utilizing RGM1 lysate, Mascot results of the excised double band revealed multiple signature peptides corresponding to rat AHNAK1 isoform 1 (Figure 22). Also, NPRC was found to associate with AHANK in 3T3-L1 preadipocytes (Figure 23). The ability of at least AHNAK1 isoform 1 to associate with NPRC was corroborated by IP Western blot analysis, while utilizing a polyclonal antibody against the carboxy terminal domain of AHNAK1, which is known to differ between the two AHNAK1 isoforms. A band corresponding to NPRC was observed after immunoprecipitating AHNAK1 with this antibody from AoSMC, RGM1, or 3T3-L1 lysates and probing for NPRC with a polyclonal antibody against the cytoplasmic domain of NPRC, as demonstrated in Figure 21C, 22C, and 23C respectively.

The C1 Domain of AHNAK1 I associates with NPRC

The association between NPRC and AHNAK1 was corroborated in AoSMCs by expression and purifying GST fusion proteins specific to each of the distinct functional domains of AHNAK1, (i.e. AHNAK1 N (amino terminal residues 2-252), AHNAK1 M (central repeat unit residues 821-1330), and two carboxy terminal domains (AHNAK1 C1, residues 4646-5145 and AHNAK1 C2, residues 5146-5643), as shown in Figure 24) and then performing GST pull-down assays. Verification of molecular weight and purity of GST-AHNAK1N, GST-AHNAK1M, GST-AHNAK1C1, and GST-AHNAK1C2 was determined by SDS-PAGE followed by Coomassie blue staining and direct Western blot analysis for GST (Fig 24B, C). Thereafter, *in vitro* GST pull-down assays were performed using cell lysate from AoSMCs and the purified GST-AHNAK1 fusion proteins. Only GST-AHNAK1C1 was able to pull-down NPRC (Figure 24D). In similar experiments, GST-AHNAK1C1 was not able to pull-down NPRA or NPRB, and in other experiments, NPRA and NPRB specific antibodies also failed to pull-down AHNAK1 (Figure 25).

Phosphorylation and occupancy of NPRC is not required for it to associate with AHNAK1

Unphosphorylated GST-NPRC was overlaid on nitrocellulose membranes containing endogenous AHNAK1 from phosphatase treated or untreated RGM1 lysate. In the presence or absence of phosphatase inhibitors, GST-NPRC was able to bind to AHNAK1 (Figure 26). GST pull-down assays demonstrated NPRC occupancy by ligand was not necessary for it to associate with AHNAK1. RGM1 cells pretreated with the

NPRC agonist cANF for increasing periods of time did not augment the association between NPRC and AHNAK1 (Figure 27).

Expression of AHNAK1, NPRs, G α_i and PLC isoforms in 3T3-L1, AoSMCs, and RGM1 cells

Endogenous protein expression levels of AHNAK1 and NPRC were assessed in the cell lines intended for use in the investigation of the role of the association between NPRC and AHNAK1. Both AHNAK1 and NPRC are coexpressed in 3T3-L1 preadipocytes, RGM1 cells, and AoSMCs (Figure 28). NPRA and NPRB proteins are expressed in 3T3-L1 preadipocytes and AoSMCs, but are not expressed in RGM1 cells (Figure 28). Because AHNAK1 and NPRC are known to activate different isoforms of PLC, these cell lines were screened for expression of various PLC isoforms. Interestingly, 3T3-L1 preadipocytes, RGM1 cells, and AoSMCs do express various levels of endogenous PLC γ 1, but do not express any appreciable levels of PLC γ 2, and do express various levels of endogenous PLC β 3 (Figure 29). Also, the expression of G α_i was investigated in these cell lines, since NPRC is known to couple to G α_i , which could potentially be involved in the function role between NPRC and AHNAK1. G α_i was found to be expressed in HeLa cells, AoSMCs, RGM1 cells, and 3T3-L1 preadipocytes (Figure 29D).

NPRC and AHNAK1 are differentially expressed during mouse adipogenesis

The progression of the differentiation of 3T3-L1 cells into mature adipocytes was monitored every other day by phase-contrast microscopy and Oil Red O staining for the

accumulation of lipid droplets (Figure 30A, B). At each corresponding day, protein expression of the NPRs, AHNAK1, and PPAR γ were assessed by Western blot analyses. There were no significant changes in NPRA or NPRB protein expression during the course of differentiation for days 0-6 (Figure 31B, C). However, AHNAK1 protein expression significantly decreased (Figure 31A, E) and NPRC protein expression significantly increased from days 0-6 (Figure 31D, F). The differential regulation of AHNAK1 and NPRs proteins during the course of 3T3-L1 differentiation was confirmed in later stages of differentiation of 3T3-L1 preadipocytes and also in mouse adipose tissues. NPRA and NPRB protein expression was low and constant in days 8-12, while NPRC protein expression was high and constant for days 8-12 of 3T3-L1 differentiation (Figure 32), and in adipose tissues from three different mouse donors for AHNAK1 and NPRs (Figure 33).

Translocation of AHNAK1 from the nucleus to the plasma membrane

Various determinants were investigated for the translocation of AHNAK1 from the nucleus to the plasma membrane. The addition of PMA resulted in a subtle increase in AHNAK1 translocation from the nucleus to the cytoplasm (Figure 34). A switch in medium containing low calcium to medium containing high calcium resulted in AHNAK1 translocation from the nucleus to the plasma membrane of 3T3-L1 preadipocytes (Figure 35). siRNA mediated knockdown of NPRC resulted in AHNAK1 accumulation in the nucleus and less AHNAK1 associated with the plasma membrane (Figure 36, 37).

Discussion

Two different types of scaffolding/adaptor proteins were identified as novel binding partners of NPRC. The β -arrestins, which are known to associate with the intracellular domains of various cell surface receptors [372] were found to associate with NPRC *in vitro*. AHNAK1, a large and versatile protein implicated in a wide range of functions was also found to associate NPRC *in vitro* and *in situ*.

Many biological processes are governed or dependent on protein-protein interactions. The interaction of two or more proteins may directly or indirectly affect various cellular functions by different means including altering the specificity of a protein for its substrate, altering the kinetic properties of an enzyme, targeting the protein for degradation, and coupling the protein to downstream signaling pathways. The interactions between proteins arise from the physical interactions between specific regions on the surface of the proteins. The association or dissociation between proteins may be dependent on various physiological conditions. Protein-protein interactions may be stable or transient in nature and either type of interaction may be strong or weak and fast or slow. Transient protein-protein interactions, which are temporary, are more prevalent in nature and are also more difficult to study than stable protein-protein interactions because the interacting proteins may dissociate during the study. Both the association between NPRC and β -arrestins and the association between NPRC and AHNAK1 may be considered to be weak and transient.

The bait-prey system is commonly used to investigate protein-protein interactions. By convention, the bait protein is the known protein or protein of interest that is used to capture the prey protein or unknown protein binding partner. The two

phases of protein-protein investigations are the discovery and the confirmation phases. It may be useful to use an endogenous source for the bait and/or prey proteins, in which both native proteins are functional to allow for physiological relevant findings. Conversely, it may be beneficial to use an artificial source for the bait and/or prey proteins to confirm a previously identified protein-protein association because it allows for the ability to work with a larger quantity of the protein than would normally be expressed in the endogenous environment, and it reduces complexities that would arise from additional interacting protein binding partners present in the endogenous environment.

NPRC is known to couple to $G\alpha_i$ and participate in the activation of the PLC cascade and inhibition of the adenylyl cyclase cascade, but the direct association between NPRC and putative protein binding partners that would mediate its role in signal transduction cascades has not been identified. Therefore, a proteomic approach to identify putative protein binding partners of NPRC was carried out in various cell lines, in which NPRC was shown to be expressed. The cell lines were used as model systems to subsequently decipher the physiological role of NPRC and its protein binding partners. Initial co-IP studies identified the β -arrestins as being putative binding partners for NPRC *in vitro*. The association between GPCRs and β -arrestins has significant implications because the 7TMRs represent the largest and most versatile family of membrane receptors. Consequently, 7TMRs regulate metabolism, secretion, cell shape, motility electrical activity in response to wide range of hormones and stimuli and are therefore the most common target of therapeutic drugs [373].

The ability of NPRC to associate with β -arrestins could contribute to the regulation of NPRC protein and the regulation of NPRC signaling. Phosphorylation and activation of NPRC by ligand binding may result in the recruitment and interaction of cytosolic β -arrestins. The association between NPRC and β -arrestins may result in the complex binding to components of the clathrin endocytic machinery, leading to downregulation, or a decrease in the number of NPRC molecules at the cell surface. Alternatively, the association between NPRC and β -arrestins may result in homologous desensitization, as the association precludes the coupling between NPRC and G_i , leading to termination of signaling by G protein effectors. Moreover, the ability of NPRC to associate with β -arrestins may implicate NP mediated activation of NPRC in in other signaling cascades in addition to AC and PLC, since β -arrestins are known to function as adaptor proteins.

Since the AHNAKs, AHNAK1 and AHNAK2, are known to possess differences between the amino and carboxy terminal domains, the utilization of a polyclonal antibody against the carboxy terminal domain of AHNAK1 was expected to pull-down AHNAK1 and not cross-react with AHNAK 2 in immunoprecipitation experiments. Although immunoprecipitating AHNAK1 with this antibody and probing for NPRC cannot be used to definitively determine the specific interacting AHNAK1 isoform, it was used to demonstrate the ability of at least AHNAK1 to associate with NPRC *in vitro*. In order to identify the specific AHNAK1 isoform that associates with NPRC, NPRC was immunoprecipitated from AoSMC or RGM1 cell lysates and the bands on Coomassie blue stained gels representing putative NPRC associated proteins were excised and subject to MS analysis for protein identification. The elutants from the NPRC

immunoprecipitation experiments may have contained AHNAK1, AHNAK2, or AHNAK-like proteins. However, Mascots results revealed multiple signature peptides corresponding only to AHNAK1, thus confirming AHNAK1 and not AHNAK 2 associates with NPRC.

After determining AHNAK1 associates with NPRC *in vitro*, GST pull-down assays utilizing distinct functional domains of AHNAK1 as GST fusion proteins were performed in order to identify the specific AHNAK1 domain that associates with NPRC *in vitro*. Although it was theoretically possible for any of the four distinct and functional domains of AHNAK1 to interact with NPRC, GST pull-down assays only revealed AHNAK1 C1 as being able to pull-down NPRC from an AoSMC lysate. Identification of the AHNAK1 domain that interacts with NPRC was necessary for the design and construction of AHNAK1 fusion proteins for investigating the role of molecular association in mediating calcium signaling *in situ*, as AHNAK1 is an extraordinary large protein and if used in its entirety, would most likely pose major difficulties in experiments involving transfection. Therefore, only a portion of AHNAK1 containing several repeating units and the carboxy terminal domain of AHNAK1 were used to create a pBIND-AHNAK1 fusion protein. Several repeating units of AHNAK1 were included because these segments are necessary for the binding and activation of PLC γ and the carboxy terminal domain of NPRC were included because this domain was shown to interact with NPRC.

Several attributes were considered for the selection of a suitable cell line for the functional interrogation of the association between NPRC and AHNAK1 *in situ*. In addition to expressing endogenous NPRC, AHNAK1, and PLC γ 1 proteins, the cell line

needed to tolerate transfection of siRNAs for knockdown of NPRC and AHNAK1 or plasmid DNA for overexpression of an AHNAK1 fusion protein. Preliminary studies for the optimization of transient transfection of the AHNAK1 fusion protein presented difficulties in RGM1 cells and in AoSMCs, while desirable transfection efficiencies were achieved in 3T3-L1 preadipocytes using the Fugene method. The cell line also needed to tolerate loading with the calcium indicator dye Fluo-3, respond to various exogenous agents in the micro molar range, and be suitable for real time live cell confocal microscopy imaging studies for motoring changes in intracellular calcium mobilization. AoSMCs and 3T3-L1 cells met these requirements and responded to various exogenous agents used as positive controls (e.g. ET-1) or used as a loading control (e.g. ionomycin). However, RGM1 cells did not tolerate Fluo-3 loading nor did it respond to any of the positive controls or loading control. As shown in Figure 31, NPRC and AHNAK1 protein expression is inversely proportional over the course of differentiation of 3T3-L1 preadipocytes into mature adipocytes after insulin, dexamethasone, and IBMX treatment. While both NPRC and AHNAK1 proteins are expressed in 3T3-L1 preadipocytes and in the early stages of differentiation, NPRC protein is overexpressed and AHNAK1 protein is attenuated in mature adipocytes. Future studies may be performed to determine if NPRC and AHNAK1 proteins are directly affected by insulin, dexamethasone, and IBMX treatment. Since 3T3-L1 preadipocytes express both NPRC and AHNAK1 proteins, tolerate transient transfection of siRNAs and plasmid DNA, and tolerate loading with Fluo-3 AM these cells were used for all *in situ* studies involving transient transfection of either siRNAs or plasmid DNA.

Haase *et al.* investigated the role of the C1 domain of AHNAK1 in the signal transduction pathway between the beta-adrenergic receptor and the L-type Ca^{2+} channel [374]. The association between the C1 domain of AHNAK1 and the $\beta 2$ subunit was shown to be dependent on PKA phosphorylation of both proteins, as the binding affinity decreased approximately 50% upon PKA phosphorylation of both protein partners [374]. Haase *et al.* suggested that the C1 domain of AHNAK1 operates as a phosphorylation-dependent suppressor of the L-type Ca^{2+} channel, and liberation of this suppression results in more available $\beta 2$ subunit to associate with the L-type Ca^{2+} channel, resulting in enhanced current density [374]. Furthermore, in another report Haase *et al.* reported the carboxy terminal domain of AHNAK1 as the interacting domain for the regulatory β subunit of L-type Ca^{2+} channels and for F-actin and suggested that this domain links the Ca^{2+} channels to the actin-based cytoskeleton. Lee *et al.* showed the M domain of AHNAK1, consisting of the repeating units of AHNAK1 function as a scaffolding motif networking PLC-gamma and PKC-alpha [239]. While considering the distinct structural domains of AHNAK1 and the reports of specific AHNAK1 domains to interact with other proteins, the ability of the C1 domain of AHNAK1 to associate with NPR-C is structurally and functionally relevant. It is plausible that the extraordinary size and conformation of AHNAK1 contributes to its distinct structural domains to be positioned or accessible for the direct interaction with its various protein binding partners. For example, the C1 domain of AHNAK1 was found to associate presumably, with the intracellular domain of NPRC. It may be expected and conceivable for either the amino terminal domain or the carboxy terminal domain of AHNAK1 to associate with NPRC and not the middle region of AHNAK1, since it is likely to be occupied after forming a

complex with PLC and PKC. Furthermore, due to the carboxy terminal domain of AHNAK1 being considerably larger and containing more putative binding regions than the amino terminal domain of AHNAK1, it would seem more likely for the carboxy terminal domain of AHNAK1 to associate with NPRC than it would for the amino terminal domain of AHNAK1 to associate with NPRC.

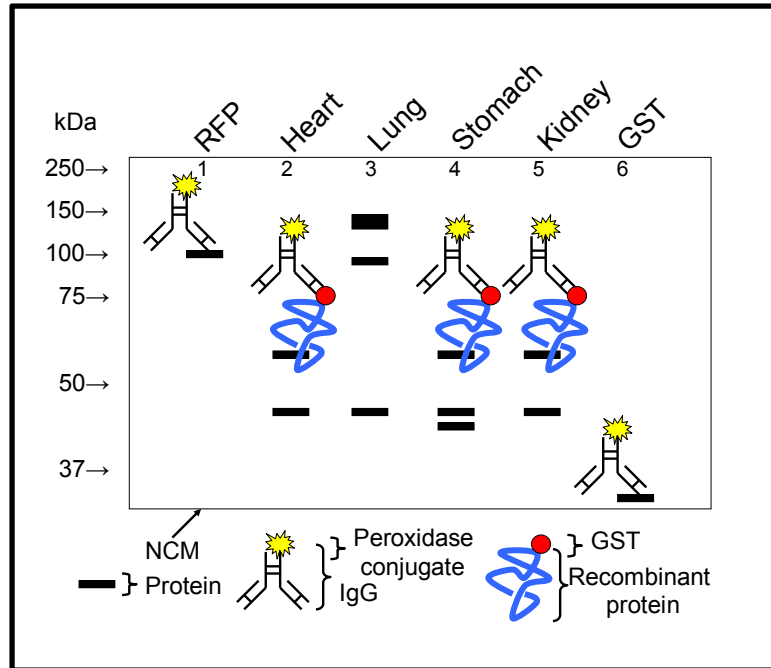


Figure 14. Schematic of the far-Western (protein overlay assay) technique. Proteins from various cell lines/tissues, the Recombinant Fusion Protein (RFP) that will be used to probe for putative protein-protein interactions, and the unfused Glutathione S Transferase (GST) protein are loaded onto separate lanes of a polyacrylamide gel so that lanes 1-6, lanes 7-12, and lanes 13-18 are analogous. Proteins are separated by SDS PAGE and then electrically transferred onto a Nitrocellulose Membrane (NCM). The NCM is cut in three identical strips to allow for two far-Westerns and one Western to be run in parallel. Two of the NCM strips are overlaid with either RFP or GST (for far-Westerns) and the third NCM strip is incubated with a specific antibody for the prey protein. For far-Westerns a peroxidase conjugated anti GST antibody is used to detect an interaction between the RFP and the prey protein. The protein interaction is confirmed by the absence of a signal in the far-Western blot using GST as the probe and by the presence of a signal for the prey protein in the Western blot using a specific antibody. In this figure the 100 kDa RFP bound to a 55 kDa prey protein present in heart, stomach, and kidney, but not lung. As controls, the peroxidase conjugated anti-GST antibody bound to the RFP in lane 1 and to GST at 26 kDa in lane 6.

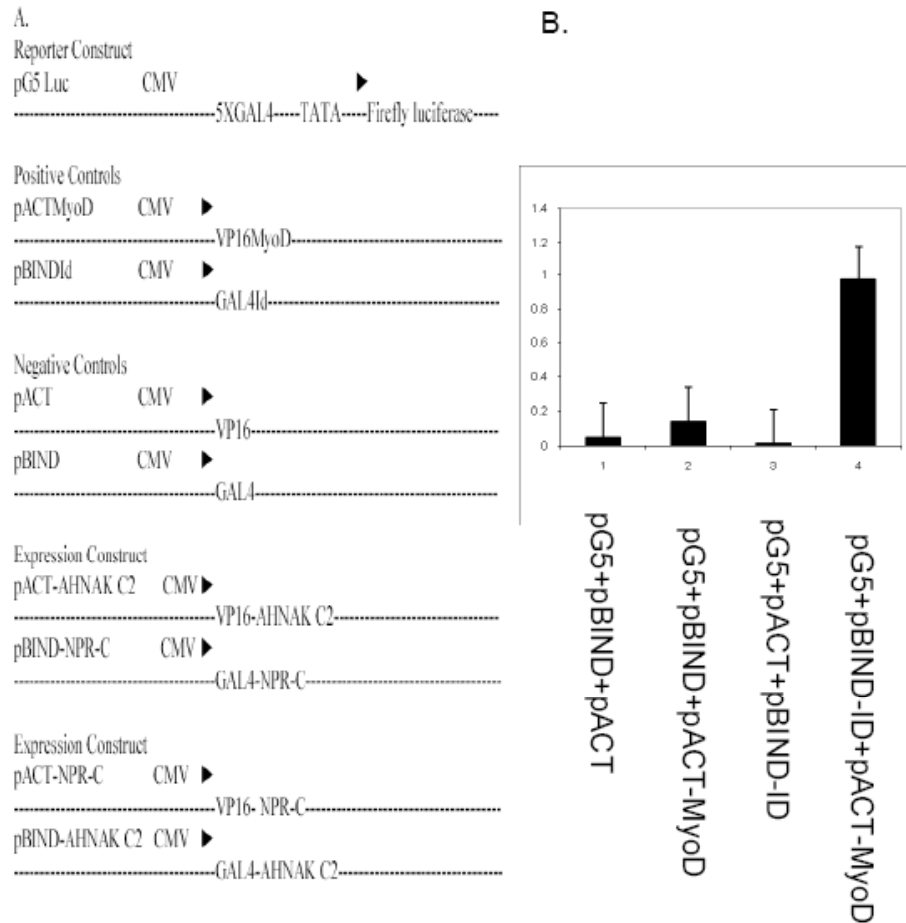


Figure 15. Representation of constructs used in the mammalian two hybrid dual luciferase assay. The reporter construct is designated pG5 Luc, positive controls known to interact are designated pACT-MyoD and pBIND-ID, negative empty vectors are designated pACT and pBIND, and expression constructs include pACT-AHNAK1C2, pBIND-AHNAK1C2, pACT-NPRC, and pBIND-NPRC. **B.** Experiments demonstrating functionality of the assay based on the fold induction of the interaction between pBIND-ID with pACT-MyoD compared to the controls.

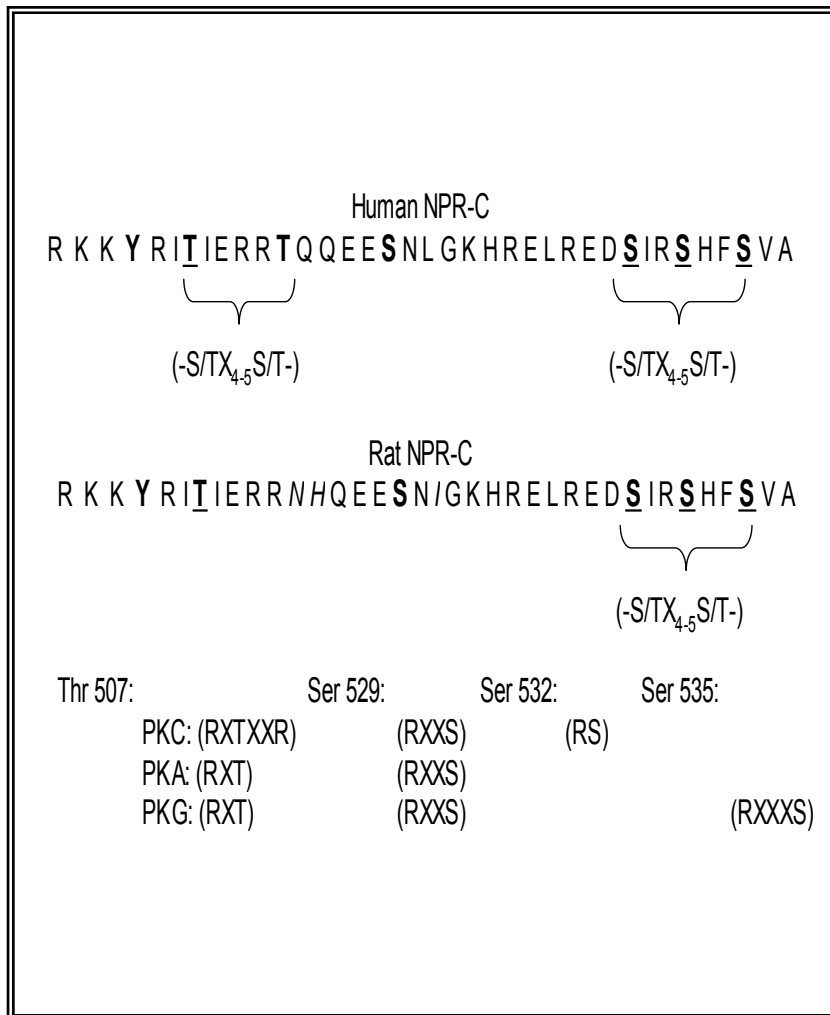


Figure 16. Sequence alignment of the 37 amino acid cytoplasmic domain of human and rat NPRC. Two independent consensus sequence binding motifs for β -arrestin (-S/TX_{4,5}S/T) are shown for human NPRC and one such motif is shown for rat NPRC. Several consensus sequences for protein kinase C, A, and G are shown for both human and rat NPRC.

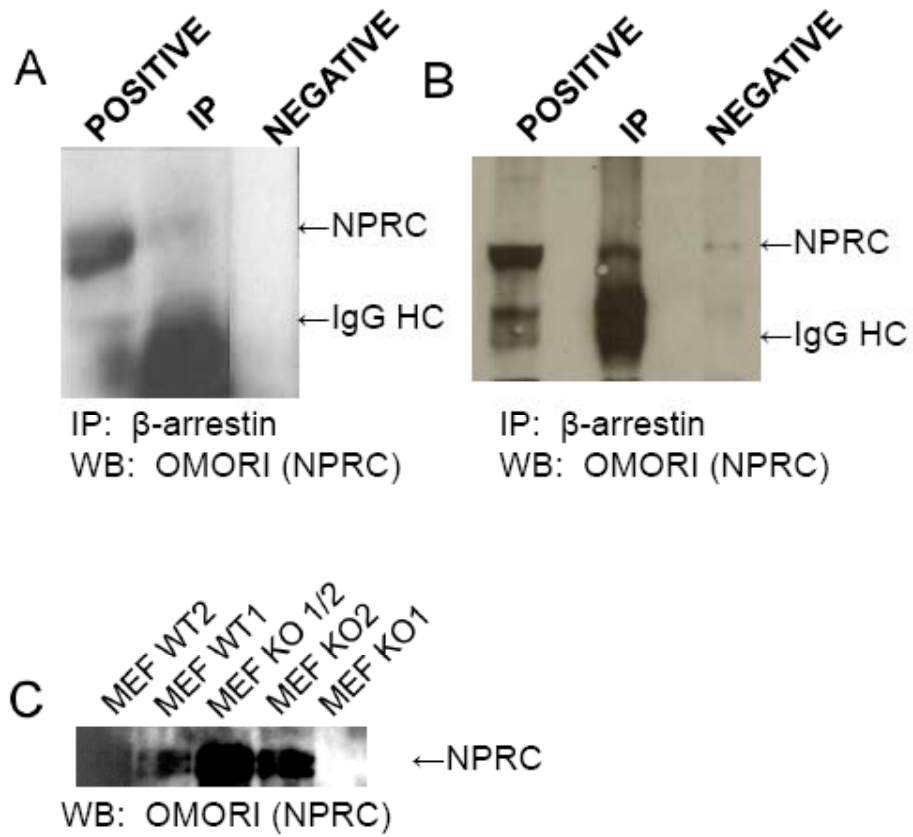


Figure 17. In vitro IP-Western demonstrating the association between NPRC and β -arrestins. A: A-10 VSMC; B: HeLa cells; C: Western blot showing NPRC expression in different β -arrestin mouse embryonic fibroblast knockouts. IgG HC refers to the heavy chain (50 kDa) of reduced and SDS-denatured rabbit IgG. POSITIVE refers to positive control consisting of whole cell lysate from NIH 3T3 cells.

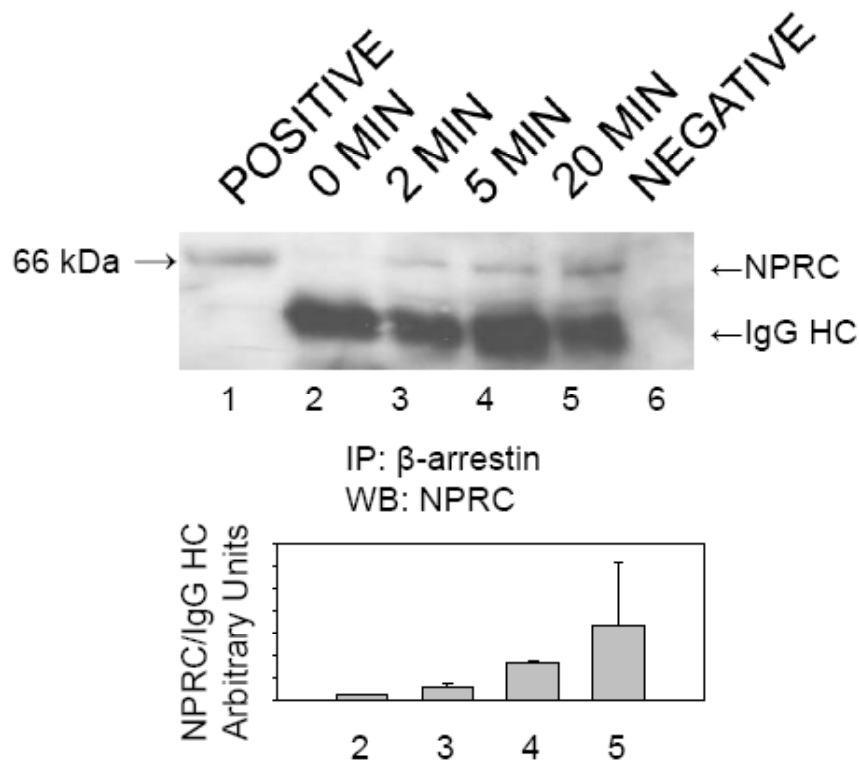


Figure 18. Effect of NPRC occupancy on its association with β -arrestins. NIH3T3 cells were treated with 1 μ M cANF for the indicated times, β -arrestin was immunoprecipitated from the lysate, and Omori anti-NPRC antibody was used to probe for NPRC protein. POSITIVE refers to positive control consisting of whole cell lysate from NIH 3T3 cells. NEGATIVE refers to negative control in which β -arrestin specific antibody was omitted and the nonspecific binding of the protein G agarose beads was assessed. IgG HC refers to heavy chain of immunoglobulin G.

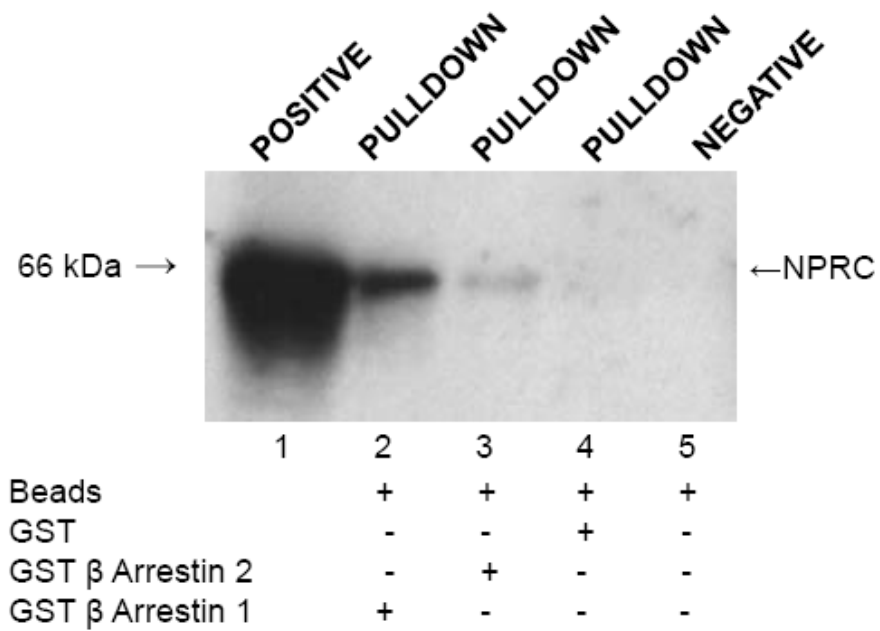


Figure 19. In vitro GST pulldown assay showing specificity of β arrestin isoforms for NRC. GST- β Arrestin1, GST- β Arrestin2, GST, or beads alone were used to pulldown NRC from RGM1 cell lysate. The blots were probed for NRC. POSITIVE refers to positive control of whole cell lysate from RGM1 cells.

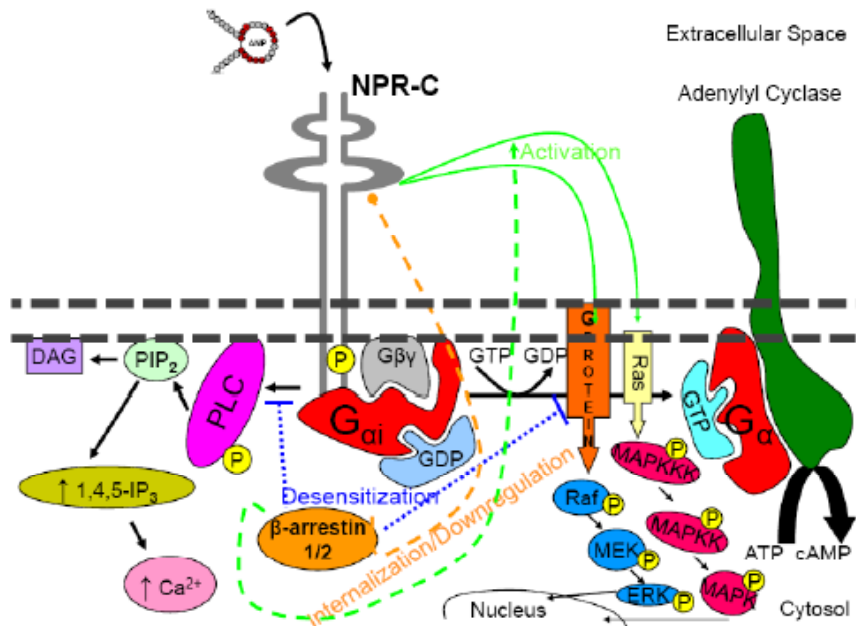


Figure 20. Model illustrating the hypothesized role of β -arrestin 1/2 in mediating NPRC signaling. Natriuretic peptides bind and activate the membrane bound phosphorylated NPRC homodimer. Thereafter, cytosolic β -arrestin is recruited and binds to specific consequence sequences within the C-terminal domain of NPRC. β -arrestin is shown (blue dotted lines) to desensitize NPRC signaling by uncoupling the receptor from G_i and further G protein dependent signaling. The association of NPRC with β -arrestin is shown to internalize and downregulate NPRC (orange dotted line). The association of NPRC with β -arrestin is shown (green lines) to activate other signaling cascades including that of MAPK and ERK. *Inhibitory guanine nucleotide-regulatory protein (G_i). 3'-5' cyclic adenosine monophosphate (cAMP), inositol triphosphate (IP₃), diacylglycerol (DAG), calcium ions (Ca^{2+}), phospholipase C (PLC), mitogen activated protein kinase (MAPK) and extracellular signal-regulated kinase (ERK).*

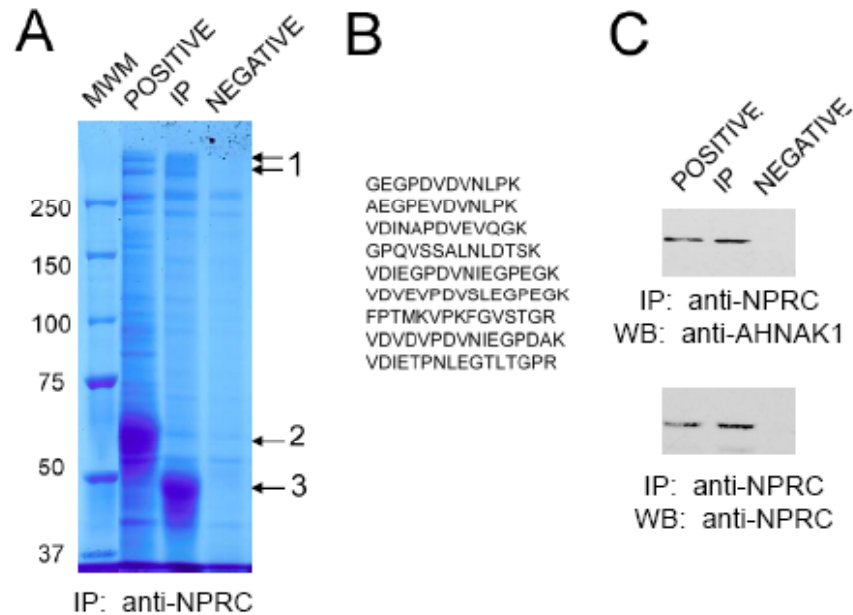


Figure 21. Molecular association of NPRC and AHNAK1 in AoSMC. **(A)** Coomassie blue staining of immunoprecipitates from AoSMC lysate using anti-NPRC antibody (JAH84) revealed a high molecular weight double band with a molecular weight above 250 kDa. **(B)** MASCOT results of the excised double band indicated in (A) revealed multiple signature peptides corresponding to human AHNAK1 isoform 1. **(C)** IP Western of immunoprecipitates from AoSMC lysate using anti-NPRC antibody probing for AHNAK1 protein (top) or NPRC protein (bottom). In panels A and C POSITIVE refers to positive control consisting of whole cell lysate and NEGATIVE refers to negative control in which NPRC specific antibody was omitted and the nonspecific binding of the protein G agarose beads was assessed. The labeled bands are AHNAK1 (1), NPRC (2), and IgG (3). Data are representative of at least three independent experiments.

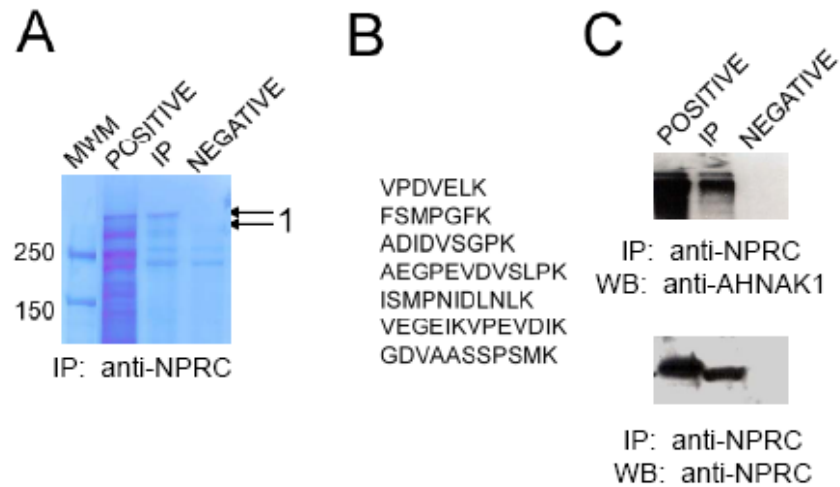


Figure 22. Molecular association of NPRC and AHNAK1 in RGM1 cells. **(A)** Coomassie blue staining of immunoprecipitates from RGM1 lysate using anti-NPRC antibody revealed a high molecular weight double band with a molecular weight above 250 kDa. **(B)** MASCOT results of the excised double band indicated in **(A)** revealed multiple signature peptides corresponding to rat AHNAK1 isoform 1. **(C)** IP Western of immunoprecipitates from RGM1 lysate using anti-NPRC antibody probing for AHNAK1 protein (top) or NPRC protein (bottom). In panels **A** and **C** POSITIVE refers to positive control consisting of whole cell lysate and NEGATIVE refers to negative control in which NPRC specific antibody was omitted and the nonspecific binding of the protein G agarose beads was assessed. The labeled bands are AHNAK1 (1), NPRC (2), and IgG (3). Data are representative of at least three independent experiments.

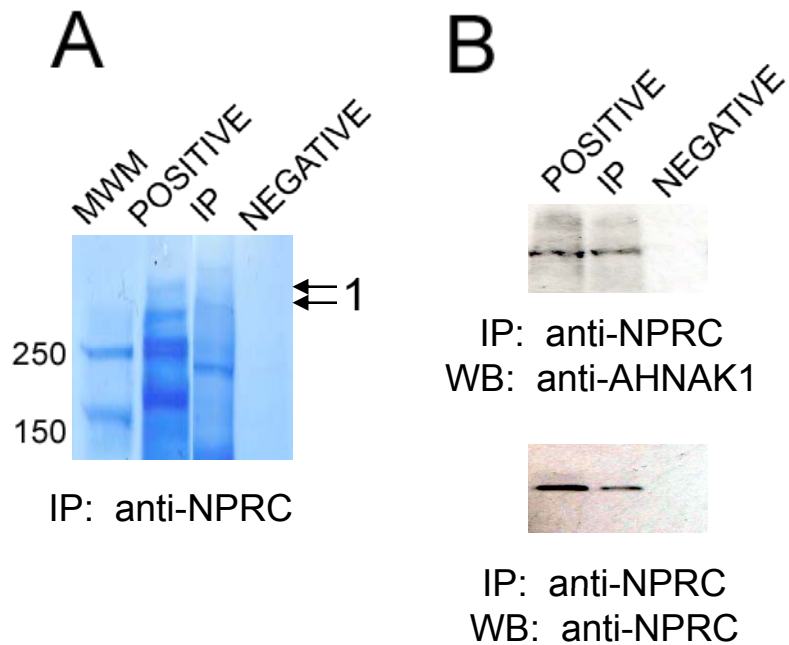


Figure 23. Molecular association of NPRC and AHNAK1 in 3T3-L1 cells. **(A)** Coomassie blue stained gel and IP Western confirming the association between NPRC and AHNAK1 in 3T3-L1 cells. **(B)** IP Western confirming the association between NPRC and AHNAK1 in 3T3-L1 preadipocytes. In panels A and B POSITIVE refers to positive control consisting of whole cell lysate and NEGATIVE refers to negative control in which NPRC specific antibody was omitted and the nonspecific binding of the protein G agarose beads was assessed. The labeled bands are AHNAK1 (1). Data are representative of at least three independent experiments.

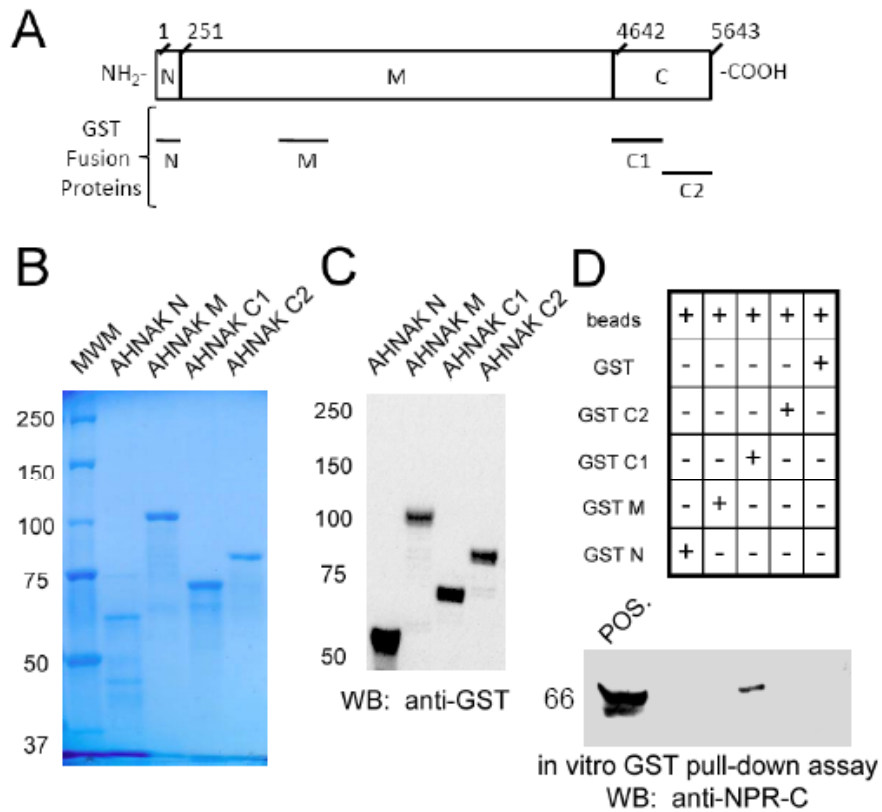


Figure 24. Identification of AHNAK1 domains that associate with NPRC in AoSMC cells. **(A)** A scheme of the molecular structure of human AHNAK1 and the location of GST fusion protein fragments AHNAK1 N (aa 2-252), AHNAK1 M (aa 821-1330), and AHNAK1 C (aa 4642-5643). The C-terminal domain was divided into two separate fragments C1 (aa 4646-5145) and C2 (aa 5146-5643). **(B)** Coomassie blue staining of purified GST-AHNAK1 domains. **(C)** Direct Western blot of purified GST-AHNAK1 domains revealed the presence of a single band for each of the purified AHNAK1 fusion proteins. **(D)** *In vitro* GST pull-down assay using AoSMC lysate and purified GST fusion proteins corresponding to each of the AHNAK1 domains or GST alone showed direct interaction between GST-AHNAK1C1 and NPRC.

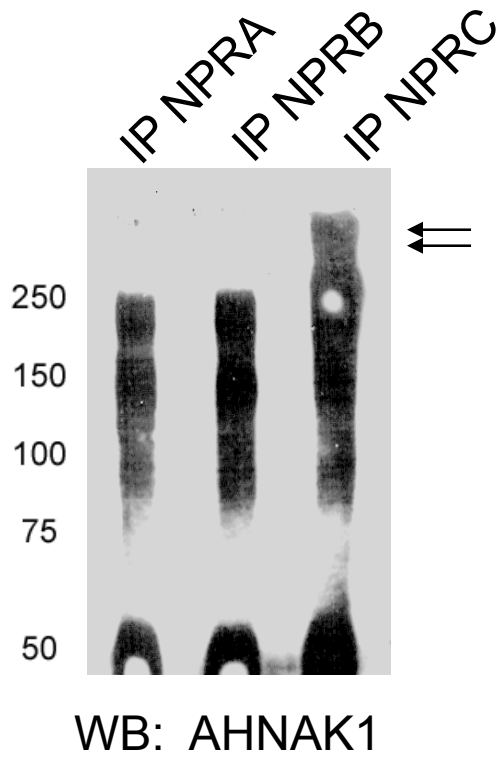


Figure 25. Specificity of the association between NPRC and AHNAK1. IP-Westerns showing NPRC and not NPRA or NPRB specific antibodies are able to pulldown AHNAK1

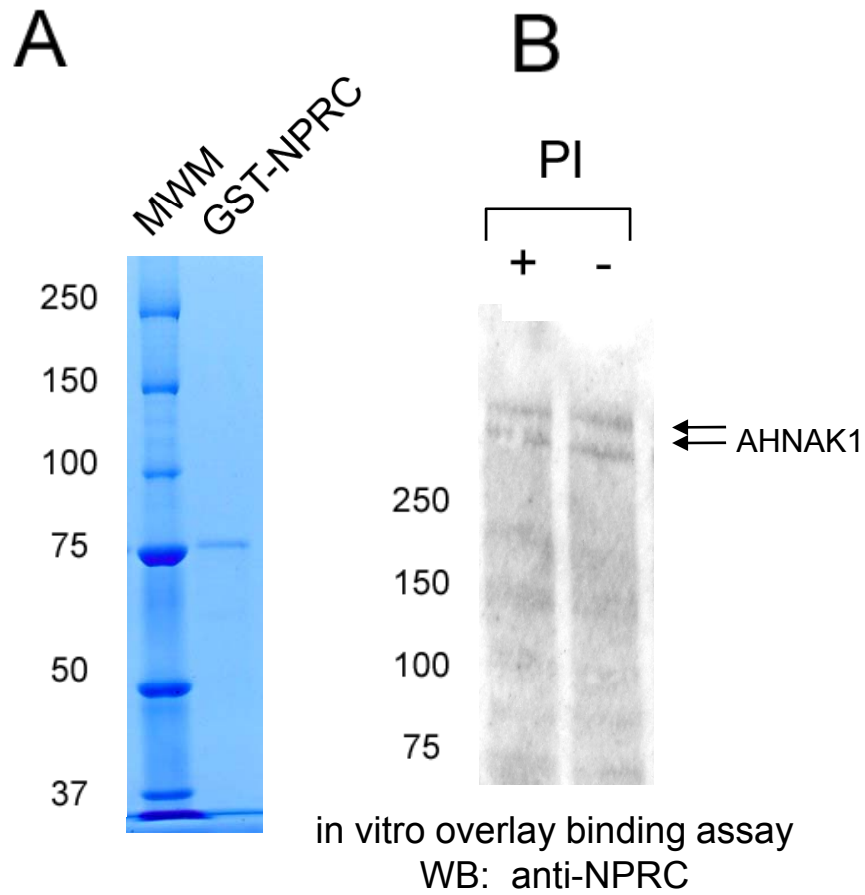


Figure 26. The role of phosphorylation in the association between NPRC and AHNAK1. (A) Coomassie blue staining of purified GST-NPRC revealed the presence of a single band. (B) *In vitro* overlay binding assay of rat gastric mucosa cell lysate treated with or without phosphatase inhibitors (PI) and overlaid with GST-NPRC and probed for GST confirmed binding of NPRC to AHNAK1 (arrow).

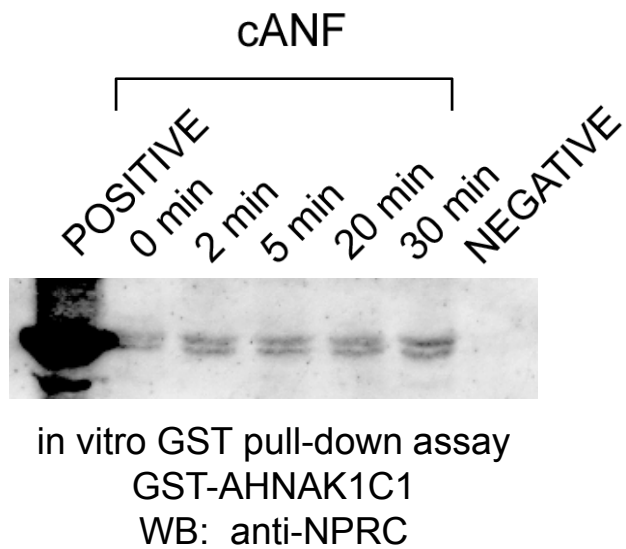


Figure 27. Effect of NPRC occupancy on the association between NPRC and AHNAK1. *In vitro* GST pull-down assay after preincubation of RGM1 cells with 1 μ M cANF for the indicated time intervals.

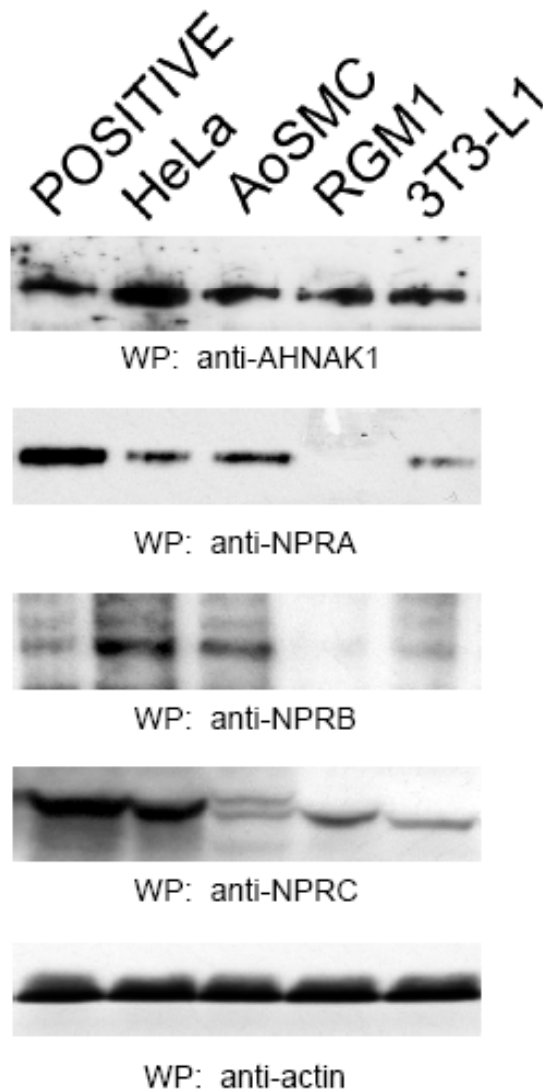


Figure 28. Expression of endogenous AHNAK1 and NPRs proteins. HeLa, AoSMC, RGM1, and 3T3-L1 cells express endogenous AHNAK1 protein (**A**) and NPRC protein (**D**). HeLa, AoSMC, and 3T3-L1 cells express NPRA protein (**B**) and NPRB protein (**C**). Blots are representative of at least three independent experiments. POSITIVE refers to positive control consisting of whole cell lysate from A-10 cells

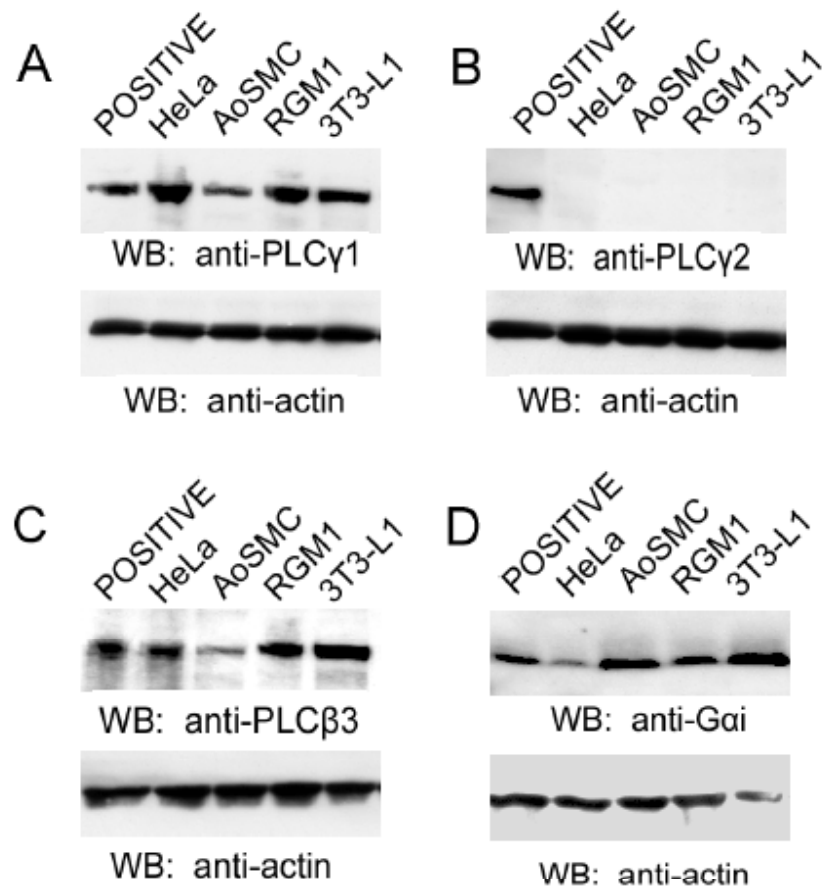


Figure 29. Expression of endogenous PLC and Gai proteins in various cell lines. HeLa, AoSMC, RGM1, and 3T3-L1 cells express varying level of endogenous PLCγ1 (A), no PLCγ2 (B), varying levels of PLCβ3 (C), and varying levels of Gai (D). Blots are representative of at least three independent experiments. POSITIVE refers to positive control consisting of whole cell lysate from NIH 3T3 cells for panels A, C, and D or whole cell lysate from Ramos cells for panel B.

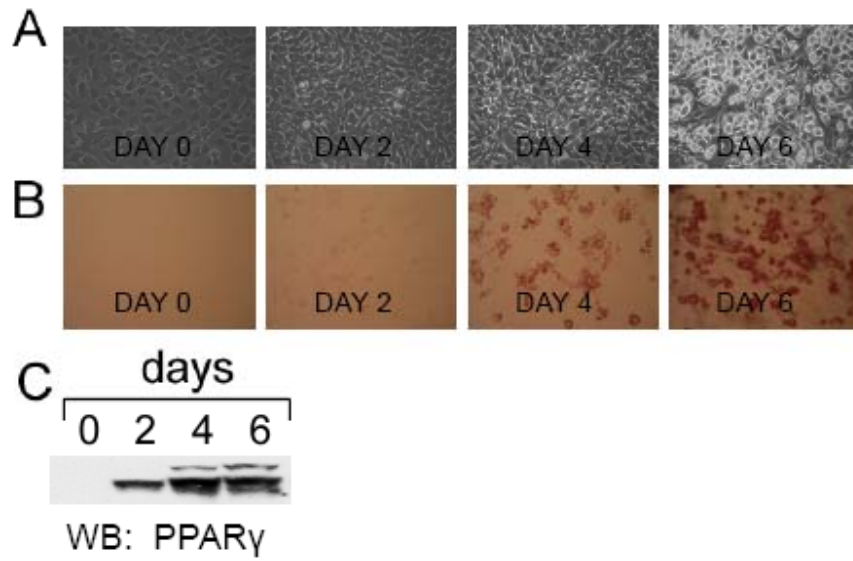


Figure 30. Assessment of the differentiation of 3T3-L1 cells. A: Phase-contrast microscopy. B: Oil Red O Staining at the indicated days. C: Western blot of peroxisome proliferator-activated receptor γ (PPAR γ) protein expression as a marker of differentiation

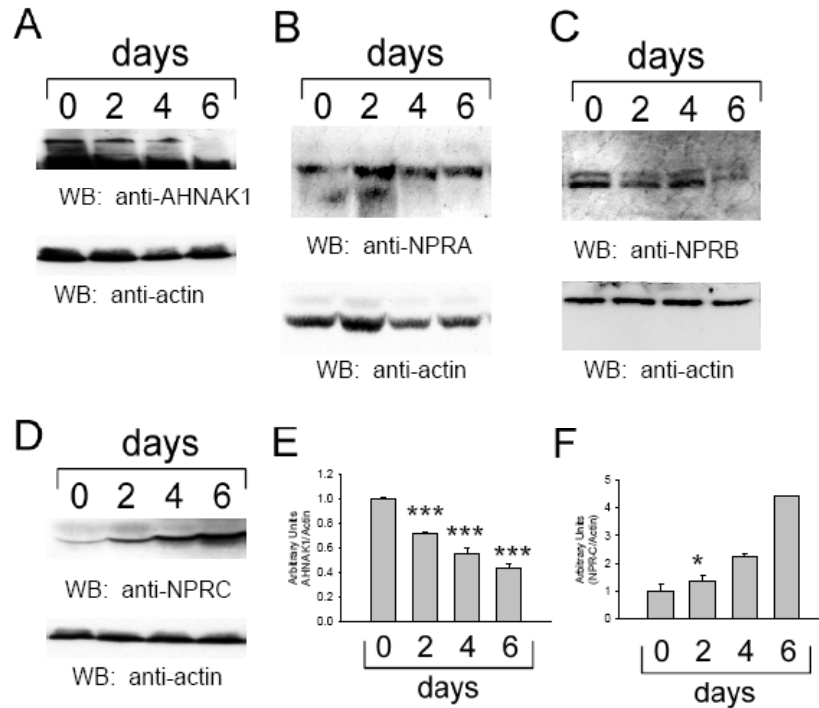


Figure 31. Regulation of AHNAK1 and NPR protein expression from day 0 to 6 of 3T3-L1 cell differentiation. AHNAK1 (A) protein expression decreases, NPRA (B) and NPRB (C) protein expression remain constant, and NPRC (D) protein expression increases with differentiation of 3T3-L1 preadipocytes. The densitometric analysis for the decrease in AHNAK1 protein expression is shown in panel E. The densitometric analysis for the increase in NPRC protein expression is shown in panel F. POSITIVE refers to positive control consisting of 3T3-L1 whole cell lysate from day 2 of 3T3-L1 preadipocyte differentiation. Student's t-test was used to compare two groups. Here, by convention * $P < 0.05$, ** $P < 0.005$, *** $P < 0.0005$

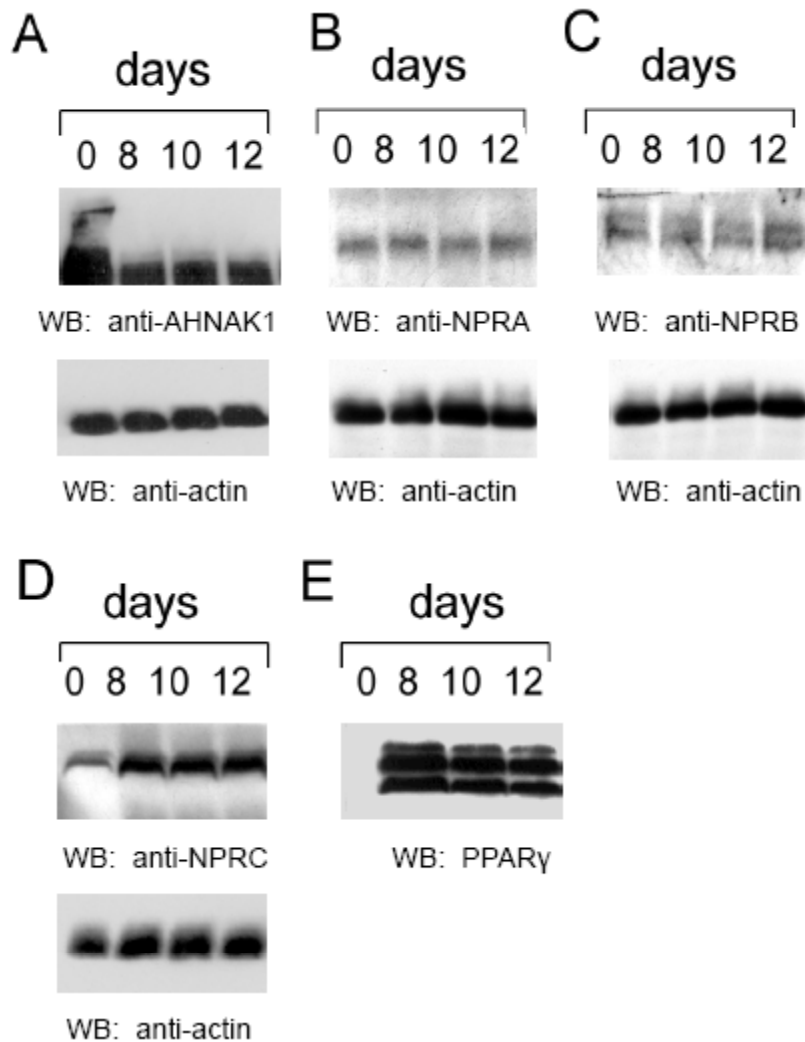


Figure 32. Regulation of AHNAK1 and NPR protein expression from day 0 to 12 of 3T3-L1 cell differentiation. AHNAK1 (A), NPRA (B), NPRB (C), and NPRC (D) protein expression does not further decrease or increase beyond day 8 of differentiation of 3T3-L1 preadipocytes. Panel E shows PPAR γ protein expression as a positive control for differentiation of 3T3-L1 preadipocytes into mature adipocytes.

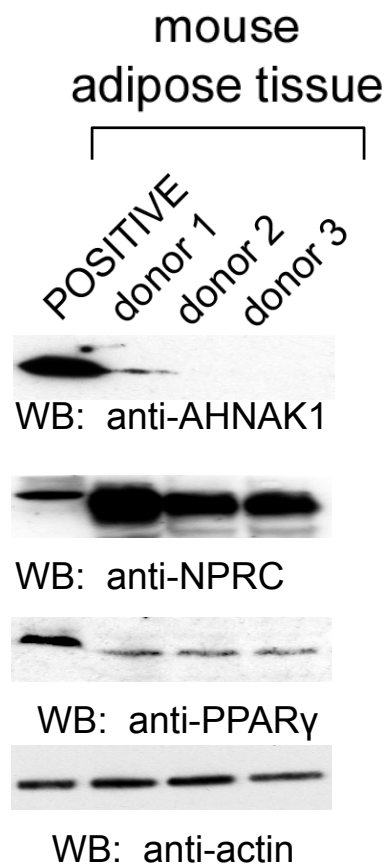


Figure 33. Endogenous expression of AHNAK1 and NPRC proteins in mouse adipose tissue. Low or no appreciable levels of AHNAK1 protein and high levels of NPRC protein were detected in adipose tissue from three different mouse donors.

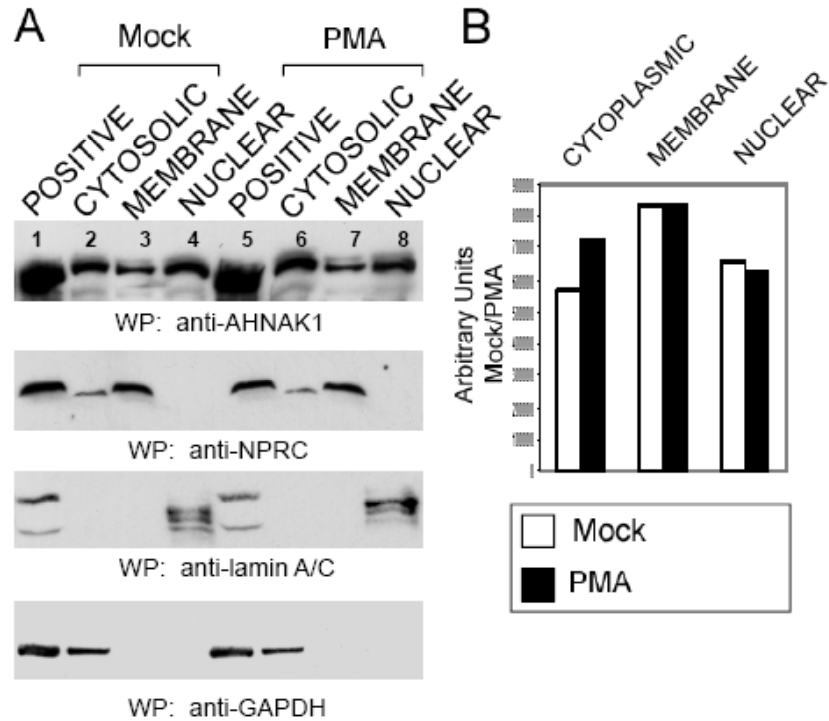


Figure 34. The effect of AHNAK1 translocation in response to PMA treatment in RGM1 cells. **(A)** Sucrose gradient centrifugation analysis of the translocation of AHNAK1 protein in response to PMA treatment. **(B)** AHNAK1 protein demonstrates more of a cytoplasmic distribution and less of a nuclear distribution with PMA treatment. NPRC was probed for as a membrane marker, Lamin A/C was probed for as a nuclear marker, and GAPDH was probed for as a cytoplasmic marker. Blots are representative of at least three independent experiments.

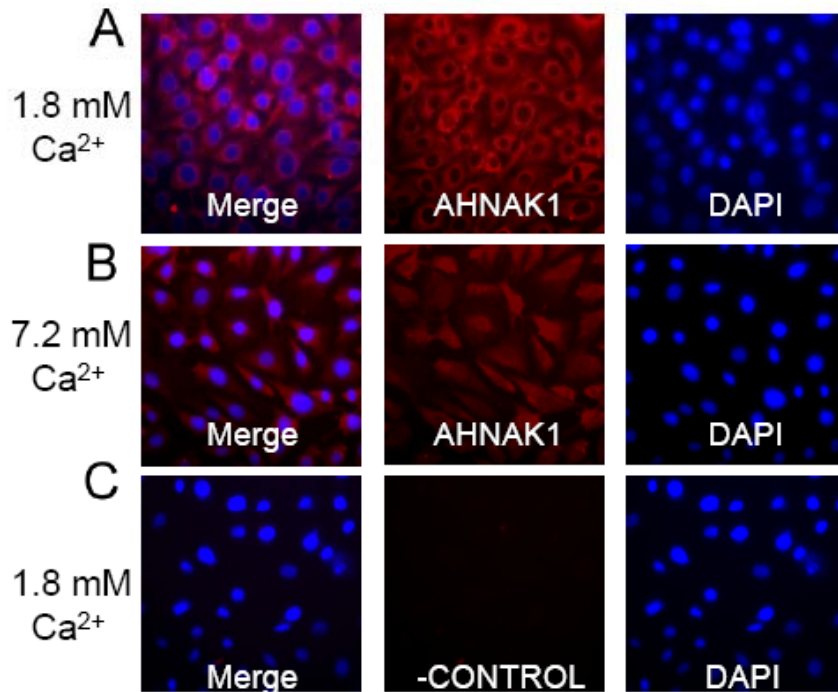


Figure 35. Immunofluorescence showing the effect of increased [Ca²⁺]_e on AHNAK1 translocation in 3T3-L1 preadipocytes. 3T3-L1 preadipocytes were initially cultured in medium containing normal Ca²⁺ (1.8 mM) and were then switched to medium containing high Ca²⁺ (7.2 mM) and cultured for an additional 6 hours before fixing the cells and staining for AHNAK1. The left column shows the merged image, the middle column shows Texas red staining for AHNAK1, and the right column shows nuclear counterstaining with DAPI

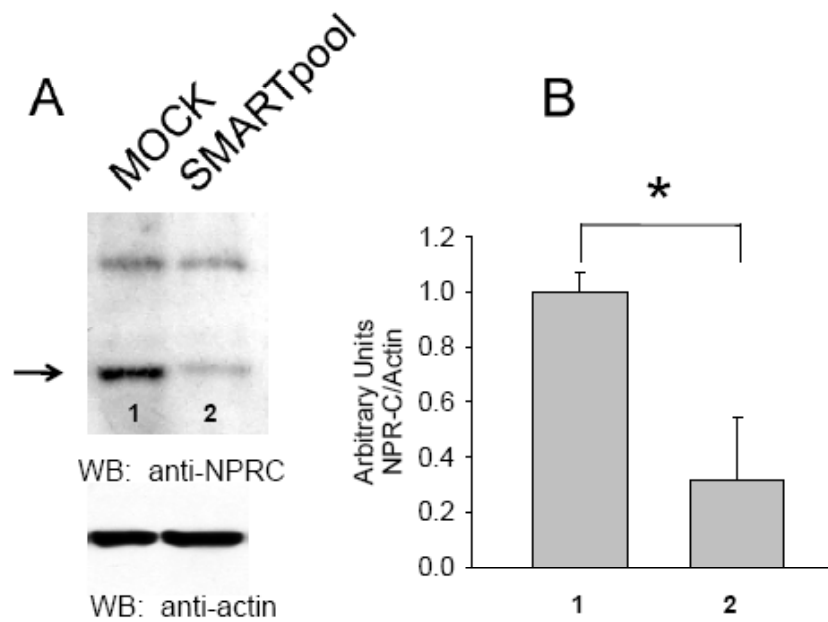


Figure 36. Knockdown of NPRC protein in 3T3-L1 preadipocytes. A: Western blot analysis in which the arrow indicates a marketed reduction in NPRC protein; B: densitometric analysis of (A). MOCK refers to the use of nontargeting siRNA instead of NPRC SMARTpool siRNA. The top band in panel A is nonspecific and the bottom band at 66 kDa corresponds to NPRC. Here, by convention * $P < 0.05$, ** $P < 0.005$, *** $P < 0.0005$

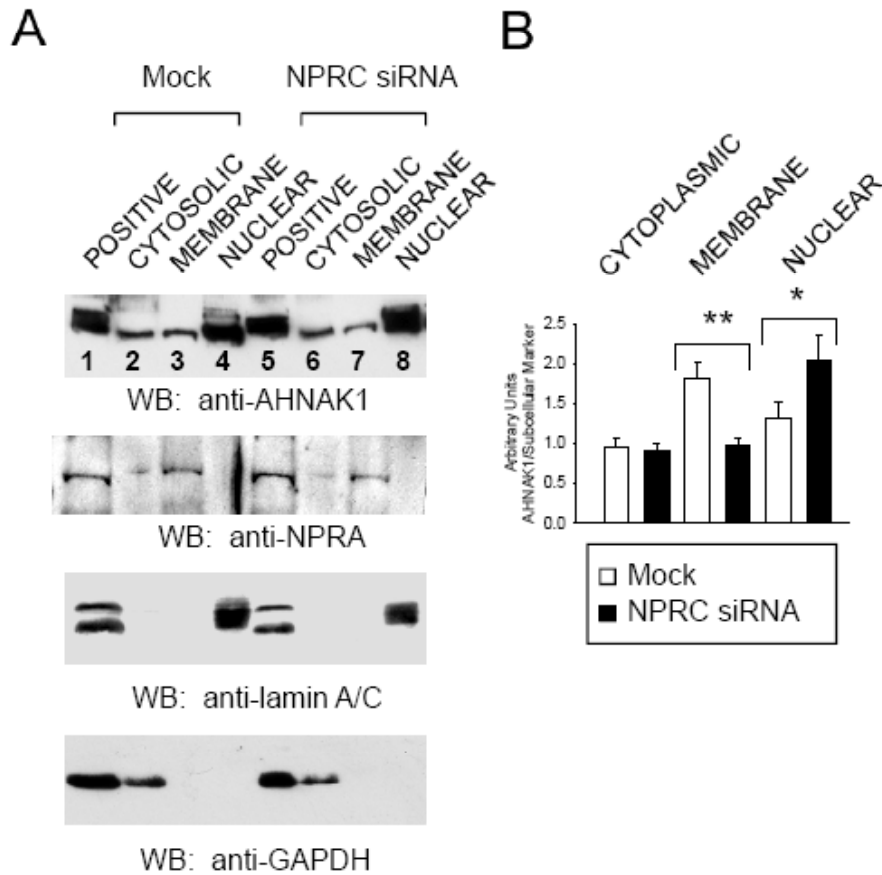


Figure 37. Role of NPRC knockdown on AHNAK1 subcellular localization in 3T3-L1 preadipocytes. A: Sucrose gradient centrifugation analysis of the translocation of AHNAK1 protein in response to NPRC knockdown. B: Densitometric analysis of (A). NPRA was probed for as a membrane marker, lamin A/C was probed for as a nuclear marker, and GAPDH was probed for as a cytoplasmic marker. Blots are representative of at least three similar independent experiments. In panel A, mock refers to the use of nontargeting siRNAs instead of NPRC SMART pool siRNAs. POSITIVE refers to positive control consisting of whole cell lysate before subcellular fractionation of the lysate. Student's t-test was used to compare two groups. Here, by convention * $P < 0.05$, ** $P < 0.005$, *** $P < 0.0005$

Chapter 3: Role of NPRC in Signal Transduction

Background

As demonstrated in the previous chapter, NPRC associates with AHNAK1 in various cell types. Both proteins are known to activate specific isoforms of PLC, as described earlier. Although AHNAK1 has been implicated in calcium signaling, its ability to associate with and modulate various proteins directly involved in maintaining calcium homeostasis is dependent on AHNAK1s recruitment/translocation to the plasma membrane. Therefore, the hypothesis is NPRC recruits and anchors AHNAK1 to the plasma membrane, where AHNAK1 serves as a receptor for AA and binds to and activates PLC γ 1.

Accordingly, a system to monitor transient changes in the second messenger downstream of the PLC signaling cascade, intracellular Ca²⁺, was employed to test this hypothesis. After demonstrating a functional system to measure small real time changes in intracellular Ca²⁺ mobilization in live cells, the physiological role and significance of the association between NPRC and AHNAK1 was investigated *in situ*. Furthermore, functional implications from the intracellular Ca²⁺ mobilization mediated by the association between NPRC and AHNAK1 were proposed for each cell type investigated.

Materials and Methods

Reagents and antibodies

In addition to the reagents and antibodies mentioned in the previous chapters, the following reagents and antibodies were purchased or acquired as described. Glass bottom culture dishes were purchased from MatTek (Ashland, MA). All other cell culture plasticware was purchased from Nalge Nunc (Rochester, NY). Fluo-3 AM dye was purchased from Molecular Probes (Eugene, OR). All other chemicals were purchased from Sigma (St. Louis, MO) unless otherwise noted. $G\alpha_i$ antibody was kindly provided by Dr. Dave Manning (University of Pennsylvania, Philadelphia, PA), NPRA and NPRB polyclonal antibodies were kindly provided by Dr. David L Garbers, University of Texas Southwestern, Dallas, TX), PLC β 3, PLC γ 1, PLC γ 2, GAPDH, Lamin A/C, and PPAR γ antibodies were purchased from Cell Signaling Technology (Danvers, MA).

Cell lines and cell culture

In addition to the cell lines mentioned in the previous chapters, the 3T3-L1 cell line was purchased from the American Type Culture Collection (Manassas, VA). All other cell culture media, antibiotic/antimycotic, and calcium-free Hank's balanced salt solution (HBSS) were purchased from GIBCO Invitrogen (Grand Island, NY). Only low passage cells were used for experiments.

3T3-L1 preadipocyte differentiation

3T3-L1 preadipocytes were cultured in high glucose DMEM Medium supplemented with 10% Newborn Calf Serum (NCS) (Sigma) and maintained at 37 °C in a 10% CO₂ humidified atmosphere. At confluency, 3T3-L1 preadipocytes were treated with 10 µg/mL insulin, 0.25 µM dexamethasone, and 0.5 mM 3-isobutyl-1-methylxanthine (IBMX), cultured in high glucose DMEM Medium supplemented with 10% FBS and maintained at 37 °C in a 10% CO₂ humidified atmosphere. Culture medium was replaced 48 hrs after differentiation with fresh culture medium containing insulin and supplemented with 10% FBS. Culture medium was replaced every 48 hrs thereafter with fresh culture medium supplemented with 10% FBS

Oil Red O Staining

3T3-L1 cells cultured to 70% confluency on chamber slides were fixed with 10% formalin in PBS, washed with 1X PBS, and stained for 1 hr at room temperature (RT) with 0.15% Oil Red O (60:40 mix of isopropanol and water). Slides were evaluated microscopically for the accumulation of lipid droplets.

SDS-PAGE, Western blotting, and Densitometric analyses

SDS-PAGE and Western blotting was performed as described in Chapter 1, but with the following modifications. Briefly, twenty five µg of protein was separated by electrophoresis for 8 hours at 25 V on 7.5% gradient polyacrylamide gels. Separated proteins were electrically transferred onto Hybond-C extra nitrocellulose membranes for 75 minutes at 100 V in Towbin buffer. Transferred proteins were stained with Ponceau

solution to confirm the transfer of the bands, destained with 1X TBS, and then blocked in 5% (w/v) nonfat powdered milk in 1X TBS at RT for 1 hour. Membranes were washed with 1X TBS and then incubated with anti-AHNAK1 or anti-NPRB antibody at a dilution of 1:500, or anti-NPRA antibody at a dilution of 1:4000, or anti NPRC, $G\alpha_i$, PLC β 3, PLC γ 1, PLC γ 2, GAPDH, Lamin A/C at a dilution of 1:1000 in 5% BSA in TBS at 4°C overnight. Membranes were washed with 1X TBS and incubated with horseradish peroxidase (HRP)-conjugated goat anti-rabbit secondary antibody (BioRad) at a dilution of 1:3000 in blocking solution at RT for 60 minutes. Immunoreactive bands were detected by SuperSignal West Pico chemiluminescent substrate according to the manufactures instructions and developed using Hyperfilm-ECL. As a loading control, membranes were probed for β -actin at a dilution of 1:10000. Densitometric analysis was performed as described in the previous chapter.

Confocal fluorescence imaging and measurement of Intracellular Calcium

Cells were cultured in complete growth media (containing calcium and FBS or NCS) in 35mm glass bottom culture dishes. At 70% confluency, cells were made quiescent by serum deprivation for 6 hrs. Cells were washed with calcium-free HBSS, loaded with the calcium-sensitive Fluo-3 AM dye at a final concentration of 10 μ M in extracellular solution (complete growth media) and incubated at 37 °C for 20 minutes. Cells were washed with calcium-free HBSS and returned to extracellular solution (complete growth media unless otherwise noted) for 10 minutes to allow for de-esterification of the dye. A confocal imaging system (Leica) equipped with an inverted microscope, an Argon 488 laser, and a 63 X 1.4NA objective lens was used to record

calcium fluorescence at RT. The excitation wavelength of the laser was set at 488 nm and the emission wavelength for monitoring fluorescence was set at 520-580nm. Images were acquired at a rate of 1 frame every 2.5 seconds and recorded with LASAF software. A field of at least 12 cells was chosen and focused in differential interference contrast (DIC) mode. After measuring baseline fluorescence for 2 minutes, 100 μ l of vehicle was added directly to the extracellular solution and fluorescence intensity was measured for an additional 2 minutes. Thereafter, 100 μ l of the test agent was added and fluorescence intensity was measured for 2 minutes. Cells were then stimulated with 10 μ M ionomycin to confirm equivalent loading.

Sucrose density gradient centrifugation

Confluent 3T3-L1 cells were harvested from 100 mm tissue culture dishes for protein in TES buffer (20 mM Tris HCl pH 7.4, 1 mM EDTA, 255 mM sucrose) supplemented with protease inhibitors. The protein lysate was subjected to moderate sonication and then centrifuged at 17 000 X g for 45 min at 4 °C. The supernatant was collected and contained the cytosolic fraction. The pellet was resuspended in 0.5 mL TES buffer and layered on 0.3 mL of a 1.12 M sucrose cushion and then centrifuged at 250 000 X g for 30 min at 4 °C in a TL 55 swinging bucket rotor. The resulting supernatant layer was carefully removed and discarded. The intermediate layer was carefully collected and contained the membrane fraction. The bottom layer was then carefully removed and discarded. The pellet was resuspended in 100 μ l of TES buffer and contained the nuclear fraction. Each fraction was quantified by the BCA assay and

subjected to SDS-PAGE and Western blot analysis using specific subcellular marker antibodies.

Transfection of siRNA and constructs

3T3-L1 cells were transfected with siGenome SMARTpool reagents (Dharmacon; Lafayette, CO) specific for mouse NPRC, AHNAK1, or nontargeting siRNA using DharmaFECT3 transfection reagent (Dharmacon; Lafayette, CO) according to the manufacturer's instructions. The different siRNA used in various experiments are listed in Table 10. Cells were harvested 72 hrs after transfection and protein knockdown was determined by Western blot and densitometric analysis. 3T3-L1 cells were transfected with pBINDAHNAK1 using FuGENE 6 according to the manufactures instructions. Cells were harvested 72 hours after transfection. Transfection efficiency was assessed by performing luciferase assays according to the manufactures instructions.

Statistics

Results are expressed as the mean \pm SD. Repeated measures ANOVA was conducted for confocal microscopy experiments. Statistical significance was set at $p < 0.05$

Results

Optimization of a system to measure intracellular Ca^{2+} mobilization in situ

Endothelin-1 (ET-1) is one of the most potent endogenous vasoconstricting agents known [375] and is also known to bind to its receptors on vascular smooth muscle cells (VSMCs) and subsequently raise the intracellular free Ca^{2+} concentration ($[Ca^{2+}]_i$) [376]. Since A-10 VSMCs have been reported to respond to ET-1 treatment with a rapid and transient increase in intracellular Ca^{2+} [377], this system was used in parallel to optimize a system to monitor realtime changes in intracellular Ca^{2+} mobilization of Fluo-3 loaded cells by confocal microscopy. The addition of 1 μ M of ET-1 to quiescent A-10 VSMCs stimulated a rapid and transient increase in intracellular Ca^{2+} compared to background fluorescence, as shown in Figure 38. There was between a two-fold to three-fold increase in intracellular Ca^{2+} of the eight randomly selected cells, when compared to baseline fluorescence and after normalizing to background fluorescence.

An increase in intracellular Ca^{2+} is observed in AoSMCs in response to exogenous AA

Next, the human equivalent to the rat A-10 VSMC line, the AoSMC line, was used to investigate the effect of exogenous AA on intracellular Ca^{2+} mobilization. Quiescent AoSMCs failed to respond to 1 μ M exogenous AA (Figure 39), but did respond with a four to ten-fold increase in intracellular Ca^{2+} in response to 10 μ M ionomycin in the presence of extracellular Ca^{2+} (Figure 40). Quiescent AoSMCs also responded with approximately a three-fold increase in intracellular Ca^{2+} in response to 25 μ M AA, and subsequently responded to ionomycin treatment in the presence of extracellular Ca^{2+} (Figure 40A,B).

Calcium is released from intracellular Ca²⁺ stores in response to AA in AoSMCs or 3T3-L1 cells

In order to determine if the source of increase of intracellular Ca²⁺ in AoSMCs was from the release of Ca²⁺ from intracellular Ca²⁺ stores or an influx of extracellular Ca²⁺, AoSMCs were stimulated with 25 μM AA in the absence of extracellular Ca²⁺ and changes in intracellular Ca²⁺ were monitored over time. The exclusion of Ca²⁺ from the extracellular medium did not affect the increase in intracellular Ca²⁺ in response 25 μM AA, as shown in Figure 41. In order to confirm the source of increase in intracellular Ca²⁺ was from intracellular Ca²⁺ stores, AoSMCs were stimulated with 1 μM of Thapsigargin (TG), then ionomycin (Figure 42), and followed by AA and PMA (data not recorded). TG stimulation inhibited the AA or PMA induced release of intracellular Ca²⁺ increase.

Effect on intracellular Ca²⁺ in AoSMCs in response to increasing concentration of exogenous AA

The fold increase in intracellular Ca²⁺ in quiescent AoSMCs did not quadruple after quadrupling the concentration of exogenous AA. Only a moderate increase in intracellular Ca²⁺ in AoSMCs was observed after increasing the concentration of exogenous AA from 25 μM to 100 μM (Figures 40 and 43). Interestingly, the response to the same concentration of ionomycin was significantly decreased after increasing the concentration of exogenous AA from 25 μM to 100 μM (Figures 40 and 43).

Effect on intracellular Ca²⁺ in AoSMCs in response to PMA

Since PMA has previously been shown to increase intracellular Ca²⁺ in NIH 3T3 cells, the ability of PMA to induce an increase in intracellular Ca²⁺ was evaluated in AoSMCs. As shown in Figure 44, PMA was able to stimulate an increase in intracellular Ca²⁺ in AoSMCs.

Addition of cANF fails to induce an increase in intracellular Ca²⁺ in AoSMCs

Since NPRC activation is known to activate PLCβ3, the ability of NPRC activation by ligand binding to elicit an increase in intracellular Ca²⁺ in AoSMCs was investigated. The addition of 1 μM of the specific NPRC agonist cANF to quiescent AoSMCs did not result in any appreciable increase in intracellular Ca²⁺, but the same cells later responded to 10 μM ionomycin (Figure 45).

Effect on intracellular Ca²⁺ in 3T3-L1 preadipocytes in response to AA or PMA

Because AoSMCs could not easily be transfected with various expression constructs or siRNAs, the 3T3-L1 cell line was used to assess the physiological significance and role of the association between NPRC and AHNAK1 in mediating the increases in intracellular Ca²⁺ in response to AA or PMA. 3T3-L1 preadipocytes responded with an increase in intracellular Ca²⁺ in response to exogenous AA (Figure 46 and 47).

Calcium is released from intracellular Ca²⁺ stores in response to AA in 3T3-L1 cells

In order to determine if the source of increase of intracellular Ca²⁺ in 3T3-L1 preadipocytes was from the release of Ca²⁺ from intracellular Ca²⁺ stores or an influx of extracellular Ca²⁺, 3T3-L1 preadipocytes were stimulated with 25 μM AA in the absence of extracellular Ca²⁺ and changes in intracellular Ca²⁺ were monitored over time. The exclusion of Ca²⁺ from the extracellular medium did not affect the increase in intracellular Ca²⁺ in response 25 μM AA, as shown in Figure 48. In order to confirm the source of increase in intracellular Ca²⁺ was from intracellular Ca²⁺ stores, 3T3-L1 preadipocytes were stimulated with 1 μM of TG, then ionomycin (Figure 49), and followed by AA and PMA (data not recorded). TG stimulation inhibited the AA or PMA induced release of intracellular Ca²⁺ increase.

Effect on intracellular Ca²⁺ in 3T3-L1 preadipocytes in response to PMA

3T3-L1 preadipocytes were used for assessing the physiological significance between NPRC and AHNAK1 because they are more similar to NIH 3T3 cells and can be transfected with better efficiency than differentiated 3T-L1 adipocytes. Accordingly, an increase in intracellular Ca²⁺ was observed in 3T3-L1 preadipocytes in response to PMA in a dose dependent manner (Figures 50, 51).

siRNA mediated knockdown of NPRC results in attenuation of the observed increase in intracellular Ca²⁺ in response to PMA

The role of NPRC in potentiating the AHNAK1 mediated AA-dependent intracellular Ca²⁺ mobilization was demonstrated by siRNA mediated knockdown of

NPRC in 3T3-L1 preadipocytes. A statistically significant decrease in intracellular Ca^{2+} in response to 25 μM PMA was observed for cells transfected with siRNA targeting NPRC compared to untreated cells (Figures 52 and 59).

Overexpression of an AHNAK1 construct results in augmentation of the observed increase in intracellular Ca^{2+} in response to PMA

In order to demonstrate a role for AHNAK1 for the increase in intracellular Ca^{2+} observed in 3T3-L1 preadipocytes and to show the response was not exclusively from PMA or AA, an AHNAK1 construct was created and transfected into 3T3-L1 preadipocytes (Appendix D-F, I-M). The AHNAK1 construct, pBIND-AHNAK1, consisted of the carboxy terminal domain of AHNAK1 and several repeating segments of AHANK, and the vector itself coded for luciferase, which was used to monitor transfection efficiency. A statistically significant augmentation of the increase in intracellular Ca^{2+} in response to PMA was observed in 3T3-L1 preadipocytes transfected with the pBIND-AHNAK1 construct compared to untreated preadipocytes (Figures 53 and 54).

siRNA mediated knockdown of AHNAK1 results in attenuation of the observed increase in intracellular Ca^{2+} in response to PMA

The role of AHNAK1 in mediating the AA-dependent intracellular Ca^{2+} mobilization was further corroborated by siRNA mediated knockdown of AHNAK1 in 3T3-L1 preadipocytes. A statistically significant decreases in intracellular Ca^{2+} in

response to 25 μM PMA was observed for cells transfected with siRNA targeting AHNAK1 compared to untreated cells (Figures 55, 56, and 59).

cPLA₂ is required for the AHNAK1 mediated intracellular Ca²⁺ mobilization in 3T3-L1 cells

In order to show the increases in intracellular Ca²⁺ were a result of endogenous AA released in response to PMA, 3T3-L1 preadipocytes were pretreated with the specific cPLA₂ inhibitor AACOCF3 for 5 minutes. Afterwards, the cells were stimulated with 25 μM PMA. A significant attenuation in the response to PMA was observed when cells pretreated with AACOCF3 (Figures 57, 59) were compared to untreated cells (Figures 50, 59).

Addition of cANF fails to induce an increase in intracellular Ca²⁺ in 3T3-L1 preadipocytes

Since NPRC activation is known to activate PLC β 3, the ability of NPRC activation by ligand binding to elicit an increase in intracellular Ca²⁺ in 3T3-L1 preadipocytes was investigated. The addition of 1 μM of the specific NPRC agonist cANF to quiescent 3T3-L1 preadipocytes did not result in any appreciable increase in intracellular Ca²⁺, but the same cells later responded to 10 μM ionomycin (Figure 58).

AHNAK1 translocates to the plasma membrane in response to an increase in extracellular Ca^{2+}

Since AHNAK1's ability to execute Ca^{2+} signaling is determined by its presence at the plasma membrane, the translocation of AHNAK1 from the nucleus to the plasma membrane was investigated in 3T3-L1 preadipocytes. The switching of 3T3-L1 preadipocytes from medium containing normal Ca^{2+} to high Ca^{2+} resulted in AHNAK1 in less AHNAK1 present in the nucleus, as shown by subcellular fraction studies, and subsequent Western blot and densitometric analysis (Figure 61A,B). Accordingly, the translocation of AHNAK1 to the cytoplasm and plasma membrane resulted in abrogation of the increase in intracellular Ca^{2+} in response to PMA stimulation (Figure 62).

Discussion

The role of NPRC in mediating AHNAK1 calcium signaling in the presence of AA was investigated in AoSMCs and in 3T3-L1 preadipocytes. The roles of NPRC and AHNAK1 in the presence of exogenous AA or through PMA induced release of endogenous AA from lipid bilayers was investigated by monitoring real time changes in intracellular Ca^{2+} mobilization in live fluo-3 loaded quiescent cells. The roles of NPRC and AHNAK1 in intracellular Ca^{2+} mobilization were corroborated by siRNA mediated knockdown of each protein or by overexpression of an AHNAK1 construct. Moreover, subcellular fraction studies demonstrated NPRC plays a role in determining the subcellular localization of AHNAK1 protein.

The 3T3-L1 cell line is an excellent model for the study of adipogenesis at the cellular level [343-345]. The results presented here suggest a functional role for NPRC and AHNAK1 in the regulation of mouse adipogenesis. Interestingly, NPRC and AHNAK1 protein expression was shown to be inversely proportional during differentiation of 3T3-L1 preadipocytes into mature adipocytes. However, the coexpression of NPRC and AHNAK1 proteins in the early stages of differentiation may suggest a role for the association between NPRC and AHNAK1 in promoting adipogenesis. Interestingly, the role of intracellular Ca^{2+} in 3T3-L1 preadipocytes has been investigated by other groups. For example, increasing levels of intracellular Ca^{2+} were reported to have an inhibitory effect in the early stages of differentiation of 3T3-L1 preadipocytes into adipocytes [378]. Ntambi and Takova demonstrated that Ca^{2+} mobilization repressed the synthesis of an intermediate involved in DNA replication to prevent the expression of transcription factors required for differentiation [378]. A report

by Jensen *et al.* provided evidence for high $[Ca^{2+}]_e$ attenuating adipogenesis in 3T3-L1 preadipocytes [379]. Jensen *et al.* reported the direct role of $[Ca^{2+}]_e$ in attenuating adipogenesis in 3T3-L1 preadipocytes was in part the result of inhibition of the C/EBP α and PPAR γ 2 transcription factors [379]. Both transcription factors have been shown in other reports to positively modulate adipogenic gene transcription [380, 381]. This group also observed that increases in $[Ca^{2+}]_e$ also interfered with the normal down-regulation of the transcription factor Pref-1, which is downregulated in differentiated 3T3-L1 preadipocytes and overexpressed in undifferentiated 3T3-L1 preadipocytes [381]. Jensen *et al.* provided compelling evidence that demonstrated calcium specifically inhibited differentiation by showing in parallel experiments that the divalent cation MgCl₂ used to offset the changes in osmolarity associated with the use of CaCl₂ did not inhibit 3T3-L1 differentiation [379]. Consistent with the findings of both Ntambi and Takova [378] and Jensen *et al.*[379], AHNAK1 translocation to the plasma membrane in response to elevated levels of extracellular calcium resulted in augmentation of intracellular calcium mobilization with the addition of PMA in 3T3-L1 preadipocytes (Figure 62). Taken together, the results presented here may suggest the association between NPRC and AHNAK1 could have an inhibitory effect in the early stages of differentiation of mouse preadipocytes into mature adipocytes. However, additional studies that actually monitor markers of differentiation, such as PPAR γ expression or the accumulation of lipid droplets would be necessary to ascertain this theory.

Several groups have reported increases in $[Ca^{2+}]_e$ modulate cell proliferation of various cell types [382-385]. As previously mentioned, calcium plays an important role in cell survival and death. Chronic elevated levels of intracellular calcium are toxic to

various cell types. In accordance with findings from Jensen *et al.*, increasing $[Ca^{2+}]_e$ by itself did not chronically elevate $[Ca^{2+}]_i$ as there was no significant change in Ca^{2+} released from intracellular stores after TG treatment [379]. Also, similar to findings from Jensen *et al.*, increasing the levels of extracellular calcium did not affect cell number or viability according to trypan blue staining. Interestingly, Jensen *et al.* presented data that showed elevated levels of $[Ca^{2+}]_e$ did not acutely or chronically impact $[Ca^{2+}]_i$ in 3T3-L1 preadipocytes [379]. This finding is in contrast to the finding presented here for the translocation of AHNAK1 to the plasma membrane upon increases in $[Ca^{2+}]_e$. However, the AHNAK1 induced mobilization of $[Ca^{2+}]_i$ is dependent on AA or PMA mediated release of AA, which was not tested in the study by Jensen *et al.* [379].

Intracellular Ca^{2+} was reported to exert a biphasic regulatory role in human adipocyte differentiation and lipid filling, as increasing levels of intracellular Ca^{2+} were found to inhibit differentiation and lipid filling in the early stages and promotion of differentiation and lipid filling in the late stages of human adipocyte differentiation [386]. Up to 48 hours of differentiation of human adipocyte differentiation, Shi *et al.* showed increasing Ca^{2+} causes a significant inhibition in PPAR γ expression, but during 48 to 72 hours of human adipocyte differentiation increasing Ca^{2+} causes a significant increase in PPAR γ expression [386]. PPAR γ expression was proposed to directly induce late differentiation gene expression, including that of fatty acid synthase (FAS), steroyl-CoA desaturase (SCD-1), and phosphoenol-pyruvate carboxykinase (PEPCK) [386]. Moreover, Shi *et al.* proposed intracellular Ca^{2+} may work synergistically with various differentiation transcriptional factors to stimulate late differentiation gene expression [386]. In other reports, increases in intracellular Ca^{2+} from the stimulation of voltage-

mediated calcium channels were found to promote triglyceride accumulation in mouse and human adipocytes by stimulating lipogenesis and suppressing lipolysis [304, 387]. The increases in intracellular Ca^{2+} were found to induce the expression and activity of FAS and inhibit both basal and agonist-stimulated lipolysis in mouse and human adipocytes [387].

Taken together, the numerous reports in the literature describing the role for $[\text{Ca}^{2+}]_i$ or $[\text{Ca}^{2+}]_e$ in modulating rodent or human adipocyte differentiation are largely limited to the *in vitro* state. Additional *in vivo* studies should be performed to demonstrate the role of $[\text{Ca}^{2+}]_i$ or $[\text{Ca}^{2+}]_e$ levels in body fat accumulation and its link to associated diseases.

TG (Tg), an endoplasmic reticulum Ca^{2+} ATPase inhibitor is a useful means to test various Ca^{2+} dependent intracellular functions since it rapidly elevates $[\text{Ca}^{2+}]_i$. Tg was used to test the source of increase in $[\text{Ca}^{2+}]_i$ in response to AA or PMA in 3T3-L1 preadipocytes transfected with NPRC or AHNAK1 specific siRNA. After depleting intracellular calcium stores with Tg, the addition of exogenous AA to 3T3-L1 preadipocytes or AoSMC failed to elicit an increase in $[\text{Ca}^{2+}]_i$, suggesting the source of increase in $[\text{Ca}^{2+}]_i$ was from release of Ca^{2+} from intracellular stores and not an influx of Ca^{2+} from the extracellular solution. Similarly, the addition of exogenous AA to either 3T3-L1 preadipocytes or AoSMC resulted in a rapid and transient increase in intracellular calcium in cells cultured in the presence or absence of calcium in the extracellular medium, further suggesting the source of increase was from the release of Ca^{2+} from intracellular stores.

The association between NPRC and AHNAK1 in human AoSMCs and the

observed increase in intracellular Ca^{2+} in response to AA or PMA seen in human AoSMCs may also have implications for vascular diseases attributed to vascular smooth muscle cell proliferation, migration, and apoptosis. Also, it is well established that intracellular calcium mobilization is crucial for VSMC contractility. Vascular smooth muscle contraction is triggered by an increase in intracellular Ca^{2+} concentration [388]. The accepted mechanism for VSMC contractility includes a series of steps, which begins with Ca^{2+} binding to calmodulin (CaM) to form the Ca^{2+} -CaM complex. The Ca^{2+} -CaM complex binds to and activates myosin light chain kinase (MLCK). The activated MLCK then catalyzes the phosphorylation of the regulatory myosin light chain (MLC), which triggers myosin-actin interaction, leading to the shortening of muscle and generation of force. The decrease in intracellular Ca^{2+} results in the dephosphorylation of myosin by myosin phosphatase, resulting in muscle relaxation [389]. Furthermore, it was reported that smooth muscle contraction is regulated by Ca^{2+} sensitization, suggesting Ca^{2+} dependent contractions may occur at lower Ca^{2+} concentration than expected [390]. Ca^{2+} sensitization may result in an increase in MLC phosphorylation due to reduced activity of myosin phosphatase. A major pathway for smooth muscle contraction involves an increase in intracellular Ca^{2+} from the opening of voltage-dependent L-type Ca^{2+} channels in response to membrane depolarization through high concentrations of extracellular K^+ [391]. Another major pathway for smooth muscle contraction involves an increase in intracellular Ca^{2+} from release of Ca^{2+} from intracellular calcium stores after G-protein coupled activation of PLC in response to various agonist [391]. Accordingly, hypercontraction is known to cause vascular diseases including increased systemic blood pressure, acute vasospasm, and microcirculatory ischemia [392-394].

Therefore, abnormal VSMC contractility may contribute to abnormal vascular tone and disorders of blood pressure regulation, including hypertension [395].

The ratiometric indicators, low-affinity indicators, long-wavelength indicators, and indicator-dextran conjugates are among the various different types of fluorescent Ca^{2+} indicators currently available. Fura-2 and indo-1 are the most widely used ratiometric indicators and both require ultraviolet excitation. Ratiometric indicators produce an excitation or emission spectral shift upon ion binding and allows for calibration of the ratio of fluorescence intensities measured at two different wavelengths. The excitation of these probes only by UV light results in significantly less interference than fluorescent compounds excited by visible wavelength. Ratiometric indicators prevent variations from artifacts including photobleaching, non-uniform loading of the indicator, and variable cell thickness, which would contribute to misinterpretation in changes of Ca^{2+} concentrations. Low-affinity indicators are useful for detecting intracellular Ca^{2+} levels in the micromolar range. Low-affinity indicators have faster ion dissociation rates to allow for the ability to better track rapid Ca^{2+} flux kinetics. Long-wavelength indicators are useful for photoactivateable “caged” probes, and argon-ion laser-based confocal microscopes and flow cytometers. Examples of long-wavelength indicators include fluo-3, fluo-4, rhod-2, and x-rhod-1, and the fura-2 analog fura-red. Dextran-linked indicators are conjugated to water-soluble dextrans and exhibit long-term intracellular retention and little vacuolar sequestration. Dextran-linked indicators are particularly useful for measuring Ca^{2+} concentrations in plant and fungal cells. There are several selection criteria for calcium indicators including the mode of measurement, dissociation constant (Kd), and the form of the indicator. The mode of measurement is

determined by whether qualitative or quantitative ion concentration data is desired. The K_d is determined by the Ca^{2+} concentration range of interest. The form of the indicator is determined by the method of cell loading and the requirements for intracellular distribution and retention of the indicator. Indicators are available in salt, acetoxymethyl (AM) ester or dextran form. Some fluorescent indicators are cell impermeant, while others are derivatized with an AM that is cell permeable. The AM form of the fluorescent indicator is designed to passively diffuse across cell membranes to inside the cell, where esterases cleave off the AM group leading to a cell-impermeant indicator [396]. Furthermore, the final intracellular concentration of the hydrolyzed Ca^{2+} indicator is dependent on factors including the concentration and type of indicator, number and type of cells loaded, and loading time and temperature [396].

The Ca^{2+} -sensitive fluorescent indicator fluo-3 was chosen to measure intracellular Ca^{2+} *in situ*. Fluo-3 is a newer generation of fluorescent Ca^{2+} indicator dyes that offers several advantages. Potential problems with fluorescent indicators include compartmentalization, intracellular buffering, autofluorescence, and cytotoxicity. Fluo-3 has a higher K_d to allow for more sensitive measurements at higher $[Ca^{2+}]_i$ in stimulated cells, and has a higher quantum yield to allow for measurement of $[Ca^{2+}]_i$ at lower cytosolic concentrations of the dye. Ca^{2+} indicators such as fluo-3 have been widely used to monitor transient increases in intracellular Ca^{2+} due to Ca^{2+} release from intracellular stores through IP_3 receptors [397-400]. Fluo 3 is especially useful for monitoring small changes in Ca^{2+} inside the cell and results in a fluorescence intensity increase of approximately 200 times when bound to calcium compared to unbound dye [401]. Confocal microscopy is often utilized to investigate localized Ca^{2+} fluorescence

events due to its small depth of field, which minimizes the accumulation of out-of-focus light [402]. The ability to monitor changes in intracellular Ca^{2+} in real-time in live fluo-3 labeled cells by confocal microscopy allows for collection and interpretation of physiologically relevant data. Although millions of cells were cultured in glass bottom tissue culture dishes for these experiments, under 63X magnification, a typical field consist of between 8-12 3T3-L1 preadipocyte cells and between 6-10 human AoSMCs under subconfluent conditions. Cells were synchronized, or made quiescent prior to imaging or the addition of any test agent by serum deprivation for 6 hours. Thereafter, the cells were loaded with the calcium indicator fluo-3 at 37 °C, washed, and then returned to completed growth medium and incubated at 37 °C to allow for deesterification of the dye. The cells were then allowed to equilibrate at room temperature prior to real time confocal imaging performed at room temperature. Cells were observed and focused in differential interference contrast mode, while changes in fluorescent intensities were measured in response to various agents.

In order to eliminate the possibility of the vehicle eliciting the observed effect, a short baseline was established, the vehicle itself was added directly to the cells, and the cells were monitored for 2 minutes. In each case, the vehicle, either DMSO diluted in HBSS without calcium or oxygen depleted water failed to elicit a response. Thereafter, the test agent was added directly to the cells and another short baseline was established before the addition of ionomycin, which served as a loading control. Changes in intracellular Ca^{2+} were monitored in real time and images were collected at a rate of no faster than 1 frame/second to prevent photobleaching. The fluorescence intensity, measured in arbitrary units, in response to the test agent was normalized to the

background fluorescence. In order to compensate for fluctuations due to focusing, data from every 25 time points were analyzed and the mean fluorescence of at least 8 independent cells were plotted as a function of time.

Several factors were taken into consideration prior to the transfection of plasmid DNA into eukaryotic cells, in order to minimize the possibility of disrupting cellular mechanisms and increase the ability to generate physiologically relevant data and achieve high transfection efficiency. Endotoxins are known to reduce transfection efficiency and subsequent protein expression levels. The levels of endotoxins that are released during the cell lysis step of plasmid preparation may vary in bacterial lysates. Endotoxin-free plasmid preparation kits were utilized to minimize the presence of endotoxins when transfecting plasmid DNA into mammalian cells. Cytotoxicity, a measurement of cell death was monitored during the transfection of mammalian cells. In addition to carefully selecting a transfection reagent characteristic of possessing low cytotoxicity, the quantity of transfection reagent used was kept to a minimum. Off-target effects may include unintended up-regulation or down-regulation of genes within transfected cells. Of the various transfection reagents used (Appendix O), the nonliposomal transfection reagent FuGENE6® provided the highest transfection efficiency of pBINDAHNAK1 into 3T3-L1 cells. The use of FuGENE6® also allowed for convenient delivery of the plasmid DNA, as it is highly efficient both in the presence and absence of serum and reduced the amount of time and effort by eliminating many handling steps. Because most DNA transfection reagents are incompatible with siRNA, DharmaFECT transfection reagent was used to transfect a pool of siRNAs into 3T3-L1 and RGM1 cells.

For either transient transfection of plasmid DNA or siRNA, transfection efficiency was determined by fluorescent microscopy and Western blot and densitometric analysis. To allow the cells to incorporate and process the plasmid DNA or siRNA, transfection efficiency was assessed between 48 and 72 hours after transfection. Since the pBINDAHNAK1 construct codes for a luciferase gene, transfection efficiency of pBINDAHNAK1 was also assessed by performing luciferase assays. Transfection reactions of plasmid DNA or siRNA were performed in the absence of antibiotic and antimycotic, as preliminary optimization experiments demonstrated the presence of either antibiotic or antimycotic significantly reduced transfection efficiency.

Due to AHNAK1's extraordinary large size, a portion containing the carboxy terminal domain and several repeating units were used to create a fusion protein for transient transfection into mammalian cells. The truncated AHNAK1 protein was subcloned into a pACT and pBIND vector to generate a VP16AHNAK1 or pACTAHNAK1 and GAL4AHNAK1 or pBINDAHNAK1. The desired AHNAK1 portion was subcloned into both the empty pACT and pBIND vectors because some constructs may demonstrate directionality depending on the insert.

Although mice completely lacking AHNAK1 do not appear to show a change in cardiac function, it is possible AHNAK2 may compensate for the deficiency in AHNAK1 production. Future studies using mouse embryonic fibroblasts deficient in AHNAK1, AHNAK2, and both AHNAKs will be necessary to determine the functional role and phenotype of AHNAK1 dysregulation. Furthermore, there are no alternative spliced variants of AHNAK1, since AHNAK1 is encoded by an intronless gene. The AHNAKs contain distinct features that allow them to function as multipurpose scaffolding proteins.

AHNAK1 contains a PI3 kinase-related regulatory site, while AHNAK2 contains a PDZ domain, and both AHNAKs contain multiple highly conserved repeating units [217]. Another attribute of the AHNAKs that may allow them to function as scaffolding proteins is their ability to translocate from the nucleus to the plasma membrane of the cell upon various stimuli and posttranslation modification (e.g. phosphorylation).

Table 4. Sequences for siRNAs used in various experiments

Target	Sequence
Mouse NPR3	UGGACGACAUAGUGCGCUA
Mouse NPR3	AGCACAAGGACACGGAAUA
Mouse NPR3	CAAGCUAAACUAAGCGUAU
Mouse NPR3	GGUCUACAGCGACGACAAA
Mouse AHNAK1	GUGCCACCAUCUACUUUGA
Mouse AHNAK1	CCGUAGCUCUGAAGUGGUU
Mouse AHNAK1	GAAGUUGCACCGUAAAGGG
Mouse AHNAK1	UGACCCAGUUGCUGAAUAC

Individually listed ON-TARGETplus set of siRNA reagents. NPR3 represents NPRC. DharmaFECT 1 or DharmaFECT 3 transfection reagents were used to deliver siRNA into cells.

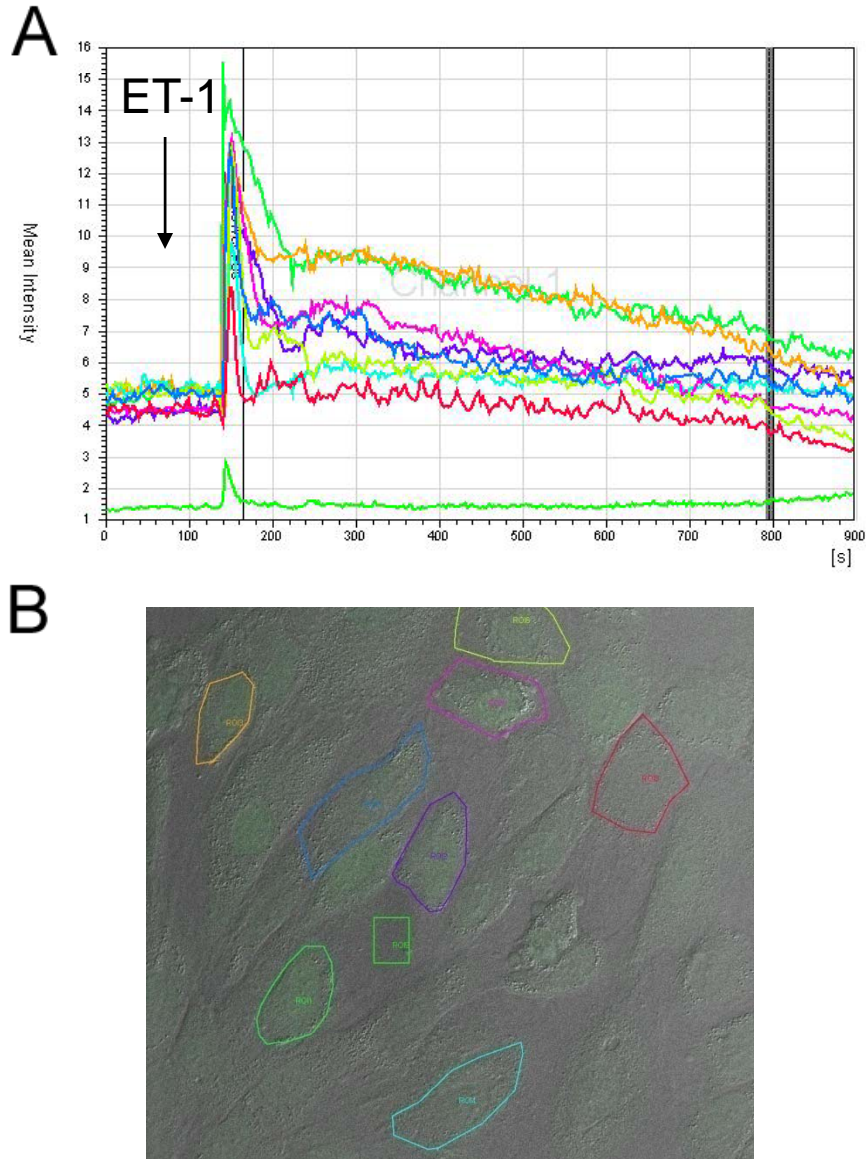


Figure 38. Response to ET-1 in A-10 VSMCs . A: Traces from eight randomly selected cells respond to 1 μ M ET-1 with a rapid and transient increase in intracellular Ca^{2+} . The transient increase in intracellular Ca^{2+} was measured by plotting the mean fluorescence intensity as a function of time (sec) and was compared to background fluorescence (green trace). B: The actual cells shown in the traces in panel A are outlined in panel B, with the green square representing background fluorescence.

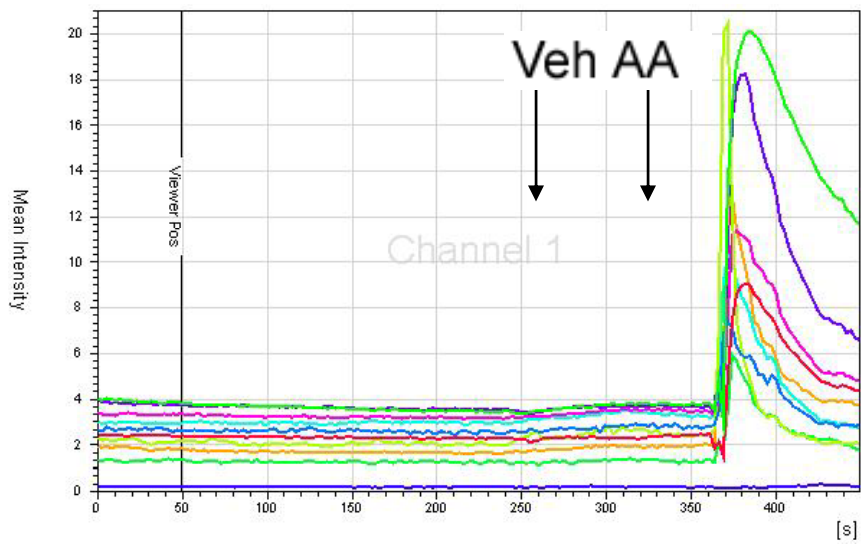


Figure 39. Intracellular Ca^{2+} mobilization in quiescent AoSMC in response to $1 \mu\text{M}$ AA. Superimposed traces showing fluo-3 fluorescence plotted as a function of time, in which each color trace represents an individual cell. AoSMC pre-loaded with Fluo-3 AM were stimulated with vehicle (Veh) and then arachidonic acid (AA) in the presence of extracellular Ca^{2+} . Fluorescent intensity was compared to background fluorescence.

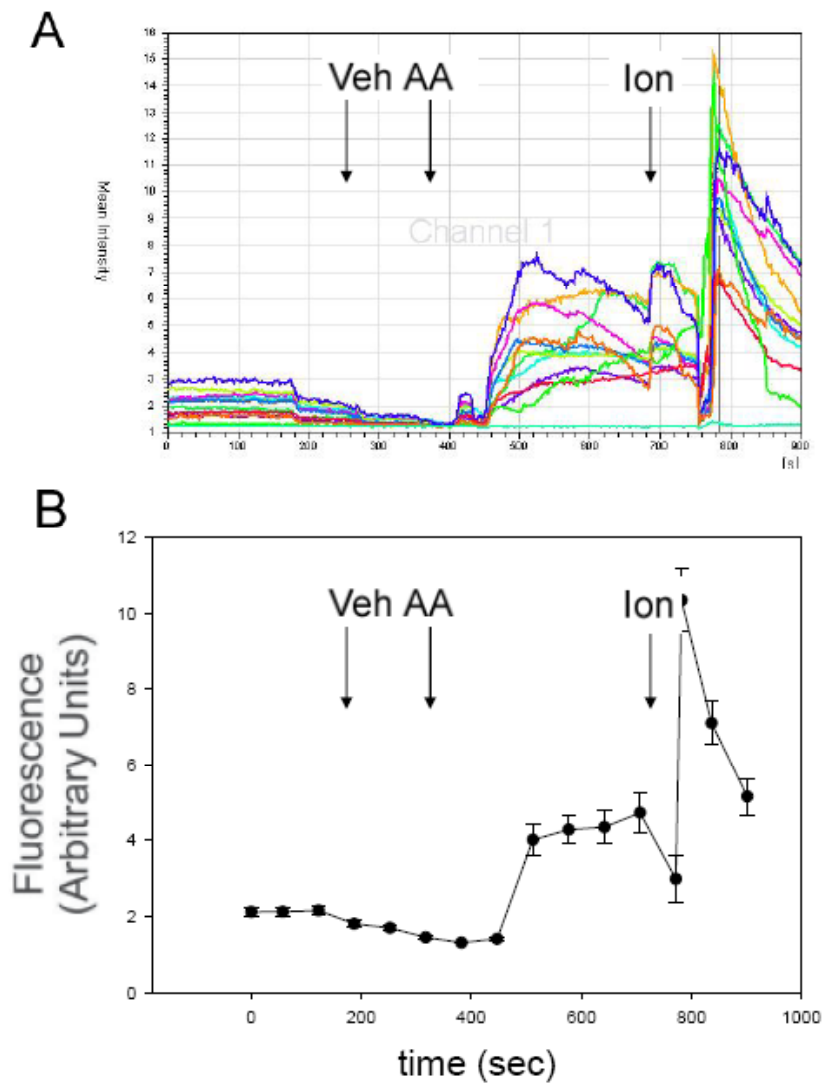


Figure 40. Intracellular Ca^{2+} mobilization in quiescent AoSMC in response to $25 \mu\text{M}$ AA. A: Superimposed traces showing fluo-3 fluorescence plotted as a function of time, in which each color trace represents an individual cell. B: Line graph showing fluo-3 fluorescence intensity plotted as a function of time for eight cells, in which every 25 time points from images captured at 1 frame/second were plotted as mean \pm SE as a function of time. AoSMC pre-loaded with Fluo-3 AM were stimulated with Veh, AA, and then ionomycin (Ion) in the presence of extracellular Ca^{2+} . Fluorescent intensity was compared to background fluorescence.

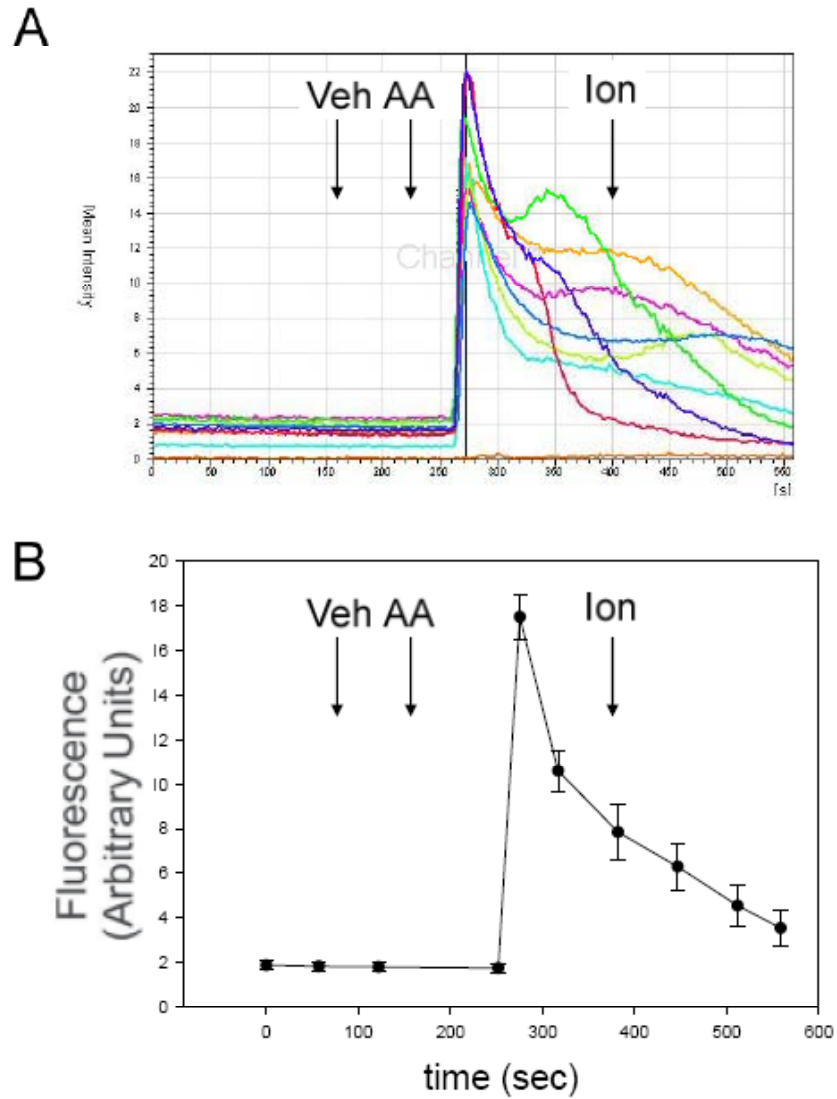


Figure 41. Intracellular Ca^{2+} mobilization in quiescent AoSMC in response to $25 \mu\text{M}$ AA in calcium free medium. A: Superimposed traces showing fluo-3 fluorescence plotted as a function of time, in which each color trace represents an individual cell. B: Line graph showing fluo-3 fluorescence intensity plotted as a function of time for eight cells, in which every 25 time points from images captured at 1 frame/second were plotted as mean \pm SE as a function of time. AoSMC pre-loaded with Fluo-3 AM were stimulated with Veh, AA, and then Ion in the absence of extracellular Ca^{2+} . Fluorescent intensity was compared to background fluorescence.

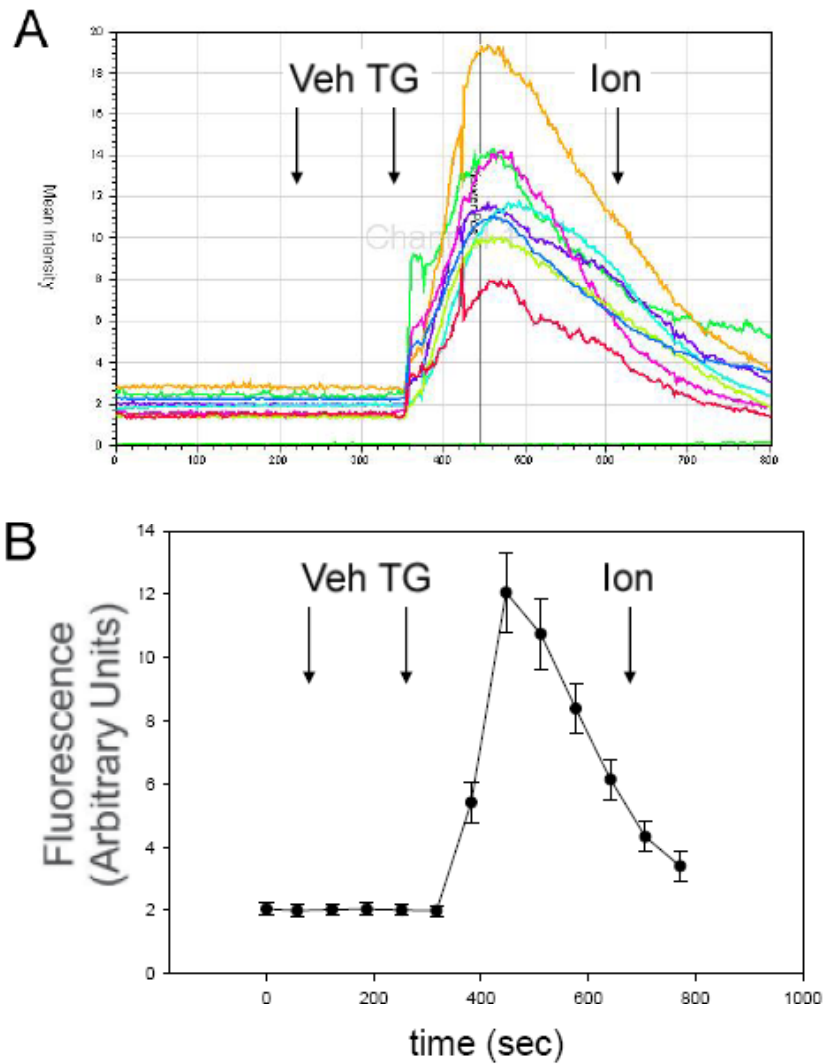


Figure 42. Intracellular Ca^{2+} mobilization in quiescent AOSMC in response to $1 \mu\text{M}$ TG. A: Superimposed traces showing fluo-3 fluorescence plotted as a function of time, in which each color trace represents an individual cell. B: Line graph showing fluo-3 fluorescence intensity plotted as a function of time for eight cells, in which every 25 time points from images captured at 1 frame/second were plotted as mean \pm SE as a function of time. AOSMC pre-loaded with Fluo-3 AM were stimulated with Veh, thapsigargin (TG) and then Ion in the absence of extracellular Ca^{2+} . Fluorescent intensity was compared to background fluorescence.

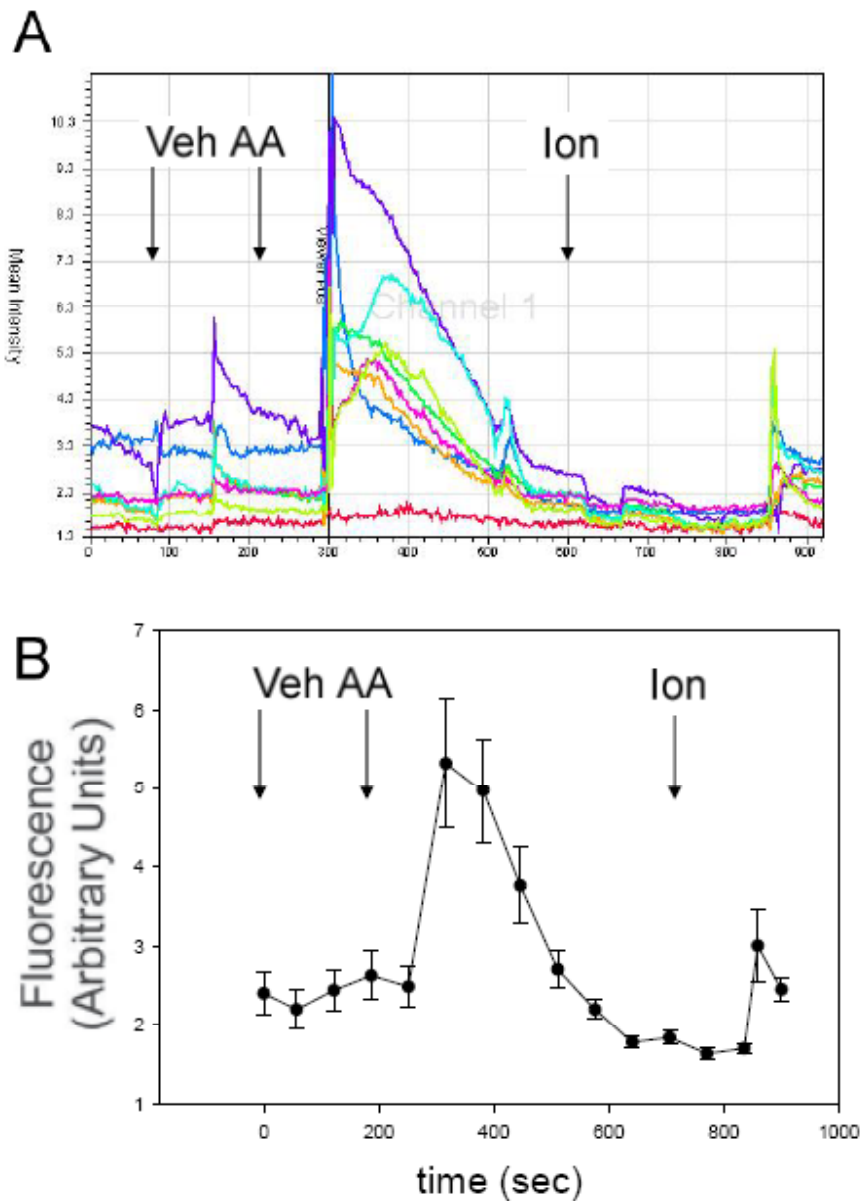


Figure 43. Intracellular Ca^{2+} mobilization in quiescent AoSMC in response to $100 \mu\text{M}$ AA. A: Superimposed traces showing fluo-3 fluorescence plotted as a function of time, in which each color trace represents an individual cell. B: Line graph showing fluo-3 fluorescence intensity plotted as a function of time for eight cells, in which every 25 time points from images captured at 1 frame/second were plotted as mean \pm SE as a function of time. AoSMC pre-loaded with Fluo-3 AM were stimulated with Veh, AA, and then Ion in the presence of extracellular Ca^{2+} . Fluorescent intensity was compared to background fluorescence.

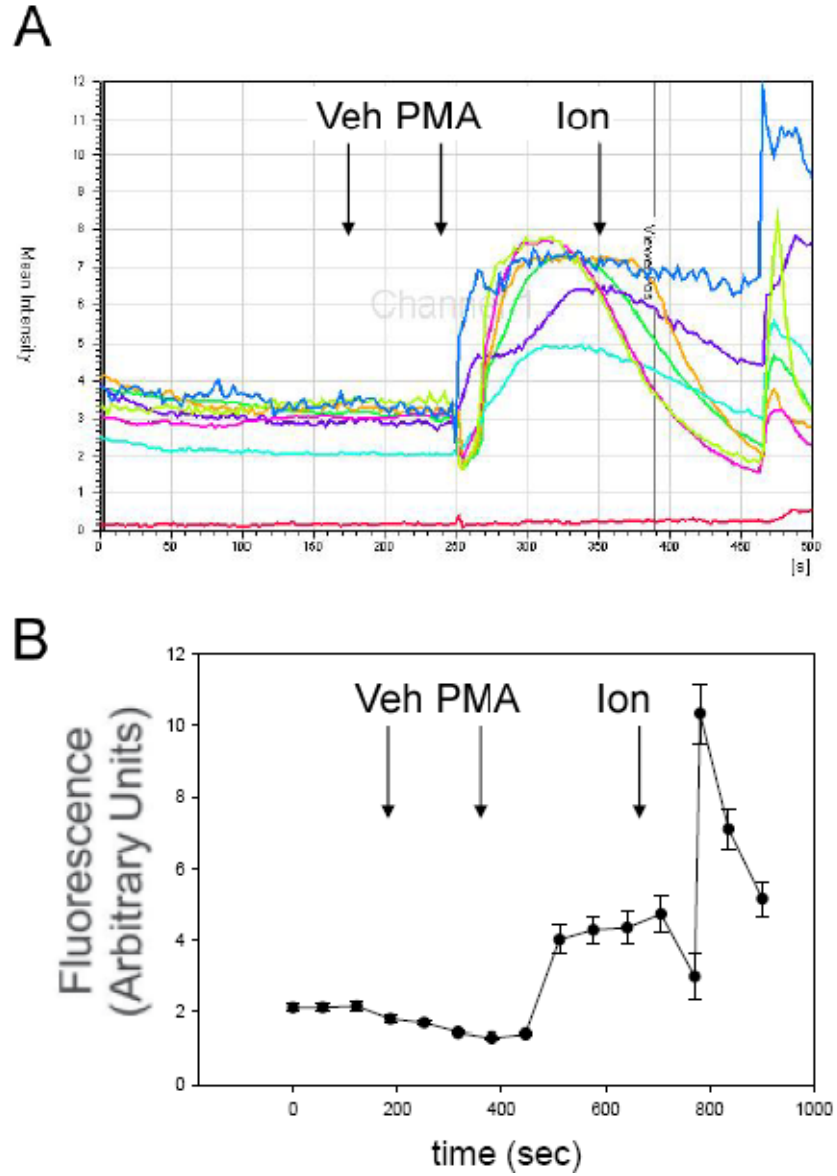


Figure 44. Intracellular Ca^{2+} mobilization in quiescent AoSMC in response to 25 μM PMA. A: Superimposed traces showing fluo-3 fluorescence plotted as a function of time, in which each color trace represents an individual cell. B: Line graph showing fluo-3 fluorescence intensity plotted as a function of time for eight cells, in which every 25 time points from images captured at 1 frame/second were plotted as mean \pm SE as a function of time. AoSMC pre-loaded with Fluo-3 AM were stimulated with Veh, Phorbol 12-myristate-13-acetate (PMA), and then Ion in the presence of extracellular Ca^{2+} . Fluorescent intensity was compared to background fluorescence.

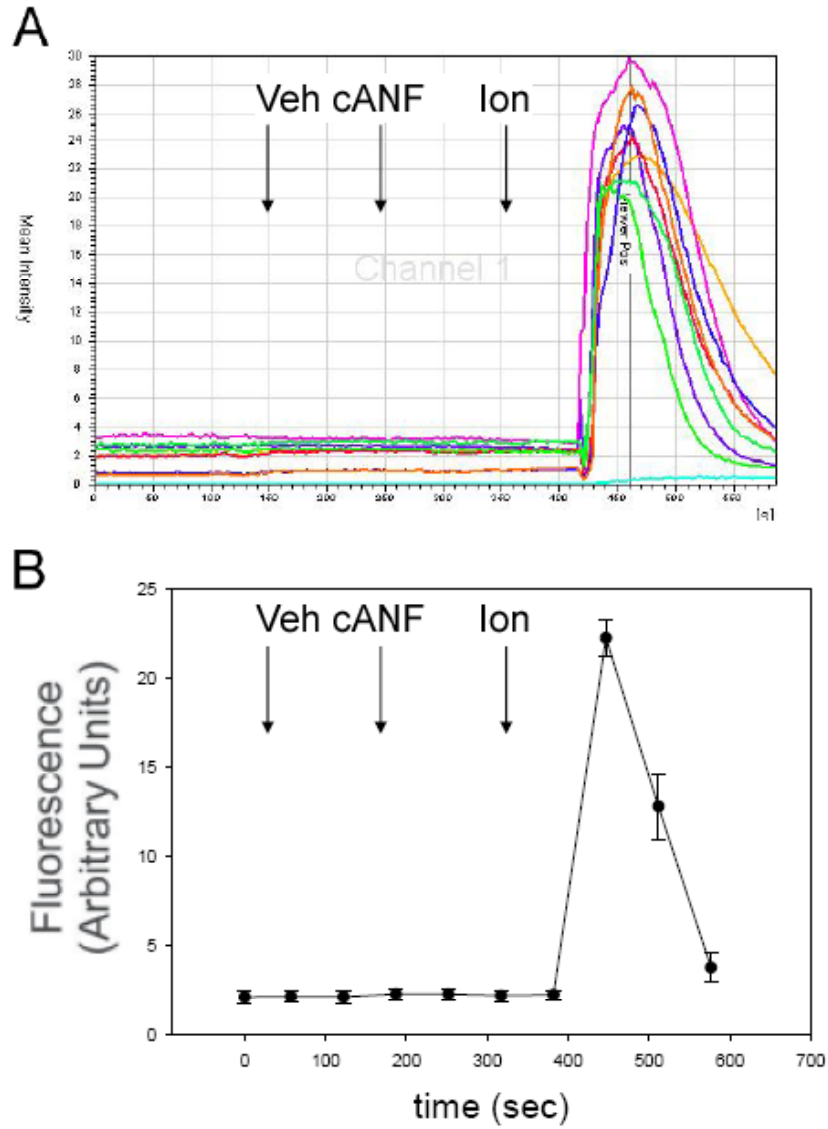


Figure 45. Intracellular Ca^{2+} mobilization in quiescent AoSMC in response to $1 \mu\text{M}$ cANF. A: Superimposed traces showing fluo-3 fluorescence plotted as a function of time, in which each color trace represents an individual cell. B: Line graph showing fluo-3 fluorescence intensity plotted as a function of time for eight cells, in which every 25 time points from images captured at 1 frame/second were plotted as mean \pm SE as a function of time. 3T3-L1 preadipocytes pre-loaded with Fluo-3 AM were stimulated with Veh, des[Gln18, Ser19, Gly20, Leu21, Gly22]-ANP(4-23)-NH₂ (cANF), and then Ion in the presence of extracellular Ca^{2+} . Fluorescent intensity was compared to background fluorescence.

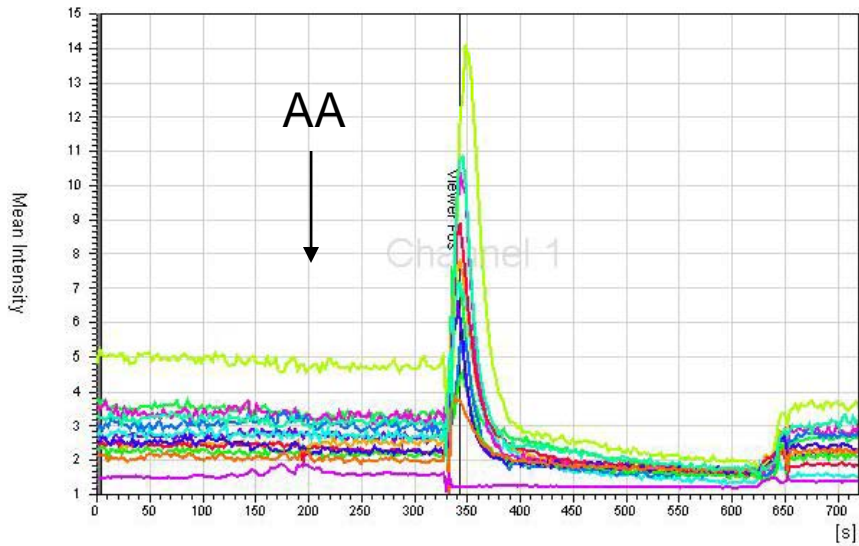


Figure 46. Intracellular Ca^{2+} mobilization in quiescent 3T3-L1 preadipocytes in response to 100 μM AA. A: Superimposed traces showing fluo-3 fluorescence plotted as a function of time, in which each color trace represents an individual cell. B: Line graph showing fluo-3 fluorescence intensity plotted as a function of time for eight cells, in which every 25 time points from images captured at 1 frame/second were plotted as mean \pm SE as a function of time. 3T3-L1 preadipocytes preloaded with Fluo-3 AM were stimulated with Veh, AA, and then lon in the presence of extracellular Ca^{2+} . Fluorescent intensity was compared to background fluorescence.

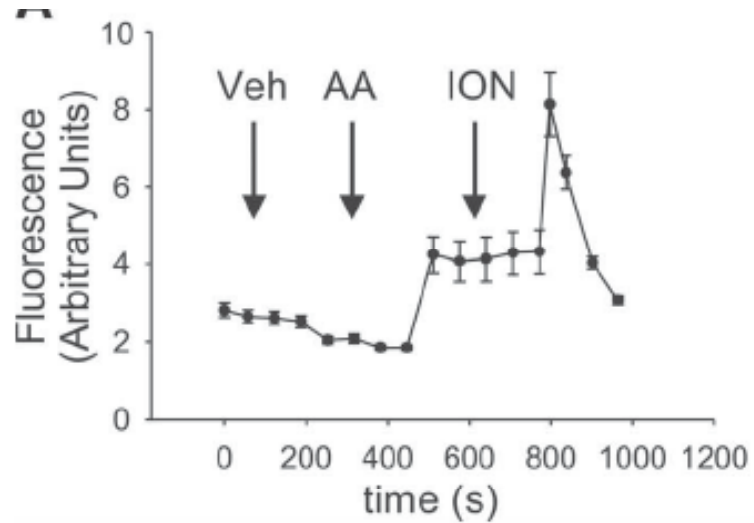


Figure 47. Intracellular Ca^{2+} mobilization in quiescent 3T3-L1 preadipocytes in response to 25 μM AA. A: Superimposed traces showing fluo-3 fluorescence plotted as a function of time, in which each color trace represents an individual cell. B: Line graph showing fluo-3 fluorescence intensity plotted as a function of time for eight cells, in which every 25 time points from images captured at 1 frame/second were plotted as mean \pm SE as a function of time. 3T3-L1 preadipocytes pre-loaded with Fluo-3 AM were stimulated with Veh, AA, and then Ion in the presence of extracellular Ca^{2+} . Fluorescent intensity was compared to background fluorescence.

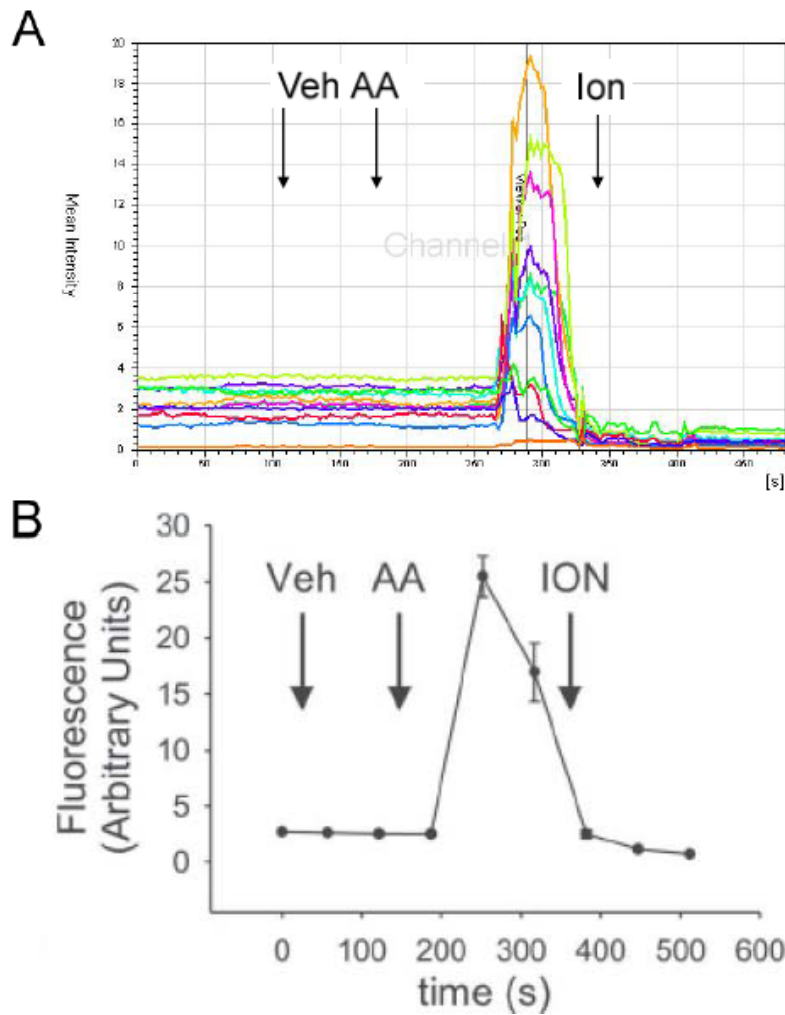


Figure 48. Intracellular Ca^{2+} mobilization in quiescent 3T3-L1 preadipocytes in response to 25 μM AA in the absence of extracellular Ca^{2+} . A: Superimposed traces showing fluo-3 fluorescence plotted as a function of time, in which each color trace represents an individual cell. B: Line graph showing fluo-3 fluorescence intensity plotted as a function of time for eight cells, in which every 25 time points from images captured at 1 frame/second were plotted as mean \pm SE as a function of time. 3T3-L1 preadipocytes pre-loaded with Fluo-3 AM were stimulated with Veh, AA, and then Ion in the absence of extracellular Ca^{2+} . Fluorescent intensity was compared to background fluorescence.

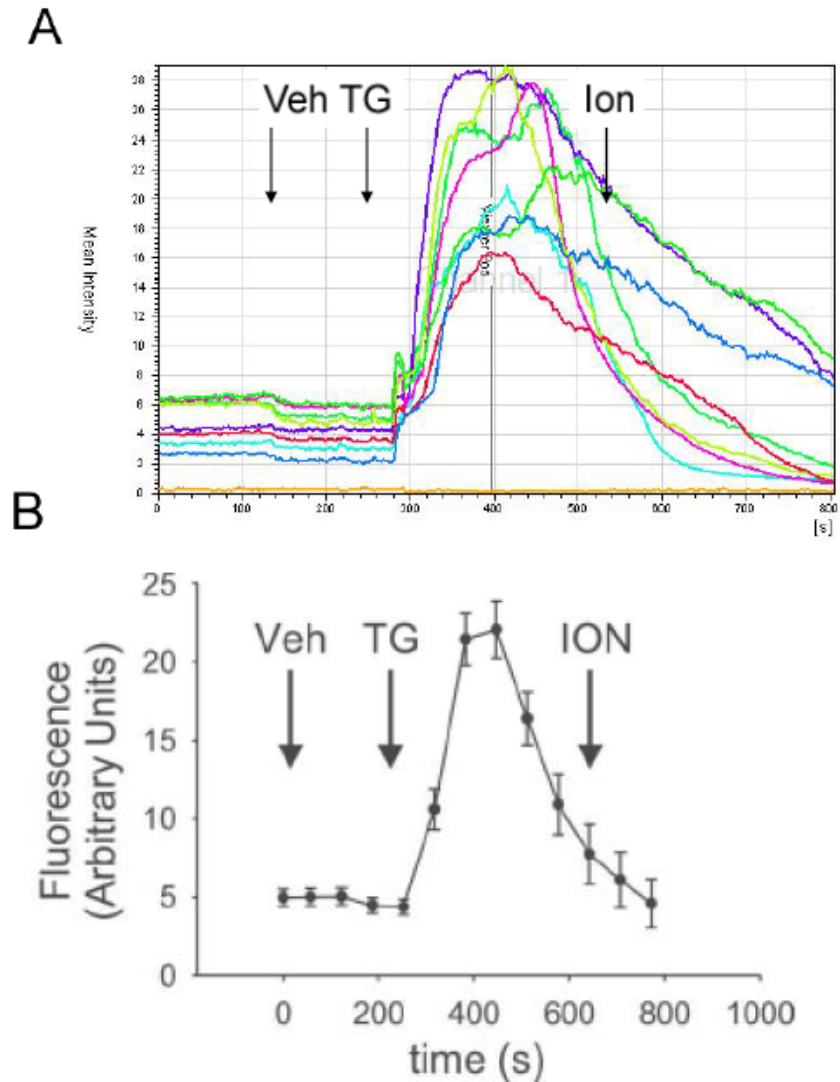


Figure 49. Intracellular Ca^{2+} mobilization in quiescent 3T3-L1 preadipocytes in response to 1 μM TG. A: Superimposed traces showing fluo-3 fluorescence plotted as a function of time, in which each color trace represents an individual cell. B: Line graph showing fluo-3 fluorescence intensity plotted as a function of time for eight cells, in which every 25 time points from images captured at 1 frame/second were plotted as mean \pm SE as a function of time. 3T3-L1 preadipocytes pre-loaded with Fluo-3 AM were stimulated with Veh, TG and then Ion in the absence of extracellular Ca^{2+} . Fluorescent intensity was compared to background fluorescence.

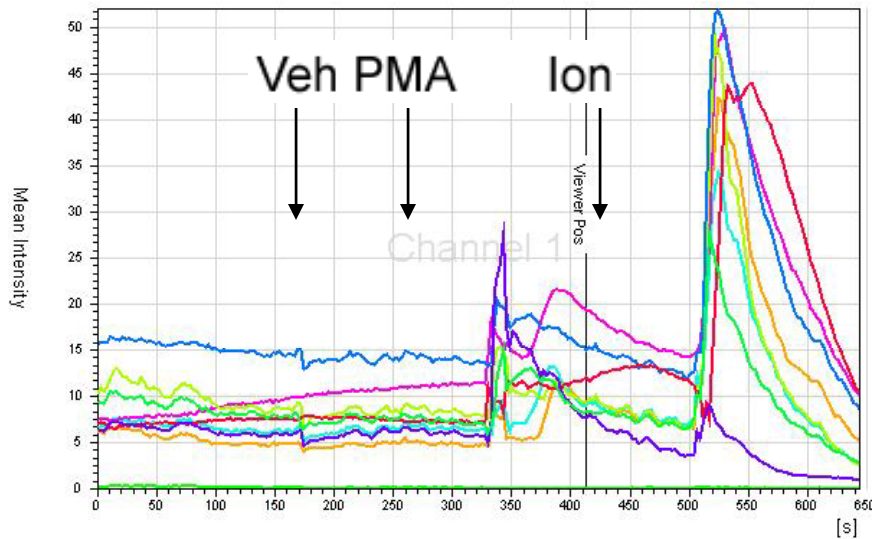


Figure 50. Intracellular Ca^{2+} mobilization in quiescent 3T3-L1 preadipocytes in response to $1 \mu\text{M}$ PMA. A: Superimposed traces showing fluo-3 fluorescence plotted as a function of time, in which each color trace represents an individual cell. B: Line graph showing fluo-3 fluorescence intensity plotted as a function of time for eight cells, in which every 25 time points from images captured at 1 frame/second were plotted as mean \pm SE as a function of time. 3T3-L1 preadipocytes preloaded with Fluo-3 AM were stimulated with Veh, PMA, and then Ion in the presence of extracellular Ca^{2+} . Fluorescent intensity was compared to background fluorescence.

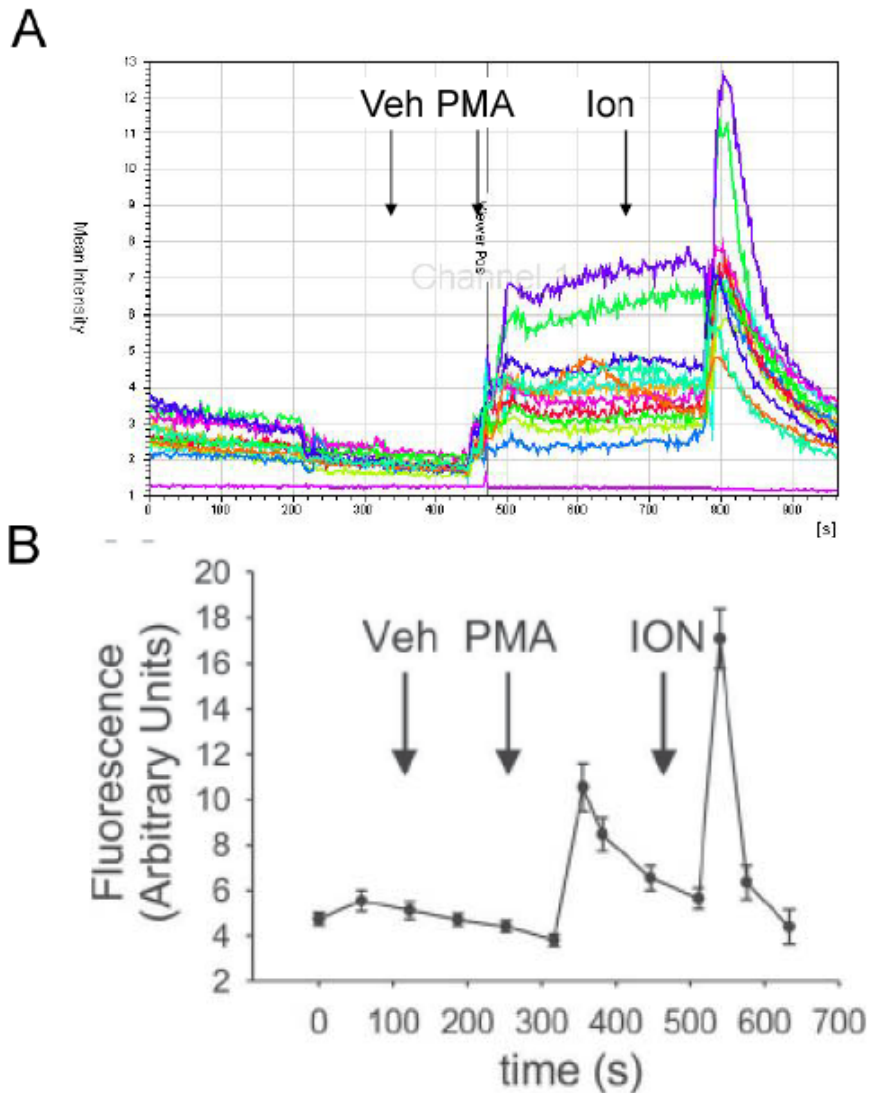


Figure 51. Intracellular Ca^{2+} mobilization in quiescent 3T3-L1 preadipocytes in response to 25 μM PMA. A: Superimposed traces showing fluo-3 fluorescence plotted as a function of time, in which each color trace represents an individual cell. B: Line graph showing fluo-3 fluorescence intensity plotted as a function of time for eight cells, in which every 25 time points from images captured at 1 frame/second were plotted as mean \pm SE as a function of time. 3T3-L1 preadipocytes pre-loaded with Fluo-3 AM were stimulated with Veh, PMA, and then Ion in the presence of extracellular Ca^{2+} . Fluorescent intensity was compared to background fluorescence.

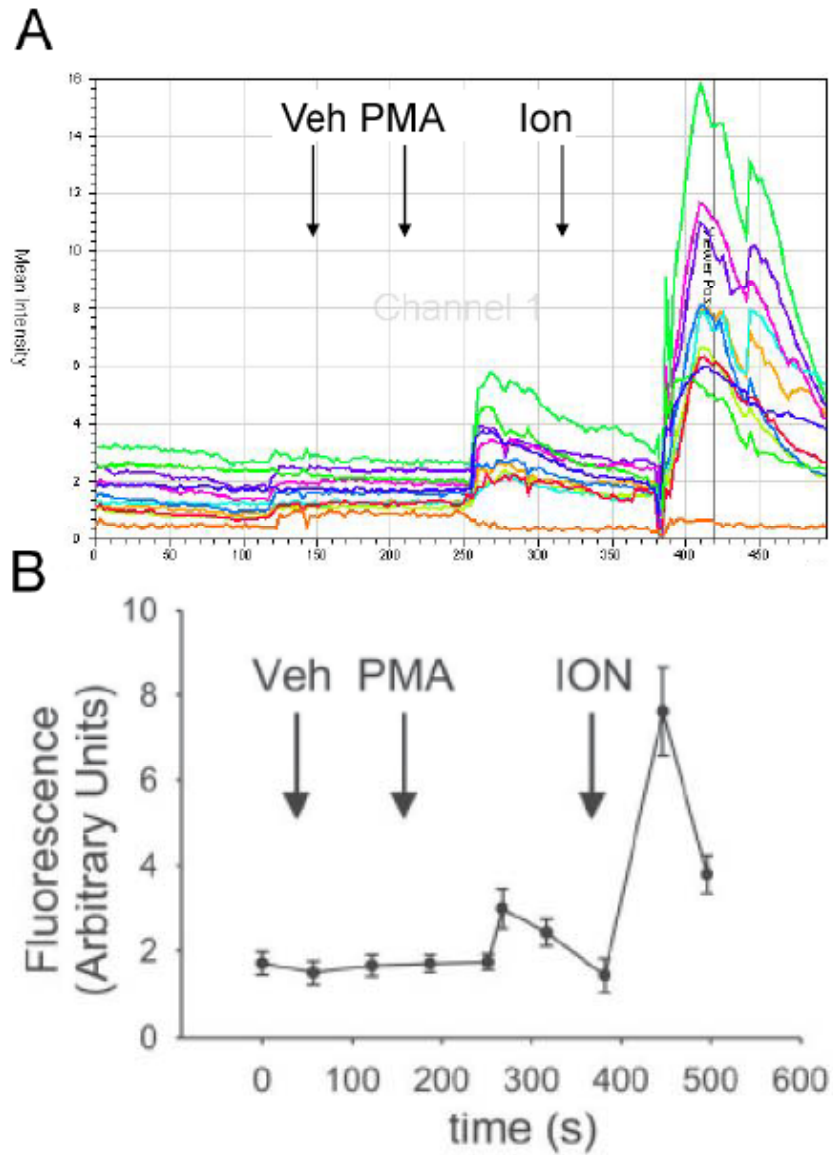


Figure 52. Effect of NPRC knockdown on intracellular Ca^{2+} mobilization in quiescent 3T3-L1 preadipocytes in response to 25 μM PMA. A: Superimposed traces showing fluo-3 fluorescence plotted as a function of time, in which each color trace represents an individual cell. B: Line graph showing fluo-3 fluorescence intensity plotted as a function of time for eight cells, in which every 25 time points from images captured at 1 frame/second were plotted as mean \pm SE as a function of time. 3T3-L1 preadipocytes pre-loaded with Fluo-3 AM were stimulated with Veh, PMA, and then Ion in the presence of extracellular Ca^{2+} . Fluorescent intensity was compared to background fluorescence.

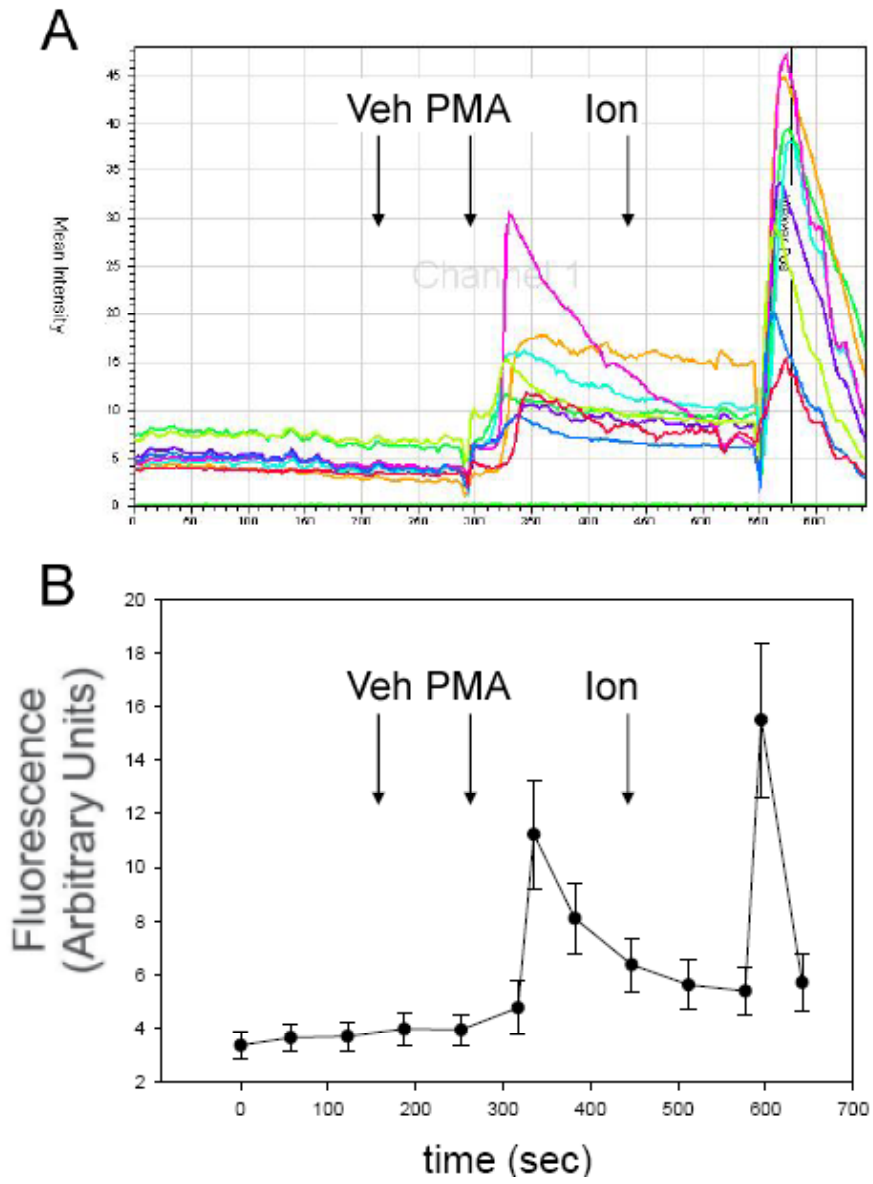


Figure 53. Effect of overexpression of an pBINDAHNAK1 construct on intracellular Ca²⁺ mobilization in quiescent 3T3-L1 preadipocytes in response to 1 μM PMA. A: Superimposed traces showing fluo-3 fluorescence plotted as a function of time, in which each color trace represents an individual cell. B: Line graph showing fluo-3 fluorescence intensity plotted as a function of time for eight cells, in which every 25 time points from images captured at 1 frame/second were plotted as mean±SE as a function of time. 3T3-L1 preadipocytes pre-loaded with Fluo-3 AM were stimulated with Veh, PMA, and then Ion in the presence of extracellular Ca²⁺. Fluorescent intensity was compared to background fluorescence.

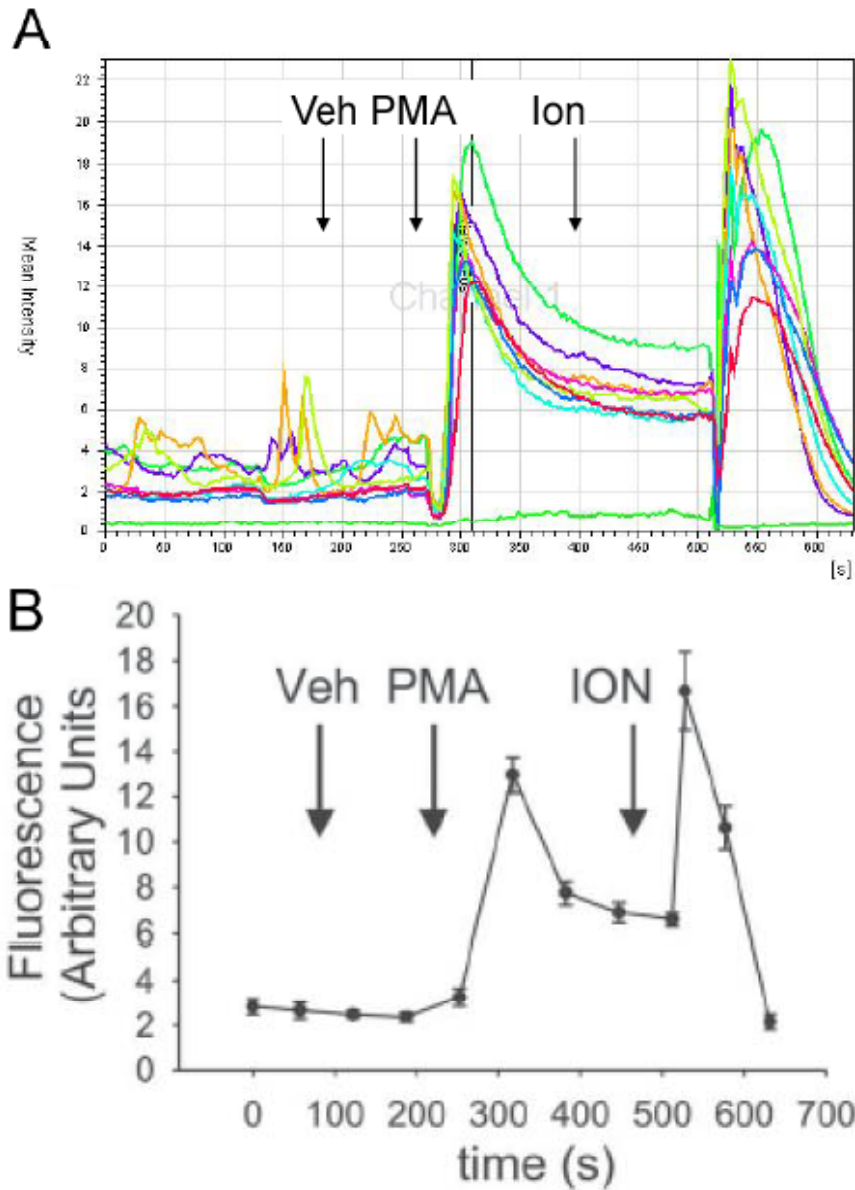


Figure 54. Effect of overexpression of an pBINDAHNAK1 construct on intracellular Ca^{2+} mobilization in quiescent 3T3-L1 preadipocytes in response to 25 μM PMA. A: Superimposed traces showing fluo-3 fluorescence plotted as a function of time, in which each color trace represents an individual cell. B: Line graph showing fluo-3 fluorescence intensity plotted as a function of time for eight cells, in which every 25 time points from images captured at 1 frame/second were plotted as mean \pm SE as a function of time. 3T3-L1 preadipocytes pre-loaded with Fluo-3 AM were stimulated with Veh, PMA, and then Ion in the presence of extracellular Ca^{2+} . Fluorescent intensity was compared to background fluorescence.

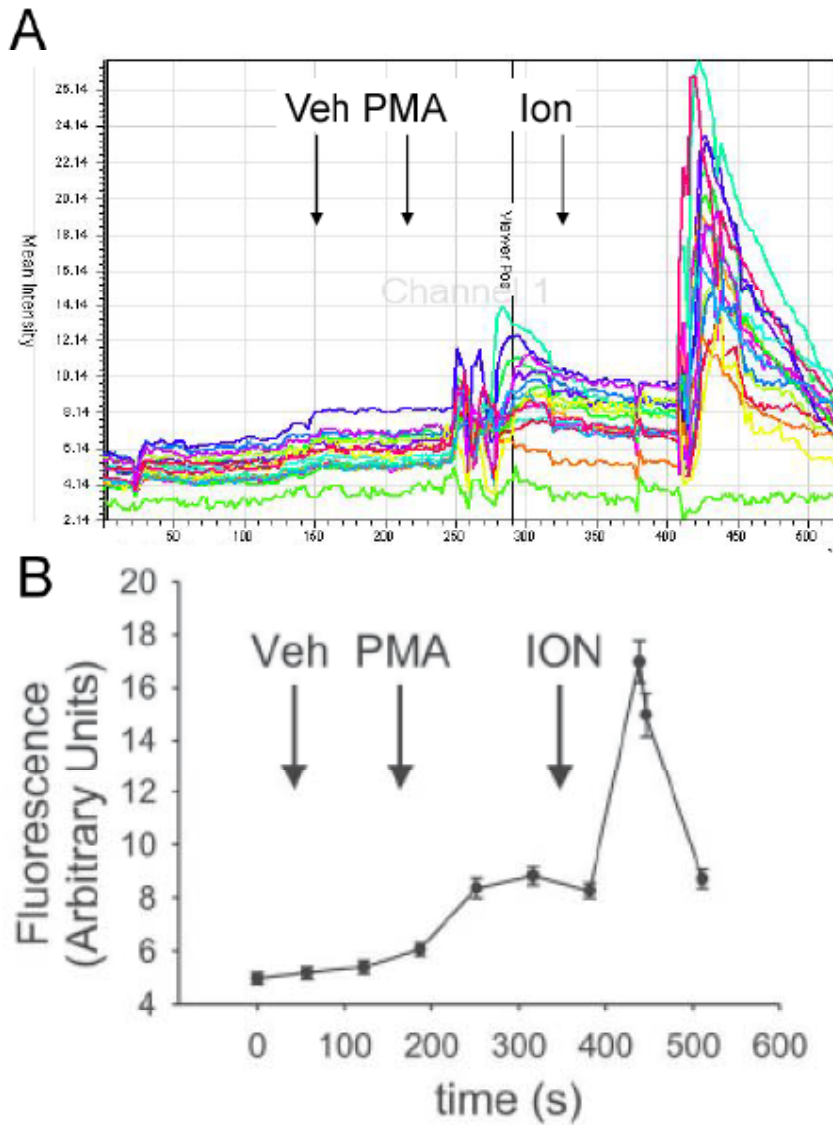


Figure 55. Effect of AHNAK1 knockdown on intracellular Ca^{2+} mobilization in quiescent 3T3-L1 preadipocytes in response to 25 μM PMA. A: Superimposed traces showing fluo-3 fluorescence plotted as a function of time, in which each color trace represents an individual cell. B: Line graph showing fluo-3 fluorescence intensity plotted as a function of time for eight cells, in which every 25 time points from images captured at 1 frame/second were plotted as mean \pm SE as a function of time. 3T3-L1 preadipocytes pre-loaded with Fluo-3 AM were stimulated with Veh, PMA, and then Ion in the presence of extracellular Ca^{2+} . Fluorescent intensity was compared to background fluorescence.

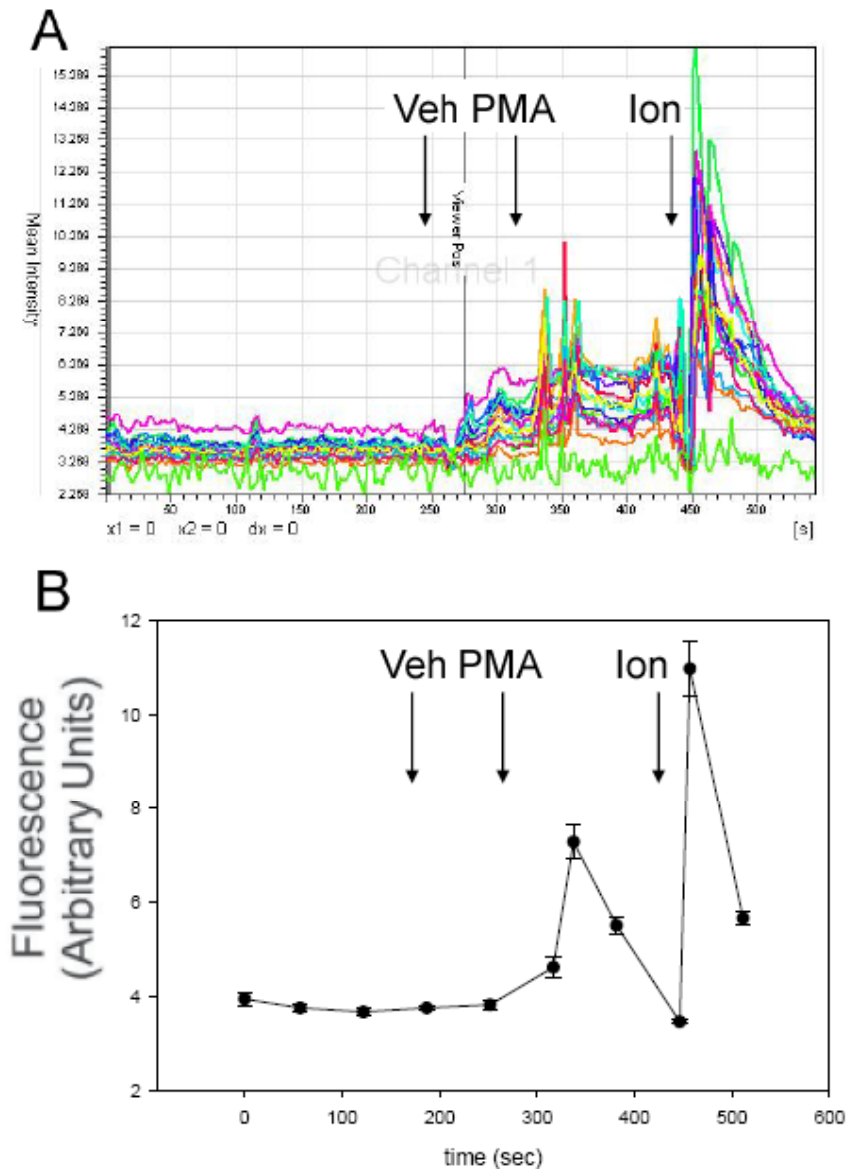


Figure 56. Effect of AHNAK1 knockdown on intracellular Ca^{2+} mobilization in quiescent day 2 differentiated 3T3-L1 preadipocytes in response to 25 μM PMA. A: Superimposed traces showing fluo-3 fluorescence plotted as a function of time, in which each color trace represents an individual cell. B: Line graph showing fluo-3 fluorescence intensity plotted as a function of time for eight cells, in which every 25 time points from images captured at 1 frame/second were plotted as mean \pm SE as a function of time. 3T3-L1 preadipocytes pre-loaded with Fluo-3 AM were stimulated with Veh, PMA, and then Ion in the presence of extracellular Ca^{2+} . Fluorescent intensity was compared to background fluorescence.

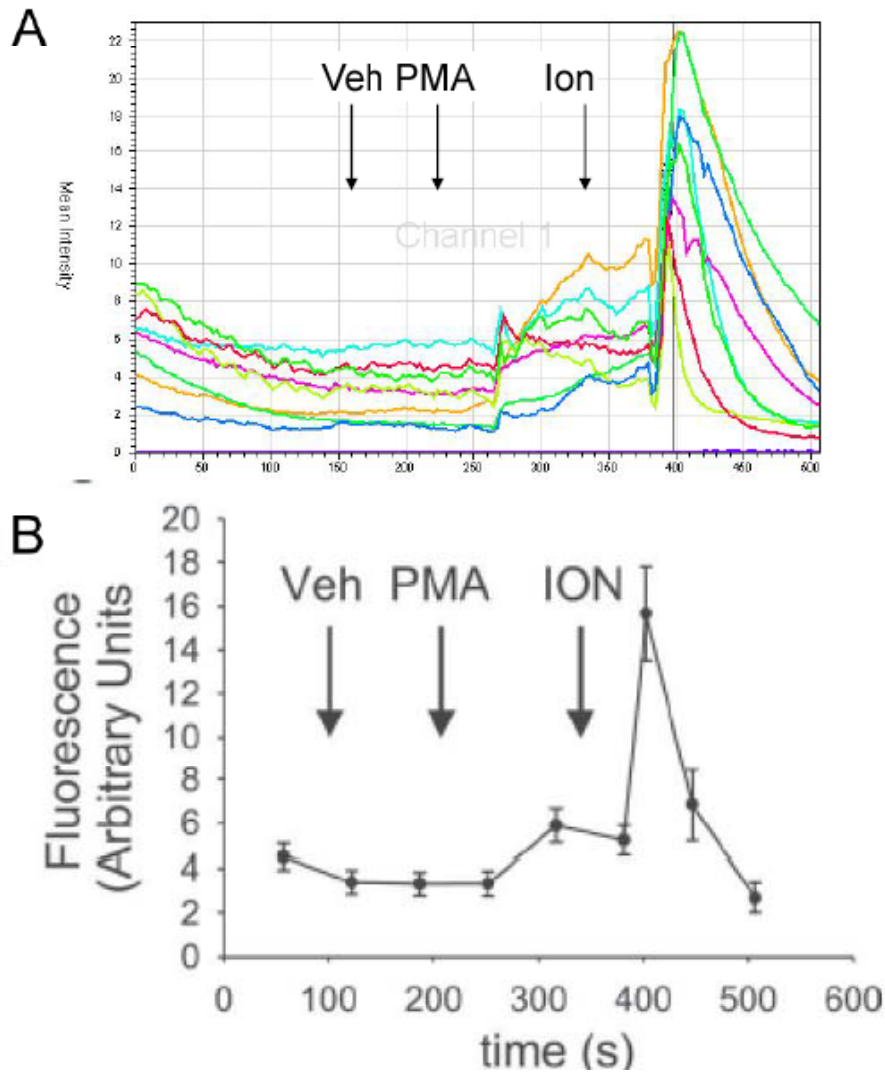


Figure 57. Intracellular Ca^{2+} mobilization in quiescent 3T3-L1 preadipocytes pretreated with AACOCF3 in response to 25 μM PMA. A: Superimposed traces showing fluo-3 fluorescence plotted as a function of time, in which each color trace represents an individual cell. B: Line graph showing fluo-3 fluorescence intensity plotted as a function of time for eight cells, in which every 25 time points from images captured at 1 frame/second were plotted as mean \pm SE as a function of time. 3T3-L1 preadipocytes pre-loaded with Fluo-3 AM were stimulated with Veh, PMA, and then Ion in the presence of extracellular Ca^{2+} . Fluorescent intensity was compared to background fluorescence.

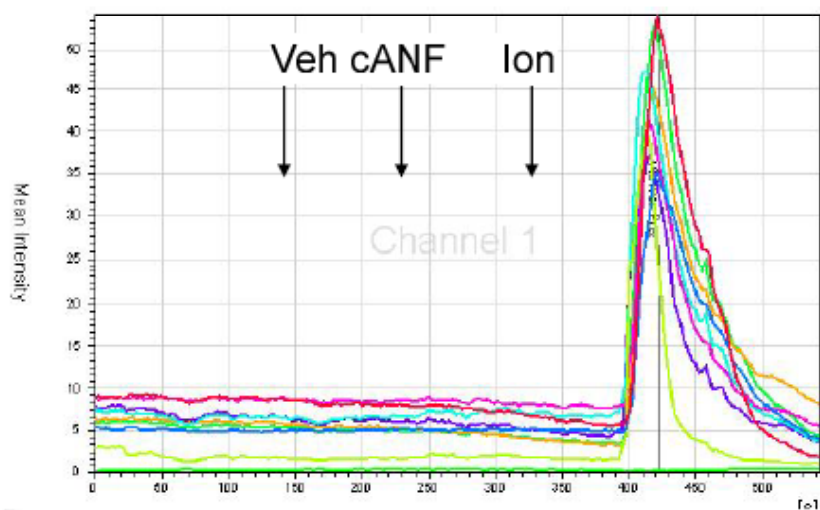
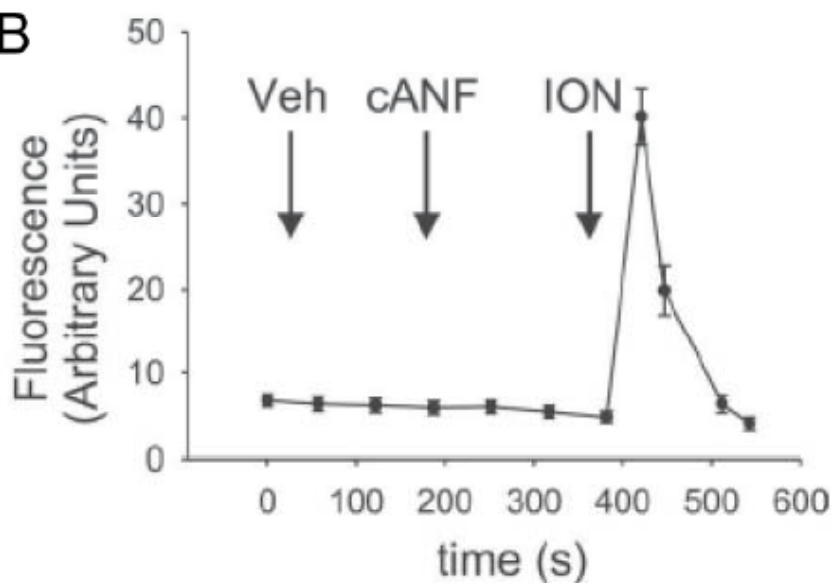
A**B**

Figure 58. Intracellular Ca^{2+} mobilization in quiescent 3T3-L1 preadipocytes in response to $1 \mu\text{M}$ cANF. A: Superimposed traces showing fluo-3 fluorescence plotted as a function of time, in which each color trace represents an individual cell. B: Line graph showing fluo-3 fluorescence intensity plotted as a function of time for eight cells, in which every 25 time points from images captured at 1 frame/second were plotted as mean \pm SE as a function of time. 3T3-L1 preadipocytes pre-loaded with Fluo-3 AM were stimulated with Veh, cANF, and then Ion in the presence of extracellular Ca^{2+} . Fluorescent intensity was compared to background fluorescence.

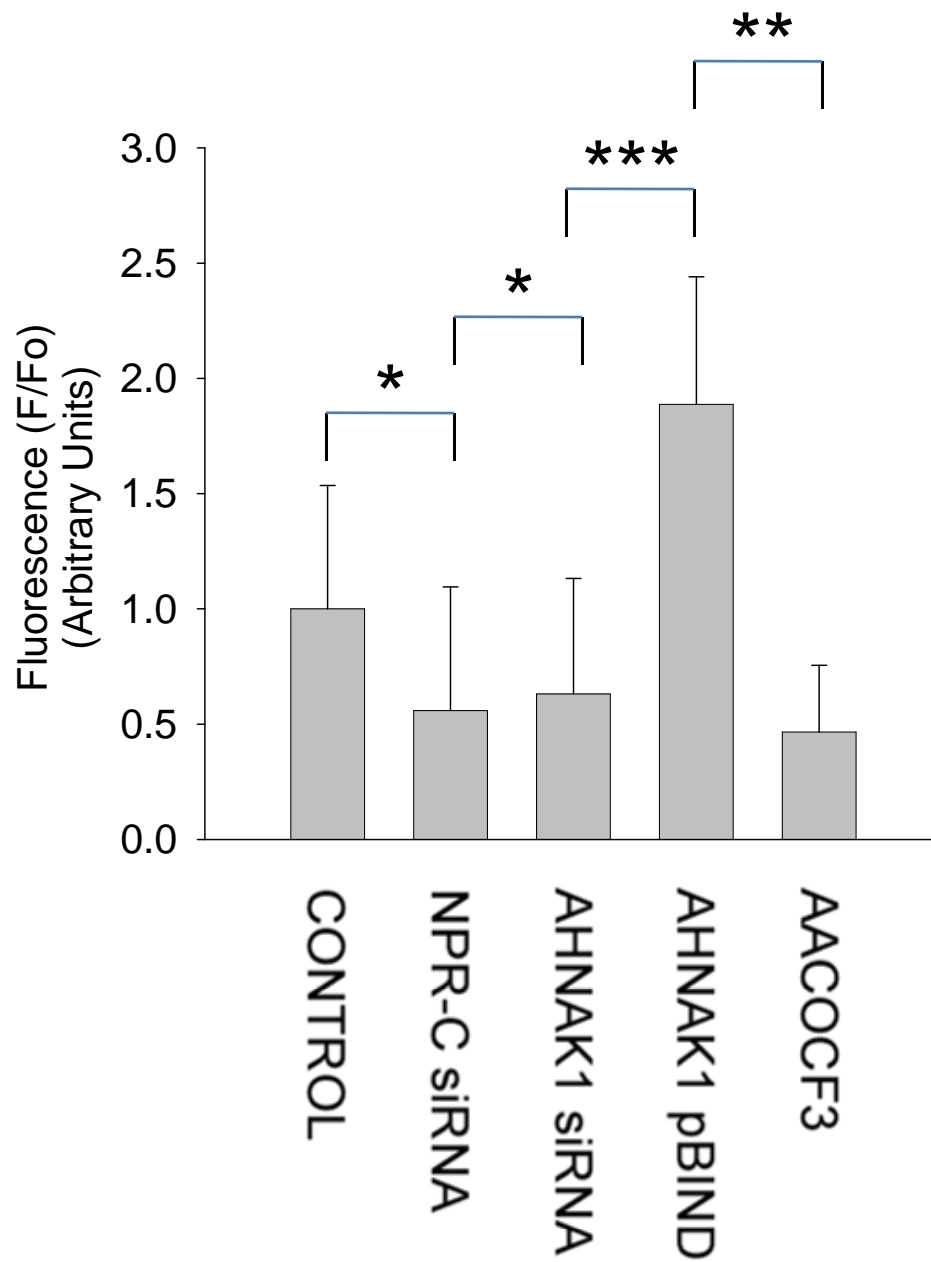


Figure 59. Comparisons of various intracellular Ca²⁺ experiments

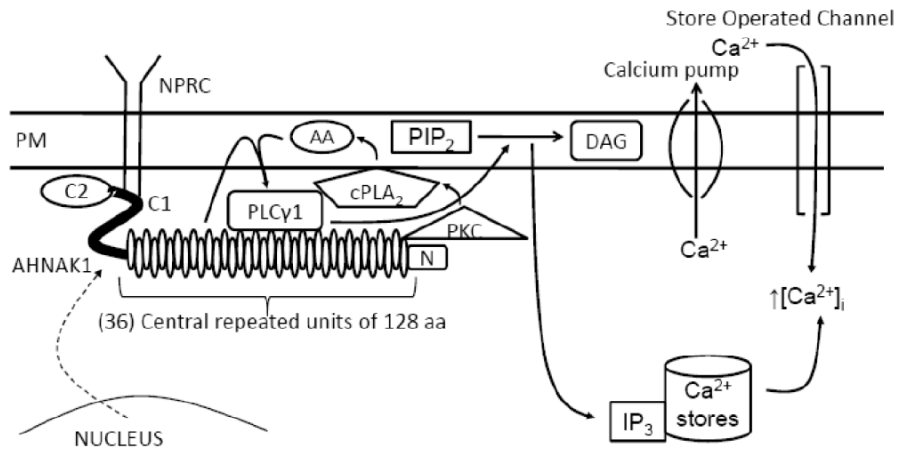


Figure 60. Proposed role of NPRC in intracellular Ca²⁺ mobilization through AHNAK1 and AA. AHNAK1 translocates from the nucleus to the plasma membrane upon various stimuli. The C1 domain of AHNAK1 associates with the cytoplasmic tail of NPRC. AHNAK1 is tethered by NPRC to the plasma membrane, where it functions as a receptor for AA liberated from membrane phospholipid bilayers by cPLA₂. Together, AHNAK1 and AA, potentiate the release of intracellular Ca²⁺ from ER stores. The highly conserved central repeating units of AHNAK1 have been reported to bind to and activate PLCγ1 in the presence of AA. The activation of cPLA₂ by PKC results in the release of AA, while the activation of PLCγ1 by AHNAK1 and free AA results in the production of IP₃. IP₃ triggers Ca²⁺ release from intracellular Ca²⁺ stores through binding to IP₃ receptors

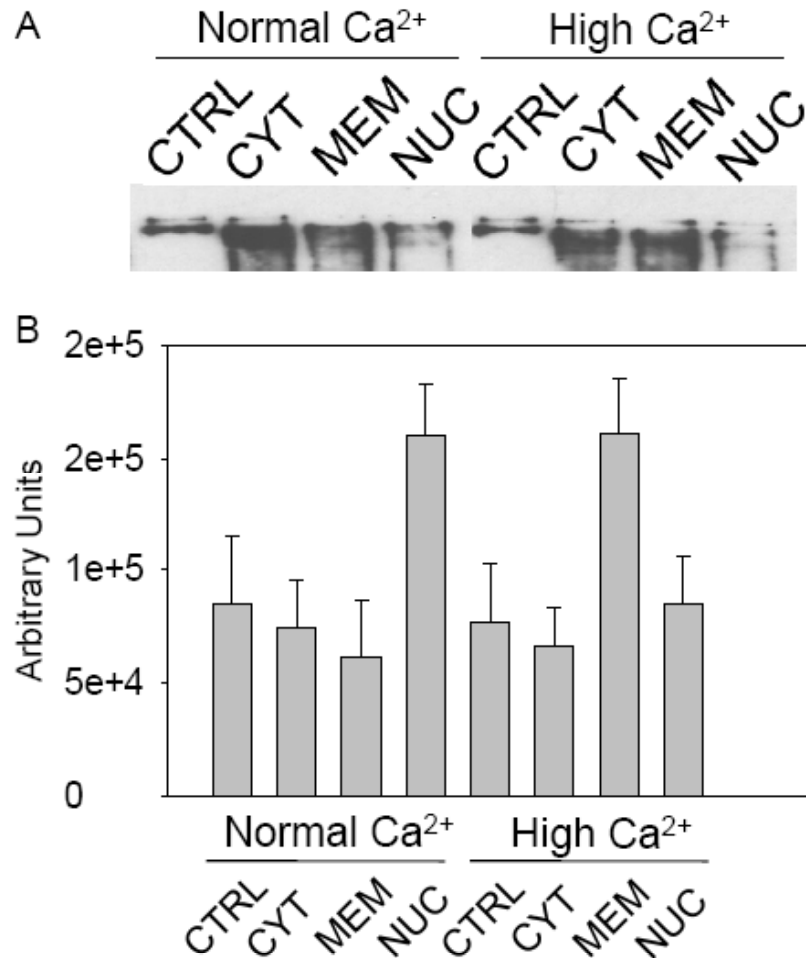


Figure 61. Western blot and densitometric analysis showing the effect of increasing $[Ca^{2+}]_e$ on AHNAK1 translocation in 3T3-L1 preadipocytes. A: Western blot analysis after subcellular fraction of 3T3-L1 preadipocytes showing less AHNAK1 in the nuclear fraction and more AHNAK1 in the membrane fraction after switching 3T3-L1 preadipocytes from normal to high Ca^{2+} . B: Densitometric analysis of (A). 3T3-L1 preadipocytes were initially cultured in medium containing normal Ca^{2+} (1.8 mM) and were then switched to medium containing high Ca^{2+} (7.2 mM) and cultured for an additional 6 hours before fixing the cells and performing subcellular fraction experiments. CTRL refers to whole cell lysate control, CYT refers to cytosolic fraction, MEM refers to membrane fraction, and NUC refers to nuclear fraction.

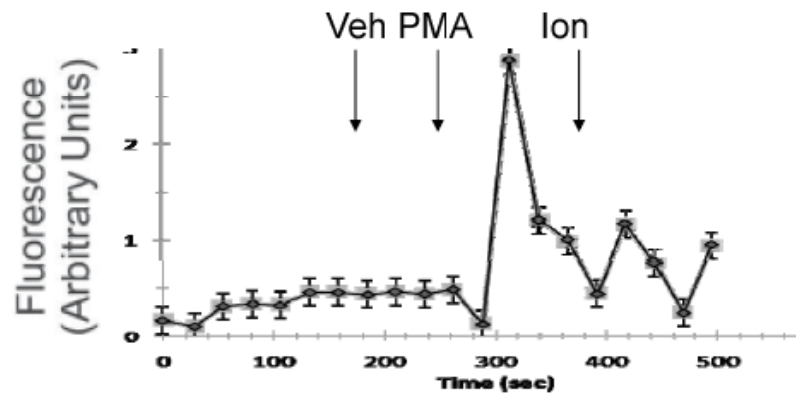


Figure 62. Effect of increased $[Ca^{2+}]_e$ on $[Ca^{2+}]_i$ mobilization in 3T3-L1 preadipocytes. 3T3-L1 preadipocytes were initially cultured in medium containing normal Ca^{2+} (1.8 mM) and were then switched to medium containing high Ca^{2+} (7.2 mM) and cultured for an additional 6 hours before loading the cells with Fluo-3 AM and monitoring changes in $[Ca^{2+}]_i$. 3T3-L1 preadipocytes pre-loaded with Fluo-3 AM were stimulated with vehicle (Veh), Phorbol 12-myristate-13-acetate (PMA), and then ionomycin (Ion) in the presence of extracellular Ca^{2+} . Fluorescent intensity was compared to background fluorescence.

Chapter 4: Post-Translational Modifications of NPRC

Background

As mentioned earlier, NPRC undergoes various posttranslational modifications. However, the role of these posttranslational modifications in mediating the structure and/or function of NPRC are either controversial or have not been thoroughly investigated. Therefore, in addition to the creating and characterizing a polyclonal antibody against NPRC (please refer to Chapter 1), a recombinant GST-NPRC fusion protein was created to investigate the requirement of glycosylation for NPRC dimerization, identify putative phosphorylation sites of NPRC, and ascertain the kinases responsible for the phosphorylation. The identification of phospho-acceptor residues and kinases responsible for the phosphorylation is a prerequisite for determining the significance of phosphorylation in context to a specific cellular process, such as NPRC mediated clearance of NPs from circulation, turnover of NPRC protein, and NPRC mediated signal transduction. In addition, the sequence and kinetics of phosphorylation and dephosphorylation events can be investigated using a combination of phospho-specific antibodies and various established methodologies.

Materials and Methods

Reagents and antibodies

In addition to the reagents and antibodies mentioned in the previous chapters, the following reagents and antibodies were purchased or acquired as described. Precast gels (5%, 7.5%, and 10% resolving with 4% stacking) were purchased from Bio-Rad (Hercules, CA). Plasmid pGEX-4T3, *E. coli* strain BL21, Glutathione-Sepharose 4B medium, and Hyperfilm-ECL were purchased from Amersham Pharmacia Biotech (Piscataway, NJ). GelCode Phosphoprotein Stain Reagent Set was purchased from Pierce (Rockford, IL). All other chemicals were purchased from Sigma (St. Louis, MO) unless otherwise noted.

Cell Culture and cell lysate preparation

Rat gastric mucosal (RGM1) epithelial cells were cultured and harvested for protein as previously described in Chapter 2.

Plasmid construction of GST-NPRC

GST-NPRC was prepared as previously described for GST- β -arrestins and the various GST-AHNAK1 domains, but with the following modifications. The cDNA fragment (**NM 012868**) encoding rat C type natriuretic peptide receptor (rNPRC) (kindly provided by Dr. David Lowe, Genentech, San Francisco, CA) was subcloned into a pGEX4T3 expression vector between EcoR1 sites and confirmed by restriction analysis and DNA sequencing (Molecular Biology Core facility at the H Lee Moffitt Cancer

Center and Research Institute; Tampa, FL). The reactions and parameters for subcloning rat NPRC into pGEX4T3 are shown in Appendix N.

Preparation of competent E.coli cells

Competent BL21 cells were prepared using the DMSO method according to Chung *et al.* [403], with modifications. Briefly, single colonies were used to inoculate 50 mL LB in a 250 mL erlenmeyer flask and then grown at 37 °C with shaking at 225 rpm. Cells were grown to an OD₆₀₀ of 0.4, harvested by centrifugation at 2500 g for 15 minutes at 4 °C, and resuspended in 5 mL of ice cold TSS buffer (Luria–Bertani (LB) broth with 10% (w/v) polyethylene glycol (PEG), 5% (v/v) dimethyl sulfoxide (DMSO), 50 mM MgCl₂, pH 6.5). Single use aliquots of the competent cells were frozen at -80 °C for use within 3 months.

Expression of GST-NPRC

The constructed expression vector was transformed into the host cell *E. coli* BL21 (DE3) strain for expression. Transformants were selected by growth on LB agar plates containing 100 µg/mL ampicillin. Single isolated colonies were used to inoculate 5 mL of 2XYTA medium (16g/L tryptone, 10 g/L yeast extract, 5g/L NaCl, pH 7.0, containing 100µg/mL ampicillin) and grown at 37 °C with shaking at 225 rpm for 12 hours. The starter culture was diluted 1:100 into fresh prewarmed 2XYTA. At an OD₆₀₀ of 0.3 to 0.6, isopropyl-d-thiogalactoside (IPTG) was added to a final concentration of 0.1 mM to 1 mM for induction of the lac promoter.

Solubilization of GST-NPRC from inclusion bodies

Recombinant fusion protein was solubilized from inclusion bodies according to Frangioni and Neel (17), with modifications. Briefly, bacterial cells were harvested at 5000 g for 10 minutes at 4 °C. The supernatant was removed and the pellet was washed once with a volume of ice cold 1X PBS (1/15 the original culture volume) (Table 5). The pellet was resuspended in a volume of ice cold STE buffer (10 mM Tris HCl, pH 8.0, 1 mM EDTA, 150 mM NaCl) (1/50th the original culture volume) (Table 5). A volume of lysozyme from chicken egg white was added (1/5000th the original culture volume) (Table 5) followed by a 15 minute incubation on ice. A volume of freshly prepared dithiothreitol (DTT) (1M) and Sarkosyl (10% w/v) was added (1/5000th and 1/350th the original culture volume, respectively) (Table 5) and then mixed by inversion three times. The lysate was sonicated twice for 5 second intervals and then centrifuged at 13000 rpm for 15 minutes to pellet cellular debris. The supernatant was transferred to a new tube and a volume of 10% Triton X-100 and STE was added (1/125th and 1/25th the original culture volume, respectively) (Table 5) and allowed to incubate at room temperature for 30 minutes.

Batch purification of GST-NPRC

A volume of prewashed 50% glutathione Sepharose 4B slurry (1/100 the lysate volume) (Table 5) was added to the lysate and incubated at 4 °C for 45 minutes with end-over-end rocking. Bound proteins were collected by centrifugation at 500 g for 2 minutes. The complex was washed twice with a volume of ice cold 1X PBS (10X the initial slurry volume) (Table 5). Protein was eluted by resuspending the complex in a

volume of elution buffer (1/1000 the culture volume) (50 mM Tris-HCl, 10 mM reduced glutathione, pH 8.0) (Table 5), incubating for 30 minutes at 4 °C with end-over-end rocking, and collecting the supernatant after centrifugation for 2 minutes at 500 g. The elution step was repeated twice and the resulting fractions were pooled.

Identification of GST-NPRC

Purity of the fusion protein was analyzed by SDS-PAGE and Coomassie blue staining using Colloidal Coomassie blue stain according to manufactures instructions (Genomic Solutions; Ann Arbor, MI). The NPRC portion of the fusion protein was identified by indirect Western blot analysis for NPRC using a polyclonal antibody (JAH84) directed against the carboxy terminal tail of NPRC. The GST portion of the fusion protein was identified by direct Western blot analysis for GST using peroxidase conjugated anti-GST polyclonal antibody (Sigma; St. Louis, MO)

Estimation of MW of GST-NPRC using a molecular weight marker kit and Ferguson plots

The electrophoretic mobilities of GST-NPRC and the different molecular weight markers were determined after subjecting them to electrophoresis on a set of gels of increasing polyacrylamide concentrations. Thereafter, the retardation coefficients of each protein were determined from the slope of the plot of the log of the electrophoretic mobilities against the percent gel concentrations. Next, the logarithm of the negative slope was plotted against the logarithm of the molecular weight of the fusion protein and

the molecular weight markers, and the resulting linear plot was used to estimate the molecular weight of GST-NPRC.

MS of GST-NPRC

MS was performed to confirm the identity of the recombinant fusion protein (Proteomics Department at the Moffitt Cancer Center, Tampa FL). Briefly, the gel band was subjected to in-gel tryptic digestion followed by liquid extraction of the gel fragments. LC-MS/MS was used to analyze collected peptides and was performed on an LTQ mass spectrometer (Thermo Electron Corporation, Waltham, MA) with an LC packings ultimate dual gradient nano-LC system (Dionex, Sunnyvale, CA). The Mascot algorithm (Matrix Science, London UK) was used to search the collected data against the nonredundant rodentia database at the National Center for Biotechnology Information (NCBIInr) with the following parameters: peptide mass tolerance, 2.5 DA; MS/MS ion mass tolerance, 0.8 DA; allowing up to 2 missed cleavages. Significant hits, defined by Mascot probability analysis and hits that exceeded the arbitrarily set acceptance threshold were regarded as positive identifications.

Circular dichroism of GST-NPRC

CD spectra were obtained using a JASCO (Easton, MD) J710 spectropolarimeter calibrated for signal intensity and wavelength maxima using an aqueous solution of *d*-10-camphosulfonic acid. UV CD spectra were obtained in 10 mM phosphate buffer, containing 0.1 mM EDTA, pH 7.0, using a cylindrical quartz cell of 0.1 cm path length (300 μ L total volume), while visible CD spectra were obtained in 10 mM MOPS buffer,

containing 0.1 mM EDTA, pH 7.0, using a cell of 1 cm path length (90 μ L total volume). All spectra were corrected for the appropriate buffer contributions and expressed in terms of molar ellipticities ($M^{-1} \text{ cm}^{-1}$).

In vitro phosphorylation of GST-NPRC

GST-NPRC immobilized on glutathione Sepharose 4B beads was incubated with 200 μ g of RGM1 cell lysate in kinase buffer (50 mM Tris [pH 7.4], 10 mM MgCl_2 , 5 mM DTT, 2 mM ATP) for a total volume of 300 μ l, and incubated at 30°C for 1 hr. The beads were rinsed three times with 1X PBS before the addition of 150 μ l of elution buffer (50 mM Tris-HCl, 10 mM reduced glutathione, pH 8.0).

Detection of phosphorylated proteins

Recombinant GST-NPRC fusion protein or RGM1 protein lysate was subjected to SDS-PAGE, then gels were stained using the GelCode Phosphoprotein Stain reagent set according to the manufactures instructions. Alternatively, proteins were transferred to nitrocellulose membranes and then membranes were probed with phosphospecific and substrate motif antibodies to identify phosphorylation of proteins.

Overlay binding assay

Overlay binding assays were performed as described in Chapter 2, but instead the membranes were overlaid with purified GST or GST-NPRC in blocking solution for 2 hours at RT, washed with 1X PBS, and probed for GST.

Results

Construction, expression, and purification of GST-NPRC

In order to create a fusion protein that would maintain the signaling function mediated by the carboxy terminal domain of NPRC, the GST tag was strategically placed on the amino terminal end of the full length sequence of rat NPRC (Figure 63). Several expression conditions of GST-NPRC, including temperature of bacterial cultivation, optical density of bacteria upon IPTG induction, IPTG concentration, and duration of IPTG induction were considered. Expression of GST-NPRC was favored at a higher temperature with IPTG induction at a lower optical density (Figure 64). Attempts to prevent misfolding of GST-NPRC by reducing the rate of expression of GST-NPRC by culturing the bacteria harboring the fusion protein at 30 °C instead of 37 °C resulted in less product, as indicated by the bands at 75 kDa in Coomassie stained gels. The expression of GST-NPRC appeared to be 5-fold less at 30 °C than at 37 °C, as indicated by densitometric analysis.

Despite the inclusion of the GST tag to facilitate solubilization of GST-NPRC, a desirable yield of purified fusion protein could not be achieved by traditional methods. Overexpression of the foreign protein in the bacteria resulted in aggregation and formation of insoluble inclusion bodies. The fusion protein was found exclusively within intracellular inclusion bodies and represented approximately 10% of total bacterial proteins as indicated by densitometric analysis. Therefore, a similar approach as originally described by Frangioni and Neel [366] to recover our fusion protein from bacterial inclusion bodies was taken. GST-NPRC was able to be purified to

homogeneity, as indicated by a single band of an apparent molecular weight of 75 kDa (Figure 65).

Next, the purity of GST-NPRC was confirmed and the NPRC portion demonstrated to be intact by MS analysis. MASCOT results only revealed several signature peptides corresponding to rat NPRC and full sequence coverage from the amino terminal domain to the carboxy terminal domain of NPRC observed (Figure 66A). However, MASCOT results did not reveal sequence coverage for the GST moiety. The expected size of GST-NPRC was between 86 and 92 kDa, since NPRC is known to have a molecular mass of between 60 and 66 kDa and GST is known to have a molecular mass of 26 kDa.

Predicted and Observed MW of GST-NPRC

A GST-NPRC fusion protein was constructed using the entire sequence of rat NPRC. The molecular weight of GST is 26 kDa and the molecular of rat NPRC is between 60 and 66 kDa. Therefore, the predicted MW of GST-NPRC is between 86 and 92 kDa. SDS-PAGE analysis of purified GST-NPRC and subsequent indirect Western blot analysis probing for NPRC resulted in an immunoreactive band at 75 kDa (Figure 66B). Similarly, direct Western blot analysis probing for GST also resulted in an immunoreactive band at 75 kDa (Figure 66C).

Native PAGE analysis of purified GST-NPRC resulted in a high molecular weight Coomassie blue stained band above 120 kDa, as indicated by a Native PAGE molecular weight marker kit. The molecular weight of the band corresponding to GST-NPRC observed in the Native PAGE studies was then estimated by using a protein molecular

weight marker kit and Ferguson plots. The estimated molecular weight of GST-NPRC's approximately 150 kDa (Figure 67).

Dimerization of GST-NPRC does not require receptor occupancy

The GST tag of GST-NPRC was removed by thrombin cleavage prior to investigating the dimerization of NPRC *in vitro*. An immunoreactive band at 66 kDa band corresponding to NPRC was detected after 18 hours of thrombin cleavage (Figure 66D). The ability of the NPRC agonist, cANF to induce dimerization of NPRC resulting from thrombin cleavage of GST-NPRC was evaluated. The addition of cANF in increasing concentrations did not augment the observed dimerization of NPRC and the primary sequence of NPRC was sufficient for its spontaneous dimerization *in vitro* (Figure 68).

The observed and theoretical secondary structures of GST-NPRC are in agreement

The GST moiety of GST-NPRC has the potential to dimerize by itself, although it is unlikely since a large portion of the tag of GST-NPRC is prematurely cleaved during the purification process. In order to determine if thrombin cleavage of GST-NPRC was necessary, the ability of the GST moiety to effect the secondary and tertiary structure of GST-NPRC was investigated. The amino acid sequences of GST and of rat NPRC were used to perform secondary structure predictions analysis. Circular Dichroism (CD) revealed a minima negative peak at 215 followed by an immediate positive peak, as indicated by the far UV CD spectra in Figure 69A. The peak profile within the region of 260 of the spectra demonstrated the fusion protein was not globular and maintained a

defined tertiary structure. The results from the CD analysis were in agreement with the proportions of α and β structures from the PSIPRED protein structure prediction server shown in Figure 69B.

The intracellular domain of NPRC contains putative phosphorylation consensus sequences

The intracellular domain of rat NPRC contains several putative phosphorylation consensus sequences, as shown in Figure 70. Two PKA, two PKB, and one PKC phosphorylation sites were identified within the 37 amino acid intracellular domain of rat NPRC.

Immobilized GST-NPRC can be phosphorylated in vitro using a crude RGM1 cellular lysate

The ability to phosphorylate GST-NPRC *in vitro* using a crude lysate from RGM1 cells was investigated. While immobilized to glutathione Sepharose 4B beads, GST-NPRC was subject to RGM1 lysate at increasing concentrations and increasing periods of time. Compared to untreated GST-NPRC, the addition of increasing concentrations of RGM1 lysate for increasing periods of time did not affect the ability to purify the fusion protein to homogeneity (Figure 71A). However, compared to untreated GST-NPRC, incubation of GST-NPRC with 600 μ g of phosphatase inhibitor treated RGM1 lysate in the presence of ATP for 1 hr resulted in a phosphostained band corresponding to 75 kDa (Fig. 71B).

Rat NPRC does not exist as a constitutively phosphorylated protein in RGM1 cells

The various different antibodies used to investigate the phosphorylation state of NPRC are listed in Table 6. A polyclonal phospho-Thr antibody, which recognizes phosphorylated Thr residues, but also phospho Ser residues was in initial experiments to determine if NPRC exist as a constitutively phosphorylated protein *in vivo*. A polyclonal NPRC specific antibody was used to immunoprecipitate NPRC from an RGM1 cell lysate treated with or without phosphatase inhibitors and was then probed for phosphorylated Thr and Ser residues using the polyclonal phospho-Thr antibody. In parallel experiments, the polyclonal phospho Thr antibody was used to immunoprecipitate total phosphorylated proteins from the RGM1 cell lysate treated with or without phosphatase inhibitors and specific NPRC antibody was used to probe for NPRC. Immunoreactive bands corresponding to phosphorylated NPRC were markedly reduced in the absence of phosphatase inhibitors, as shown in Figure 72. In other experiments a monoclonal phospho Thr specific antibody, which only detects phosphorylated Thr residues was also used to probe for phosphorylated Thr residues after immunoprecipitation NPRC with NPRC specific antibody. Accordingly, the monoclonal phospho Thr specific antibody was used to immunoprecipitate total phosphorylated proteins from the RGM1 cell lysate treated with or without phosphatase inhibitors and NPRC specific antibody was used to probe for NPRC. In each case, NPRC phosphorylation at threonine residues was essentially nondetectable in the absence of phosphatase inhibitors after probing with a phosphospecific antibody that recognizes only phosphorylated threonine residues (Figure 72A).

Rat NPRC is a substrate for PKA

In order to determine if NPRC was a substrate for a specific kinase, NPRC was immunoprecipitated from the RGM1 cell lysate and probed for phosphorylation using PKA, PKB, and PKC substrate motif antibodies (Table 6). Probing for phosphorylation with PKB and PKC substrate motif antibodies did not reveal any immunoreactive bands corresponding to NPRC. However, probing for phosphorylation with a PKA substrate motif antibody did reveal an immunoreactive band at 66 kDa corresponding to NPRC that was markedly reduced in the absence of phosphate inhibitors (Figure 72C). However, immunoreactive NPRC bands of equal intensity were detected after probing NPRC with specific NPRC antibody from both phosphatase treated and untreated RGM1 cell lysates (Figure 72D).

Rat NPRC is phosphorylated on Thr 505

Global phosphorylation of NPRC by PKA was investigated using a PKA consensus sequence prediction algorithm, pkaPS [404]. Six distinct phosphorylation sites were identified over the entire sequence of rat NPRC (Table 7). However, only one of these sites included a threonine residue, Thr 505 (Table 7).

Discussion

A recombinant GST-NPRC fusion protein was created and used to investigate posttranslational modifications of NPRC. The expected molecular mass of GST-NPRC was predicted to be between 86 and 92 kDa, since NPRC is known to have a molecular mass of between 60 and 66 kDa and GST is known to have a molecular mass of 26 kDa. However, Western blot analysis consistently revealed an immunoreactive band at 75 kDa, using a polyclonal antibody against the cytoplasmic domain of NPRC (Figure 66B). Accordingly, a GST peroxidase antibody also revealed an immunoreactive band at 75 kDa (Figure 66C). Although it was apparent the GST-NPRC fusion protein was truncated, it was immediately apparent that the GST fusion tag and not the NPRC parent protein was most likely truncated, since each of the polyclonal antibody against NPRC used in the Western blot analysis is against the a region within the last 37 amino acids of the carboxy terminal domain of NPRC. Thrombin cleavage of GST-NPRC revealed an immunoreactive band at approximately 66 kDa (Figure 66D), which was also observed in Western blots of uncleaved GST-NPRC, suggesting the fusion protein may be cleaved as a result of proteolysis. Since the entire sequence of GST was used to create the peroxidase conjugated GST antibody it was expected the antibody would recognize multiple epitopes of GST. It was also expected that the presence of only a few amino acids of GST would be necessary for recognition of this antibody. MS sequence analysis revealed multiple signature peptides corresponding to rat NPRC spanning from the first amino acid at the amino terminal domain to the last amino acid of the carboxy terminal domain of NPRC.

Since proteins are neither uniform in charge/mass ratio nor in shape, the molecular weight of GST-NPRC was assessed in parallel with molecular weight standards while performing non-denaturing native polyacrylamide gel electrophoresis (PAGE), as described by others [405, 406]. The estimation of the molecular weight of GST-NPRC by this method minimized the influence of charge/mass ratio, but conformational differences between GST-NPRC and the molecular weight standards could influence an accurate estimation. Ferguson plots and a protein molecular weight marker kit were also used to further confirm NPRC was intact by indirectly estimating the molecular weight of GST-NPRC (Figure 67). Because all proteins have the same backbone, the nature of the side chains comprising the backbone determines the overall three-dimensional structure of the protein. In some cases, the primary structure of a protein alone may be sufficient to dictate the three-dimensional shape or tertiary structure of the protein. In other cases, protein chaperonins may induce protein folding. It was expected that in the absence of β -mercaptoethanol, S-S bridges will remain intact and a mixture of GST-NPRC monomer and GST-NPRC homodimers, formed from spontaneous dimerization would be present after performing native PAGE. Although the exact site of cleavage of GST could not be determined by these methods, the truncation of the GST moiety was not a concern since it was removed by thrombin cleavage in some experiments.

The molecular design of GST-NPRC involved using the entire coding sequence of rat NPRC instead of a partial sequence, because the original intent was to be able to study global posttranslational modifications of NPRC. Endogenous NPRC exists as a monomer and a disulfide-linked homodimer [82, 83], but the dimeric structure of NPRC is not

necessary for ligand binding activity [83]. It is generally thought that the cytoplasmic domain of NPRC is phosphorylated upon ligand binding [370]. Under non-denaturing native-PAGE conditions dimerization of GST-NPRC (Figure 68) or NPRC alone in both the absence and presence of increasing amounts of the NPRC ligand, cANF was observed. In addition to using the GST-NPRC fusion protein as a tool to study the phosphorylation state of NPRC, it could also be used to study the importance of glycosylation of NPRC for its ability to dimerize, bind ligand, and mediate signal transduction. NPRC undergoes N terminal glycosylation as its extracellular (ECD) contains multiple N-linked glycosylation sites, but the role of NPRC glycosylation remains controversial. Glycosylation and ligand binding are thought to contribute to the homodimerization and subsequent activation of NPRC. Furthermore, ligand induced dimerization of single transmembrane spanning receptors, such as cytokine receptors and growth factor receptors appear to be a general mechanism for receptor activation and downstream signaling [407, 408]. Multiple groups have shown glycosylation of NPRA and NPRB is important for ligand binding [409, 410]. Heim *et al.* demonstrated that inhibition of *N*-glycosylation of NPRA by tunicamycin did not alter the ability of ANP, but did affect ANP analogs to bind to rat glioma cells stably transfected with NPRA and activate guanylyl cyclase [411]. Fenrick *et al.* showed lower guanylyl cyclase activity after deglycosylation of NPRB compared to fully glycosylated receptor [409]. Independent from its role in modulating ligand binding, glycosylation does not appear to be required for distribution of NPRs to the cell surface [409, 410]. Glycosylation of NPRC has not been shown to be a prerequisite for its ligand binding. Preliminary results suggest N terminal glycosylation of NPRC is not required for NPRC homodimerization,

since GST-NPRC spontaneously dimerized *in vitro* and the addition of ligand, in increasing amounts did not further enhance the dimerization (Figure 68). This finding suggests the primary sequence of NPRC alone is sufficient for its dimerization *in vitro*. Furthermore, because GST-NPRC completely lacks glycosylation, as this posttranslational modification is absent in *E. coli*, GST-NPRC could provide a simplified means to investigate the requirement of glycosylation for the NPRC activation and function.

Several methods exist for prediction of the secondary structure of various proteins. The de novo PSIPRED [412, 413], JNET [414] and PHD [415] secondary structure prediction programs are among the best secondary structure prediction methods available and can achieve a performance or Q3 score of between 75-77% [416]. These methods utilize BLAST searches of the non-redundant protein sequence database to obtain evolutionary information which is then fed into a multi-layered feed-forward neural network to acquire sequence/structure patterns, which are subsequently used to predict the secondary structure of the query protein [417].

Since mammalian posttranslational modifications including phosphorylation are absent in bacteria, the GST-NPRC fusion protein may be useful for the investigation of phosphorylation events of NPRC. MS and site-directed mutagenesis are commonly used to investigate the phosphorylation state of a protein. Alternatively, the availability of phosphospecific antibodies can be used to probe for protein phosphorylation. Phosphorylation motif antibodies are useful resources for the identification and characterization of the phosphorylation state of a protein. Consensus sequences are commonly used as substrate specificity determinants for protein kinases [418]. The

carboxy terminal domain of NPRC is rich in serine and threonine residues and consensus sequence motifs for PKA, PKB, and PKC. In one report, NPRC was shown to be phosphorylated exclusively on serine residues in rat aortic smooth muscle cells. It is possible multiple serine residues of NPRC are phosphorylated simultaneously or sequentially by one or more kinases. In agreement with a recent report, evidence is provided here for the phosphorylation of Thr 505 of NPRC in RGM1 cells. The discrepancy between the phosphorylated residues of NPRC may be attributed to the phosphorylation state of NPRC being species and cell type dependent. A future study that may be performed to confirm the phosphorylation of NPRC at Thr 505 include mutating Thr 505 to an Ala and then performing *in vitro* phosphorylation assays, while comparing the mutant construct to wildtype NPRC. The functional significance of the phosphorylation of NPRC at Thr-505 in RGM1 cells may be evaluated by utilizing the mutant construct and wildtype NPRC, while performing I¹²⁵ ligand binding experiments after transiently transfecting and radiolabeling RGM1 cells to assess the clearance function of NPRC. Similarly, other cell lines, capable of being transiently transfected can be used to determine the role of phosphorylation of NPRC at Thr-505. Phosphorylation of Thr-505 of NPRC may have significant implications because it is within the intracellular domain of NPRC. The intracellular domain of NPRC has been reported to contain G protein activator sequences and participate in signal transduction. Therefore, the functional significance of the phosphorylation of NPRC at Thr-505 on NPRC signaling mediated by Gi or independent of G-proteins (i.e. via AHNAK1) can be studied while utilizing the mutant construct and wildtype NPRC. Although this is the first report of phosphorylation of NPRC at Thr-505 by PKA, NPRC has been reported to be

phosphorylated on Thr-505 by PKG [419]. The Thr-505 residue of NPRC was reported to be part of a consensus sequence for phosphorylation by cGMP-dependent protein kinase (PKG) [419]. After expression of various NPRC mutants into COS-1 cells, desensitization by PKG was found to be mediated by phosphorylation of Thr-505 of NPRC [419].

In order to identify the kinase responsible for phosphorylation of Thr-505 substrate motif antibodies for various kinases were utilized. Only a PKA substrate motif antibody and not PKB or PKC substrate motif antibodies resulted in immunoreactive bands after immunoprecipitating NPRC from RGM1 lysate with NPRC specific antibody. PKA phosphorylates proteins on Serine (Ser) and Threonine (Thr) residues within the motif Arg-X-X-Ser/Thr, where X may represent any amino acid residue. The motif is not absolute and some variations in basic residues and spacing are allowed. It has been reported that the 2nd or 3rd position prior to the phosphorylated serine or threonine should be occupied by an arginine. Several algorithms exist for predicting putative PKA phosphorylation sites. The pkaPS algorithm was used because it offers both high sensitivity and specificity for predicting PKA phosphorylation sites of a given protein sequence based on various parameters. PkaPS was used to identify all putative PKA phosphorylation sites within the entire sequence of rat NPRC. Of the six predicted phosphorylation sites (Table 7), only amino acid 505 contained a Thr residue. Since the phospho-Thr specific antibody used in IP-Western blot analyses only recognizes phosphorylated Thr residues and does not cross-react with phosphorylated Ser residues, Thr-505 of rat NPRC is most likely phosphorylated by PKA. NPRC may be phosphorylated on multiple residues, but does not exist as a constitutively phosphorylated

protein in RGM1 cells, since treatment of RGM1 lysate with phosphatase inhibitors was necessary to achieve phosphorylation.

MS is routinely used to identify phosphorylation sites of a protein of interest. However, the ability to accurately detect phosphorylated residues is dependent on the abundance of the phosphorylation. Therefore, it was not surprising that the MS approach to detect phosphorylation of NPRC failed, since there is no evidence of NPRC being abundantly phosphorylated. The ability to detect NPRC phosphorylation by MS in future experiments can be improved by incorporating a separation technique, such as immobilized metal affinity chromatography (IMAC). The IMAC method may be used to enrich for phosphopeptides that are present at low amounts and is therefore useful for a more accurate identification of phosphorylation sites by LC-MS/MS. Furthermore, protein phosphorylation is dynamic and constantly changes over time. As shown in Figure 72, NPRC does not exist as a constitutively phosphorylated protein and most likely undergoes a series of phosphorylation and dephosphorylation events. This finding may be used to troubleshoot future experiments, in which a specific kinase may be overexpressed in the cell line of interest by transient transfection, or the cells may be treated with an activator of a specific kinase in order to enhance the phosphorylation.

Future studies will be necessary to determine if this phosphorylation is conserved in other species and to determine sequential phosphorylation and dephosphorylation events. Additional studies will also be necessary to determine if PKA phosphorylation of NPRC is necessary for receptor homodimerization, activation, desensitization, and/or internalization.

Table 5. Solubilization and purification scheme for GST-NPRC

Culture volume	60 mL culture	500 mL culture
Centrifugation (5000 g for 10 min. at 4 °C)		
<i>1X PBS wash buffer</i>	4 mL	33 mL
<i>Resuspension buffer (STE)</i>	1.2 mL	10 mL
<i>Lysozyme</i>	12 µl	100 µl
<i>1M DTT</i>	12 µl	100 µl
<i>10% Sarkosyl</i>	170 µl	1.43 mL
Sonication (2X for 5 sec. intervals)		
Centrifugation (3000 rpm for 15 min. at room temp.)		
<i>10% Triton X-100</i>	480 µl	4 mL
<i>STE</i>	2.4 mL	20 mL
Incubation (30 min. at room temp.)		
Elution		
<i>Glutathione Sepharose Bed Volume</i>	30 µl	240 µl
<i>Glutathione elution buffer</i>	60 µl	500 µl
<i>1X PBS wash buffer (2X)</i>	300 µl	2.4 mL
<i>Approx. GST-NPRC yield</i>	30 µg	200 µg

Approximate volumes for a 60 mL culture and 500 mL culture are provided

Table 6. Various antibodies used to characterize the phosphorylational state of NPRC

Antibody	Specificity/Sensitivity	Motif	Source
JAH84	Total NPRC	None	Our laboratory
Phospho-Thr-polyclonal	Phospho-Try, Ser, Thr	None	Cell Signaling
Phospho-Thr-monoclonal	Phospho-Thr	None	Cell Signaling
Phospho-PKA Substrate	Phospho-Ser, Thr	(RRXS/T)	Cell Signaling
Phospho-PKB (Akt) Substrate	Phospho-Ser, Thr	(R/K)X(R/K)XX(T/S)	Cell Signaling
Phospho-PKC Substrate	Phospho-Ser	(R/K)X(S)(Hyd)(R/K)	Cell Signaling

Table 7. Prediction of NPRC phosphorylation by PKA using the pkaPS algorithm

Position	Residue	Score	Profile
193	S	0.04	0.82
337	S	0.31	1.08
441	S	0.65	1.09
505	T	0.41	0.74
527	S	0.14	0.81
533	S	0.18	0.40

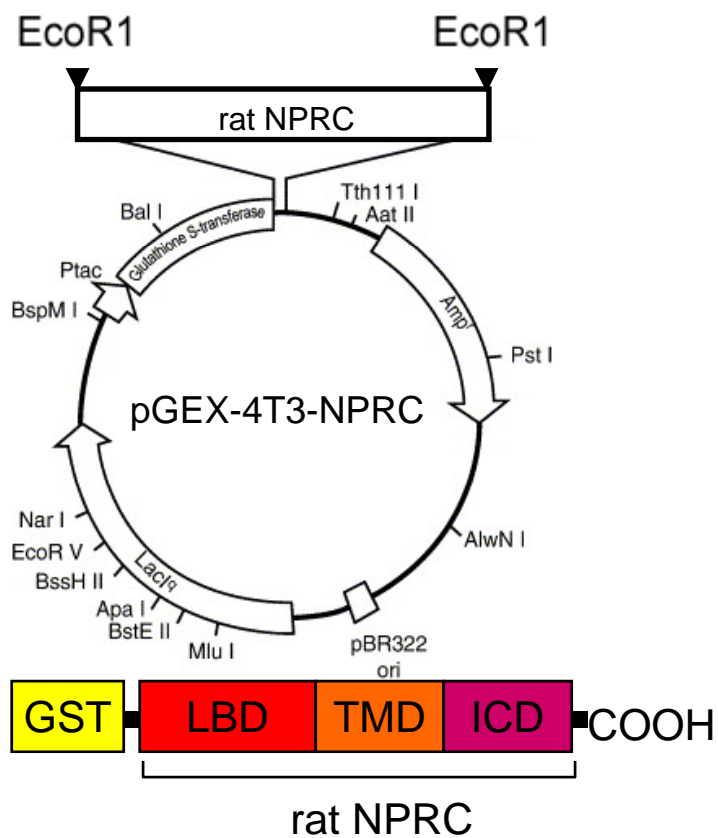
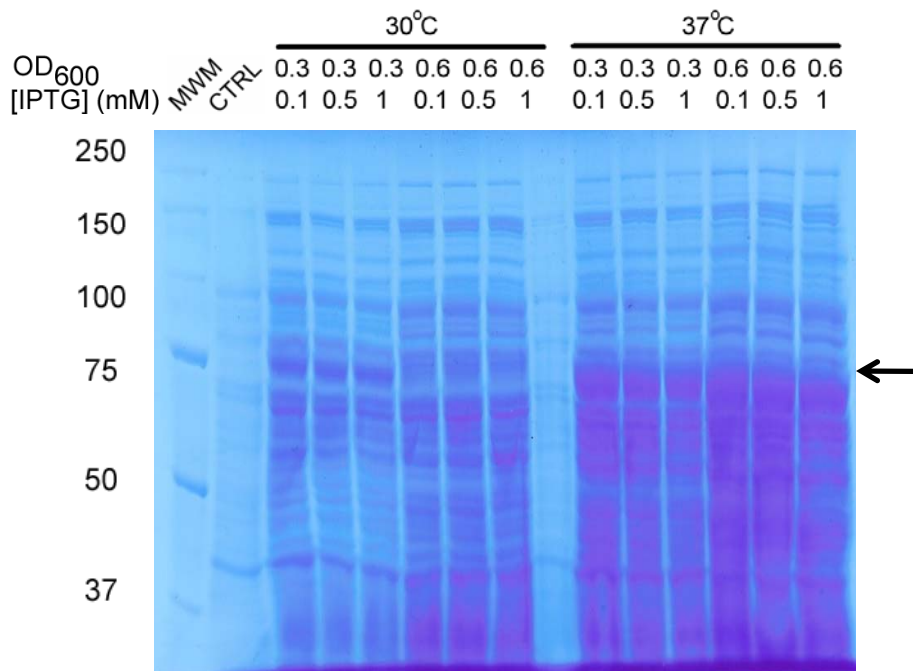


Figure 63. Construction of recombinant GST-NPRC. Schematic of the pGEX4T3-NPRC construct and domains of GST-NPRC. The ligand binding domain (LBD), transmembrane domain (TMD), and intracellular domain (ICD) of NPRC are depicted



SDS-PAGE

Figure 64. Optimization of the expression conditions of GST-NPRC. Coomassie blue stained gel illustrating the effects of temperature, cell density, and IPTG concentration on the expression of GST-NPRC. The arrow indicates expression of the GST-NPRC fusion protein. Lysates were obtained from *E. coli* BL21 cells transformed with the pGEX4T3-NPRC construct. Lane 1, unstained molecular weight markers (MWM). CTRL in lane 2 refers to control, in which lysate from pGEX4T3 empty vector was compared to lysate from pGEX4T3-NPRC (GST-NPRC) as shown in each of the other indicated lanes.

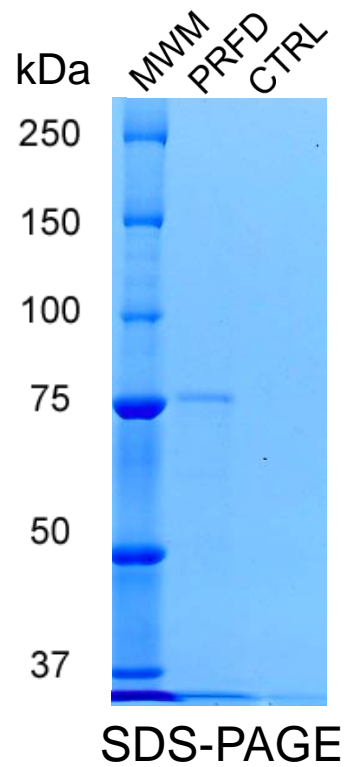


Figure 65. Coomassie blue stained gel showing the purification of GST-NPRC. Lane 1, unstained molecular weight markers (MWM). Lane 2, purified fraction (PRFD) of GST-NPRC. Lane 3, control (CTRL) in which lysate from empty vector was purified in parallel with lysate from bacteria harboring the GST-NPRC construct.

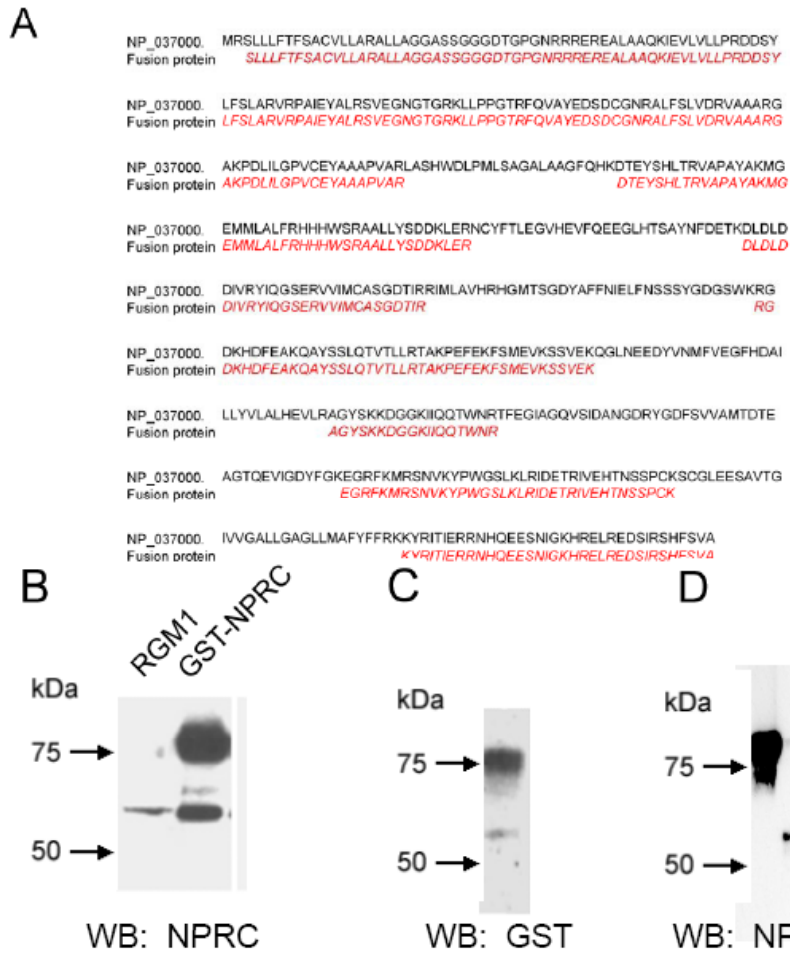


Figure 66. Confirmation of the sequence of GST-NPRC. **(A)** Sequence alignment/Mascot results from LC-MS/MS. Matched peptides are italicized in red. **(B)** Indirect Western blot showing an immunoreactive band of an apparent molecular mass of 75 kDa using anti-NPRC antibody. The band at 66 kDa from RGM1 lysate and purified GST-NPRC corresponds to the GST-NPRC fusion protein in which GST is truncated and NPRC is intact. **(C)** Direct Western blot showing an immunoreactive band of an apparent molecular mass of 75 kDa using a peroxidase conjugated anti GST antibody. **(D)** Indirect Western blot showing an immunoreactive band of an apparent molecular mass of approximately 60 kDa after thrombin cleavage of GST-NPRC.

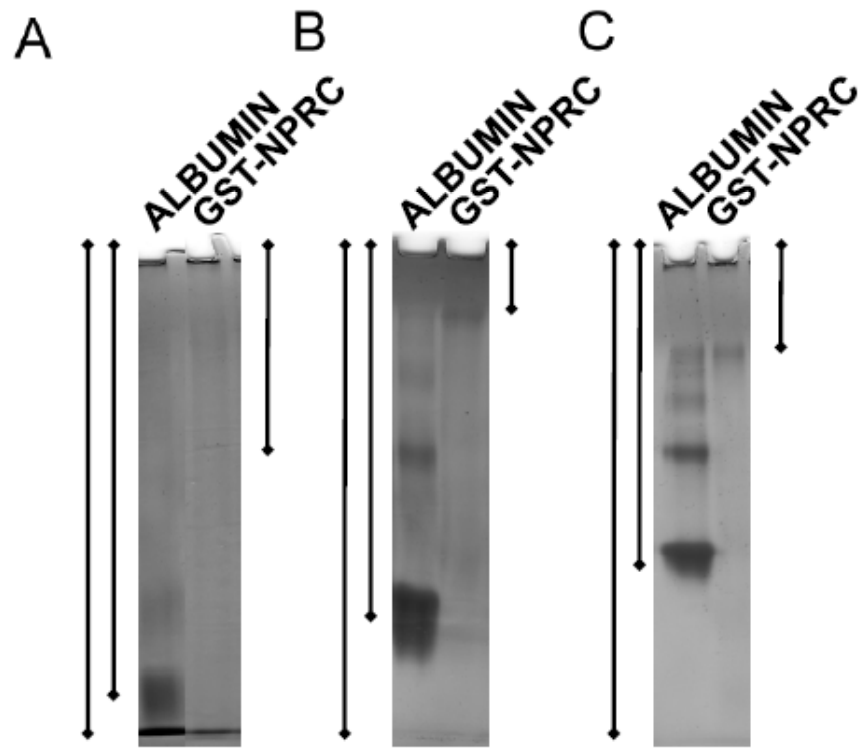


Figure 67. Grayscale of Coomassie blue stained gels used to determine the molecular weight of GST-NPRC under native PAGE conditions. R_f = distance of protein migration / distance of tracking dye migration. A: 5% gel; B: 7.5% gel; C: 10% gel

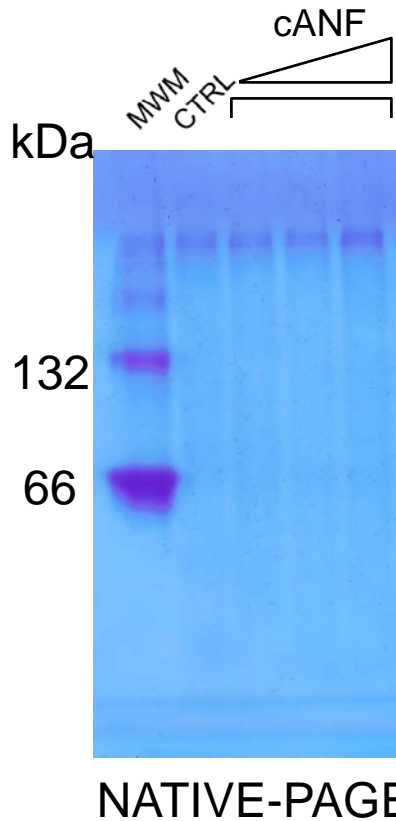


Figure 68. Spontaneous versus ligand induced dimerization of GST-NPRC . Native PAGE (nonreducing and nondenaturing conditions) analysis of GST-NPRC using a 10% Tris HCl gel and after Coomassie blue staining. Lane 1, albumin dimer at 132 kDa and monomer at 66 kDa . Lane 2, control (CTRL) of untreated GST-NPRC. Lanes 3-5, incubation of GST-NPRC with increasing amounts of cANF. GST-NPRC was able to dimerize spontaneously independent of ligand.

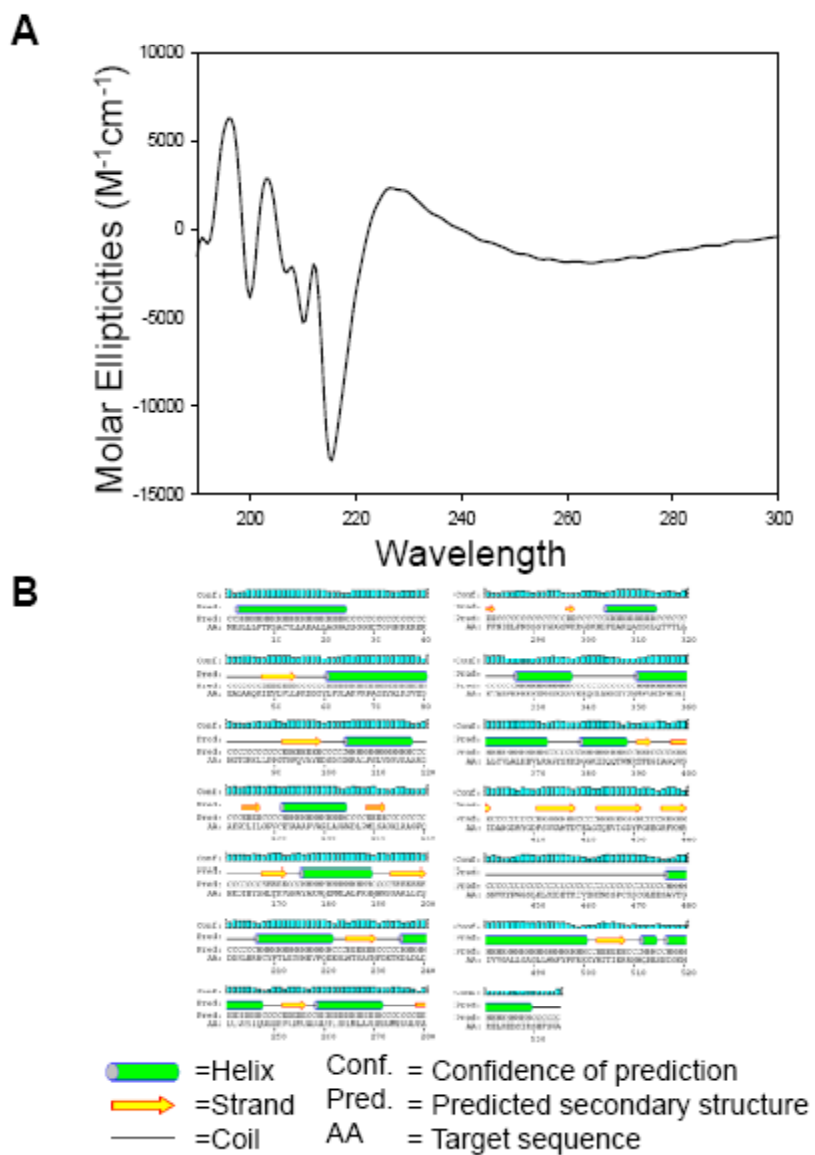


Figure 69. Predicted secondary structure for GST-NPRC. **(A)** Far UV CD spectra; the region around 260 indicates the protein has a defined tertiary structure and is not globular. The minima at 215 followed by an immediate positive peak indicates the protein is mainly helical. **(B)** PSIPRED protein structure prediction server results for rat GST-NPRC.

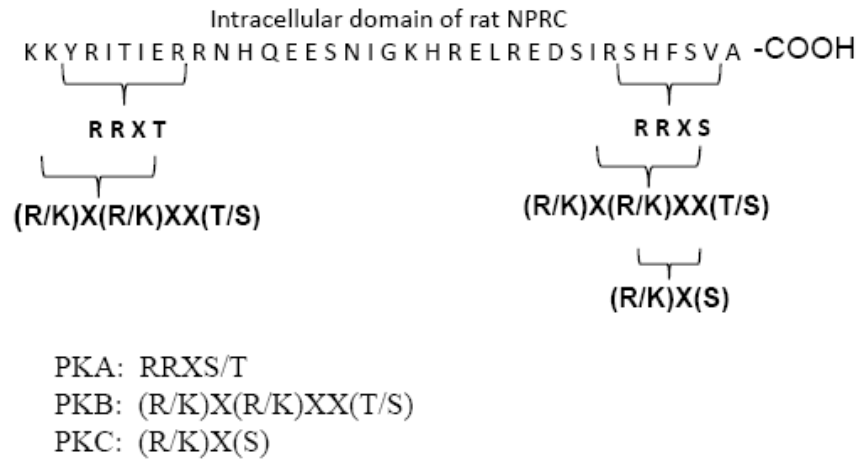


Figure 70. Phosphorylation consensus sequences within the intracellular domain of rat NPRC. Two phosphorylation consensus sequences are shown for PKA, two phosphorylation consensus sequences are shown for PKB, and one phosphorylation consensus sequence is shown for PKC

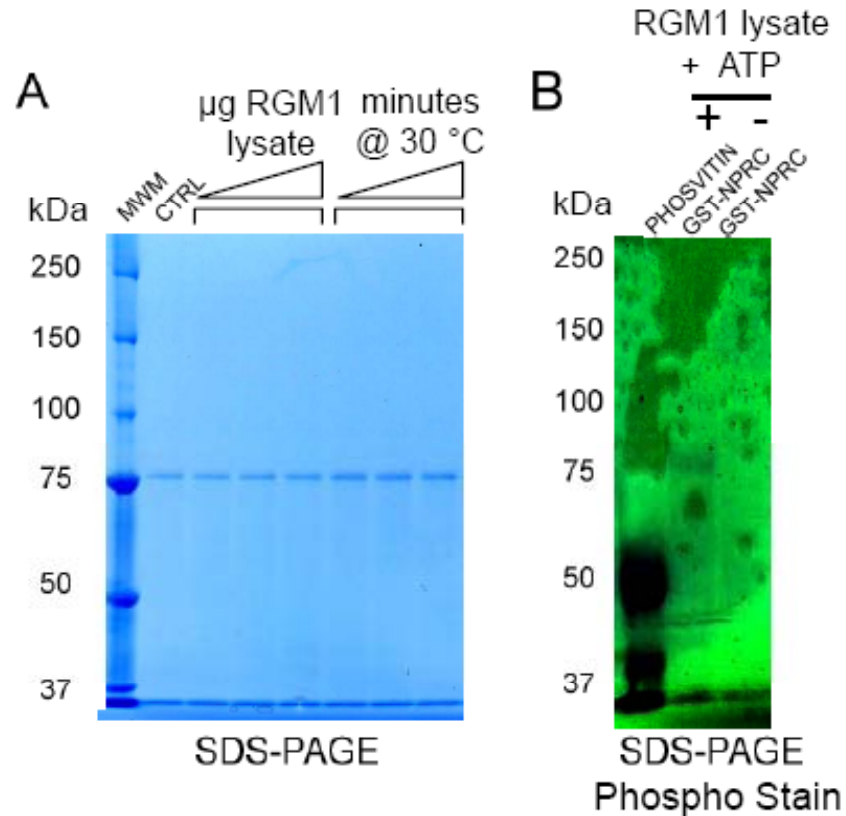


Figure 71. In vitro phosphorylation of GST-NPRC (A) Lane 1, molecular weight marker (MWM). Lane 2, untreated control (CTRL). Lanes 3-5, purification of GST-NPR fusion protein after incubating the fusion protein, immobilized on glutathione Sepharose 4B beads with increasing amounts of RGM1 cell lysate (200, 400, or 600 µg, respectively) for 30 min in the presence of ATP. Lanes 6-8, purification of GST-NPRC fusion protein after incubating the fusion protein, immobilized on glutathione Sepharose 4B beads for increasing time intervals (15 min, 30 min, 1 hour, respectively) with 400 µg of RGM1 lysate in the presence of ATP. (B) Phosphostained gel after SDS-PAGE, in which GST-NPRC was treated with or without 400 µg RGM1 lysate and ATP for 1 hour.

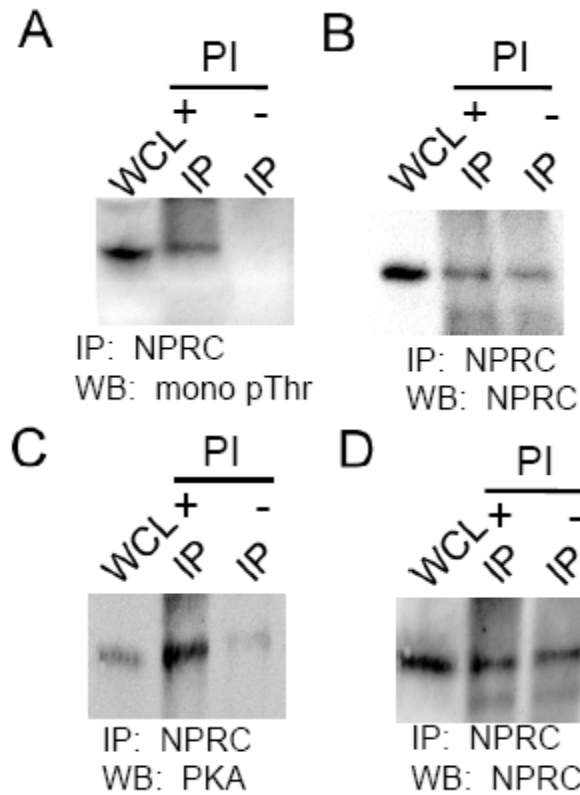


Figure 72. Identification of putative residues and kinases involved in NPRC phosphorylation. **(A)** IP Western blot analysis after immunoprecipitating NPRC from RGM1 whole cell lysate (WCL) treated with phosphatase inhibitors (+ PI) and probing with phospho-Thr specific antibody revealed an immunoreactive band at 66 kDa. The immunoreactive band at 66 kDa was absent after immunoprecipitating NPRC from untreated (- PI) RGM1 lysate and probing with phospho-Thr specific antibody **(B)** Similarly, IP Western blot analysis after immunoprecipitating with NPRC specific antibody and probing with NPRC specific antibody revealed an immunoreactive band at 66 kDa. **(C)** IP Western blot analysis after immunoprecipitating NPRC from RGM1 lysate treated with phosphatase inhibitors and probing with a PKA substrate motif antibody revealed an immunoreactive band at 66 kDa. The immunoreactive band at 66 kDa was attenuated after immunoprecipitating NPRC from untreated RGM1 lysate and probing with PKA substrate motif antibody. **(D)** Similarly, IP Western blot analysis after immunoprecipitating with NPRC specific antibody and probing with NPRC specific antibody revealed an immunoreactive band at 66 kDa.

Chapter 5: Potential Functions of AHNAK1

Background

As mentioned earlier, the AHNAK family of proteins has been implicated in several different cell-type dependent functions, and there may be other possible functions that are still unknown. While considering the versatility of AHNAK1 to serve as an adaptor/scaffolding protein and its ability to associate with a wide range of proteins, the identification of AHNAK1 protein expression in different cell types is a preliminary step for discovering novel functions of this protein. As demonstrated earlier, AHNAK1 associates with NPRC in RGM1 cells. Since AHNAK1 is a barrier protein and the RGM1 cell line demonstrates barrier type properties, the role of AHNAK1 in modulating the paracellular permeability of normal rat gastric epithelial cells was investigated. Also, the expression profile of AHNAK1 in normal human stomach organ donors was investigated to correlate the findings from studies in which the RGM1 cell line was used as a model system and to further elucidate the functional significance of AHNAK1.

Materials and Methods

Reagents and antibodies

In addition to the reagents and antibodies mentioned in the previous chapters, the following reagents and antibodies were purchased or acquired as described. ZO-2 antibody was purchased from Cell Signaling Technologies.

Cell culture

RGM1 cells were cultured as described in Chapter 2.

SDS-PAGE, Western blotting, and densitometric analysis

SDS-PAGE, Western blotting, and densitometric analyses were performed as described in the previous chapters.

Immunohistochemistry and immunofluorescence

Immunohistochemistry and immunofluorescence was performed as described in Chapter 1, but with the following modifications. ZO-2 antibody was used at a dilution of 1:250.

Sucrose density-gradient centrifugation

Sucrose density-gradient centrifugation studies were performed exactly as described in Chapter 3.

siRNA Transfection

AHNAK1 specific SMARTpool siRNAs (Table 4) or negative control nontargeting siRNA were purchased from Dharmacon (Lafayette, CO). siRNAs were transfected into RGM1 cells using DharmaFECT Transfection Reagent (Dharmacon) according to the manufactures instructions.

In vitro Cell Permeability Assay

Permeation of fluorescein isothiocyanate (FITC)-dextran (MW: 2000 kD) across RGM1 monolayers was assessed by *in vitro* Permeability Assay kit (Millipore, Billerica, MA) according to the manufactures instructions, but with the modifications. Briefly, RGM1 cells were transfected with non-targeting siRNA or AHNAK1 specific SMARTpool siRNA and allowed to reach confluency. As controls, permeation of FITC-dextran was also assessed across collagen coated inserts without an RGM1 monolayer, and across RGM1 monolayers treated with 50 μ M EDTA for 20 minutes.

Statistical analysis

Results are presented as mean \pm SEM. Statistical analyses were performed using Student's *t* test or one-way ANOVA. All data are representative of at least two independent experiments.

Results

AHNAK1 colocalizes with ZO-2 in confluent RGM1 cells

In order to determine if AHNAK1 could affect the integrity of the junctional complex of epithelial cells (Figure 73), colocalization of AHNAK1 and ZO-2 was initially investigated. Both AHNAK1 and ZO-2 were found to colocalize along the cell boundary of confluent RGM1 cells, as shown in Figure 74A. Strong AHNAK1 immunoreactivity, using polyclonal AHNAKC2 antibody (Figure 74B) and strong ZO-2 immunoreactivity, using monoclonal ZO-2 antibody (Figure 74C) was observed after staining RGM1 cells cultured on type 1 collagen chamber slides.

AHNAK1 is predominantly plasma membrane bound in confluent RGM1 cells

Subcellular fraction studies and Western blot analysis revealed AHNAK1 protein expression in the cytoplasmic, membrane, and nuclear fraction (Figure 75A). Pan-Cadherin was probed for as a membrane marker, Lamin A/C was probed for as a nuclear marker, and GAPDH was probed for as a cytoplasmic marker (Figure 75A). The highest level of AHNAK1 protein expression was found in the cytoplasmic fraction (Figure 75A). Immunofluorescence staining revealed strong cytoplasmic and membrane staining for AHNAK1, but very weak nuclear staining for AHANK1 (Figure 75B).

AHNAK1 is expressed in various regions of healthy human stomach organ donors

As shown in the schematic shown in Figure 76, the stomach is composed of various types of cells that perform specialized functions. Haematoxylin and eosin (H&E) staining and PAS/alcian blue staining demonstrated tissue samples taken from three

different human organ stomach donors were normal and were from healthy individuals (Figure 77). Western blot analysis demonstrated AHNAK1 expression in the antrum and body of three different human organ stomach donors (Figure 78A). Actin was probed for as a loading control (Figure 78A). Immunohistochemical analysis revealed AHNAK1 is expressed at the basolateral plasma membrane in surface epithelial cells (Figure 79). Also, immunohistochemical analysis showed AHNAK1 is expressed in the capillaries and muscle of the stomach (Figure 79).

AHNAK1 protein knockdown results in increased paracellular permeability

As demonstrated by Western blot (Figure 80A) and densitometric analysis (Figure 80B), transfection of siRNAs targeting AHNAK1 into RGM1 cells resulted in approximately a 50% knockdown in AHNAK1 protein. The knockdown in AHNAK1 protein resulted in increased permeability to FITC-Dextran in confluent RGM1 cells (Figure 81). The increased permeability to FITC-Dextran seen after siRNA mediated knockdown of AHNAK1 protein was greater than the increased permeability to FITC-Dextran observed after EDTA treatment of RGM1 cells in adjacent wells (Figure 81).

Discussion

AHNAK1 is a versatile protein that has been implicated in several cell-type dependent functions. Novel findings presented here for AHNAK1 include AHNAK1 protein expression in normal rat gastric mucosal cells and in surface epithelial cells of the antrum and body of healthy human stomach organ donors, AHNAK1 co-expression with ZO-2 in confluent RGM1 cells, and increased paracellular permeability with siRNA mediated knockdown of AHNAK1 protein in RGM1 cells.

Gentil *et al.* demonstrated the co-localization of AHNAK1 with ZO-1 in the brain [232]. The co-localization of AHNAK1 with ZO-1 or other ZOs in other tissues has not been reported. This may in part be due to AHNAK1 and the different ZOs being highly tissue specific and serving nonredundant functions. The evidence provided here for the expression of AHNAK1 in RGM1 cells and its association with ZO-2 may have significant implications. An important function of gastric epithelial cells is to provide a protective barrier and selective permeability of various substances between the external and internal compartments of the stomach. Paracellular permeability and intramembrane diffusion of various components between the apical and basolateral membranes of epithelial cells is attributed to TGs. TJs are a major component of the junctional complex of epithelial cells (Figure 73) and are composed of different types of transmembrane proteins, which connect to the cytoskeleton via adaptor/scaffold proteins including the ZOs. Therefore, the association with AHNAK1 with ZO-2 may affect the integrity of TGs of normal gastric epithelial cells. AHNAK1 does not possess any transmembrane domains, and therefore its expression and function is not at the site of the TGs located between epithelial cells, but instead is mostly likely nuclear and/or cytoplasmic. Although

AHNAK1 was found to co-localize with ZO-2 at the cell boundary in confluent RGM1 cells, additional experiments will be necessary to determine if AHNAK1 associates with ZO-2 in the nucleus, which could prevent its translocation to the plasma membrane, where it binds to the cytoplasmic C termini of junctional transmembrane proteins and link them to the actin cytoskeleton. The existence of ZO-2 in the nucleus has been reported, as Traweger *et al.* identified the localization of ZO-2 to the nucleus of migratory EC and subconfluent epithelial cells in response to environmental stress [420].

The function of AHNAK1 protein may be dependent on its ability to translocate from the nucleus to the plasma membrane. The cell type-dependent subcellular distribution of AHNAK1 is likely attributed to AHNAK1's ability to translocate from the nucleus to the plasma membrane. For example, in epithelial cells AHNAK1 has been shown to translocate from the nucleus to the plasma membrane in response to an increase in extracellular Ca^{2+} or stimulation of PKC [224]. Furthermore, AHNAK1's ability to associate with the plasma membrane may be due to N-myristoylation, as AHNAK1 contains nine potential *in vitro* N-myristoylation sites, in which N-myristoylation promotes membrane association [234]. In addition to being cell type-dependent, it is also plausible that AHNAK1's recruitment to the plasma membrane is cell cycle-dependent, as the phosphorylation state of AHNAK1 is substantially repressed in quiescent cells and its expression increases in the G₀ stage of the cell cycle [421].

The organization and integrity of epithelial cells is crucial for its function. Benaud *et al.* showed down-regulation of AHNAK1 affects the cell membrane cytoarchitecture of epithelial cells [226]. A report by Hieda *et al.* provided evidence of desmoyokin/AHNAK1 being restricted to the desmosome of bovine snout epidermis and

was suggested to play an role in plaque assembly [228]. Salim *et al.* reported a role for AHNAK1 in the establishment of cell-matrix contacts of Schwann cells [221]. Taken together, these findings may suggest a role for AHNAK1 in the regulation of epithelial cell adhesion and permeability.

Although this is the first report of AHNAK1 expression in surface epithelial cells of the stomach, Gentil *et al.* reported AHNAK1 positive staining in the muscularis mucosae and smooth muscle layers in the stomach of adult mice [219]. Similar to Gentil *et al.*, AHNAK1 expression in the muscularis mucosae and smooth muscle in the stomach of healthy human organ donors was observed (Figure 79). There are several explanations for AHNAK1 not previously being observed in the different secretory epithelial cells of the stomach. A difference in species, the use of different antibodies, and epitope accessibility are some explanations for the discrepancies in AHNAK1 immunoreactivity in the stomach.

In addition to providing a selective barrier, the epithelium signals to innate immune cells in the mucosa to combat infection and repair wounds [422]. The gastric mucosal barrier is routinely exposed to trauma, and since gastric mucosal restoration involves cell migration and proliferation (23), AHNAK1 may also serve a role in mediating each of these processes. The non-transformed RGM1 cell line was found to be an excellent model to investigate gastric epithelial restoration *in vitro* [342], as it displays a tight phenotype *in vitro*. Therefore, the RGM1 cell line is suitable for the determination of epithelial-regeneration and permeability changes in future studies.

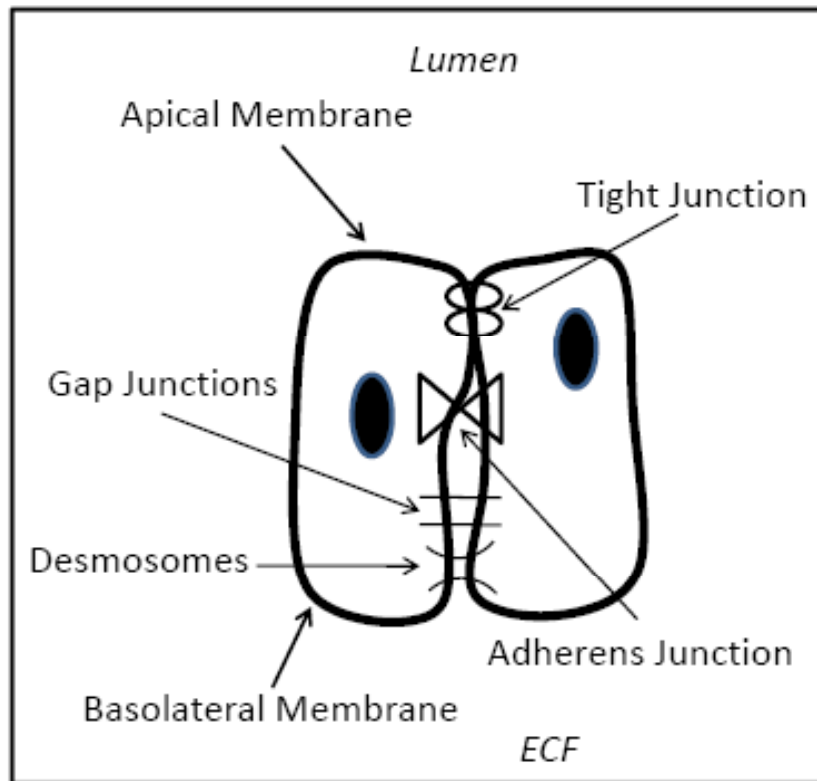


Figure 73. Schematic of the junctional complex of epithelial cells. The tight junctions (TJs) constitute the most apical component of the junctional complex. The adherens junctions (Ajs) anchors the cells together through Ca^{2+} -dependent cell adhesion molecules. The desmosomes junctions hold cells together and provide anchoring sites for intermediate filaments. Gap junctions allow small molecules to pass from the cytoplasm of neighboring cells.

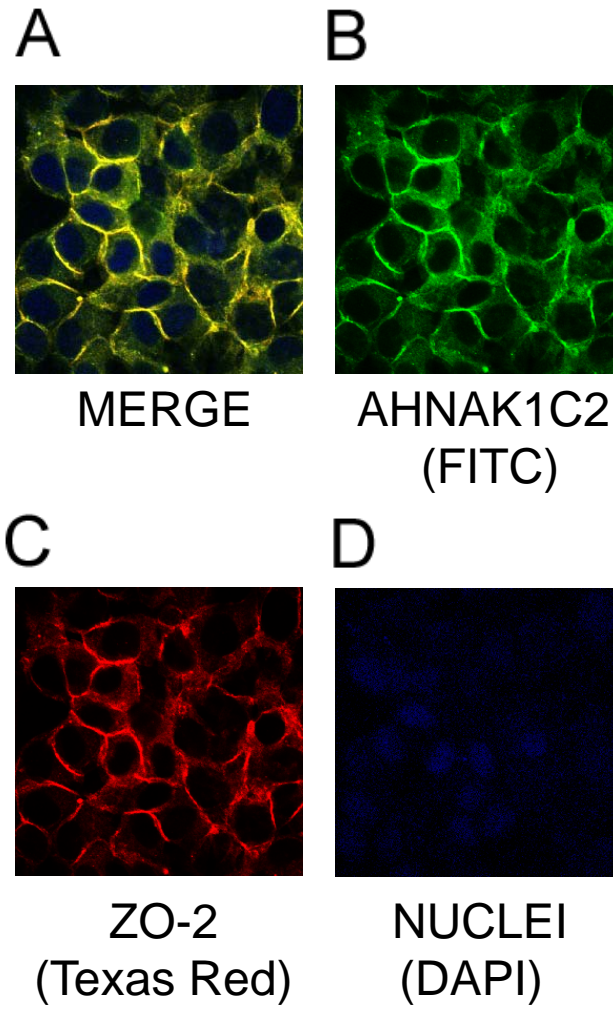


Figure 74. Colocalization of AHNAK1 and ZO-2 proteins in confluent RGM1 cells. DAPI was used to counterstain nuclei. Negative control (omission of AHNAK1 specific antibody)

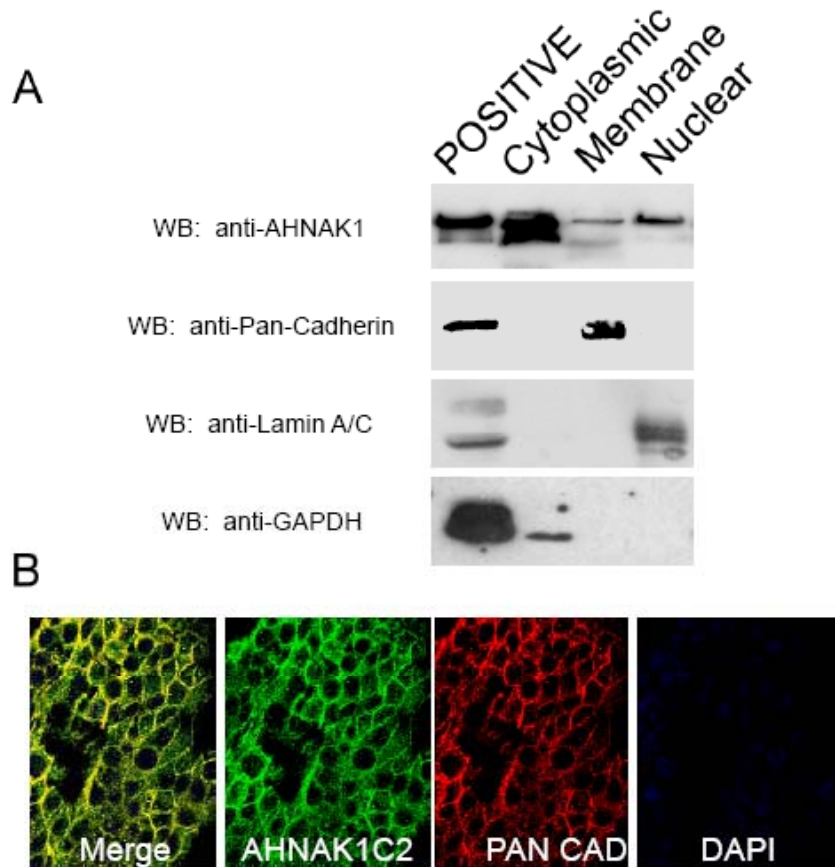


Figure 75. Subcellular localization of AHNAK1 in RGM1 cells. B: Immunofluorescent staining of RGM1 cells using antibody specific for AHNAK1 C2 illustrates the presence of AHNAK1 (FITC green) predominantly localized in the cytoplasm and at the plasma membrane. DAPI was used to counterstain the nucleus. Negative control (omission of AHNAK1 specific antibody)

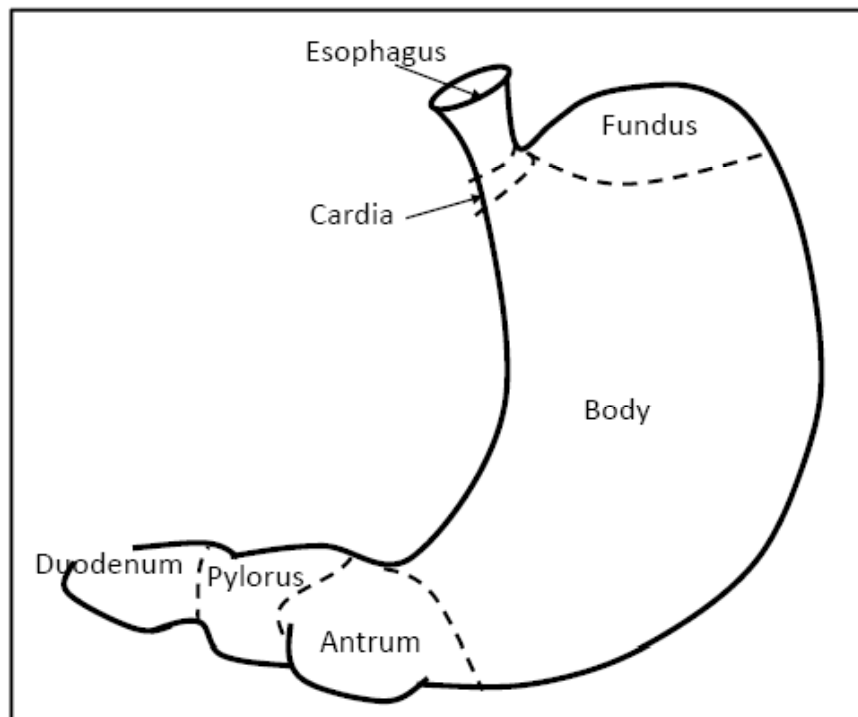


Figure 76. Schematic illustrating the various sections of the stomach. Each section is composed of different cells with specialized functions.

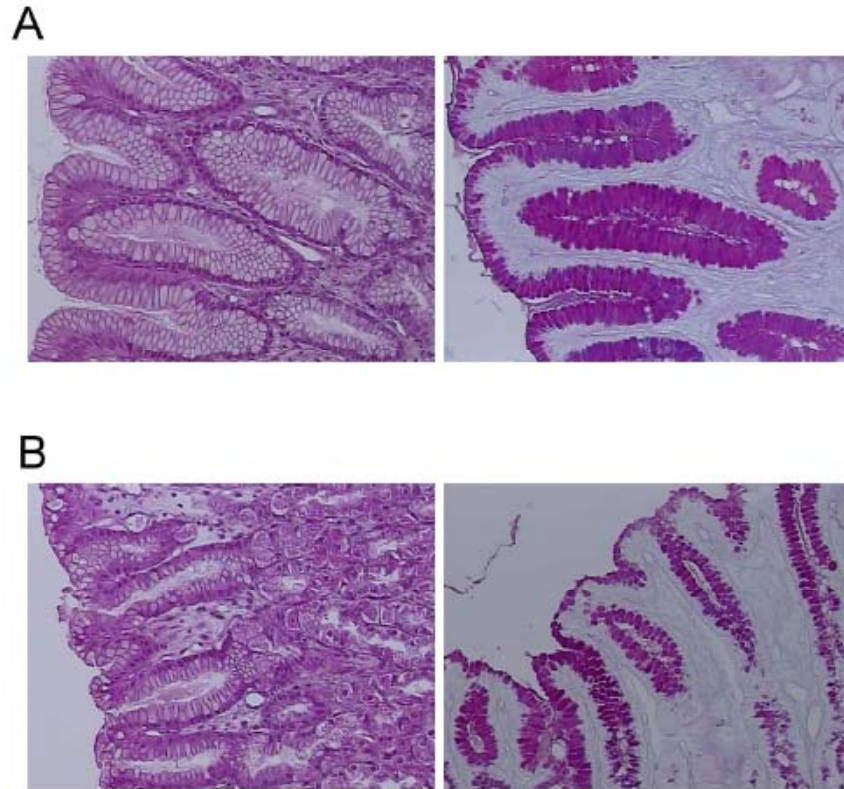


Figure 77. Histochemical analysis of representative tissue sections from healthy human organ stomach donors. Human stomach antrum (A) and body (B); Haematoxylin and Eosin (H and E) (left) PAS/Alcian Blue staining (right)

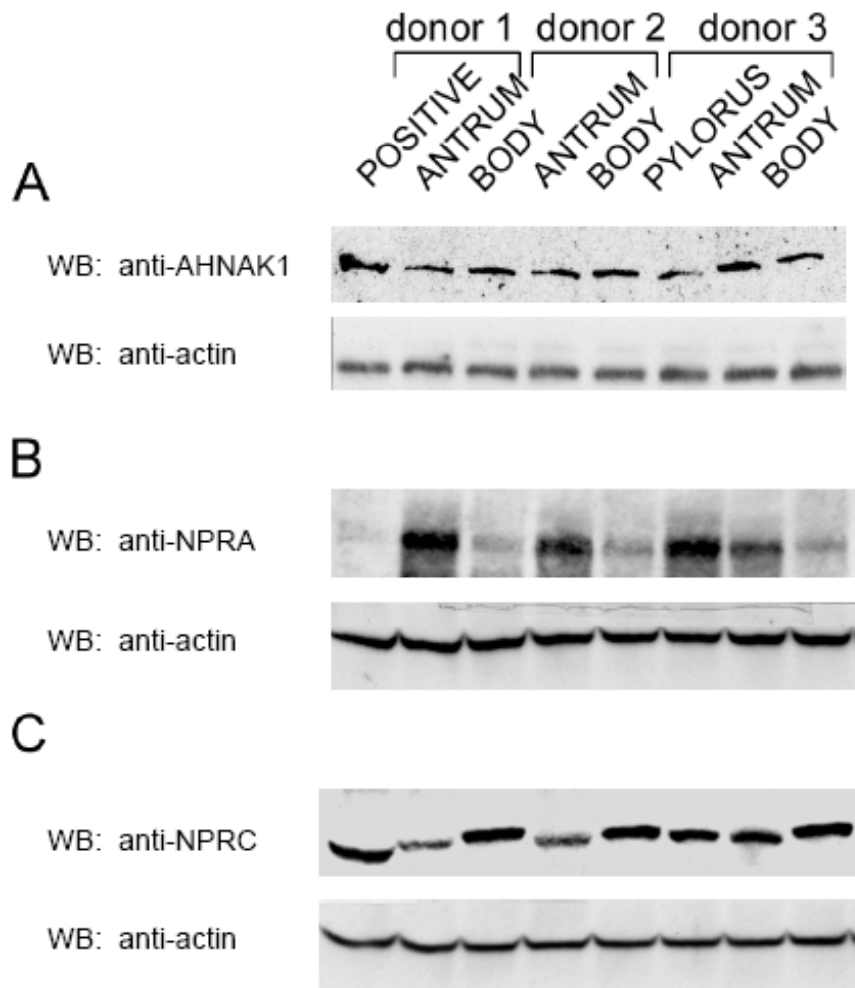


Figure 78. Western blot analysis of endogenous AHNAK1, NPRA, and NPRC protein expression in healthy human stomach.. (A) Immunoblot analysis showing (A) AHNAK1; (B) NPRA; (C) NPRC protein expression in different regions from three healthy human organ stomach donors

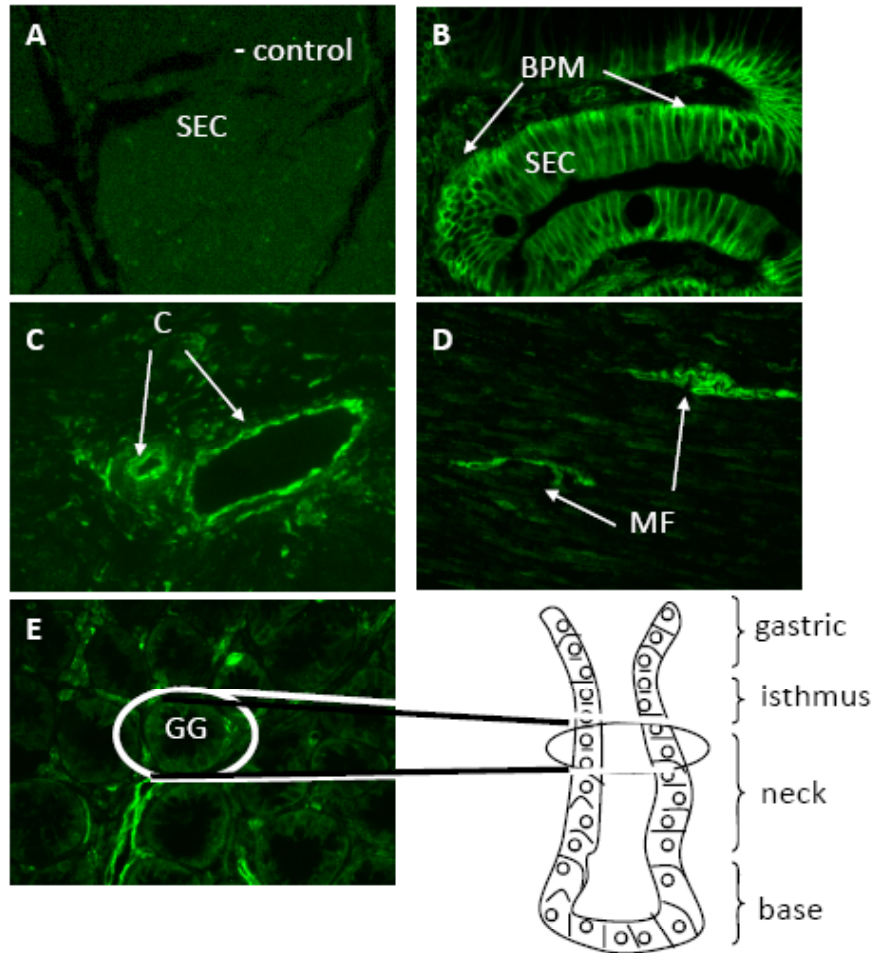


Figure 79. Immunohistochemistry analysis of endogenous AHNAK1 in healthy human stomach. A: Negative control (staining in the absence of AHNAK1 specific antibody); B: AHNAK1 protein immunoreactivity in surface epithelial cells (SEC) and at the basolateral plasma membrane (BPM); C: AHNAK1 protein immunoreactivity in capillaries (C); D: AHNAK1 protein immunoreactivity in muscle fibers (MF) from the muscularis mucosae; E: AHNAK1 protein immunoreactivity in the lamina propria but not in the cells of the gastric gland (GG)

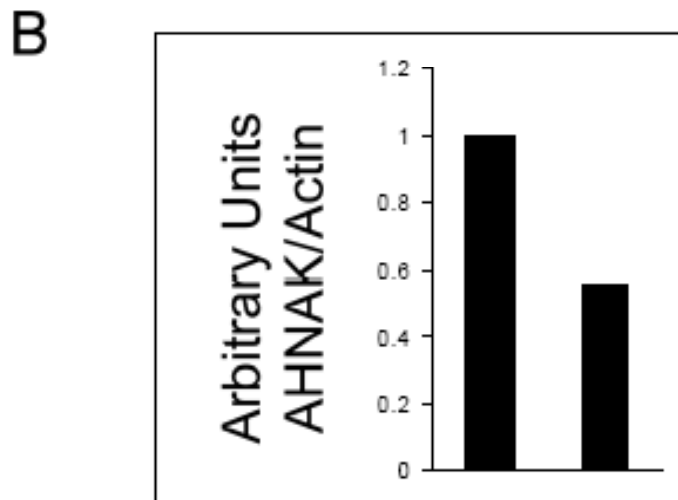
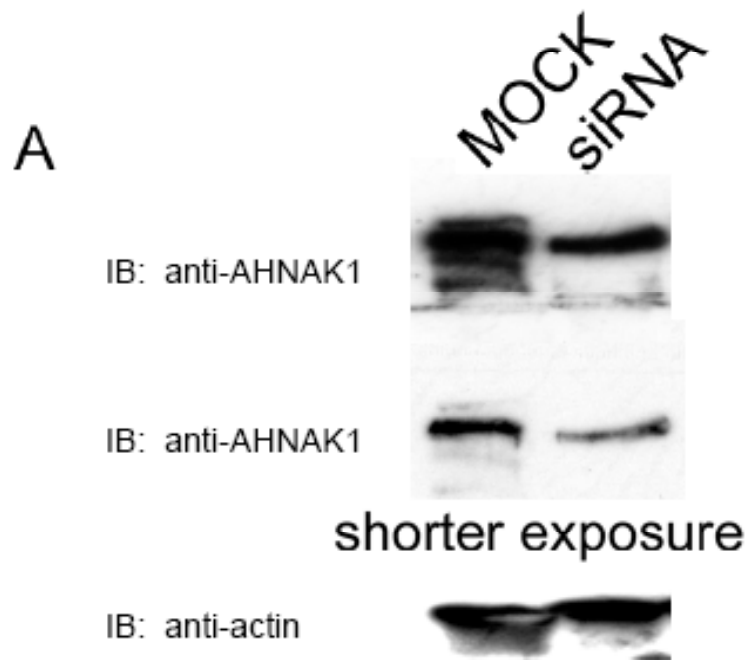


Figure 80. Knockdown of AHNAK1 protein in RGM1 cells. A: Western blot analysis of AHNAK1 after siRNA knockdown. B: Densitometric analysis of (A). MOCK refers to the use of nontargeting siRNA instead of AHNAK1 SMARTpool siRNA.

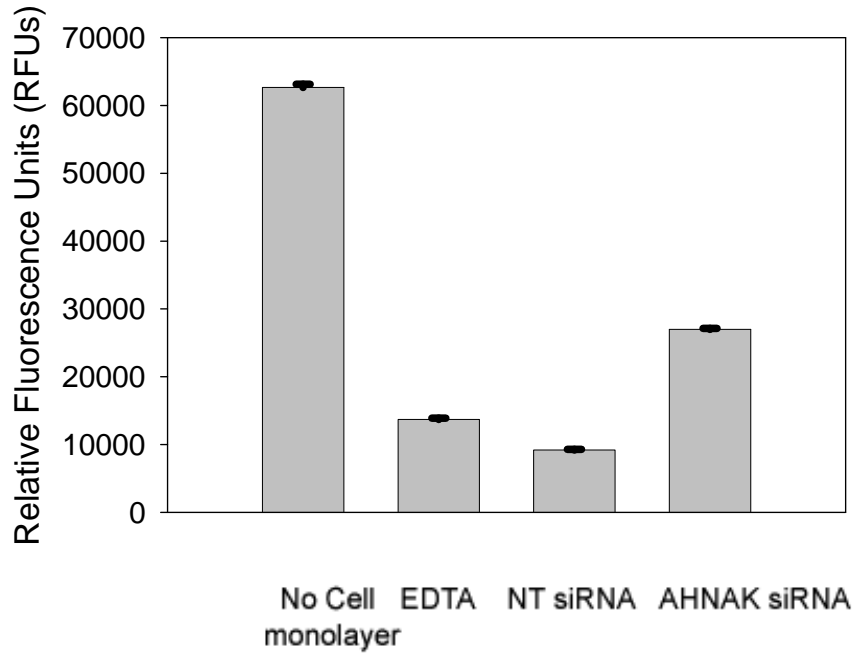


Figure 81. In vitro permeability assay demonstrating the role of AHNAK1 in maintaining paracellular cellular permeability and the barrier properties of RGM1 cells. Each group was performed in triplicates and the results shown are representative of two independent experiments. Controls shown include the absence of a cell monolayer, EDTA treatment for 20 minutes, and the use of nontargeting (NT) siRNA instead of AHNAK1 SMARTpool siRNA.

References

1. Daniels, L.B. and A.S. Maisel, *Natriuretic peptides*. J Am Coll Cardiol, 2007. **50**(25): p. 2357-68.
2. Wilkins, M.R., J. Redondo, and L.A. Brown, *The natriuretic-peptide family*. Lancet, 1997. **349**(9061): p. 1307-10.
3. Wu, F., et al., *Processing of pro-atrial natriuretic peptide by corin in cardiac myocytes*. J Biol Chem, 2002. **277**(19): p. 16900-5.
4. Yandle, T.G., *Biochemistry of natriuretic peptides*. J Intern Med, 1994. **235**(6): p. 561-76.
5. Vesely, D.L., et al., *Atrial natriuretic hormone, vessel dilator, long-acting natriuretic hormone, and kaliuretic hormone decrease the circulating concentrations of CRH, corticotropin, and cortisol*. J Clin Endocrinol Metab, 2001. **86**(9): p. 4244-9.
6. Vesely, D.L., *Natriuretic peptides and acute renal failure*. Am J Physiol Renal Physiol, 2003. **285**(2): p. F167-77.
7. Sawada, Y., et al., *Stretch-induced hypertrophic growth of cardiocytes and processing of brain-type natriuretic peptide are controlled by proprotein-processing endoprotease furin*. J Biol Chem, 1997. **272**(33): p. 20545-54.
8. Martinez-Rumayor, A., et al., *Biology of the natriuretic peptides*. Am J Cardiol, 2008. **101**(3A): p. 3-8.
9. de Bold, A.J., B.G. Bruneau, and M.L. Kuroski de Bold, *Mechanical and neuroendocrine regulation of the endocrine heart*. Cardiovasc Res, 1996. **31**(1): p. 7-18.
10. de Bold, A.J., *Tissue fractionation studies on the relationship between an atrial natriuretic factor and specific atrial granules*. Can J Physiol Pharmacol, 1982. **60**(3): p. 324-30.
11. de Bold, A.J., et al., *A rapid and potent natriuretic response to intravenous injection of atrial myocardial extract in rats. Reprinted from Life Sci. 28:89-94, 1981*. J Am Soc Nephrol, 2001. **12**(2): p. 403-9; discussion 403-8, 408-9.
12. Ruskoaho, H., *Atrial natriuretic peptide: synthesis, release, and metabolism*. Pharmacol Rev, 1992. **44**(4): p. 479-602.
13. Rebsamen, M.C., et al., *Role of cAMP and calcium influx in endothelin-1-induced ANP release in rat cardiomyocytes*. Am J Physiol, 1997. **273**(5 Pt 1): p. E922-31.
14. Levin, E.R., D.G. Gardner, and W.K. Samson, *Natriuretic peptides*. N Engl J Med, 1998. **339**(5): p. 321-8.
15. Bonow, R.O., *New insights into the cardiac natriuretic peptides*. Circulation, 1996. **93**(11): p. 1946-50.
16. Cheung, B.M. and C.R. Kumana, *Natriuretic peptides--relevance in cardiovascular disease*. Jama, 1998. **280**(23): p. 1983-4.

17. Anand-Srivastava, M.B. and G.J. Trachte, *Atrial natriuretic factor receptors and signal transduction mechanisms*. Pharmacol Rev, 1993. **45**(4): p. 455-97.
18. Hutchinson, H.G., et al., *Mechanisms of natriuretic-peptide-induced growth inhibition of vascular smooth muscle cells*. Cardiovasc Res, 1997. **35**(1): p. 158-67.
19. Cao, L. and D.G. Gardner, *Natriuretic peptides inhibit DNA synthesis in cardiac fibroblasts*. Hypertension, 1995. **25**(2): p. 227-34.
20. Garg, U.C. and A. Hassid, *Nitric oxide-generating vasodilators and 8-bromocyclic guanosine monophosphate inhibit mitogenesis and proliferation of cultured rat vascular smooth muscle cells*. J Clin Invest, 1989. **83**(5): p. 1774-7.
21. Vesely, B.A., et al., *Four peptides decrease the number of human pancreatic adenocarcinoma cells*. Eur J Clin Invest, 2003. **33**(11): p. 998-1005.
22. Dong, M.Q., et al., *[Comparison of inhibitory effects of three natriuretic peptides on the proliferation of pulmonary artery smooth muscle cells of rats]*. Sheng Li Xue Bao, 2000. **52**(3): p. 252-4.
23. Hamad, A.M., S.R. Johnson, and A.J. Knox, *Antiproliferative effects of NO and ANP in cultured human airway smooth muscle*. Am J Physiol, 1999. **277**(5 Pt 1): p. L910-8.
24. Wu, C.F., N.H. Bishopric, and R.E. Pratt, *Atrial natriuretic peptide induces apoptosis in neonatal rat cardiac myocytes*. J Biol Chem, 1997. **272**(23): p. 14860-6.
25. Suenobu, N., et al., *Natriuretic peptides and nitric oxide induce endothelial apoptosis via a cGMP-dependent mechanism*. Arterioscler Thromb Vasc Biol, 1999. **19**(1): p. 140-6.
26. Rose, R.A., A.E. Lomax, and W.R. Giles, *Inhibition of L-type Ca²⁺ current by C-type natriuretic peptide in bullfrog atrial myocytes: an NPR-C-mediated effect*. Am J Physiol Heart Circ Physiol, 2003. **285**(6): p. H2454-62.
27. Rose, R.A. and W.R. Giles, *Natriuretic peptide C receptor signalling in the heart and vasculature*. J Physiol, 2008. **586**(2): p. 353-66.
28. Rose, R.A., et al., *C-type natriuretic peptide inhibits L-type Ca²⁺ current in rat magnocellular neurosecretory cells by activating the NPR-C receptor*. J Neurophysiol, 2005. **94**(1): p. 612-21.
29. Trachte, G.J., et al., *C-type natriuretic peptide neuromodulates via "clearance" receptors*. Am J Physiol, 1995. **268**(4 Pt 1): p. C978-84.
30. Murthy, K.S., et al., *G protein-dependent activation of smooth muscle eNOS via natriuretic peptide clearance receptor*. Am J Physiol, 1998. **275**(6 Pt 1): p. C1409-16.
31. Murthy, K.S., et al., *G(i-1)/G(i-2)-dependent signaling by single-transmembrane natriuretic peptide clearance receptor*. Am J Physiol Gastrointest Liver Physiol, 2000. **278**(6): p. G974-80.
32. Barletta, G., et al., *Low-dose C-type natriuretic peptide does not affect cardiac and renal function in humans*. Hypertension, 1998. **31**(3): p. 802-8.
33. Pham, I., et al., *Renal and vascular effects of C-type and atrial natriuretic peptides in humans*. Am J Physiol, 1997. **273**(4 Pt 2): p. R1457-64.

34. Chauhan, S.D., et al., *Release of C-type natriuretic peptide accounts for the biological activity of endothelium-derived hyperpolarizing factor*. Proc Natl Acad Sci U S A, 2003. **100**(3): p. 1426-31.
35. Komatsu, Y., et al., *Regulation of endothelial production of C-type natriuretic peptide in coculture with vascular smooth muscle cells. Role of the vascular natriuretic peptide system in vascular growth inhibition*. Circ Res, 1996. **78**(4): p. 606-14.
36. Yamahara, K., et al., *Significance and therapeutic potential of the natriuretic peptides/cGMP/cGMP-dependent protein kinase pathway in vascular regeneration*. Proc Natl Acad Sci U S A, 2003. **100**(6): p. 3404-9.
37. Chusho, H., et al., *Dwarfism and early death in mice lacking C-type natriuretic peptide*. Proc Natl Acad Sci U S A, 2001. **98**(7): p. 4016-21.
38. Komatsu, Y., et al., *Significance of C-type natriuretic peptide (CNP) in endochondral ossification: analysis of CNP knockout mice*. J Bone Miner Metab, 2002. **20**(6): p. 331-6.
39. Mericq, V., et al., *Regulation of fetal rat bone growth by C-type natriuretic peptide and cGMP*. Pediatr Res, 2000. **47**(2): p. 189-93.
40. Yasoda, A., et al., *Natriuretic peptide regulation of endochondral ossification. Evidence for possible roles of the C-type natriuretic peptide/guanylyl cyclase-B pathway*. J Biol Chem, 1998. **273**(19): p. 11695-700.
41. Agoston, H., et al., *C-type natriuretic peptide regulates endochondral bone growth through p38 MAP kinase-dependent and -independent pathways*. BMC Dev Biol, 2007. **7**: p. 18.
42. Maack, T., et al., *Physiological role of silent receptors of atrial natriuretic factor*. Science, 1987. **238**(4827): p. 675-8.
43. Roques, B.P., et al., *Neutral endopeptidase 24.11: structure, inhibition, and experimental and clinical pharmacology*. Pharmacol Rev, 1993. **45**(1): p. 87-146.
44. Steinhilber, M.E., K.L. Cochrane, and L.J. Field, *Hypotension in transgenic mice expressing atrial natriuretic factor fusion genes*. Hypertension, 1990. **16**(3): p. 301-7.
45. Oliver, P.M., et al., *Natriuretic peptide receptor 1 expression influences blood pressures of mice in a dose-dependent manner*. Proc Natl Acad Sci U S A, 1998. **95**(5): p. 2547-51.
46. John, S.W., et al., *Blood pressure and fluid-electrolyte balance in mice with reduced or absent ANP*. Am J Physiol, 1996. **271**(1 Pt 2): p. R109-14.
47. Lopez, M.J., et al., *Salt-resistant hypertension in mice lacking the guanylyl cyclase-A receptor for atrial natriuretic peptide*. Nature, 1995. **378**(6552): p. 65-8.
48. Lopez, M.J., D.L. Garbers, and M. Kuhn, *The guanylyl cyclase-deficient mouse defines differential pathways of natriuretic peptide signaling*. J Biol Chem, 1997. **272**(37): p. 23064-8.
49. Matsukawa, N., et al., *The natriuretic peptide clearance receptor locally modulates the physiological effects of the natriuretic peptide system*. Proc Natl Acad Sci U S A, 1999. **96**(13): p. 7403-8.
50. Tsutamoto, T., et al., *Attenuation of compensation of endogenous cardiac natriuretic peptide system in chronic heart failure: prognostic role of plasma*

- brain natriuretic peptide concentration in patients with chronic symptomatic left ventricular dysfunction.* Circulation, 1997. **96**(2): p. 509-16.
51. Ellinor, P.T., et al., *Discordant atrial natriuretic peptide and brain natriuretic peptide levels in lone atrial fibrillation.* J Am Coll Cardiol, 2005. **45**(1): p. 82-6.
 52. Dries, D.L., *Relevance of molecular forms of brain natriuretic peptide for natriuretic peptide research.* Hypertension, 2007. **49**(5): p. 971-3.
 53. Mukoyama, M., et al., *Increased human brain natriuretic peptide in congestive heart failure.* N Engl J Med, 1990. **323**(11): p. 757-8.
 54. Mukoyama, M., et al., *Brain natriuretic peptide as a novel cardiac hormone in humans. Evidence for an exquisite dual natriuretic peptide system, atrial natriuretic peptide and brain natriuretic peptide.* J Clin Invest, 1991. **87**(4): p. 1402-12.
 55. Lang, C.C., et al., *Effect of haemodialysis on plasma levels of brain natriuretic peptide in patients with chronic renal failure.* Clin Sci (Lond), 1992. **82**(2): p. 127-31.
 56. Naruse, M., et al., *Atrial and brain natriuretic peptides in cardiovascular diseases.* Hypertension, 1994. **23**(1 Suppl): p. I231-4.
 57. Cody, R.J., et al., *Atrial natriuretic factor in normal subjects and heart failure patients. Plasma levels and renal, hormonal, and hemodynamic responses to peptide infusion.* J Clin Invest, 1986. **78**(5): p. 1362-74.
 58. Crozier, I.G., et al., *Haemodynamic effects of atrial peptide infusion in heart failure.* Lancet, 1986. **2**(8518): p. 1242-5.
 59. Sabbatini, M.E., et al., *Atrial natriuretic factor stimulates exocrine pancreatic secretion in the rat through NPR-C receptors.* Am J Physiol Gastrointest Liver Physiol, 2003. **285**(5): p. G929-37.
 60. Sabbatini, M.E., et al., *C-type natriuretic peptide enhances amylase release through NPR-C receptors in the exocrine pancreas.* Am J Physiol Gastrointest Liver Physiol, 2007. **293**(5): p. G987-94.
 61. Sabbatini, M.E., et al., *Atrial natriuretic factor negatively modulates secretin intracellular signaling in the exocrine pancreas.* Am J Physiol Gastrointest Liver Physiol, 2007. **292**(1): p. G349-57.
 62. Sabbatini, M.E., et al., *NPR-C receptors are involved in C-type natriuretic peptide response on bile secretion.* Regul Pept, 2003. **116**(1-3): p. 13-20.
 63. Sabbatini, M.E., et al., *C-type natriuretic peptide stimulates pancreatic exocrine secretion in the rat: role of vagal afferent and efferent pathways.* Eur J Pharmacol, 2007. **577**(1-3): p. 192-202.
 64. Puurunen, J. and H. Ruskoaho, *Vagal-dependent stimulation of gastric acid secretion by intracerebroventricularly administered atrial natriuretic peptide in anaesthetized rats.* Eur J Pharmacol, 1987. **141**(3): p. 493-5.
 65. Stapelfeldt, W., et al., *Effect of naloxone on vagally-induced gastric acid secretion in rats.* Neuropeptides, 1988. **12**(1): p. 13-20.
 66. Gower, W.R., Jr., et al., *Atrial natriuretic peptide gene expression in the rat gastrointestinal tract.* Biochem Biophys Res Commun, 1994. **202**(1): p. 562-70.
 67. Gower, W.R., Jr., et al., *Regulation of atrial natriuretic peptide gene expression in gastric antrum by fasting.* Am J Physiol Regul Integr Comp Physiol, 2000. **278**(3): p. R770-80.

68. Schulz, S. and S.A. Waldman, *The guanylyl cyclase family of natriuretic peptide receptors*. Vitam Horm, 1999. **57**: p. 123-51.
69. Garbers, D.L., *The guanylyl cyclase receptors*. Zygote, 2000. **8 Suppl 1**: p. S24-5.
70. Drewett, J.G. and D.L. Garbers, *The family of guanylyl cyclase receptors and their ligands*. Endocr Rev, 1994. **15**(2): p. 135-62.
71. Yuen, P.S. and D.L. Garbers, *Guanylyl cyclase-linked receptors*. Annu Rev Neurosci, 1992. **15**: p. 193-225.
72. Garbers, D.L., *Guanylyl cyclase-linked receptors*. Pharmacol Ther, 1991. **50**(3): p. 337-45.
73. Wedel, B.J. and D.L. Garbers, *New insights on the functions of the guanylyl cyclase receptors*. FEBS Lett, 1997. **410**(1): p. 29-33.
74. Garbers, D.L., *Guanylyl cyclase receptors and their endocrine, paracrine, and autocrine ligands*. Cell, 1992. **71**(1): p. 1-4.
75. Garbers, D.L. and D.G. Lowe, *Guanylyl cyclase receptors*. J Biol Chem, 1994. **269**(49): p. 30741-4.
76. Potter, L.R., S. Abbey-Hosch, and D.M. Dickey, *Natriuretic peptides, their receptors, and cyclic guanosine monophosphate-dependent signaling functions*. Endocr Rev, 2006. **27**(1): p. 47-72.
77. Koller, K.J., et al., *Selective activation of the B natriuretic peptide receptor by C-type natriuretic peptide (CNP)*. Science, 1991. **252**(5002): p. 120-3.
78. Suga, S., et al., *Receptor selectivity of natriuretic peptide family, atrial natriuretic peptide, brain natriuretic peptide, and C-type natriuretic peptide*. Endocrinology, 1992. **130**(1): p. 229-39.
79. Potter, L.R. and T. Hunter, *Guanylyl cyclase-linked natriuretic peptide receptors: structure and regulation*. J Biol Chem, 2001. **276**(9): p. 6057-60.
80. Potthast, R. and L.R. Potter, *Phosphorylation-dependent regulation of the guanylyl cyclase-linked natriuretic peptide receptors*. Peptides, 2005. **26**(6): p. 1001-8.
81. Potter, L.R. and T. Hunter, *Identification and characterization of the phosphorylation sites of the guanylyl cyclase-linked natriuretic peptide receptors A and B*. Methods, 1999. **19**(4): p. 506-20.
82. Anand-Srivastava, M.B., *Natriuretic peptide receptor-C signaling and regulation*. Peptides, 2005. **26**(6): p. 1044-59.
83. Itakura, M., H. Suzuki, and S. Hirose, *Structural analysis of natriuretic peptide receptor-C by truncation and site-directed mutagenesis*. Biochem J, 1997. **322** (Pt 2): p. 585-90.
84. Brown, J. and Z. Zuo, *Receptor proteins and biological effects of C-type natriuretic peptides in the renal glomerulus of the rat*. Am J Physiol, 1994. **266**(4 Pt 2): p. R1383-94.
85. Ogawa, H., et al., *Crystal structure of hormone-bound atrial natriuretic peptide receptor extracellular domain: rotation mechanism for transmembrane signal transduction*. J Biol Chem, 2004. **279**(27): p. 28625-31.
86. Scarborough, R.M., et al., *Truncated atrial natriuretic peptide analogs. Comparison between receptor binding and stimulation of cyclic GMP accumulation in cultured vascular smooth muscle cells*. J Biol Chem, 1986. **261**(28): p. 12960-4.

87. Vesely, D.L., et al., *Four cardiac hormones eliminate up to two-thirds of human breast cancers in athymic mice. In vivo*, 2007. **21**(6): p. 973-8.
88. Vesely, D.L., et al., *Elimination of up to 80% of human pancreatic adenocarcinomas in athymic mice by cardiac hormones. In vivo*, 2007. **21**(3): p. 445-51.
89. Vesely, B.A., et al., *Urodilatin and four cardiac hormones decrease human renal carcinoma cell numbers. Eur J Clin Invest*, 2006. **36**(11): p. 810-9.
90. Vesely, B.A., et al., *Four peptide hormones' specific decrease (up to 97%) of human prostate carcinoma cells. Eur J Clin Invest*, 2005. **35**(11): p. 700-10.
91. Eichelbaum, E.J., et al., *Four cardiac hormones eliminate up to 82% of human medullary thyroid carcinoma cells within 24 hours. Endocrine*, 2006. **30**(3): p. 325-32.
92. Vesely, B.A., et al., *Four cardiac hormones eliminate 4-fold more human glioblastoma cells than the green mamba snake peptide. Cancer Lett*, 2007. **254**(1): p. 94-101.
93. Gower, W.R., et al., *Four peptides decrease human colon adenocarcinoma cell number and DNA synthesis via cyclic GMP. Int J Gastrointest Cancer*, 2005. **36**(2): p. 77-87.
94. Vesely, B.A., et al., *Four cardiac hormones cause cell death of melanoma cells and inhibit their DNA synthesis. Am J Med Sci*, 2007. **334**(5): p. 342-9.
95. Vesely, B.A., et al., *Primary malignant tumors of the heart: four cardiovascular hormones decrease the number and DNA synthesis of human angiosarcoma cells. Cardiology*, 2006. **105**(4): p. 226-33.
96. Vesely, B.A., et al., *Five cardiac hormones decrease the number of human small-cell lung cancer cells. Eur J Clin Invest*, 2005. **35**(6): p. 388-98.
97. Eichelbaum, E.J., et al., *Cardiac and kidney hormones cure up to 86% of human small-cell lung cancers in mice. Eur J Clin Invest*, 2008. **38**(8): p. 562-70.
98. Anand-Srivastava, M.B., *Downregulation of atrial natriuretic peptide ANP-C receptor is associated with alterations in G-protein expression in A10 smooth muscle cells. Biochemistry*, 2000. **39**(21): p. 6503-13.
99. Alli, A.A. and W.R. Gower, Jr., *The C type natriuretic peptide receptor tethers AHNAK1 at the plasma membrane to potentiate arachidonic acid induced calcium mobilization. Am J Physiol Cell Physiol*, 2009.
100. Burgess, M.D., et al., *C-type natriuretic peptide receptor expression in pancreatic alpha cells. Histochem Cell Biol*, 2009. **132**(1): p. 95-103.
101. Cohen, D., et al., *Molecular determinants of the clearance function of type C receptors of natriuretic peptides. J Biol Chem*, 1996. **271**(16): p. 9863-9.
102. Nussenzveig, D.R., J.A. Lewicki, and T. Maack, *Cellular mechanisms of the clearance function of type C receptors of atrial natriuretic factor. J Biol Chem*, 1990. **265**(34): p. 20952-8.
103. Rademaker, M.T., et al., *Clearance receptors and endopeptidase: equal role in natriuretic peptide metabolism in heart failure. Am J Physiol*, 1997. **273**(5 Pt 2): p. H2372-9.
104. Chiu, P.J., et al., *Influence of C-ANF receptor and neutral endopeptidase on pharmacokinetics of ANF in rats. Am J Physiol*, 1991. **260**(1 Pt 2): p. R208-16.

105. Kukkonen, P., O. Vuolteenaho, and H. Ruskoaho, *Basal and volume expansion-stimulated plasma atrial natriuretic peptide concentrations and hemodynamics in conscious rats: effects of SCH 39.370, an endopeptidase inhibitor, and C-ANF-(4-23), a clearance receptor ligand*. *Endocrinology*, 1992. **130**(2): p. 755-65.
106. Charles, C.J., et al., *Clearance receptors and endopeptidase 24.11: equal role in natriuretic peptide metabolism in conscious sheep*. *Am J Physiol*, 1996. **271**(2 Pt 2): p. R373-80.
107. Wegner, M., D. Ganten, and J.P. Stasch, *Neutral endopeptidase inhibition potentiates the effects of natriuretic peptides in renin transgenic rats*. *Hypertens Res*, 1996. **19**(4): p. 229-38.
108. Stults, J.T., et al., *The disulfide linkages and glycosylation sites of the human natriuretic peptide receptor-C homodimer*. *Biochemistry*, 1994. **33**(37): p. 11372-81.
109. He, X., et al., *Allosteric activation of a spring-loaded natriuretic peptide receptor dimer by hormone*. *Science*, 2001. **293**(5535): p. 1657-62.
110. Sarzani, R., et al., *Fasting inhibits natriuretic peptides clearance receptor expression in rat adipose tissue*. *J Hypertens*, 1995. **13**(11): p. 1241-6.
111. Chabrier, P.E., et al., *Regulation of atrial natriuretic factor receptors by angiotensin II in rat vascular smooth muscle cells*. *J Biol Chem*, 1988. **263**(26): p. 13199-202.
112. Yoshimoto, T., et al., *Angiotensin II-dependent down-regulation of vascular natriuretic peptide type C receptor gene expression in hypertensive rats*. *Endocrinology*, 1996. **137**(3): p. 1102-7.
113. Boumati, M., Y. Li, and M.B. Anand-Srivastava, *Modulation of ANP-C receptor signaling by endothelin-1 in A-10 smooth muscle cells*. *Arch Biochem Biophys*, 2002. **401**(2): p. 178-86.
114. Kishimoto, I., et al., *Natriuretic peptide clearance receptor is transcriptionally down-regulated by beta 2-adrenergic stimulation in vascular smooth muscle cells*. *J Biol Chem*, 1994. **269**(45): p. 28300-8.
115. Agui, T., et al., *Opposite actions of transforming growth factor-beta 1 on the gene expression of atrial natriuretic peptide biological and clearance receptors in a murine thymic stromal cell line*. *J Biochem*, 1995. **118**(3): p. 500-7.
116. Sun, J.Z., et al., *Tyrosine kinase receptor activation inhibits NPR-C in lung arterial smooth muscle cells*. *Am J Physiol Lung Cell Mol Physiol*, 2001. **281**(1): p. L155-63.
117. Itoh, K., et al., *Gene regulation of atrial natriuretic peptide A, B, and C receptors in rat glomeruli*. *Exp Nephrol*, 1999. **7**(4): p. 328-36.
118. Ardaillou, N., et al., *Dexamethasone upregulates ANP C-receptor protein in human mesangial cells without affecting mRNA*. *Am J Physiol*, 1996. **270**(3 Pt 2): p. F440-6.
119. Lu, S.Y., et al., *Down-regulation of C-type natriuretic peptide receptor by vasonatin peptide in cardiac myocytes and fibroblasts*. *Acta Pharmacol Sin*, 2004. **25**(4): p. 424-30.
120. Hirata, Y., et al., *Regulation of atrial natriuretic peptide receptors in cultured vascular smooth muscle cells of rat*. *Biochem Biophys Res Commun*, 1986. **138**(1): p. 405-12.

121. Arejian, M., Y. Li, and M.B. Anand-Srivastava, *Nitric oxide attenuates the expression of natriuretic peptide receptor C and associated adenylyl cyclase signaling in aortic vascular smooth muscle cells: role of MAPK*. *Am J Physiol Heart Circ Physiol*, 2009. **296**(6): p. H1859-67.
122. Gower, W.R., Jr., et al., *Identification, regulation and anti-proliferative role of the NPR-C receptor in gastric epithelial cells*. *Mol Cell Biochem*, 2006. **293**(1-2): p. 103-18.
123. Klinger, J.R., et al., *Downregulation of pulmonary atrial natriuretic peptide receptors in rats exposed to chronic hypoxia*. *J Appl Physiol*, 1994. **77**(3): p. 1309-16.
124. Li, H., et al., *Selective downregulation of ANP-clearance-receptor gene expression in lung of rats adapted to hypoxia*. *Am J Physiol*, 1995. **268**(2 Pt 1): p. L328-35.
125. Sun, J.Z., et al., *Hypoxia reduces atrial natriuretic peptide clearance receptor gene expression in ANP knockout mice*. *Am J Physiol Lung Cell Mol Physiol*, 2000. **279**(3): p. L511-9.
126. Sun, J.Z., et al., *Dietary salt supplementation selectively downregulates NPR-C receptor expression in kidney independently of ANP*. *Am J Physiol Renal Physiol*, 2002. **282**(2): p. F220-7.
127. Nagase, M., et al., *Role of natriuretic peptide receptor type C in Dahl salt-sensitive hypertensive rats*. *Hypertension*, 1997. **30**(2 Pt 1): p. 177-83.
128. Luk, J.K., E.F. Wong, and N.L. Wong, *Downregulation of atrial natriuretic factor clearance receptors in experimental chronic renal failure rats*. *Am J Physiol*, 1995. **269**(3 Pt 2): p. H902-8.
129. Naruse, M., et al., *[Pathophysiological significance of the natriuretic peptide system: receptor subtype as another key factor]*. *Nippon Yakurigaku Zasshi*, 1998. **112**(3): p. 147-54.
130. Lefkowitz, R.J., *Seven transmembrane receptors: something old, something new*. *Acta Physiol (Oxf)*, 2007. **190**(1): p. 9-19.
131. Anand-Srivastava, M.B. and M. Cantin, *Atrial natriuretic factor receptors are negatively coupled to adenylate cyclase in cultured atrial and ventricular cardiocytes*. *Biochem Biophys Res Commun*, 1986. **138**(1): p. 427-36.
132. Anand-Srivastava, M.B., A.K. Srivastava, and M. Cantin, *Pertussis toxin attenuates atrial natriuretic factor-mediated inhibition of adenylate cyclase. Involvement of inhibitory guanine nucleotide regulatory protein*. *J Biol Chem*, 1987. **262**(11): p. 4931-4.
133. Anand-Srivastava, M.B., P.D. Sehl, and D.G. Lowe, *Cytoplasmic domain of natriuretic peptide receptor-C inhibits adenylyl cyclase. Involvement of a pertussis toxin-sensitive G protein*. *J Biol Chem*, 1996. **271**(32): p. 19324-9.
134. Pagano, M. and M.B. Anand-Srivastava, *Cytoplasmic domain of natriuretic peptide receptor C constitutes Gi activator sequences that inhibit adenylyl cyclase activity*. *J Biol Chem*, 2001. **276**(25): p. 22064-70.
135. Zhou, H. and K.S. Murthy, *Identification of the G protein-activating sequence of the single-transmembrane natriuretic peptide receptor C (NPR-C)*. *Am J Physiol Cell Physiol*, 2003. **284**(5): p. C1255-61.

136. Kiemer, A.K., et al., *Inhibition of cyclooxygenase-2 by natriuretic peptides*. *Endocrinology*, 2002. **143**(3): p. 846-52.
137. Levin, E.R. and H.J. Frank, *Natriuretic peptides inhibit rat astroglial proliferation: mediation by C receptor*. *Am J Physiol*, 1991. **261**(2 Pt 2): p. R453-7.
138. Hu, R.M., et al., *Atrial natriuretic peptide inhibits the production and secretion of endothelin from cultured endothelial cells. Mediation through the C receptor*. *J Biol Chem*, 1992. **267**(24): p. 17384-9.
139. Johnson, B.G., G.J. Trachte, and J.G. Drewett, *Neuromodulatory effect of the atrial natriuretic factor clearance receptor binding peptide, cANF(4-23)-NH₂ in rabbit isolated vasa deferentia*. *J Pharmacol Exp Ther*, 1991. **257**(2): p. 720-6.
140. Drewett, J.G., R.J. Ziegler, and G.J. Trachte, *Neuromodulatory effects of atrial natriuretic peptides correlate with an inhibition of adenylate cyclase but not an activation of guanylate cyclase*. *J Pharmacol Exp Ther*, 1992. **260**(2): p. 689-96.
141. Mouawad, R., Y. Li, and M.B. Anand-Srivastava, *Atrial natriuretic peptide-C receptor-induced attenuation of adenylyl cyclase signaling activates phosphatidylinositol turnover in A10 vascular smooth muscle cells*. *Mol Pharmacol*, 2004. **65**(4): p. 917-24.
142. Prins, B.A., et al., *Atrial natriuretic peptide inhibits mitogen-activated protein kinase through the clearance receptor. Potential role in the inhibition of astrocyte proliferation*. *J Biol Chem*, 1996. **271**(24): p. 14156-62.
143. Rose, R.A., et al., *Effects of C-type natriuretic peptide on ionic currents in mouse sinoatrial node: a role for the NPR-C receptor*. *Am J Physiol Heart Circ Physiol*, 2004. **286**(5): p. H1970-7.
144. Cahill, P.A. and A. Hassid, *Clearance receptor-binding atrial natriuretic peptides inhibit mitogenesis and proliferation of rat aortic smooth muscle cells*. *Biochem Biophys Res Commun*, 1991. **179**(3): p. 1606-13.
145. Itoh, H., et al., *Atrial natriuretic polypeptide as a novel antigrowth factor of endothelial cells*. *Hypertension*, 1992. **19**(6 Pt 2): p. 758-61.
146. Lelievre, V., et al., *Proliferative actions of natriuretic peptides on neuroblastoma cells. Involvement of guanylyl cyclase and non-guanylyl cyclase pathways*. *J Biol Chem*, 2001. **276**(47): p. 43668-76.
147. Hempel, A., et al., *Atrial natriuretic peptide clearance receptor participates in modulating endothelial permeability*. *Am J Physiol*, 1998. **275**(5 Pt 2): p. H1818-25.
148. Pedram, A., et al., *Vasoactive peptides modulate vascular endothelial cell growth factor production and endothelial cell proliferation and invasion*. *J Biol Chem*, 1997. **272**(27): p. 17097-103.
149. Jaubert, J., et al., *Three new allelic mouse mutations that cause skeletal overgrowth involve the natriuretic peptide receptor C gene (*Npr3*)*. *Proc Natl Acad Sci U S A*, 1999. **96**(18): p. 10278-83.
150. Murakami, A., et al., *X-arrestin: a new retinal arrestin mapping to the X chromosome*. *FEBS Lett*, 1993. **334**(2): p. 203-9.
151. Shinohara, T., et al., *Primary and secondary structure of bovine retinal S antigen (48-kDa protein)*. *Proc Natl Acad Sci U S A*, 1987. **84**(20): p. 6975-9.

152. Lohse, M.J., et al., *beta-Arrestin: a protein that regulates beta-adrenergic receptor function*. Science, 1990. **248**(4962): p. 1547-50.
153. Attramadal, H., et al., *Beta-arrestin2, a novel member of the arrestin/beta-arrestin gene family*. J Biol Chem, 1992. **267**(25): p. 17882-90.
154. Luttrell, L.M. and R.J. Lefkowitz, *The role of beta-arrestins in the termination and transduction of G-protein-coupled receptor signals*. J Cell Sci, 2002. **115**(Pt 3): p. 455-65.
155. Pierce, K.L., R.T. Premont, and R.J. Lefkowitz, *Seven-transmembrane receptors*. Nat Rev Mol Cell Biol, 2002. **3**(9): p. 639-50.
156. Lefkowitz, R.J., *A magnificent time with the "magnificent seven" transmembrane spanning receptors*. Circ Res, 2003. **92**(4): p. 342-4.
157. Lefkowitz, R.J., K.L. Pierce, and L.M. Luttrell, *Dancing with different partners: protein kinase a phosphorylation of seven membrane-spanning receptors regulates their G protein-coupling specificity*. Mol Pharmacol, 2002. **62**(5): p. 971-4.
158. Shenoy, S.K. and R.J. Lefkowitz, *Seven-transmembrane receptor signaling through beta-arrestin*. Sci STKE, 2005. **2005**(308): p. cm10.
159. Ahn, S., et al., *Desensitization, internalization, and signaling functions of beta-arrestins demonstrated by RNA interference*. Proc Natl Acad Sci U S A, 2003. **100**(4): p. 1740-4.
160. Reiter, E. and R.J. Lefkowitz, *GRKs and beta-arrestins: roles in receptor silencing, trafficking and signaling*. Trends Endocrinol Metab, 2006. **17**(4): p. 159-65.
161. Premont, R.T., et al., *Identification, purification, and characterization of GRK5, a member of the family of G protein-coupled receptor kinases*. J Biol Chem, 1994. **269**(9): p. 6832-41.
162. Yang, W. and S.H. Xia, *Mechanisms of regulation and function of G-protein-coupled receptor kinases*. World J Gastroenterol, 2006. **12**(48): p. 7753-7.
163. Sobierajska, K., H. Fabczak, and S. Fabczak, *[Mechanisms of regulation and function of G-protein coupled receptor kinases]*. Postepy Biochem, 2005. **51**(4): p. 421-9.
164. Pitcher, J.A., N.J. Freedman, and R.J. Lefkowitz, *G protein-coupled receptor kinases*. Annu Rev Biochem, 1998. **67**: p. 653-92.
165. Palczewski, K. and J.L. Benovic, *G-protein-coupled receptor kinases*. Trends Biochem Sci, 1991. **16**(10): p. 387-91.
166. Zidar, D.A., et al., *Selective engagement of G protein coupled receptor kinases (GRKs) encodes distinct functions of biased ligands*. Proc Natl Acad Sci U S A, 2009. **106**(24): p. 9649-54.
167. Violin, J.D. and R.J. Lefkowitz, *Beta-arrestin-biased ligands at seven-transmembrane receptors*. Trends Pharmacol Sci, 2007. **28**(8): p. 416-22.
168. Lefkowitz, R.J., *G protein-coupled receptor kinases*. Cell, 1993. **74**(3): p. 409-12.
169. Krupnick, J.G., et al., *Arrestin/clathrin interaction. Localization of the clathrin binding domain of nonvisual arrestins to the carboxy terminus*. J Biol Chem, 1997. **272**(23): p. 15011-6.

170. Laporte, S.A., et al., *The interaction of beta-arrestin with the AP-2 adaptor is required for the clustering of beta 2-adrenergic receptor into clathrin-coated pits.* J Biol Chem, 2000. **275**(30): p. 23120-6.
171. Lin, F.T., et al., *Feedback regulation of beta-arrestin1 function by extracellular signal-regulated kinases.* J Biol Chem, 1999. **274**(23): p. 15971-4.
172. Shenoy, S.K., et al., *Regulation of receptor fate by ubiquitination of activated beta 2-adrenergic receptor and beta-arrestin.* Science, 2001. **294**(5545): p. 1307-13.
173. Shenoy, S.K., et al., *Beta-arrestin-dependent signaling and trafficking of 7-transmembrane receptors is reciprocally regulated by the deubiquitinase USP33 and the E3 ligase Mdm2.* Proc Natl Acad Sci U S A, 2009. **106**(16): p. 6650-5.
174. Sibley, D.R., et al., *Phosphorylation/dephosphorylation of the beta-adrenergic receptor regulates its functional coupling to adenylate cyclase and subcellular distribution.* Proc Natl Acad Sci U S A, 1986. **83**(24): p. 9408-12.
175. Ferguson, S.S., *Evolving concepts in G protein-coupled receptor endocytosis: the role in receptor desensitization and signaling.* Pharmacol Rev, 2001. **53**(1): p. 1-24.
176. DeWire, S.M., et al., *Beta-arrestins and cell signaling.* Annu Rev Physiol, 2007. **69**: p. 483-510.
177. Ali, N. and D.K. Agrawal, *Guanine nucleotide binding regulatory proteins: their characteristics and identification.* J Pharmacol Toxicol Methods, 1994. **32**(4): p. 187-96.
178. Macara, I.G., et al., *The Ras superfamily of GTPases.* Faseb J, 1996. **10**(5): p. 625-30.
179. Feig, L.A., *Guanine-nucleotide exchange factors: a family of positive regulators of Ras and related GTPases.* Curr Opin Cell Biol, 1994. **6**(2): p. 204-11.
180. Schmidt, A. and A. Hall, *Guanine nucleotide exchange factors for Rho GTPases: turning on the switch.* Genes Dev, 2002. **16**(13): p. 1587-609.
181. Olson, M.F., *Guanine nucleotide exchange factors for the Rho GTPases: a role in human disease?* J Mol Med, 1996. **74**(10): p. 563-71.
182. Overbeck, A.F., et al., *Guanine nucleotide exchange factors: activators of Ras superfamily proteins.* Mol Reprod Dev, 1995. **42**(4): p. 468-76.
183. Quilliam, L.A., et al., *Guanine nucleotide exchange factors: activators of the Ras superfamily of proteins.* Bioessays, 1995. **17**(5): p. 395-404.
184. Scheffzek, K. and M.R. Ahmadian, *GTPase activating proteins: structural and functional insights 18 years after discovery.* Cell Mol Life Sci, 2005. **62**(24): p. 3014-38.
185. Gamblin, S.J. and S.J. Smerdon, *GTPase-activating proteins and their complexes.* Curr Opin Struct Biol, 1998. **8**(2): p. 195-201.
186. Ross, E.M., *G protein GTPase-activating proteins: regulation of speed, amplitude, and signaling selectivity.* Recent Prog Horm Res, 1995. **50**: p. 207-21.
187. Bollag, G. and F. McCormick, *GTPase activating proteins.* Semin Cancer Biol, 1992. **3**(4): p. 199-208.
188. Donovan, S., K.M. Shannon, and G. Bollag, *GTPase activating proteins: critical regulators of intracellular signaling.* Biochim Biophys Acta, 2002. **1602**(1): p. 23-45.

189. Turner, S.J., et al., *Effects of lovastatin on Rho isoform expression, activity, and association with guanine nucleotide dissociation inhibitors*. *Biochem Pharmacol*, 2008. **75**(2): p. 405-13.
190. Marrari, Y., et al., *Assembly and trafficking of heterotrimeric G proteins*. *Biochemistry*, 2007. **46**(26): p. 7665-77.
191. Johnston, C.A. and D.P. Siderovski, *Receptor-mediated activation of heterotrimeric G-proteins: current structural insights*. *Mol Pharmacol*, 2007. **72**(2): p. 219-30.
192. Oldham, W.M. and H.E. Hamm, *Structural basis of function in heterotrimeric G proteins*. *Q Rev Biophys*, 2006. **39**(2): p. 117-66.
193. Hampoelz, B. and J.A. Knoblich, *Heterotrimeric G proteins: new tricks for an old dog*. *Cell*, 2004. **119**(4): p. 453-6.
194. Hildebrandt, J.D., *Role of subunit diversity in signaling by heterotrimeric G proteins*. *Biochem Pharmacol*, 1997. **54**(3): p. 325-39.
195. Hunt, T.W., R.C. Carroll, and E.G. Peralta, *Heterotrimeric G proteins containing G alpha i3 regulate multiple effector enzymes in the same cell. Activation of phospholipases C and A2 and inhibition of adenylyl cyclase*. *J Biol Chem*, 1994. **269**(47): p. 29565-70.
196. Rebois, R.V., et al., *Heterotrimeric G proteins form stable complexes with adenylyl cyclase and Kir3.1 channels in living cells*. *J Cell Sci*, 2006. **119**(Pt 13): p. 2807-18.
197. Wittpoth, C., et al., *Regions on adenylyl cyclase that are necessary for inhibition of activity by beta gamma and G(alpha) subunits of heterotrimeric G proteins*. *Proc Natl Acad Sci U S A*, 1999. **96**(17): p. 9551-6.
198. Wing, M.R., et al., *Activation of phospholipase C-epsilon by heterotrimeric G protein betagamma-subunits*. *J Biol Chem*, 2001. **276**(51): p. 48257-61.
199. Jiang, H., D. Wu, and M.I. Simon, *Activation of phospholipase C beta 4 by heterotrimeric GTP-binding proteins*. *J Biol Chem*, 1994. **269**(10): p. 7593-6.
200. Katz, A., D. Wu, and M.I. Simon, *Subunits beta gamma of heterotrimeric G protein activate beta 2 isoform of phospholipase C*. *Nature*, 1992. **360**(6405): p. 686-9.
201. Domenighini, M., et al., *Computer modelling of the NAD binding site of ADP-ribosylating toxins: active-site structure and mechanism of NAD binding*. *Mol Microbiol*, 1991. **5**(1): p. 23-31.
202. Merritt, E.A. and W.G. Hol, *AB5 toxins*. *Curr Opin Struct Biol*, 1995. **5**(2): p. 165-71.
203. el Baya, A., et al., *Pertussis toxin. Entry into cells and enzymatic activity*. *Adv Exp Med Biol*, 1997. **419**: p. 83-6.
204. Chinnapen, D.J., et al., *Rafting with cholera toxin: endocytosis and trafficking from plasma membrane to ER*. *FEMS Microbiol Lett*, 2007. **266**(2): p. 129-37.
205. Sunahara, R.K. and R. Taussig, *Isoforms of mammalian adenylyl cyclase: multiplicities of signaling*. *Mol Interv*, 2002. **2**(3): p. 168-84.
206. Hanoune, J. and N. Defer, *Regulation and role of adenylyl cyclase isoforms*. *Annu Rev Pharmacol Toxicol*, 2001. **41**: p. 145-74.
207. Nowak, J.Z. and J.B. Zawilska, *[Adenylyl cyclase--isoforms, regulation and function]*. *Postepy Hig Med Dosw*, 1999. **53**(2): p. 147-72.

208. Dessauer, C.W. and A.G. Gilman, *The catalytic mechanism of mammalian adenylyl cyclase. Equilibrium binding and kinetic analysis of P-site inhibition.* J Biol Chem, 1997. **272**(44): p. 27787-95.
209. Dessauer, C.W., et al., *The interactions of adenylate cyclases with P-site inhibitors.* Trends Pharmacol Sci, 1999. **20**(5): p. 205-10.
210. Xia, Z., et al., *The type III calcium/calmodulin-sensitive adenylyl cyclase is not specific to olfactory sensory neurons.* Neurosci Lett, 1992. **144**(1-2): p. 169-73.
211. Buck, J., et al., *Cytosolic adenylyl cyclase defines a unique signaling molecule in mammals.* Proc Natl Acad Sci U S A, 1999. **96**(1): p. 79-84.
212. Chiono, M., et al., *Capacitative Ca²⁺ entry exclusively inhibits cAMP synthesis in C6-2B glioma cells. Evidence that physiologically evoked Ca²⁺ entry regulates Ca(2+)-inhibitable adenylyl cyclase in non-excitabile cells.* J Biol Chem, 1995. **270**(3): p. 1149-55.
213. Braun, T., *Purification of soluble form of adenylyl cyclase from testes.* Methods Enzymol, 1991. **195**: p. 130-6.
214. Johnson, R.A. and I. Shoshani, *Preparation and use of "P"-site-targeted affinity ligands for adenylyl cyclases.* Methods Enzymol, 1994. **238**: p. 56-71.
215. Hashimoto, T., et al., *Desmoyokin, a 680 kDa keratinocyte plasma membrane-associated protein, is homologous to the protein encoded by human gene AHNAK.* J Cell Sci, 1993. **105** (Pt 2): p. 275-86.
216. Shtivelman, E., F.E. Cohen, and J.M. Bishop, *A human gene (AHNAK) encoding an unusually large protein with a 1.2-microns polyionic rod structure.* Proc Natl Acad Sci U S A, 1992. **89**(12): p. 5472-6.
217. Komuro, A., et al., *The AHNAKs are a class of giant propeller-like proteins that associate with calcium channel proteins of cardiomyocytes and other cells.* Proc Natl Acad Sci U S A, 2004. **101**(12): p. 4053-8.
218. Kudoh, J., et al., *Localization of the human AHNAK/desmoyokin gene (AHNAK) to chromosome band 11q12 by somatic cell hybrid analysis and fluorescence in situ hybridization.* Cytogenet Cell Genet, 1995. **70**(3-4): p. 218-20.
219. Gentil, B.J., et al., *Expression of the giant protein AHNAK (desmoyokin) in muscle and lining epithelial cells.* J Histochem Cytochem, 2003. **51**(3): p. 339-48.
220. Kingsley, P.D., et al., *Subtractive hybridization reveals tissue-specific expression of ahnak during embryonic development.* Dev Growth Differ, 2001. **43**(2): p. 133-43.
221. Salim, C., et al., *The giant protein AHNAK involved in morphogenesis and laminin substrate adhesion of myelinating Schwann cells.* Glia, 2009. **57**(5): p. 535-49.
222. Matza, D., et al., *Requirement for AHNAK1-mediated calcium signaling during T lymphocyte cytolysis.* Proc Natl Acad Sci U S A, 2009. **106**(24): p. 9785-90.
223. Nie, Z., et al., *C-Terminus of desmoyokin/AHNAK protein is responsible for its translocation between the nucleus and cytoplasm.* J Invest Dermatol, 2000. **114**(5): p. 1044-9.
224. Hashimoto, T., et al., *Regulation of translocation of the desmoyokin/AHNAK protein to the plasma membrane in keratinocytes by protein kinase C.* Exp Cell Res, 1995. **217**(2): p. 258-66.

225. Sussman, J., et al., *Protein kinase B phosphorylates AHNAK and regulates its subcellular localization*. J Cell Biol, 2001. **154**(5): p. 1019-30.
226. Benaud, C., et al., *AHNAK interaction with the annexin 2/S100A10 complex regulates cell membrane cytoarchitecture*. J Cell Biol, 2004. **164**(1): p. 133-44.
227. Zuber, J., et al., *A genome-wide survey of RAS transformation targets*. Nat Genet, 2000. **24**(2): p. 144-52.
228. Hieda, Y., S. Tsukita, and S. Tsukita, *A new high molecular mass protein showing unique localization in desmosomal plaque*. J Cell Biol, 1989. **109**(4 Pt 1): p. 1511-8.
229. Gentil, B.J., et al., *The giant protein AHNAK is a specific target for the calcium- and zinc-binding S100B protein: potential implications for Ca²⁺ homeostasis regulation by S100B*. J Biol Chem, 2001. **276**(26): p. 23253-61.
230. Borgonovo, B., et al., *Regulated exocytosis: a novel, widely expressed system*. Nat Cell Biol, 2002. **4**(12): p. 955-62.
231. Huang, Y., et al., *AHNAK, a novel component of the dysferlin protein complex, redistributes to the cytoplasm with dysferlin during skeletal muscle regeneration*. Faseb J, 2007. **21**(3): p. 732-42.
232. Gentil, B.J., et al., *Specific AHNAK expression in brain endothelial cells with barrier properties*. J Cell Physiol, 2005. **203**(2): p. 362-71.
233. Haase, H., et al., *Signaling from beta-adrenoceptor to L-type calcium channel: identification of a novel cardiac protein kinase A target possessing similarities to AHNAK*. Faseb J, 1999. **13**(15): p. 2161-72.
234. Hohaus, A., et al., *The carboxyl-terminal region of ahnak provides a link between cardiac L-type Ca²⁺ channels and the actin-based cytoskeleton*. Faseb J, 2002. **16**(10): p. 1205-16.
235. Stiff, T., et al., *AHNAK interacts with the DNA ligase IV-XRCC4 complex and stimulates DNA ligase IV-mediated double-stranded ligation*. DNA Repair (Amst), 2004. **3**(3): p. 245-56.
236. Matza, D., et al., *A scaffold protein, AHNAK1, is required for calcium signaling during T cell activation*. Immunity, 2008. **28**(1): p. 64-74.
237. Sekiya, F., et al., *AHNAK, a protein that binds and activates phospholipase C-gamma1 in the presence of arachidonic acid*. J Biol Chem, 1999. **274**(20): p. 13900-7.
238. Rhee, S.G., *Regulation of phosphoinositide-specific phospholipase C*. Annu Rev Biochem, 2001. **70**: p. 281-312.
239. Lee, I.H., et al., *AHNAK-mediated activation of phospholipase C-gamma1 through protein kinase C*. J Biol Chem, 2004. **279**(25): p. 26645-53.
240. Skoldberg, F., et al., *Identification of AHNAK as a novel autoantigen in systemic lupus erythematosus*. Biochem Biophys Res Commun, 2002. **291**(4): p. 951-8.
241. Haase, H., et al., *The carboxyl-terminal ahnak domain induces actin bundling and stabilizes muscle contraction*. Faseb J, 2004. **18**(7): p. 839-41.
242. Brash, A.R., *Arachidonic acid as a bioactive molecule*. J Clin Invest, 2001. **107**(11): p. 1339-45.
243. Bogatcheva, N.V., et al., *Arachidonic acid cascade in endothelial pathobiology*. Microvasc Res, 2005. **69**(3): p. 107-27.

244. Brash, A.R., et al., *Molecular cloning of a second human 15S-lipoxygenase and its murine homologue, an 8S-lipoxygenase. Their relationship to other mammalian lipoxygenases.* Adv Exp Med Biol, 1999. **447**: p. 29-36.
245. Spector, A.A., *Structure and lipid binding properties of serum albumin.* Methods Enzymol, 1986. **128**: p. 320-39.
246. Abumrad, N., C. Coburn, and A. Ibrahimi, *Membrane proteins implicated in long-chain fatty acid uptake by mammalian cells: CD36, FATP and FABPm.* Biochim Biophys Acta, 1999. **1441**(1): p. 4-13.
247. Pohl, J., et al., *Role of FATP in parenchymal cell fatty acid uptake.* Biochim Biophys Acta, 2004. **1686**(1-2): p. 1-6.
248. Stahl, A., *A current review of fatty acid transport proteins (SLC27).* Pflugers Arch, 2004. **447**(5): p. 722-7.
249. Dutta-Roy, A.K., *Cellular uptake of long-chain fatty acids: role of membrane-associated fatty-acid-binding/transport proteins.* Cell Mol Life Sci, 2000. **57**(10): p. 1360-72.
250. Glatz, J.F., et al., *Role of membrane-associated and cytoplasmic fatty acid-binding proteins in cellular fatty acid metabolism.* Prostaglandins Leukot Essent Fatty Acids, 1997. **57**(4-5): p. 373-8.
251. Van Nieuwenhoven, F.A., G.J. Van der Vusse, and J.F. Glatz, *Membrane-associated and cytoplasmic fatty acid-binding proteins.* Lipids, 1996. **31 Suppl**: p. S223-7.
252. Levick, S.P., et al., *Arachidonic acid metabolism as a potential mediator of cardiac fibrosis associated with inflammation.* J Immunol, 2007. **178**(2): p. 641-6.
253. Capdevila, J.H., J.R. Falck, and J.D. Imig, *Roles of the cytochrome P450 arachidonic acid monooxygenases in the control of systemic blood pressure and experimental hypertension.* Kidney Int, 2007. **72**(6): p. 683-9.
254. Marnett, L.J., et al., *Arachidonic acid oxygenation by COX-1 and COX-2. Mechanisms of catalysis and inhibition.* J Biol Chem, 1999. **274**(33): p. 22903-6.
255. Chandrasekharan, N.V., et al., *COX-3, a cyclooxygenase-1 variant inhibited by acetaminophen and other analgesic/antipyretic drugs: cloning, structure, and expression.* Proc Natl Acad Sci U S A, 2002. **99**(21): p. 13926-31.
256. Feng, L., et al., *Cloning two isoforms of rat cyclooxygenase: differential regulation of their expression.* Arch Biochem Biophys, 1993. **307**(2): p. 361-8.
257. Johnson, J.L., et al., *Purification and characterization of prostaglandin H synthase-2 from sheep placental cotyledons.* Arch Biochem Biophys, 1995. **324**(1): p. 26-34.
258. Kennedy, B.P., et al., *Cloning and expression of rat prostaglandin endoperoxide synthase (cyclooxygenase)-2 cDNA.* Biochem Biophys Res Commun, 1993. **197**(2): p. 494-500.
259. Masferrer, J.L., et al., *Selective inhibition of inducible cyclooxygenase 2 in vivo is antiinflammatory and nonulcerogenic.* Proc Natl Acad Sci U S A, 1994. **91**(8): p. 3228-32.
260. O'Neill, G.P. and A.W. Ford-Hutchinson, *Expression of mRNA for cyclooxygenase-1 and cyclooxygenase-2 in human tissues.* FEBS Lett, 1993. **330**(2): p. 156-60.

261. Ding, X.Z., R. Hennig, and T.E. Adrian, *Lipoxygenase and cyclooxygenase metabolism: new insights in treatment and chemoprevention of pancreatic cancer*. Mol Cancer, 2003. **2**: p. 10.
262. Yamamoto, S., H. Suzuki, and N. Ueda, *Arachidonate 12-lipoxygenases*. Prog Lipid Res, 1997. **36**(1): p. 23-41.
263. Kuhn, H. and S. Borngraber, *Mammalian 15-lipoxygenases. Enzymatic properties and biological implications*. Adv Exp Med Biol, 1999. **447**: p. 5-28.
264. Oltman, C.L., et al., *Epoxyeicosatrienoic acids and dihydroxyeicosatrienoic acids are potent vasodilators in the canine coronary microcirculation*. Circ Res, 1998. **83**(9): p. 932-9.
265. Weintraub, N.L., et al., *Potentiation of endothelium-dependent relaxation by epoxyeicosatrienoic acids*. Circ Res, 1997. **81**(2): p. 258-67.
266. Burke, J.E. and E.A. Dennis, *Phospholipase A2 structure/function, mechanism, and signaling*. J Lipid Res, 2009. **50 Suppl**: p. S237-42.
267. Burke, J.R., et al., *BMS-229724 is a tight-binding inhibitor of cytosolic phospholipase A2 that acts at the lipid/water interface and possesses anti-inflammatory activity in skin inflammation models*. J Pharmacol Exp Ther, 2001. **298**(1): p. 376-85.
268. Boyanovsky, B.B. and N.R. Webb, *Biology of secretory phospholipase A2*. Cardiovasc Drugs Ther, 2009. **23**(1): p. 61-72.
269. Xing, M. and P.A. Insel, *Protein kinase C-dependent activation of cytosolic phospholipase A2 and mitogen-activated protein kinase by alpha 1-adrenergic receptors in Madin-Darby canine kidney cells*. J Clin Invest, 1996. **97**(5): p. 1302-10.
270. Hooks, S.B. and B.S. Cummings, *Role of Ca²⁺-independent phospholipase A2 in cell growth and signaling*. Biochem Pharmacol, 2008. **76**(9): p. 1059-67.
271. Street, I.P., et al., *Slow- and tight-binding inhibitors of the 85-kDa human phospholipase A2*. Biochemistry, 1993. **32**(23): p. 5935-40.
272. Piomelli, D., *Arachidonic acid in cell signaling*. Curr Opin Cell Biol, 1993. **5**(2): p. 274-80.
273. Hjelte, L.E. and A. Nilsson, *Arachidonic acid and ischemic heart disease*. J Nutr, 2005. **135**(9): p. 2271-3.
274. Rebecchi, M.J. and O.M. Rosen, *Stimulation of polyphosphoinositide hydrolysis by thrombin in membranes from human fibroblasts*. Biochem J, 1987. **245**(1): p. 49-57.
275. Berridge, M.J., P. Lipp, and M.D. Bootman, *The versatility and universality of calcium signalling*. Nat Rev Mol Cell Biol, 2000. **1**(1): p. 11-21.
276. El Boustany, C., et al., *Capacitative calcium entry and transient receptor potential canonical 6 expression control human hepatoma cell proliferation*. Hepatology, 2008. **47**(6): p. 2068-77.
277. Lipskaia, L., J.S. Hulot, and A.M. Lompre, *Role of sarco/endoplasmic reticulum calcium content and calcium ATPase activity in the control of cell growth and proliferation*. Pflugers Arch, 2009. **457**(3): p. 673-85.
278. Schwarz, E.C., et al., *Calcium dependence of T cell proliferation following focal stimulation*. Eur J Immunol, 2007. **37**(10): p. 2723-33.

279. McCord, A.M., J. Cuevas, and B.E. Anderson, *Bartonella-induced endothelial cell proliferation is mediated by release of calcium from intracellular stores*. DNA Cell Biol, 2007. **26**(9): p. 657-63.
280. Wilkerson, M.K., et al., *Inositol trisphosphate receptor calcium release is required for cerebral artery smooth muscle cell proliferation*. Am J Physiol Heart Circ Physiol, 2006. **290**(1): p. H240-7.
281. Munaron, L., S. Antoniotti, and D. Lovisolo, *Intracellular calcium signals and control of cell proliferation: how many mechanisms?* J Cell Mol Med, 2004. **8**(2): p. 161-8.
282. Antoniotti, S., et al., *Control of endothelial cell proliferation by calcium influx and arachidonic acid metabolism: a pharmacological approach*. J Cell Physiol, 2003. **197**(3): p. 370-8.
283. Fiorio Pla, A. and L. Munaron, *Calcium influx, arachidonic acid, and control of endothelial cell proliferation*. Cell Calcium, 2001. **30**(4): p. 235-44.
284. Huang, R., et al., *B cell differentiation factor-induced human B cell maturation: stimulation of intracellular calcium release*. Cell Immunol, 1995. **164**(2): p. 227-33.
285. Morley, P. and J.F. Whitfield, *The differentiation inducer, dimethyl sulfoxide, transiently increases the intracellular calcium ion concentration in various cell types*. J Cell Physiol, 1993. **156**(2): p. 219-25.
286. Black, B.L. and J.E. Smith, *Regulation of goblet cell differentiation by calcium in embryonic chick intestine*. Faseb J, 1989. **3**(14): p. 2653-9.
287. Pillai, S., et al., *Uncoupling of the calcium-sensing mechanism and differentiation in squamous carcinoma cell lines*. Exp Cell Res, 1991. **192**(2): p. 567-73.
288. Rong, Y. and C.W. Distelhorst, *Bcl-2 protein family members: versatile regulators of calcium signaling in cell survival and apoptosis*. Annu Rev Physiol, 2008. **70**: p. 73-91.
289. Schroter, A., et al., *Nitric oxide applications prior and simultaneous to potentially excitotoxic NMDA-evoked calcium transients: cell death or survival*. Brain Res, 2005. **1060**(1-2): p. 1-15.
290. Zhou, G. and G. Zhang, *[Indomethacin induces apoptosis of K562 cells through activation of caspases and elevation of intracellular free calcium]*. Zhonghua Xue Ye Xue Za Zhi, 2001. **22**(5): p. 241-4.
291. Zhang, Q.H., H.P. Sheng, and T.T. Loh, *bcl-2 protects HL-60 cells from apoptosis by stabilizing their intracellular calcium pools*. Life Sci, 2001. **68**(25): p. 2873-83.
292. Hofer, A.M., *Another dimension to calcium signaling: a look at extracellular calcium*. J Cell Sci, 2005. **118**(Pt 5): p. 855-62.
293. Brown, E.M., *The extracellular Ca²⁺-sensing receptor: central mediator of systemic calcium homeostasis*. Annu Rev Nutr, 2000. **20**: p. 507-33.
294. Riccardi, D. and G. Gamba, *The many roles of the calcium-sensing receptor in health and disease*. Arch Med Res, 1999. **30**(6): p. 436-48.
295. Riccardi, D., *Calcium ions as extracellular, first messengers*. Z Kardiol, 2000. **89** **Suppl 2**: p. 9-14.
296. Riccardi, D. and D. Maldonado-Perez, *The calcium-sensing receptor as a nutrient sensor*. Biochem Soc Trans, 2005. **33**(Pt 1): p. 316-20.

297. Riccardi, D., et al., *Novel regulatory aspects of the extracellular Ca²⁺-sensing receptor, CaR*. Pflugers Arch, 2009. **458**(6): p. 1007-22.
298. Ward, D.T., *Calcium receptor-mediated intracellular signalling*. Cell Calcium, 2004. **35**(3): p. 217-28.
299. Hermans, E. and R.A. Challiss, *Structural, signalling and regulatory properties of the group I metabotropic glutamate receptors: prototypic family C G-protein-coupled receptors*. Biochem J, 2001. **359**(Pt 3): p. 465-84.
300. Quist, A.P., et al., *Physiological role of gap-junctional hemichannels. Extracellular calcium-dependent isosmotic volume regulation*. J Cell Biol, 2000. **148**(5): p. 1063-74.
301. Babini, E., et al., *Alternative splicing and interaction with di- and polyvalent cations control the dynamic range of acid-sensing ion channel 1 (ASIC1)*. J Biol Chem, 2002. **277**(44): p. 41597-603.
302. Rosen, E.D. and B.M. Spiegelman, *Molecular regulation of adipogenesis*. Annu Rev Cell Dev Biol, 2000. **16**: p. 145-71.
303. Rajala, M.W. and P.E. Scherer, *Minireview: The adipocyte--at the crossroads of energy homeostasis, inflammation, and atherosclerosis*. Endocrinology, 2003. **144**(9): p. 3765-73.
304. Jones, B.H., et al., *Upregulation of adipocyte metabolism by agouti protein: possible paracrine actions in yellow mouse obesity*. Am J Physiol, 1996. **270**(1 Pt 1): p. E192-6.
305. Kopelman, P.G., *Obesity as a medical problem*. Nature, 2000. **404**(6778): p. 635-43.
306. MacDougald, O.A. and S. Mandrup, *Adipogenesis: forces that tip the scales*. Trends Endocrinol Metab, 2002. **13**(1): p. 5-11.
307. Spiegelman, B.M., et al., *PPAR gamma and the control of adipogenesis*. Biochimie, 1997. **79**(2-3): p. 111-2.
308. Michalik, L. and W. Wahli, *Peroxisome proliferator-activated receptors: three isotypes for a multitude of functions*. Curr Opin Biotechnol, 1999. **10**(6): p. 564-70.
309. El-Jack, A.K., et al., *Reconstitution of insulin-sensitive glucose transport in fibroblasts requires expression of both PPARgamma and C/EBPalpha*. J Biol Chem, 1999. **274**(12): p. 7946-51.
310. Cohen, P., *Protein kinases--the major drug targets of the twenty-first century?* Nat Rev Drug Discov, 2002. **1**(4): p. 309-15.
311. Slice, L.W. and S.S. Taylor, *Expression of the catalytic subunit of cAMP-dependent protein kinase in Escherichia coli*. J Biol Chem, 1989. **264**(35): p. 20940-6.
312. Alto, N., et al., *Intracellular targeting of protein kinases and phosphatases*. Diabetes, 2002. **51 Suppl 3**: p. S385-8.
313. Scott, J.D., *Cyclic nucleotide-dependent protein kinases*. Pharmacol Ther, 1991. **50**(1): p. 123-45.
314. Faux, M.C. and J.D. Scott, *Molecular glue: kinase anchoring and scaffold proteins*. Cell, 1996. **85**(1): p. 9-12.

315. Li, Q. and G.D. Zhu, *Targeting serine/threonine protein kinase B/Akt and cell-cycle checkpoint kinases for treating cancer*. *Curr Top Med Chem*, 2002. **2**(9): p. 939-71.
316. van den Heuvel, A.P., et al., *Binding of protein kinase B to the plakin family member periplakin*. *J Cell Sci*, 2002. **115**(Pt 20): p. 3957-66.
317. Uchiyama, T., et al., *Role of Akt signaling in mitochondrial survival pathway triggered by hypoxic preconditioning*. *Circulation*, 2004. **109**(24): p. 3042-9.
318. Hirai, K., et al., *PI3K inhibition in neonatal rat brain slices during and after hypoxia reduces phospho-Akt and increases cytosolic cytochrome c and apoptosis*. *Brain Res Mol Brain Res*, 2004. **124**(1): p. 51-61.
319. Dempsey, E.C., et al., *Protein kinase C isozymes and the regulation of diverse cell responses*. *Am J Physiol Lung Cell Mol Physiol*, 2000. **279**(3): p. L429-38.
320. Gould, C.M. and A.C. Newton, *The life and death of protein kinase C*. *Curr Drug Targets*, 2008. **9**(8): p. 614-25.
321. Newton, A.C., *Regulation of the ABC kinases by phosphorylation: protein kinase C as a paradigm*. *Biochem J*, 2003. **370**(Pt 2): p. 361-71.
322. Ebnet, K., *Organization of multiprotein complexes at cell-cell junctions*. *Histochem Cell Biol*, 2008. **130**(1): p. 1-20.
323. Denker, B.M. and S.K. Nigam, *Molecular structure and assembly of the tight junction*. *Am J Physiol*, 1998. **274**(1 Pt 2): p. F1-9.
324. Mese, G., G. Richard, and T.W. White, *Gap junctions: basic structure and function*. *J Invest Dermatol*, 2007. **127**(11): p. 2516-24.
325. Green, K.J. and J.C. Jones, *Desmosomes and hemidesmosomes: structure and function of molecular components*. *Faseb J*, 1996. **10**(8): p. 871-81.
326. Collins, J.E., et al., *Cloning and sequence analysis of desmosomal glycoproteins 2 and 3 (desmocollins): cadherin-like desmosomal adhesion molecules with heterogeneous cytoplasmic domains*. *J Cell Biol*, 1991. **113**(2): p. 381-91.
327. Schafer, S., P.J. Koch, and W.W. Franke, *Identification of the ubiquitous human desmoglein, Dsg2, and the expression catalogue of the desmoglein subfamily of desmosomal cadherins*. *Exp Cell Res*, 1994. **211**(2): p. 391-9.
328. Koch, P.J., et al., *Complexity and expression patterns of the desmosomal cadherins*. *Proc Natl Acad Sci U S A*, 1992. **89**(1): p. 353-7.
329. Herrmann, H. and U. Aebi, *Intermediate filaments: molecular structure, assembly mechanism, and integration into functionally distinct intracellular Scaffolds*. *Annu Rev Biochem*, 2004. **73**: p. 749-89.
330. Rudini, N. and E. Dejana, *Adherens junctions*. *Curr Biol*, 2008. **18**(23): p. R1080-2.
331. Geiger, B., et al., *The molecular basis for the assembly and modulation of adherens-type junctions*. *Cell Differ Dev*, 1990. **32**(3): p. 343-53.
332. Nagafuchi, A., *Molecular architecture of adherens junctions*. *Curr Opin Cell Biol*, 2001. **13**(5): p. 600-3.
333. Shin, K., V.C. Fogg, and B. Margolis, *Tight junctions and cell polarity*. *Annu Rev Cell Dev Biol*, 2006. **22**: p. 207-35.
334. Haskins, J., et al., *ZO-3, a novel member of the MAGUK protein family found at the tight junction, interacts with ZO-1 and occludin*. *J Cell Biol*, 1998. **141**(1): p. 199-208.

335. Jesaitis, L.A. and D.A. Goodenough, *Molecular characterization and tissue distribution of ZO-2, a tight junction protein homologous to ZO-1 and the Drosophila discs-large tumor suppressor protein*. J Cell Biol, 1994. **124**(6): p. 949-61.
336. Gumbiner, B., T. Lowenkopf, and D. Apatira, *Identification of a 160-kDa polypeptide that binds to the tight junction protein ZO-1*. Proc Natl Acad Sci U S A, 1991. **88**(8): p. 3460-4.
337. Beatch, M., et al., *The tight junction protein ZO-2 contains three PDZ (PSD-95/Discs-Large/ZO-1) domains and an alternatively spliced region*. J Biol Chem, 1996. **271**(42): p. 25723-6.
338. Cordenosi, M., et al., *Cingulin contains globular and coiled-coil domains and interacts with ZO-1, ZO-2, ZO-3, and myosin*. J Cell Biol, 1999. **147**(7): p. 1569-82.
339. Yamamoto, T., et al., *The Ras target AF-6 interacts with ZO-1 and serves as a peripheral component of tight junctions in epithelial cells*. J Cell Biol, 1997. **139**(3): p. 785-95.
340. Mattagajasingh, S.N., et al., *Characterization of the interaction between protein 4.1R and ZO-2. A possible link between the tight junction and the actin cytoskeleton*. J Biol Chem, 2000. **275**(39): p. 30573-85.
341. Kobayashi, I., et al., *RGMI, a cell line derived from normal gastric mucosa of rat*. In vitro Cell Dev Biol Anim, 1996. **32**(5): p. 259-61.
342. Osada, T., et al., *Effect of mechanical strain on gastric cellular migration and proliferation during mucosal healing: role of Rho dependent and Rac dependent cytoskeletal reorganisation*. Gut, 1999. **45**(4): p. 508-15.
343. Green, H. and O. Kehinde, *An established preadipose cell line and its differentiation in culture. II. Factors affecting the adipose conversion*. Cell, 1975. **5**(1): p. 19-27.
344. Green, H. and O. Kehinde, *Spontaneous heritable changes leading to increased adipose conversion in 3T3 cells*. Cell, 1976. **7**(1): p. 105-13.
345. Green, H. and M. Meuth, *An established pre-adipose cell line and its differentiation in culture*. Cell, 1974. **3**(2): p. 127-33.
346. Kohn, A.D., et al., *Expression of a constitutively active Akt Ser/Thr kinase in 3T3-L1 adipocytes stimulates glucose uptake and glucose transporter 4 translocation*. J Biol Chem, 1996. **271**(49): p. 31372-8.
347. Rubin, C.S., et al., *Development of hormone receptors and hormonal responsiveness in vitro. Insulin receptors and insulin sensitivity in the preadipocyte and adipocyte forms of 3T3-L1 cells*. J Biol Chem, 1978. **253**(20): p. 7570-8.
348. Yablonka-Reuveni, Z., B. Christ, and J.M. Benson, *Transitions in cell organization and in expression of contractile and extracellular matrix proteins during development of chicken aortic smooth muscle: evidence for a complex spatial and temporal differentiation program*. Anat Embryol (Berl), 1998. **197**(6): p. 421-37.
349. Fisher, S.A. and M. Ikebe, *Developmental and tissue distribution of expression of nonmuscle and smooth muscle isoforms of myosin light chain kinase*. Biochem Biophys Res Commun, 1995. **217**(2): p. 696-703.

350. Ross, S.A., G.H. Fick, and L. Alima, *Factors influencing the estimation of the albumin excretion rate in subjects with diabetes mellitus*. Clin Invest Med, 1997. **20**(3): p. 152-61.
351. Dyson, M.R., et al., *Production of soluble mammalian proteins in Escherichia coli: identification of protein features that correlate with successful expression*. BMC Biotechnol, 2004. **4**: p. 32.
352. Mercado-Pimentel, M.E., N.C. Jordan, and G.O. Aisemberg, *Affinity purification of GST fusion proteins for immunohistochemical studies of gene expression*. Protein Expr Purif, 2002. **26**(2): p. 260-5.
353. Zhan, Y., X. Song, and G.W. Zhou, *Structural analysis of regulatory protein domains using GST-fusion proteins*. Gene, 2001. **281**(1-2): p. 1-9.
354. Chatton, B., et al., *Eukaryotic GST fusion vector for the study of protein-protein associations in vivo: application to interaction of ATF α with Jun and Fos*. Biotechniques, 1995. **18**(1): p. 142-5.
355. Braun, P., et al., *Proteome-scale purification of human proteins from bacteria*. Proc Natl Acad Sci U S A, 2002. **99**(5): p. 2654-9.
356. Eshaghi, S., et al., *An efficient strategy for high-throughput expression screening of recombinant integral membrane proteins*. Protein Sci, 2005. **14**(3): p. 676-83.
357. Wilkinson, D.L. and R.G. Harrison, *Predicting the solubility of recombinant proteins in Escherichia coli*. Biotechnology (N Y), 1991. **9**(5): p. 443-8.
358. Baneyx, F., *Recombinant protein expression in Escherichia coli*. Curr Opin Biotechnol, 1999. **10**(5): p. 411-21.
359. Hammarstrom, M., et al., *Rapid screening for improved solubility of small human proteins produced as fusion proteins in Escherichia coli*. Protein Sci, 2002. **11**(2): p. 313-21.
360. Shi, P.Y., N. Maizels, and A.M. Weiner, *Recovery of soluble, active recombinant protein from inclusion bodies*. Biotechniques, 1997. **23**(6): p. 1036-8.
361. Youssoufian, H., *Immunoaffinity purification of antibodies against GST fusion proteins*. Biotechniques, 1998. **24**(2): p. 198-200, 202.
362. Carrio, M.M. and A. Villaverde, *Protein aggregation as bacterial inclusion bodies is reversible*. FEBS Lett, 2001. **489**(1): p. 29-33.
363. Garcia-Fruitos, E., A. Aris, and A. Villaverde, *Localization of functional polypeptides in bacterial inclusion bodies*. Appl Environ Microbiol, 2007. **73**(1): p. 289-94.
364. Mukhopadhyay, A., *Inclusion bodies and purification of proteins in biologically active forms*. Adv Biochem Eng Biotechnol, 1997. **56**: p. 61-109.
365. Kiefer, H., K. Maier, and R. Vogel, *Refolding of G-protein-coupled receptors from inclusion bodies produced in Escherichia coli*. Biochem Soc Trans, 1999. **27**(6): p. 908-12.
366. Frangioni, J.V. and B.G. Neel, *Solubilization and purification of enzymatically active glutathione S-transferase (pGEX) fusion proteins*. Anal Biochem, 1993. **210**(1): p. 179-87.
367. Schrodell, A. and A. de Marco, *Characterization of the aggregates formed during recombinant protein expression in bacteria*. BMC Biochem, 2005. **6**: p. 10.
368. Wagner, S., et al., *Consequences of membrane protein overexpression in Escherichia coli*. Mol Cell Proteomics, 2007. **6**(9): p. 1527-50.

369. Fujishige, K., et al., *Localization of clearance receptor in rat lung and trachea: association with chondrogenic differentiation*. *Am J Physiol*, 1998. **274**(3 Pt 1): p. L425-31.
370. Pedro, L., et al., *Characterization of the phosphorylation state of natriuretic peptide receptor-C*. *Mol Cell Biochem*, 1998. **178**(1-2): p. 95-101.
371. Alli, A., and Gower, W.R., Jr., *Characterization of a polyclonal antibody against the cytoplasmic domain of the C-type natriuretic peptide receptor*. *J Clin Ligand Assay*, 2009. **31**: p. 3-7.
372. Cen, B., et al., *Direct and differential interaction of beta-arrestins with the intracellular domains of different opioid receptors*. *Mol Pharmacol*, 2001. **59**(4): p. 758-64.
373. Gudermann, T., B. Nurnberg, and G. Schultz, *Receptors and G proteins as primary components of transmembrane signal transduction. Part 1. G-protein-coupled receptors: structure and function*. *J Mol Med*, 1995. **73**(2): p. 51-63.
374. Haase, H., et al., *Ahnak is critical for cardiac Ca(V)1.2 calcium channel function and its beta-adrenergic regulation*. *Faseb J*, 2005. **19**(14): p. 1969-77.
375. Yanagisawa, M., et al., *A novel potent vasoconstrictor peptide produced by vascular endothelial cells*. *Nature*, 1988. **332**(6163): p. 411-5.
376. Iwamuro, Y., et al., *Activation of three types of voltage-independent Ca²⁺ channel in A7r5 cells by endothelin-1 as revealed by a novel Ca²⁺ channel blocker LOE 908*. *Br J Pharmacol*, 1999. **126**(5): p. 1107-14.
377. Danthuluri, N.R. and T.A. Brock, *Endothelin receptor-coupling mechanisms in vascular smooth muscle: a role for protein kinase C*. *J Pharmacol Exp Ther*, 1990. **254**(2): p. 393-9.
378. Ntambi, J.M. and T. Takova, *Role of Ca²⁺ in the early stages of murine adipocyte differentiation as evidenced by calcium mobilizing agents*. *Differentiation*, 1996. **60**(3): p. 151-8.
379. Jensen, B., et al., *High extracellular calcium attenuates adipogenesis in 3T3-L1 preadipocytes*. *Exp Cell Res*, 2004. **301**(2): p. 280-92.
380. Wu, Z., et al., *Cross-regulation of C/EBP alpha and PPAR gamma controls the transcriptional pathway of adipogenesis and insulin sensitivity*. *Mol Cell*, 1999. **3**(2): p. 151-8.
381. Gregoire, F.M., *Adipocyte differentiation: from fibroblast to endocrine cell*. *Exp Biol Med (Maywood)*, 2001. **226**(11): p. 997-1002.
382. Huang, S., V.M. Maher, and J.J. McCormick, *Extracellular Ca²⁺ stimulates the activation of mitogen-activated protein kinase and cell growth in human fibroblasts*. *Biochem J*, 1995. **310** (Pt 3): p. 881-5.
383. Molostvov, G., et al., *Extracellular calcium-sensing receptor mediated signalling is involved in human vascular smooth muscle cell proliferation and apoptosis*. *Cell Physiol Biochem*, 2008. **22**(5-6): p. 413-22.
384. Kwak, J.O., et al., *The extracellular calcium sensing receptor is expressed in mouse mesangial cells and modulates cell proliferation*. *Exp Mol Med*, 2005. **37**(5): p. 457-65.
385. Yamaguchi, T., et al., *Mouse osteoblastic cell line (MC3T3-E1) expresses extracellular calcium (Ca²⁺o)-sensing receptor and its agonists stimulate*

- chemotaxis and proliferation of MC3T3-E1 cells.* J Bone Miner Res, 1998. **13**(10): p. 1530-8.
386. Shi, H., et al., *Role of intracellular calcium in human adipocyte differentiation.* Physiol Genomics, 2000. **3**(2): p. 75-82.
387. Xue, B., et al., *The agouti gene product inhibits lipolysis in human adipocytes via a Ca²⁺-dependent mechanism.* Faseb J, 1998. **12**(13): p. 1391-6.
388. Sanders, K.M., *Invited review: mechanisms of calcium handling in smooth muscles.* J Appl Physiol, 2001. **91**(3): p. 1438-49.
389. Walsh, M.P., *Regulation of vascular smooth muscle tone.* Can J Physiol Pharmacol, 1994. **72**(8): p. 919-36.
390. Somlyo, A.P. and A.V. Somlyo, *Signal transduction by G-proteins, rho-kinase and protein phosphatase to smooth muscle and non-muscle myosin II.* J Physiol, 2000. **522 Pt 2**: p. 177-85.
391. Somlyo, A.P. and A.V. Somlyo, *Signal transduction and regulation in smooth muscle.* Nature, 1994. **372**(6503): p. 231-6.
392. Bohr, D.F., A.F. Dominiczak, and R.C. Webb, *Pathophysiology of the vasculature in hypertension.* Hypertension, 1991. **18**(5 Suppl): p. III69-75.
393. Mohri, M., et al., *Angina pectoris caused by coronary microvascular spasm.* Lancet, 1998. **351**(9110): p. 1165-9.
394. Mulvany, M.J. and C. Aalkjaer, *Structure and function of small arteries.* Physiol Rev, 1990. **70**(4): p. 921-61.
395. Mendelsohn, M.E., *In hypertension, the kidney is not always the heart of the matter.* J Clin Invest, 2005. **115**(4): p. 840-4.
396. Takahashi, A., et al., *Measurement of intracellular calcium.* Physiol Rev, 1999. **79**(4): p. 1089-125.
397. Parker, I. and Y. Yao, *Regenerative release of calcium from functionally discrete subcellular stores by inositol trisphosphate.* Proc Biol Sci, 1991. **246**(1317): p. 269-74.
398. Bootman, M., et al., *Imaging the hierarchical Ca²⁺ signalling system in HeLa cells.* J Physiol, 1997. **499 (Pt 2)**: p. 307-14.
399. Nelson, M.T., et al., *Relaxation of arterial smooth muscle by calcium sparks.* Science, 1995. **270**(5236): p. 633-7.
400. Klein, M.G., et al., *Two mechanisms of quantized calcium release in skeletal muscle.* Nature, 1996. **379**(6564): p. 455-8.
401. Harkins, A.B., N. Kurebayashi, and S.M. Baylor, *Resting myoplasmic free calcium in frog skeletal muscle fibers estimated with fluo-3.* Biophys J, 1993. **65**(2): p. 865-81.
402. Zou, H., et al., *Using total fluorescence increase (signal mass) to determine the Ca²⁺ current underlying localized Ca²⁺ events.* J Gen Physiol, 2004. **124**(3): p. 259-72.
403. Chung, C.T., S.L. Niemela, and R.H. Miller, *One-step preparation of competent Escherichia coli: transformation and storage of bacterial cells in the same solution.* Proc Natl Acad Sci U S A, 1989. **86**(7): p. 2172-5.
404. Neuberger, G., G. Schneider, and F. Eisenhaber, *pkaPS: prediction of protein kinase A phosphorylation sites with the simplified kinase-substrate binding model.* Biol Direct, 2007. **2**: p. 1.

405. Chrambach, A. and D. Rodbard, *Polyacrylamide gel electrophoresis*. Science, 1971. **172**(982): p. 440-51.
406. Hedrick, J.L. and A.J. Smith, *Size and charge isomer separation and estimation of molecular weights of proteins by disc gel electrophoresis*. Arch Biochem Biophys, 1968. **126**(1): p. 155-64.
407. Lemmon, M.A. and J. Schlessinger, *Regulation of signal transduction and signal diversity by receptor oligomerization*. Trends Biochem Sci, 1994. **19**(11): p. 459-63.
408. Heldin, C.H., *Dimerization of cell surface receptors in signal transduction*. Cell, 1995. **80**(2): p. 213-23.
409. Fenrick, R., N. McNicoll, and A. De Lean, *Glycosylation is critical for natriuretic peptide receptor-B function*. Mol Cell Biochem, 1996. **165**(2): p. 103-9.
410. Lowe, D.G. and B.M. Fendly, *Human natriuretic peptide receptor-A guanylyl cyclase. Hormone cross-linking and antibody reactivity distinguish receptor glycoforms*. J Biol Chem, 1992. **267**(30): p. 21691-7.
411. Heim, J.M., S. Singh, and R. Gerzer, *Effect of glycosylation on cloned ANF-sensitive guanylyl cyclase*. Life Sci, 1996. **59**(4): p. PL61-8.
412. McGuffin, L.J., K. Bryson, and D.T. Jones, *The PSIPRED protein structure prediction server*. Bioinformatics, 2000. **16**(4): p. 404-5.
413. Jones, D.T., *Protein secondary structure prediction based on position-specific scoring matrices*. J Mol Biol, 1999. **292**(2): p. 195-202.
414. Cuff, J.A. and G.J. Barton, *Application of multiple sequence alignment profiles to improve protein secondary structure prediction*. Proteins, 2000. **40**(3): p. 502-11.
415. Rost, B., C. Sander, and R. Schneider, *PHD--an automatic mail server for protein secondary structure prediction*. Comput Appl Biosci, 1994. **10**(1): p. 53-60.
416. Montgomerie, S., et al., *PROTEUS2: a web server for comprehensive protein structure prediction and structure-based annotation*. Nucleic Acids Res, 2008. **36**(Web Server issue): p. W202-9.
417. Montgomerie, S., et al., *Improving the accuracy of protein secondary structure prediction using structural alignment*. BMC Bioinformatics, 2006. **7**: p. 301.
418. Kennelly, P.J. and E.G. Krebs, *Consensus sequences as substrate specificity determinants for protein kinases and protein phosphatases*. J Biol Chem, 1991. **266**(24): p. 15555-8.
419. Zhou, H., and Murthy, K. S, *PKG-induced desensitization of the single-transmembrane NPR-C receptor is mediated by phosphorylation of a single threonine residue in the intracellular domain (Abstract)*. Gastroenterology, 2002. **122**.
420. Traweger, A., et al., *The tight junction protein ZO-2 localizes to the nucleus and interacts with the heterogeneous nuclear ribonucleoprotein scaffold attachment factor-B*. J Biol Chem, 2003. **278**(4): p. 2692-700.
421. Shtivelman, E. and J.M. Bishop, *The human gene AHNAK encodes a large phosphoprotein located primarily in the nucleus*. J Cell Biol, 1993. **120**(3): p. 625-30.
422. Blikslager, A.T., et al., *Restoration of barrier function in injured intestinal mucosa*. Physiol Rev, 2007. **87**(2): p. 545-64.

Appendices

Appendix A: EMBOSS alignment needle program results of AHANK1 and AHNAK2

1	0	1013	GEGFEFDVNLKSNVDISAPKVDNAPDLSLEGPEGLKGGKFKMPEMHF	1062
1	50	965	----EVDVQAKKAKLDGAWLEGDSLADKDVIAKDSKFKMFKMPSFGV	1010
1	0	1063	RAPKMSLFDVLDLKGPKMKGNVDISAPKIEGEMQVF-----	1099
51	100	1011	SAP-----GKSIKALVDVSAKVEADLSLPSMQGDLKTTDLSTI	1048
1	46	1100	----DVIDIRGPKVDIKAPD---VEGQGLDWSLKIPMMKMKFSPMLSG	1141
101	150	1049	QPASTDLKQADQVDVWLPEGHLEPAGAGLGH---PKVEMFSPKMPKVAL	1096
47	96	1142	EGPEVDVNLKADVWVSGPKVDIEAPDVSELEGPEGLKGGKFKMPEMHF	1191
151	197	1097	KGPDVWVKGKLD--LKSFKAEVTFADV-----	1122
97	146	1192	TPKISMPDVLHLKGGPKVGDVVDVSPKVEGEMKVPDVEIKGPKMIDAP	1241
198	238	1123	--EVSLSPEVDVEAPGAKLD---SARLEGELSL-----A	1152
147	186	1242	DVEVQSPDHLKMPKMKPKF---SMPGFKGEGREVDVNLKADIVSGPK	1289
239	278	1153	DKDVIAKDSKFKMFKMPSFGASAPG-KSTEASVDVSAKVEADVSLFS	1201
187	226	1290	V--DVEVFDVS-----LEG--PEG-----KLGK	1308
279	328	1202	MQGDLKTTDLSTIQPPSADLEVHAGQVDVWVLEGHVPEGAGFKGHLKPKVM	1251
227	275	1309	PKFMPMPEMHFKAPKISMPDVLNLKGGPKL---GDVDSLEPEVEGEMKVP	1355
329	355	1252	PSLKMFKVLDLKGQVVEVKGPKLGLGKHAETAHEVAVSLSPVVDVQAP	1301
276	320	1356	DVIDIKGPKV--DISAPDVVHGGPDWHLKMPKMKPKF---SMPGFKGEGPE	1401
356	377	1302	GAKLDGAGLDGDSLADKDVIAKDSKFKMFKMPSFGVSAFG-KSIEAS	1350
321	370	1402	VDVLPKADVWVSGPKM--DAEVPDVNIEGPDADKLGKFKMPEMHFKIQ	1449
378	414	1351	VDSLAKVEADMSLPSMQGDLKTTDLSTIQPPSTDL---ELQAGOLDVWKLK	1397
371	417	1450	KISIPDVGHLKGG--PKMKGDDVTVKVEGEIKAPDVIDIKGPKVDINAP	1497
415	457	1398	EGVPE--GAGLKGHLKPKMP--SFKVPKV--DLKSPIDIKGPKLDKLD	1443
418	452	1498	DVEVHGGPDWHLKMPKMKPKFSPMPGFKGEGREVDVNLKADIVSGPKVD	1547
458	507	1444	KVEVTFADVVEVSLPSV-----EVDVEAPGAKLDGGRLEED	1478
453	502	1548	IDVFDVNLKADVEGPKLGGKFKMPSMNIQTHKISMPDVLNLKADIVSGPK	1597
508	533	1479	MSLADKDLTTKDSKFKMFKMPSFGVSAFGKSI-EASVDVSAKVV--EA	1525
503	548	1598	DVSLPKVEGDLKGPEDVWVAKPKMVDVW--GDIIEGEPGK-----LKG-	1638
534	576	1526	DVSLPSMQGDLKATDLSTIQPPSADLEVQAGQVDVWVLEGSPVSEAGLKG	1575
549	592	1639	----PKFMPMPEMHFKAPKISMPDVLHLKGGPKVGMVDSVSPKVEGEM	1682
577	622	1576	LKPKVMPSPKMPKVDLKGQDIDVKGPKLDLKGPKV---EVTAPDVKMSL	1621
593	623	1683	KVPDVIDIKGPKVDIDAP----DVEVHDPDHLKMPKMKMKFSPMGFKAE	1728
623	672	1622	SSMEVDVQAPRAKLDGAGLEDSLADKDVIAKDSKFKMFKMPSFGV	1671
624	673	1729	GP-----EVDVNLKADIVSGVSDVTD-----APLDIEG--	1759
673	714	1672	APGKSIASVDVSEPKVEADVSLPSMQGDLKTTDLSTIQSPSADLEVQAGQ	1721
674	713	1760	----PEGKL-KGSKFK--MPKL---NIKAPKVSMPDVLNLKGGPKLGE	1798
715	756	1722	VNVKLEPGLPEGAGFKGHLKPKVQMPSLKMPKVALKPKQMDVKGPKL---	1768
714	762	1799	IDASVPELEGDLRGPQDVKGPVFAEAVP---DVELECP-----	1834
757	799	1769	-----DLKPKAEVWAPDVEVSLPSVEVDVVEAPGAKLDSVRLEGD	1808
763	812	1835	-----DAKLGPKFKMPEMHFKAPKISMPDVLHLKGGPKVKGDA	1873
800	844	1809	LSLADKDVIAKDSKFKMFKMPSFGVSAFGKSI-EASVDVSAKVV--EA	1855
813	862	1874	DVSVFKLEGLDTPGSPVEVPE-----DVELECPD-----AKLKG-	1907
845	877	1856	EVSLSPSMQGDLKTTDLSTIQPPSADLEVQAGQVDVWVLEGSPVSEAGLKG	1905
863	912	1908	----PKFMPMPEMHFKAPKISMPDVLHLKGGPKV---GDVDSVSP---	1945
878	896	1906	LKPKVMPSPKMPKVDLKGQDIDVWVAKPKMVDVW--GDIIEGEPGK-----	1955
913	962	1946	-----KLEGLDTPGSPVEVPE-----DVELECPD-----AKLKG-	1982
897	936	1956	VDVQAKKAKLDGAWLEGDSLADKDVIAKDSKFKMFKMPSFGV	1998
963	1012			
937	964			

1983	HFKTFKISMPDVLHLKGVKMGDMVSPKVEGEMKVPDVIKGGKMD-	2031	ADLDVSGPKVDIDVDPVNIIEGPEGLKGPFKMPEMNIKAKPISMPDIDL	3098
1999	GVSAPGRSI-EASVDFEAFKV--EADVSLPSMQGDLKTTDLIQPPSADL	2045	AKLDGARLEGDSLADKDVTAKDSKFKMPEMNIKAKPISMPDIDL	3001
2032	-IDAPDVLVHGGPDWHL-----KMPKMKMFKSMPGFKAEQPEVDVNL	2072	NLKGPKVKGMDVSLPKVEGDMKPEVDVDIRGP--KVDINAPDVLVHGGPDW	3146
2046	KVQIGQVDVVKLPEGVPEAGLKGHLPKVEMPSLKMFKVGLKGPQVDIKG	2095	DVSAPKV--EAEVSLPSMQGDLKTTDLISIEPPSAQLEVAQAGVDLKLPEG	3049
2073	PKADVVSQPKVDVVEPDSLEGPEGLKGPVKMPEMNIKAKPISMPDVL	2122	HL-----KMPKMKMFKSMPGFKAEQPEVDVNLKADLVSQPKVDV	3188
2096	PKLD--LKDPKVEMRVPDVL-----EVSLSFMS	2119	HVPEGAGLKGHLKGLKQMPFKMPEMNIKAKPISMPDIDLKADLVSQPKVDV	3050
2123	DLHLKGPVKVDVSLPKLEGLDITGSPVDEVDVELECPDAMLKGEKFK	2172	DVPD-----VNIIEGPEGLKGPVKMPEMNIKAKPISMPDIDL	3206
2120	EVDVQAPRAKLD---SAHQGLDIT-----LANKDLTIDKDSKFKMPEKFK	2158	TAPDVEVSQPGMEVDVEAFGAKLDGARLEGDSLADKDVTAKDSKFKMPEKFK	3147
2173	KMPMFKTFKISMPDVLNHLKGPVKMGDMVSPKVEGEMKVPDVIKGGKMD	2222	FKMPEMNIKAKPISMPDIDLNLKGPVKMGDMVSPKVEGEMKVPDVIKGGKMD	3256
2159	KMPSFGVSAP-----GKSIEASVDSVSPKVEADM	2187	FKMPSFGVSAPGKSIIEVL--VDVSAPKV--EADLPSMQGDLKTTDLISIE	3194
2223	PKVDIDAPDVLVHGGPDWHLKMPKMKMFKSMPGFKAEQPEVDVNLKADL	2270	GP--KIDVADPIDIDHGGPDWHLKMPKMKMPEMNIKAKPISMPDIDLNLKGP	3304
2188	-----SLPSMQGDLKTTDLISIQPLISA	2208	PSPSAQLEVAQAGVDV-----KLPESHV-----LEG	3219
2271	DVDVSGPKVDVVEPDSLEGP---EGKLGK--PKFMPEMNIKAKPISMPDVL	2315	SKLKGVDVSGPKVLE--GDHKAPSLDITGPEVDVSGPKVLEGGKSKSFK	3353
2209	DVKVQAQVDVVKL-----LEGFVPEEVLKGLKGLKQMPFS--FKVQKV---	2249	AGLKGHL---PKLQMPFSFKMPEMNIKAKPISMPDIDLKADLVSQPKVDV	3253
2316	DVDVNLKGPVKIGDVSAPKLEGLKGPVLDVKGPKLDAIMPEVAVEGF	2365	LKPFNFSGSKVQIPEVDVKGKKEPDIIDITGPKVDINAPDVEVQGVKGSKF	3403
2250	-----DLKGPVLDVKGPKLDAIMPEVAVEGF	2275	-----DLKGPVLDVKGPKLDAIMPEVAVEGF	3268
2366	NGKWKTKPKFMPEMNIKAKPISMPDIDLHLKSPKAKGEVDVVKLEGLD	2415	KMPFLSISSPKSMPDVLNHLKSPKAKGEVDVVKLEGLD	3453
2276	D-----VEVSLPSVEVDVKAPGAK---LDGARLEGDM	2304	-----VSPQSMVEVDVEAFGAKLD---GARLEGDM	3293
2416	KGPHVDVSGPDIDIEGPEGLKGPVKMPEMNIKAKPISMPDVLNHLKGP	2465	PEVNLNAPDVLVHGGPDWHLKMPKMKMPEMNIKAKPISMPDIDLKADLVSQ	3490
2305	-----SLADKDVTAKDSKFKMPEMNIKAKPISMPDVLNHLKGP	2344	-----LADKDVTAKDSKFKMPEMNIKAKPISMPDVLNHLKGP	3339
2466	KIKGVDVSVPEVEGKLEVDPMNIRGP-----KVDINAPDVLVHGGPD	2505	---PDVAVDLKPGDINIEGSPMNIIE--GPDINVEGPEG-----GLKG	3528
2345	ALKVEADVSLPSMQGDLKTTDLISVQPSADLEVAQAGVDVVKLPEGVPEGS	2394	ADVSLPSMQGDLKTTDLISVQPSADLEVAQAGVDVVKLPEGVPEGVPEGS	3389
2506	---NHLKMPKMKMPEMNIKAKPISMPDIDLHLKSPKAKGEVDVVKLEGLD	2551	PKFMPEMNIKAKPISMPDIDLNLKGPVKMGDMVSPKVEGEMKVPDVIKGGKMD	3578
2395	AGLKGHL---PKLQMPFSFKMPEMNIKAKPISMPDIDLKADLVSQPKVDV	2440	-----HLKPEVMP-----SKMPEMNIKAKPISMPDIDLKADLVSQPKVDV	3412
2552	D-----VNIIEGPEGLKGPVKL-----MPEMNIKAKPISMPDIDL	2581	IKGPKVDINAPDVLVHGGPDWHLKMPKMKMPEMNIKAKPISMPDIDLKADL	3628
2441	DVEVSVQPSVEVDVEAFGAKLDGAWLEGDSLADKDVTAKDSKFKMPEKFK	2490	IKGPKLDLVEKAEVTVDPVVEVSLPSV-----EVDVQAPR	3447
2582	PDFDLHLKGPVKIGDVSAPKLEGLKGPVLDVKGPKLDAIMPEVAVEGF	2618	ADIDISGPNVDVDPVNIIEGPEGLKGPVKMPEMNIKAKPISMPDIDL	3678
2491	PSFGVSAPGKSIIEASVDSVSAFKVEADGSLSSMQGDLKTTDLISIQPPSADL	2540	AKLDGARLEGDSLADKDVTAKDSKFKMPEMNIKAKPISMPDIDLKADLVSQ	3496
2619	---KVDINAPD-----VGVQGPDWHLMKPKMPEMNIKAKPISMPDIDL	2657	NLKGPKMKGMDVSLPKVEGDMKPEVDVDIRGP--KVDINAPDVLVHGGPDW	3728
2541	EVQAQVDVVKLPEGVPEAGLKG---HL--PKVQMPFSFKMPEMNIKAKPISMPD	2585	EVQAQVDVVKLPEGVPEAGLKG---HL--PKVQMPFSFKMPEMNIKAKPISMPD	3542
2658	GDVVKPKADIDVSGPKVDIEGPD-----VNIIEGPEGLKGPVKL-----	2692	GDVVKPKADIDVSGPKVDIEGPD-----VNIIEGPEGLKGPVKL-----	2633
2586	LDVKGPK--LDLKGPKAEVTVDPVEMSLSMEVDVQAPRAKLDGARLEGDM	2633	-----PKFMPEMNIKAKPISMPDIDLNLKGPVKMGDMVSPKVEGEMKVPD	2724
2693	-----PKFMPEMNIKAKPISMPDIDLNLKGPVKMGDMVSPKVEGEMKVPD	2724	-----PKFMPEMNIKAKPISMPDIDLNLKGPVKMGDMVSPKVEGEMKVPD	2679
2634	LSLADKDVTAKDSKFKMPEMNIKAKPISMPDIDLNLKGPVKMGDMVSPKVEGEMKVPD	2679	-----KVDIDAPDVLVHGGPDWHL	2764
2725	VDVSLPKVEGDMKPEVDVDIRGP--KVDIDAPDVLVHGGPDWHL	2764	ADMSLPSMQGDLKTTDLISIQPPSAQLEVAQAGVDVVKLPEGVPEAGLKG	2729
2680	ADMSLPSMQGDLKTTDLISIQPPSAQLEVAQAGVDVVKLPEGVPEAGLKG	2729	KMPKMKMFKSMPGFKAEQPEVDVNLKADLVSQPKVDVVECPDAMLKGEKFK	2814
2765	KMPKMKMFKSMPGFKAEQPEVDVNLKADLVSQPKVDVVECPDAMLKGEKFK	2814	HLKQMPFSFKMPEMNIKAKPISMPDIDLKADLVSQPKVDVVKLPEGVPEAGLKG	2763
2730	HLKQMPFSFKMPEMNIKAKPISMPDIDLKADLVSQPKVDVVKLPEGVPEAGLKG	2763	EGKWSKPKFMPEMNIKAKPISMPDIDLNLKGPVKMGDMVSPKVEGEMKVPD	2864
2815	EGKWSKPKFMPEMNIKAKPISMPDIDLNLKGPVKMGDMVSPKVEGEMKVPD	2864	KAEVTVDPVEMSLSMEVDVQAPRAKLD---GARLEGDM	2799
2764	KAEVTVDPVEMSLSMEVDVQAPRAKLD---GARLEGDM	2799	KGPEVDLKGPKVDIDVDPVNIIEGPEGLKGPVKMPEMNIKAKPISMPDIDL	2912
2865	KGPEVDLKGPKVDIDVDPVNIIEGPEGLKGPVKMPEMNIKAKPISMPDIDL	2912	-----SLADKDVTAKDSKFKMPEMNIKAKPISMPDIDLKADLVSQ	2834
2800	-----SLADKDVTAKDSKFKMPEMNIKAKPISMPDIDLKADLVSQ	2834	EVDVNLKADLVSQPKVDVVECPDAMLKGEKFK	2951
2913	EVDVNLKADLVSQPKVDVVECPDAMLKGEKFK	2951	SVDSSELKVEADGSPSQGDLKTTDLISIQPPSAQLEVAQAGVDVVKLPEG	2884
2835	SVDSSELKVEADGSPSQGDLKTTDLISIQPPSAQLEVAQAGVDVVKLPEG	2884	KMPE--MNKA--PKIMPDFDLHLKGPVKMGDMVSLPKVEGDMKPEVDV	2998
2952	KMPE--MNKA--PKIMPDFDLHLKGPVKMGDMVSLPKVEGDMKPEVDV	2998	HVPEGAGLKGHLKGLKQMPFS-----KMPKMKMFKSMPGFKAEQPEVDVNL	2917
2885	HVPEGAGLKGHLKGLKQMPFS-----KMPKMKMFKSMPGFKAEQPEVDVNL	2917	IRGQVDIDVDPVNIIEGPEGLKGPVKMPEMNIKAKPISMPDIDLKADLVSQ	3048
2999	IRGQVDIDVDPVNIIEGPEGLKGPVKMPEMNIKAKPISMPDIDLKADLVSQ	3048	VKGPVLDLKGPKAEVTVDPVVEVSLPSV-----EVDVQAPR	2952
2918	VKGPVLDLKGPKAEVTVDPVVEVSLPSV-----EVDVQAPR	2952		

Appendix B: reverse and forward sequence for pACT-NPRC and pBIND-NPRC

LNPRCPACT+T3

AGGCCTTAGTTATTCAGGTACCTGCGGCCGCTCTAGAGTCGACCGTTTCATTGATGTCTTTCAACCCGCTATCTCCT
TAAAGAATCTCAGGCAGAAAAAAGTGGGGGGCTTCCTTTAAGCTACTGAAAAATGGGATCTGATGGAATCTTCC
CGTAATCCCAGATGTTTTCCAAGGTTACTTTCTTCTTGGTTCGCCTCTCAATGGTTATTCTGTATTTCTTCTGAA
AAAGTAGAAGGCCATTAGCAAGCCAGCTCCTAGTAAAGCCCCACGACAATTCCTGTCACTGCCGATTCTTCTAGGC
CACATGATTTGCAGGGAGAGCTGTTTGTATGCTCTACAATTCGGTTTTTCATCTATTCTCAGTTTTAAAGGGCCCCAAG
GATATTTGACATTCGGCCGATTTCAAACGACCTTCTTTTCAAATAATCACCATAACCTCCTGGGTGCCCGCT
CCACATCAGTCATGGCAATCACAGAGAAATCCCATATCGGTCTCCGTTGGCATCTATGGACACCTGCCCGGCGATA
CCTTCAAATGTTCTGTTCCAAGTCTGCTGTATAATTTCCCTCCATCCTTTTTGCTGTAACCAAGCTCTGAGTACTTCATG
TAGAGCCAAGACGTAGAGGAGGATGGCATCGTGGAAATCCTTCAACAAACATGTTAACGTAATCCTCCATATTGAGCC
CTTGTTTTCTCAACTGAACTTTTACCTCCATGAAAACTTCTCAAACCTCAGTTTTCACTGTCTCAGTAGAGTGACTGT
CTGGAGGACGAGTATGCTTGGCTTAAAGTCTGATCGTGGTGTCTCCTCTCTCCATGAGCCATCCATAGGAAGA
GCTGTTGAAGAGCTCAATGTTGAAGAAGCGTAGTCTCCACTGGTATGCCATGCCTGTGCGCCACCAGCATGATGCT
CCGGATGGTGTACTGCTCGCACACATGATCACCCTCTCTCACT

LNPRCPACT+T7

AGCTGAGCAGCCTCCTGAAGATGAAGCTACTGTCTTCTATCGAACAAGCATGCCAAAAAAGAAGAGAAAGGTAGAT
GAATCCCAGGGATCTCGACGGCCCCCGACCGATGTGAGCCTGGGGGACGAGCTCCACTTAGACGGCGAGGAC
GTGGCGATGGCGCATGCCGACGCGTAGACGATTTGATGCTGGACATGTTGGGGGACGGGGATTCCCCGGGTCCG
GGATCGCCAGGGATCCGTCGACTTGACGCGTTGATATCGAATTCCTGCAGGTGACCGGGGGCAGAAGGGCGAGT
CGGCGGCGGCGAGGGCAAGCTCTTTCTTGGCGCACGATGCCGTCTCTGCTGGTGTCACTTTCTCCCCGTGCGTAC
TACTCGGCTGGGCGTTGCTGGCCGGCGGCACCGGTGGCGGTGGCGTTGGCGGCGGCGGCGGTGGCGCGGGCATA
GGCGGGCGGACGCCAGGAGAGAGAGGGCGCTGCCGCCACAGAAGATCGAGGTGCTGGTGTACTGCCCCAGGATGAC
TCGTAATTTGTTTTCACTCACCCTGGGTGCGCCGGCCATCGATGCTCTGCGCAGCGTGGAGGGCAACGGGACTG
GGAGGGCGGCTTCTGCCGCCGGGCACTCGCTTCCAGGTGGCTTACGAGGATTCAGACTGTGGGAACCGTGCCTCTT
CAGCTTGGTGGACCGGTGGCGGCGGCGCGGGGGCGCAAGCCAGACCTTATCCTGGGGCCAGTGTGCGAGTATG
CAGCAGCGCCAGTGGCCCGGCTTGCATCGCACTGGGACCTGCCATGCTGTGCGCTGGGGCGCTGGCCGCTGGCT
TCCAGCACAAAGGACTCTGAGTACTCGCACCTCACGCGGTGGCGCCCGCCTACGCCAAGATGGCGAGATGATGCT
CGCCCTGTTCCGCCACCACCCTGGAGCCGCGCTGCACTGGTCTACAGCGACGACAGTGC

LNPRCPBIND+T3

AGGCCTTAGTTATTCAGGTACCTGCGGCCGCTCTAGAGTCGACCGTTTCATTGATGTCTTTCAACCCGCTATCTCCT
TAAAGAATCTCAGGCAGAAAAAAGTGGGGGGCTTCCTTTAAGCTACTGAAAAATGGGATCTGATGGAATCTTCC
CGTAATCCCAGATGTTTTCCAAGGTTACTTTCTTCTTGGTTCGCCTCTCAATGGTTATTCTGTATTTCTTCTGAA
AAAGTAGAAGGCCATTAGCAAGCCAGCTCCTAGTAAAGCCCCACGACAATTCCTGTCACTGCCGATTCTTCTAGGC
CACATGATTTGCAGGGAGAGCTGTTTGTATGCTCTACAATTCGGTTTTTCATCTATTCTCAGTTTTAAAGGGCCCCAAG
GATATTTGACATTCGGCCGATTTCAAACGACCTTCTTTTCAAATAATCACCATAACCTCCTGGGTGCCCGCT
CCACATCAGTCATGGCAATCACAGAGAAATCCCATATCGGTCTCCGTTGGCATCTATGGACACCTGCCCGGCGATA
CCTTCAAATGTTCTGTTCCAAGTCTGCTGTATAATTTCCCTCCATCCTTTTTGCTGTAACCAAGCTCTGAGTACTTCATG
TAGAGCCAAGACGTAGAGGAGGATGGCATCGTGGAAATCCTTCAACAAACATGTTAACGTAATCCTCCATATTGAGCC
CTTGTTTTCTCAACTGAACTTTTACCTCCATGAAAACTTCTCAAACCTCAGTTTTCACTGTCTCAGTATGAGTGACTGT
CTGGAGGGACGAGTATGCTTGGCTTAAAGTCTGATCGTGGTGTCTCCTCTCTCCATGAGCCATCTCCATAGGAAGA
GCTGTTGAAGAGCTCAATGTTGAAGAAGCGTAGTCTCCACTGGTATGCCATGCCTGTGCGCCACCAGCATGATGCT
CCGGATGGTGTACTGCTCGCACACATGATCACCCTCTCTCACTGGCTGGATATTGCGCACGAT

LNPRCPBIND+T7

GCTGAGCAGCCTCCTGAAGATGAAGCTACTGTCTTCTATCGAACAAGCATGCGATATTTGCCGACTTAAAAAGCTCA
AGTGCTCCAAAGAAAAACCGAAGTGCGCCAAGTGTCTGAAGAACAAGTGGGAGTGTGCTACTCTCCAAAAACAAA
AGGTCTCCGCTGACTAGGGCACATCTGACAGAAGTGAATCAAGGCTAGAAAGACTGGAACAGCTATTTCTACTGAT
TTTTCTCGAGAAGACCTTGACATGATTTGAAAATGGATTCTTTACAGGATATAAAAGCATTGTTAACAGGATATTTG
TACAAGATAATGTGAATAAAGATGCCGTACAGATAGATTGGCTTCACTGGAGACTGATATGCCTCTAACATTGAGAC
AGCATAGAATAAGTCCGACATCATATCGGAAGAGATAGTACAACAAGTCAAAGACAGTTGACTGTATCGCCGGAA
TTCCCGGGGATCCGTCGACTTGACGCGTTGATATCGAATTCCTGCAGGTGACCGGGGGCAGAAGGGCGAGTGGG
CGGCGGCGAGGGCAAGCTCTTTCTTGGCGCACGATGCCGTCTCTGCTGGTGTCACTTTCTCCCCGTGCGTACTAC
TCGGCTGGGCGTTGCTGGCCGGCGGCACCGGTGGCGGTGGCGTTGGCGGCGGCGGCGGTGGCGCGGGCATAGG
CGGCGGACGGCAGGAGAGAGAGGGCGCTGCCGCCACAGAAGATCGAGGTGCTGGTGTACTGCCCCAGGATGACTC
GTACTTGTATTTCACTCACCCTGGGTGCGCCGGCCATCGAGTATGCTCTGCGCAGCGTGGAGGGCAACGGGACTGG
GAGGCGGCTTCTGCCCGGGCACTCGCTTCCAGGTGGCTTACGAGGATTCAGACTGTGGGAACCGTGCCTCTTC
AGCTTGGTGGACCGCGTGGCGGCGGCGGGGGCGCAAGCCAGACCTTATCCTGGGGCCAGTGTGCGAGT

Appendix C: sequence for pACT- β -arrestin and pBIND- β -arrestin

BAR-PACT+VP16

ACGCGTTGATATCATCTAGAATGGGCGACAAAGGGACACGAGTGTTCAAGAAGGCAAGCCCCAATGGAAAGCTCAC
CGTCTACCTGGGAAAGCGGGACTTTGTGGACCACATTGACCTGGTGGACCCCGTGGATGGCGTGGTCTGGTGGAT
CCTGAGTATCTCAAAGAAAGGCGAGTCTACGTGACACTGACCTGCGCCTTCCGGTATGGCCGGGAAGACCTGGATG
TCTTGGGTCTGACTTTTCGAAAGACCTGTTTGTGGCTAACGTGCAGTCCTTCCCACCGGCCCTGAGGACAAGAAG
CCACTGACTCGGCTACAAGAGCGACTCATCAAGAAGCTGGGCGAGCATGCCTACCCCTTACCTTTGAGATCCCGC
CAAACCTTCCGTGCTCAGTCACATTGCAACCTGGGCTGAGGAC

BAR-PBIND+GAL4

TGACGCGTTGATATCATCTAGAATGGGCGACAAAGGGACACGAGTGTTCAAGAAGGCAAGCCCCAATGGAAAGCTCA
CCGTCTACCTGGGAAAGCGGGACTTTGTGGACCACATTGACCTGGTGGACCCCGTGGATGGCGTGGTCTGGTGGAT
TCCTGAGTATCTCAAAGAAAGGCGAGTCTACGTGACACTGACCTGCGCCTTCCGGTATGGCCGGGAAGACCTGGAT
GTCTTGGGTCTGACTTTTCGAAAGACCTGTTTGTGGCTAACGTGCAGTCCTTCCCACCGGCCCTGAGGACAAGAAG
GCCACTGACTCGGCTACAAGAGCGACTCATCAAGAAGCTGGGCGAGCATGCCTACCCCTTACCTTTGAGATCCCG
CCAAACCTTCCGTGCTCAGTCACATTGCAACCTGGGCTG

Appendix D: reverse and forward sequence for pBIND-AHNAK1

PZF187PBIND+T3

GGCTTAGTTATTCAGGTACCTGCGGCCGCCACTCTTTCTTTGTGGAAACTGACAGCTCCACCTCGGGAAGCTGGAT
GCCAACCTTATCCCCTGTCAATTGCTAGAAGAGGAGGACAGTCGGGACTTCTTAGAGGCCAGGGACACCCCACTCC
CCTGTAACCTTGCCTGTCTCATCATCGCTCCCAGTCACCTCATAATGACCTTTGCTCTTTGACCCCAATCCACCAAAGG
TACCGAATTTACAGCTTCCCGTGTTCCTTTAACTTTCCACCTTCCAGAGACTTCCCACCTTCAAACCTCCAGCGT
CCCCGTGGGGTGGAAAGTCCAGAGAACTCTTTCATCACTGAATGAATTTGAGCGGTGCCGTGGCTTCTTACTTT
TAAATAAGGAAATTTGCCTTTCCGGTGAAGAGGCTTCGGCTCTGCCTCTCCTTCCAGAGACGCCAGGCTGGCCTTT
GAACTTTTAGGTTGACTTTTGGACCCAGAAATTTGATGCTTCTGGTGAGCCAGTGACACCACTTTCCCTTTAGGTTG
GAAAAATTAACCTTGGCATTGATCTTGGACTTTTCTGATTTGACTTTCAGACTTCCCACTCGCCGTCTCCAGCAC
CAGCTTGGATGCTGGCCTCTGCTTTAGGGAAGTGAACATCCACCCCACTTCTCTGCCAACCACTCACGGCCAGAG
AAGGTAATTTGGGGATCTTCAATTTAGGGAATGTTACTTTTCCAGATCCACTTTCCAAGTGACCTTGAAGCCAGAC
ACACTCAGCCCAGGACCTGGAGTCCAATCTGACCTCCTTTACACCTCCTTCCACCTTTGGTCTGAGAAATGAAG
GCCCCAGCAAACCT

PZF187PBIND+T7

GCTGAGCAGCCTCCTGAAAGATGAAGCTACTGTCTTCTATCGAACAAGCATGCGATATTTGCCGACTTAAAAAGCTCA
AGTGCTCCAAAGAAAACCGAAGTGCGCCAAGTGTCTGAAGAACAAGTGGGAGTGTGCTACTCTCCAAAACCAA
AGGTCTCCGCTGACTAGGGCACATCTGACAGAAGTGGAAATCAAGGCTAGAAAAGACTGGAACAGCTATTTCTACTGAT
TTTTCTCGAGAAGACCTTGACATGATTTTGAATGGATTCTTTACAGGATATAAAAAGCATTGTTAACAGGATATTTG
TACAAGATAATGTGAATAAAGATGCCGTCACAGATAGATTGCTTTCAGTGGAGACTGATATGCCTCTAACATTGAGAC
AGCATAGAATAAGTGGCAGATCATCATCGGAAGAGAGTAGTAACAAAGGTCAAAGACAGTTGACTGTATCGCCGGAA
TTCCCGGGATCCGCTGACTTGACGCTTGATATCGAATTCCTGCAGGTCGACCGGGGGCAGAAGGGCGAGTCGG
CGGCGGCGAGGGCAAGCTCTTTCTTGGGACGATGCCGTCTGCTGGTGGTCACTTTCTCCCGTGGTACTAC
TCGGCTGGGCTTGTGCGCGGCGCACCGGTGGCGGTGGCGTGGCGGGCGGCGGTTGGCGGGCGGCGGATAGG
CGGCGGACGCGAGAGAGAGAGGCGCTGCCGCCACAGAAGATCGAGGTGCTGGTGTACTGCCCCAGGATGACTC
GTACTTGTCTTCACTACCCGGGTGCGGCGGCCATCGAGTATGCTCTGCGCAGCGTGGAGGGCAACGGGACTGG
GAGGCGGCTTCTGCCCGGGCACTCGCTTCCAGGTGGCTTACGAGGATTCAGACTGTGGGAACCGTCCGCTCTTC
AGCTTGGTGGACCGCGTGGCGGGCGGGGCGCCAAGCCAGACCTTATCCTGGGGCCAGTGTGCGAGT

Appendix E: reverse and forward sequence for AHNAK1 construct 2

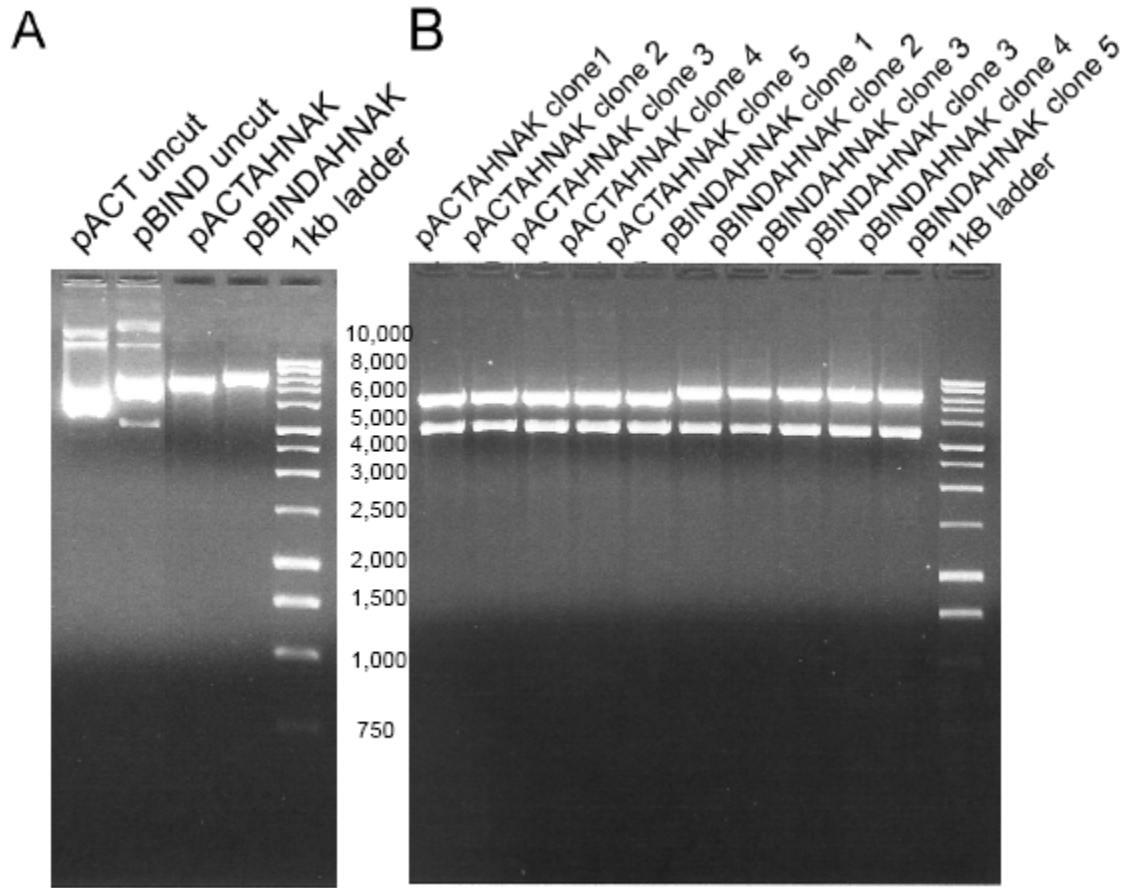
PZ21+M13FORWARD

AATTGGGTACCGGGCCCCCCTCGAGGTGACGGTATCGATAAGCTTGATATCGAATTCGGTGAAGTCCACATCAG
GCATGGAGATCTTGGGGGCCCTTGATATTCATCTCTGGCATCTTGAACCTGGGGCCCTTCAGCTTTCCTTCAGGTCCCT
CAATATTCACATCTGGAACCTCAACACCCACCTTGGGTCCTGAGATGTCCACATCAGCCTTGGGCAGGTTACATCCA
CTTCTGGGCCCTCTGCTTTGAAGCCAGGCATGCTGAACCTGGGCATTTTCATCTTGGGCATCTTCAGGTGCCAGTCT
GGGCCTTGAACCTCCACATCTGGGACATCAATGTCCATTTTGGCACTTTTAAGTTCAACATCAGGAACCTTAAATCTCAC
TTTCAACCTTTGGCATTGTGACATCATATTCTCCCTTTACGTTAGGGCCCTTTCAGATGTAAGTCCACATCAGGCATGGA
GATCTTGGGGACTTTGATGTTTCATCTCAGGCATCTTAACTTGGGCCCTTTCATTTCCCTTCTGGTTCCTCAATGCTC
ACATCAGGAGCAGTAACATCTATCTTGGGCCCGGAAATGTCCACATCAGCCTTGGGCAGGTTCCACATCCACTTCTGG
GCCCTCTGCTTTGAACCCTGGCACACTGAATTTGGGCATTTTCATCTTGGGCATCTTCAAGTGCCAGTCTGGGCCATG
AACATCCACATCTGGGGCATCAATGTCCACTTTTGGGCCCTTTGAGTTCTCCTTCCAGCTTTGGTACAGTTACATCATA
TCTCCCTTACCTTTGTACCTTTCACGTGCAAATCTACATCAGGCATGGAGATCTTTGGTGTCTTGACACTCATATCAG
GCAGCTTAACATCGGGGCCCTTAAAGTTTTCCCCCAGACCCTCCAAGTTGACATCTGGGGCTTCCACATTGACCTTG
GGCCTGAAATACTGATATCTCCTTTGGGTAGAGTCATATGAACATCTGGACCTTCCCTTTGGCTCCTGGAGTGCTG
AACGTGGGCATTTTCATCTTGGGCAT

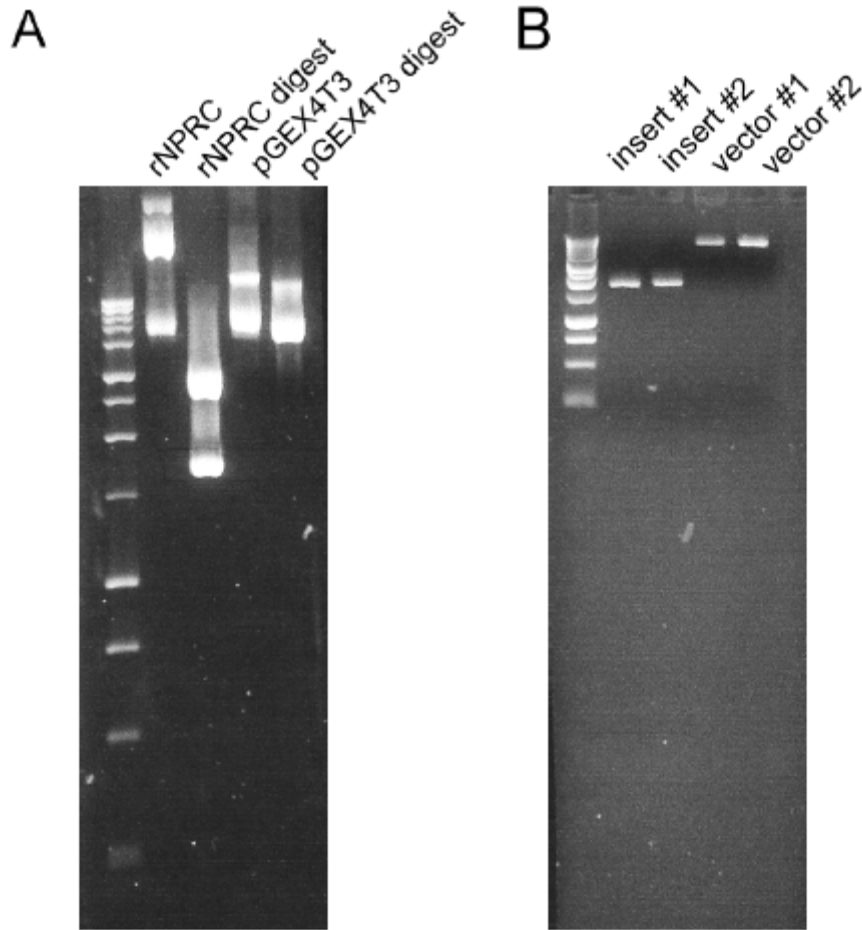
pZ21+M13REVERSE

AACAAAAGCTGGAGCTCCACCGCGGTGGCGGCCGCTCTAGAAGTGTGGATCCCCGGGCTGCAGGAATTCGGCT
GAAGTCGGAAGATGGAGTGGAAGGAGACCTCGGGGAGACCCAGAGCCGTACCATCACAGTGACCAGAAGGGTCAC
GGCCTACACTGTGGATGTGACTGGCCGGGAAGGAGCCAAGGACATAGACATCAGTAGCCCTGAATTCAGATCAAG
ATTCGAAGACATGAACTGACTGAAATCTCAAATGTGGATGTGGAGACCCAGTCTGGGAAGACCGTGATCAGACTGCC
CTCGGGCTCGGGGGCAGCCTCTCCGACAGGCTCTGCTGTGGATATCCGAGCAGGGGCCATTTCTGCTTCAGGACCA
GAGCTCCAAGGTGCTGGCCACTCGAAGCTCCAGGTCACCATGCCTGGGATAAAGGTGGGAGGCTCAGGTGTCAATG
TCAATGCAAAGGGCTTGGACTTGGGTGGCAGAGGAGGGGTCCAAGTTCCAGCAGTGGACATTTTCATCTTCTCTTGGG
GGTAGGGCAGTAGAGGTACAGGGCCCATCTCTGGAGAGTGGTGTATCATGGCAAAATTAATTTCCACCATGAAAGT
GCCGAAATTTGGTGTCTAACAGGGCGTGAGGGCCAGACACCAAAGGCAGGGCTGAGGGTTTCTGCACCTGAAGTC
TCTGTGGGGCACAAGGGCGGCAAGCCAGGCTTGACTATCCAAGCCCCTCAGCTGGAAGTCAGTGTGCCCTTGCCA
ATATTGAGGGCCTTGAGGGGAAGCTGAAGGGCCCCCAAATCACTGGGCCATCACTTGAAGGTGACCTAGGCCTGAA
AGGTGCCAAGCCACAGGGGCACATTGGGGTGGATGCCTCTGCTCCCCAAATTGGGGGTAGCATCACTGGCCCCAGT
GTGGAAGTTCAGGCCCTGACATTGATGTTCAAGGGCCCTGGGAGCAAACCTGAATGTGCCCAAGATGAAAGTCCCCA
AGTTCTCTGTATCAGGTGCAAAGGGAGAGGAACTGGGATTGATGTGACACTGCCTACAGGTG

Appendix F: Construction of pACT and pBIND AHNAK1 fusion proteins



Appendix G: Construction of pGEX4T3NPRC



Appendix H: Sequence for rat GST-NPRC

RNPR-C+PGEX-3

```

ATCGTCAGTCAGTCACGATGCGGCCGCTCGAGTCGACCCGGGAATTCTCCAAGAACACCCCTTCTGTTCCATTGATG
TCTGTCCTTCAACTATCTCTTTAAGGAATCTCAAGCAGACAAAGCAAGGGGGGCATTTCTTTTAAGCCACCGAAAAAT
GTGATCTGATGGAATCTTCCCGCAGCTCTCGATGTTTCCCAATGTTGCTTTCTTCTGGTGATTTGCGCTCTCAATGGT
TATTCTGATTTCTTCTGAAAAAGTAGAAGGCCATTAGCAAACCAGCACCTAGTAGGGCCCCCACAACAATTCCTGT
CACTGCTGATTCTTCTAGGCCACATGATTTGCAAGGAGAGCTGTTGGTGTGCTCCACAATTCTGGTTTCATCTATTCT
CAATTCAAAGAGCCCCAAGGATATTTGACATTGGATCGCATTTTGAACCGCCTTCTTTTCAAAGTAATCACCAATG
ACCTCCTGGGTACCTGCTTCTGTATCAGTCATGGCAACCACAGAGAAGTCTCCATACCGATCCCCATTAGCATCTATG
GACACCTGCCCGCGATACCTTCAAATGTCCTGTTCCAAGTCTGCTGGATGATTTTCCCCCATCCTTCTTGCTGTAG
CCAGCTCTGAGCACTTTCATGCAAAGCCAGAACGTAGAGGAGGATGGCATCATGGAAGCCTTCAACGAACATGTTTAC
GTAATCCTCCTCATTGAGCCCTTGTCTCAACAGAACTTTTACCTCCATGGAAAACCTTCTCAAACCTCAGGCTTCGCG
GTCCTCAGCAGGGTGACTGTTTGGAGGGATGAGTAAGCTTGCTTAGCTTCAAAGTCGTGTTTGTCCCCTCTTCCAC
GAGCCATCTCCGTAAGAAGAACTGTTGAAGAGTTCAATGTTGAAGAAAGCATAGTCTCCACTGGTCATGCCGTGCT
GTGCACCGCCAACATGATTCTCCGAATGGTGTACCAC
    
```

Appendix I. Primers used with the QuikChange site-directed mutagenesis kit

CGG GCT GCA GGA ATT CCG CTT GCT GGC AAC AGG ATG CGG TCC

5'- GGC TGC AGG AGA CGC GTT GGC TGG CAA CAG GAT GCG -3'

5'- CGC ATC CTG TTG CCA GCC AAC GCG TCT CCT GCA GCC -3'

Appendix J: Site-directed mutagenesis reaction

Volume (µL)	Reagent
39.5 µL	Water
5 µL	10X reaction buffer
1.25 µL	Diluted primer #1
1.25 µL	Diluted primer #2
1 µL	Diluted DNA
1 µL	dNPT mix
50 µL	

Reagents were added sequentially in the order listed.

Appendix K: Cycling parameters for site-directed mutagenesis reaction

# of Cycles	Temperature	Time
1	95 °C	30 sec
16	95 °C	30 sec
	55 °C	1 min
	68 °C	14 min
	4 °C	Hold

Appendix L: Ligation reaction for construction of pACT and pBIND AHNAK1

Vector	DEPC H2O	T4 DNA ligase 10X buffer	Insert	Ligase
5 µL pACTAHNAK1	2 µL	2 µL	10 µL pzdoube	1 µL
5 µL pBINDAHNAK1	2 µL	2 µL	10 µL pzdoube	1 µL

Appendix M: Restriction digest reaction for verification of pACT and pBIND AHNAK1

Sample	10X reaction buffer	100X BSA	DEPC H2O	Enzyme
5 µL pACTAHNAK1	2.5 µL	0.3 µL	15.2 µL	0.75 µL NOT1 0.75 µL Mlu1
5 µL pBINDAHNAK1	2.5 µL	0.3 µL	15.2 µL	0.75 µL NOT1 0.75 µL Mlu1

Appendix N: Reactions and parameters for the subcloning of rat NPRC into pGEX4T3

Restriction Digestion of rNPRC:

<u>Sample</u>	<u>10X Buffer H</u>	<u>100X BSA</u>	<u>DEPC H₂O</u>	<u>Enzyme</u>
5 μ L rNPRC (5 μ g/ μ L) EcoR1	10 μ L	1 μ L	79 μ L	5 μ L
30 μ L pGEX4T3 (0.54 μ g/ μ L) EcoR1	10 μ L	1 μ L	54 μ L	5 μ L

Gel Electrophoresis

<u>Sample</u>	<u>TBE</u>	<u>LB</u>
1 μ L rNPRC (0.5 μ g/ μ L)	9 μ L	2 μ L
2.5 μ L rNPRC digest	7.5 μ L	2 μ L
1 μ L pGEX4T3	9 μ L	2 μ L
2.5 μ L pGEX4T3 digest	7.5 μ L	2 μ L
5 μ L ladder	5 μ L	2 μ L

Samples were heated for 15 minutes for 65 °C before load the gel for electrophoresis

Dephosphorylation of pGEX4T3 vector digest:

A 100 μ L reaction was set up as follows:

10 μ L 10X NEB3

49 μ L DEPC H₂O

1 μ L CIP

The reaction incubated for 1hr at 37 °C in a thermocycler

Ligation Reaction:

<u>Vector</u>	<u>H₂O</u>	<u>10X Buffer</u>	<u>Ligase</u>	<u>Insert</u>
2 μL pGEX4T2	15 μL	2 μL	1 μL	none
2μL pGEX4T2 rNPRC	14 μL	2 μL	1 μL	1 μL
3 μL pGEX4T2 rNPRC	13μL	2 μL	1 μL	1 μL

Samples were ligated overnight at 16 °C in a thermocycler

The purity and concentration of the ligation was estimated by gel electrophoresis

1-5 μL the ligation was transformed into competent cells

Appendix O: Transfection reagents used for delivery of plasmid DNA or siRNA

Transfection Reagent	Application	Cell type
Lipofectamine™	Transfection of plasmid DNA	Adherent/suspension cell lines
Lipofectamine™ 2000	Transfection of plasmid DNA	Adherent/suspension cell lines
FuGENE®	Transfection of plasmid DNA	Adherent/suspension cell lines
FuGENE® HD	Transfection of plasmid DNA	Adherent/suspension cell lines
Dharmafect1	Transfection of siRNA	Adherent
Dharmafect3	Transfection of siRNA	Adherent

Appendix P: Relevant publications

Articles in peer reviewed scholarly journals:

1. **Alli, A. A.**, and Gower, W. R., Jr. (2009) The C type natriuretic peptide receptor tethers AHNAK1 at the plasma membrane to potentiate arachidonic acid induced calcium mobilization. *Am J Physiol Cell Physiol*, *in press*
2. **Alli, A. A.**, and Gower, W.R., Jr. (2009) Characterization of a polyclonal antibody against the Cytoplasmic domain of the C-type natriuretic peptide receptor. *J Clin Ligand Assay* **31**, 3-7

Manuscripts submitted for publication:

1. **Alli, A.A.**, and Gower, W.R. Jr. Molecular approaches to examine the phosphorylation state of the C type natriuretic peptide receptor

Manuscripts in preparation:

1. **Alli, A.A.**, et al. Expression of AHNAK1 in surface epithelial cells of the stomach and its role in maintaining gastric epithelial permeability barrier properties

Presentations, proceedings, and published abstracts:

- Abdel A. Alli**, Drew A. Rideout, Gay M Carter, and William R. Gower, Jr. (2009) AHNAK expression and subcellular localization in gastric surface epithelial cells *The FASEB Journal*.

Experimental Biology (ASBMB); New Orleans, LA.

Abdel A. Alli, Gay M Carter, and William R. Gower, Jr. (2009) Expression and localization of natriuretic peptide receptor types A and C in human stomach *The FASEB Journal*.

Experimental Biology (APS); New Orleans, LA.

Abdel A. Alli and William R. Gower, Jr. (2009) Association between NPRC and AHNAK1 may regulate arachidonic acid dependent intracellular Ca²⁺ mobilization in human AoSMCs. Weinstein Cardiovascular Development Conference; San Francisco, CA.

Abdel A. Alli and William R. Gower, Jr. 2008. Novel methodology for obtaining recombinant proteins from bacterial inclusion bodies: advantages and applications. CLAS' 34th International Meeting; Coral Springs Marriot & Golf, Coral Springs, FL.

Abdel A. Alli and William R. Gower, Jr. 2008. The C type natriuretic peptide receptor may activate phospholipase C independently of G proteins through its association with AHNAK.

CLAS' 34th International Meeting; Coral Springs Marriot & Golf, Coral Springs, FL.

Abdel A. Alli and William R. Gower, Jr. 2008. The association between the C type

natriuretic peptide receptor and AHNAK may reveal novel roles for natriuretic peptides in human vascular smooth muscle cells. *2nd Annual Cardiovascular Symposium*; Tampa, FL.

Abdel A Alli and William R Gower (2008) The C type natriuretic peptide receptor associates with AHNAK in human aortic vascular smooth muscle cells *The FASEB Journal*. 22:1046.5
Experimental Biology (ASBMB); San Diego, CA.

Abdel A. Alli, Barrett Z. McCormick, and William R. Gower, Jr. 2007. Characterization of a Novel Polyclonal Antibody Against the C-type Natriuretic Peptide Receptor. *The American Society for Cell Biology*; Washington, DC.

Abdel A. Alli and William R. Gower, Jr. 2007. Efficient recovery of correctly folded GST fusion proteins from bacterial inclusion bodies. *1st Annual Department of Molecular Medicine Graduate Research in Progress Symposium*. Brooksville, FL.

Abdel A. Alli, Dayami Lopez, and William R. Gower, Jr. 2007. C type natriuretic peptide receptor associates with AHNAK in A-10 vascular smooth muscle cells. *1st Annual Cardiovascular Symposium*; Tampa, FL.

Abdel A. Alli, Gay M. Carter, Eric Thomas, William R. Gower, Jr. 2007. Expression,

purification, and characterization of a functional C type natriuretic peptide receptor fusion protein. *Experimental Biology (ASBMB)*; Washington, DC.

Abdel A. Alli, Dayami Lopez, and William R. Gower, Jr. 2007. Novel association between NPRC and AHNAK in the stomach. *Digestive Disease Week (AGA)*; Washington, DC.

Abdel A. Alli, Dayami Lopez, Kun Jiang, Gay M. Carter, Saras Arasu, Kristen Diehl, and William R. Gower, Jr. 2007. Novel In vitro association between C-type natriuretic peptide receptor and beta-arrestins. *Endocrine Society*; Toronto, Canada.

About the Author

Abdel A. Alli received a Bachelor's of Science Degree in Biology, cum laude, from the University of South Florida, College of Arts and Sciences in the Fall of 2003. He then graduated with a Master's of Public Health Degree in Tropical Health/Communicable Diseases and a Graduate Certificate in Infection Control from the University of South Florida, College of Public Health in the Fall of 2004. He then earned a Master's of Science Degree in Medical Sciences from the University of South Florida, College of medicine in the Spring of 2009.

During his tenor as a doctoral student, Abdel earned an American Heart Association predoctoral fellowship and several awards for his research, including the Golden Bull award, distinguished Graduate Student Achievement award, and the Excellence in Research Award. Abdel has coauthored several peer reviewed journal articles and has earned several travel awards to present his research at various National/International scientific meetings.